![University of Glasgow logo]

Mallon, Jennifer (2023) *Quantifying the benthic metabolism of tropical coral reefs and seagrasses in a changing climate.* PhD thesis.

http://theses.gla.ac.uk/83381/

Quantifying the Benthic Metabolism of

Tropical Coral Reefs and Seagrasses

in a Changing Climate

Jennifer Mallon

BSc Hons. Marine Biology

Submitted in fulfilment of the requirements for the Degree of

Doctor of Philosophy

School of Geographical and Earth Sciences

College of Science and Engineering

University of Glasgow

March 2022

Abstract

Tropical coastal regions are home to around a third of the world's population, where entire communities depend upon ecosystem services derived from an interconnected network of coral reefs, seagrasses, mangroves, and associated fauna. The tropical coastal zone incorporates numerous unique and widely distributed habitats, from mangroves to mud flats, however this thesis focusses on two interconnected marine tropical ecosystems. Coral reefs and seagrasses are global biodiversity hotspots with high rates of productivity which fuel coastal biogeochemical cycling. Seagrasses support blue carbon sequestration, sediment retention, and provide critical habitat. Biogenic calcification by coral reef organisms constructs massive calcium carbonate ($CaCO_3$) structures, as calcifying organisms deposit skeletons over thousands of years. This robust $CaCO_3$ structure protects coastlines from storms by absorbing the impact of wave energy and is critical for maintaining healthy shores. Coral skeletons form a uniquely intricate architecture which provides habitat for diverse ecological communities and many economically important species. However, anthropogenic climate change threatens the ecological function of these systems. High concentrations of carbon dioxide (CO_2) are absorbed into the oceans, resulting in ocean acidification and warming waters, with catastrophic impacts on calcifying organisms. As the global climate crisis threatens coastal ecosystems and the services they provide, the development of metrics to track and predict changes to ecosystem function are essential for advancing scientific conservation efforts.

Biogeochemical measurements of benthic metabolism are proposed as an efficient tool for long-term and high-resolution tracking of changes to species composition and ecosystem function. Benthic metabolism in coastal ecosystems describes carbon cycling driven by biological processes: inorganic (calcification – dissolution) and organic carbon metabolism (photosynthesis – respiration). These processes can be measured from changes in sea water chemistry; specifically dissolved oxygen (DO), dissolved inorganic carbon (DIC), and total alkalinity (TA). Changes to these parameters can be used to measure net metabolic flux between the benthos and seawater and can be used to quantify the carbon cycling processes of coastal ecosystems. Calculating the balance of net community calcification (NCC) to net community production (NCP) provides insight into benthic composition and ecological function and has potential as a method for monitoring change. This approach has been particularly useful for coral reef ecosystems, as their ecological complexity and biodiversity presents a unique logistical challenge for research.

Coral reefs are already substantially degraded and highly vulnerable to the impact of climate change effects such as ocean warming and acidification. Catastrophic declines in coral cover and the negative impact of warming and ocean acidification on calcifying organisms threatens the potential for coral reef structural growth and maintenance, and some reefs are already net dissolving. In response to declines in calcifying corals, reef restoration efforts aim to rebuild coral reefs using a variety of techniques to propagate coral fragments and produce juvenile corals which can be transplanted on the reef. However, differences in the physiological processes of the species used in such programs require further evaluation. To address this research gap, rates of metabolism were measured in individual fragments of important coral reef calcifiers, with significant differences detected between species of coral and between coral and crustose coralline algae (CCA). The organisms selected for this study have distinct functions in terms of reef calcification. *Acropora cervicornis* have rapid-growth rates and an intricate branching morphology, while *Orbicella faveolata* and *Siderastrea Siderea* are slow-growth, massive reef-builders. The abundant and opportunistic *Porites astreoides* are known for their increasing dominance on degraded coral reefs, and crustose coralline algae create a cement-like covering which encrusts and strengthens reef substrate. Ex-situ incubations under natural ambient light demonstrated that individual rates of calcification and photosynthesis are different between species, and shift in response to light over a diurnal cycle. The highest photosynthesis and calcification values were measured at solar noon for all species, followed by a plateau, reflecting a hyperbolic relationship with light. Metabolism-irradiance models demonstrated similar light-response curves in the 2 massive coral species and the opportunistic *P. astreoides*, while branching *A. cervicornis* metabolism was lower and aligned more closely with CCA than the other coral species. Metabolic maxima for photosynthesis (P_{max}) and calcification (G_{max}) were extracted from the models and demonstrated a positive linear relationship between the different organisms, indicating a link between the energy produced by photosynthesis and respiration with calcification across functional groups. The data were interpreted in the context of total carbon metabolism (M_{tot}), and this was proposed as a novel metric for quantifying the balance of inorganic to organic carbon cycling.

A range of methods have been developed to quantify benthic metabolism in the field; from isolation of the benthic community using incubation chambers to autonomous sensor deployments for instantaneous measurements of ecosystem metabolism, each with unique advantages and limitations. In-situ measurements are critical for quantifying metabolism of complex communities, which cannot be reliably

recreated in ex-situ settings. Due to the myriad of environmental influences affecting benthic metabolism in the field, benthic incubation chambers have been used to isolate benthic organisms and the water surrounding them so that any biogeochemical changes in the water column are the result of biological activity within the chamber. Benthic chambers usually consist of transparent enclosures which allow sunlight to penetrate, and often have a submersible pump installed to drive water flow over the study organisms. A sampling port facilitates measurement of dissolved oxygen and carbonate chemistry so that metabolic rates can be tracked. Following a review of the benthic chamber designs currently available, a gap was identified for a chamber that is low-cost, made from easily accessible materials, large enough to incubate a community, and minimally invasive. A simple benthic chamber design was created and trialled to address these design criteria. The benthic chamber performed in line with the other existing chamber designs available, while substantially cutting costs. The chambers were deployed in two case studies to measure productivity of seagrass and coral reef patches. Productivity measurements agreed with previous estimates for both ecosystems tested, and the coral reef patches incubated also showed a hyperbolic relationship with light, aligning with the diurnal trends measured in the ex-situ incubations of individual coral reef calcifiers. The benthic chamber presented here is an affordable and feasible option for field studies of benthic metabolism.

At the broader ecosystem or large community scale, benthic metabolism can be tracked over large bodies of water and over longer time scales. Using flow respirometry and benthic boundary layer approaches, it is possible to measure biogeochemical flux in coastal waters without interrupting natural flow and environmental drivers. In the final experiment of this thesis, multiple methods were used to measure benthic metabolism of a seagrass-sediment dominated bay. The methods selected represent some of the key approaches developed over the last ~70 years. Lagrangian flow, control volume, and benthic ecosystem and acidification measurement systems (BEAMS) approaches were tested over 48 hours, alongside benthic incubation chambers and discrete water sampling. There was strong agreement between Lagrangian, control volume and BEAMS for net community production (NCP) measurements, and integrated rates were aligned with results from chamber incubations. Net community calcification (NCC) was relatively low, and the Lagrangian approach was more sensitive to the NCC signal than BEAMS. The metabolic rates scaled with light conditions following a hyperbolic model, with variations in coefficients and model fits between the data sets collected. Linear regressions between NCC and NCP demonstrated distinct relationships between night

and day, again highlighting the importance of diel cycles in quantifying coastal carbon cycles.

The findings of this thesis enhance the current understanding of the metabolic processes taking place in tropical marine ecosystems and supports future research by providing novel metrics and methods for quantifying benthic metabolism. At each scale, from the organism to the ecosystem, the influence of light was established as a key driver of benthic metabolism. This research has direct impact and application for conservation of coral reefs and seagrasses and will support future endeavours to quantify carbon cycling of coastal ecosystems.

Table of Contents

List of Tables

List of Figures

Acknowledgements

Author's Declaration

The material presented in this thesis is the result of research conducted between October 2017 and March 2022, under the supervision of Dr Adrian Bass (primary) and Dr Thorsten Balke, the University of Glasgow; Prof Anastazia Banaszak, National Autonomous University of Mexico, Dr Dan Exton at Operation Wallacea; and Dr Tyler Cyronak at the Nova Southeastern University. This work is based on individual research carried out by myself, and any published or un-published material not of my own has been fully acknowledged in the text.

Definitions/Abbreviations

AEC	Aquatic eddy covariance
BEAMS	Benthic Ecosystem and Acidification Measurement System
C	Carbon
$CaCO_3$	Calcium carbonate
CCA	Crustose coralline algae
CO_2	Carbon dioxide
DIC	Dissolved inorganic carbon
DO	Dissolved oxygen
G	Calcification
G_{dark}	Dark calcification
G_{net}	Net calcification
LEC	Light enhanced calcification
NCC	Net community calcification
NCP	Net community production
O_2	Oxygen
OA	Ocean acidification
P	Photosynthesis
P_{DIC}	Photosynthesis measured from dissolved inorganic carbon assimilation
P_{DO}	Photosynthesis measured from oxygen production
P_{net}	Net production
R	Respiration
SD	Standard deviation
SST	Sea surface temperature
TA	Total alkalinity

1 Introduction

1.1 Coastal marine carbon

Oceans are the largest active reservoir of carbon on Earth (Millero 2007), and they play a critical role in carbon sequestration, cycling, and storage (Nellemann et al. 2009). Carbon sequestration by marine organisms began some 3.5 million years ago when photosynthesis evolved as a metabolic process in the ocean and contributed to the balance of O_2 and CO_2 in the atmosphere, fundamental to the persistence of life on Earth (Ver et al. 1999). Today, the ocean continues to sequester atmospheric carbon into the oceanic carbon sink where it can be stored for hundreds of thousands of years, regulating climate and maintaining ecosystem functions and services (McKinley et al. 2017). Estimates of the carbon sequestration value of marine productivity were well underway over 100 years ago, with early research focussed on the role of oceanic phytoplankton (Boysen-Jensen 1914). However, the role of marine vegetative systems in sequestering and locking down atmospheric carbon has since become the focus of research into biological carbon sequestration into the ocean sink (Duarte et al. 2013a; Macreadie et al. 2019; Serrano et al. 2019).

The coastal ocean is the interface between open ocean and terrestrial ecosystems and plays a disproportionate role in biogeochemical cycling despite taking up just 8% of the world's ocean area (Smith and Hollibaugh 1993; Hyndes et al. 2014; Silbiger and Sorte 2018). In 2009, the concept of 'blue carbon' was introduced to describe the exceptional capacity of some marine ecosystems to capture and store carbon compared to land-based ecosystems (Nellemann et al. 2009). Around 55% of the ocean's carbon budget is sequestered in the coastal zone, where highly productive ecosystems draw down carbon before it is transferred to long-term sediments or adjacent coastal biomes (Sabine et al. 2004; Nellemann et al. 2009). The high rates of carbon sequestration and storage in the coastal ocean are due to photosynthetic activity of marine macrophytes, which thrive in shallow, oligotrophic waters where sunlight penetrates to the seafloor, driving high rates of productivity. In contrast to highly productive terrestrial ecosystems, carbon is cycled within the coastal ocean, stored in sediments and / or exported to the deeper open ocean carbon sink (Mackenzie et al. 2005; Howard et al. 2014). The coastal ocean is considered a major component of the global carbon cycle, which has increased in carbon sink capacity

since the onset of anthropogenic increases in CO_2 (Bauer et al. 2013) . However, global climate change threatens the longevity of coastal marine ecosystems (He and Silliman 2019; Barnard et al. 2021). Therefore, it is critical to investigate and define carbon fluxes within and between ecosystems of the coastal ocean in order to predict future trajectories.

Despite accounting for only 0.1% of the coastal zone, seagrass meadows play an important role in coastal biogeochemical cycling and are highly valued as blue carbon ecosystems (Greiner et al. 2013; Duarte et al. 2013c; Costanza et al. 2014). Seagrass meadows have some of the highest rates of productivity of all biomes (Hemminga and Duarte 2000; Larkum et al. 2006; Duarte et al. 2010). They are considered a critical ecosystem for climate change mitigation (Macreadie et al. 2014; Trevathan-Tackett et al. 2015; Howard et al. 2017; Serrano et al. 2019), and seagrass restoration is being explored as a potential tool for drawing down anthropogenic CO_2 (Greiner et al. 2013; Duarte et al. 2013c; Macreadie et al. 2021). The carbon captured by seagrass photosynthesis is stored in underground biomass (López-Mendoza et al. 2020) and long-term marine sediments, which are around 40 times more efficient at organic carbon storage than the soils of terrestrial forests (Nellemann et al. 2009). There is variability in their carbon storage capacity, with distinct quantities and sources of organic carbon found stored in sediments across a single seagrass ecosystem (Ricart et al. 2020). Seagrasses occur on all continents in the shallow coastal ocean, up to depths of 50 metres, where transparent waters facilitate photosynthesis (Hemminga and Duarte 2000). The canopy of the seagrass meadow traps particulate matter from the water column by attenuating currents and filtering sea water, contributing to build up of sediments which are then retained in the meadow bed by their underground root-like network of rhizomes (Hendriks et al. 2008; Duarte et al. 2013b). Around half of the carbon which accumulates in seagrass sediments originates from non-seagrass sources (Kennedy et al. 2010; Oreska et al. 2018), likely imported from adjacent habitats (Duarte and Cebrián 1996). The most productive seagrass meadows are multispecies, and productivity of seagrass meadows is enhanced by autotrophic epiphytes, which can account for 20 – 60% of seagrass productivity (Hemminga and Duarte 2000). It is estimated that seagrasses account for around 1% of global net marine primary production (Duarte and Chiscano 1999) and 10% of annual organic carbon burial in the world's oceans (Fourqurean et al. 2012).

While the role of seagrasses in coastal carbon capture and storage is well-established, the carbon value of coral reef ecosystems has been contested since the 1990s (Frankignoulle et al. 1994; Gattuso et al. 1999b), with ongoing research to constrain coral reef carbon and carbonate budgets in the face of a changing climate (e.g., Naumann et al. 2012; Alldredge et al. 2013; Jones et al. 2015; Albright et al. 2015; Takeshita et al. 2018; Enochs et al. 2019; Stoltenberg et al. 2019; Molina-Hernández et al. 2020). Coral reefs host high rates of organic carbon production, supporting their ability to build inorganic calcium carbonate structures through biogenic calcification (Gattuso et al. 1999a). However, the process of calcification by corals and other important benthic organisms, such as calcifying and crustose coralline algae, release carbon at a rate higher than it sequesters (Ware et al. 1991; Gattuso et al. 1999b). In calcification, for each mole of $CaCO_3$ precipitated, 0.6 moles of CO_2 are released, whereas for photosynthesis, the production of 1 mole of organic carbon (CH_2O) results in fixation of 1 mole of CO_2. Respiration also releases CO_2; therefore, a calcifying reef has a net flux of CO_2 to the atmosphere (Frankignoulle et al. 1994). The potential for coral reefs as long-term carbon burial systems is considered insignificant in the overall marine carbon budget (Gattuso et al. 1996; Watanabe and Nakamura 2019). Therefore, coral reefs are not considered in blue carbon budgeting and generally act as a source of carbon to the atmosphere, rather than a sink (Frankignoulle et al. 1994; Gattuso et al. 1999b; Gattuso and Buddemeier 2000).

Despite the relatively low level of carbon lockdown of typical coral reefs, their position in the interconnected coastal biome means that understanding and quantifying carbon transfer within these ecosystems is critical for predicting and mitigating climate change. Coral reefs have a critical role in protecting blue carbon-rich ecosystems such as seagrasses and sediments from erosion by the open ocean, and the biodiversity they contain supports ocean-wide carbon cycling and trophic energy networks. As global climate change threatens the persistence of corals and coral reef ecosystems, it is likely that their role in coastal carbon budgets will change. As the irreversible degradation of coral reefs is well underway (Bellwood et al. 2004; Hughes et al. 2017b; Reverter et al. 2021), it is critical that the longstanding questions regarding their carbon cycling capabilities, and the biological processes driven this, be addressed.

1.2 Ecological function and services of coral reefs and seagrasses

Coastal areas are around three times more densely populated than inland regions, and human populations in these areas are growing exponentially (UNEP 2006). These communities depend directly on the ecosystem services provided by marine and coastal ecosystems (Lau et al. 2019). Coral reefs, seagrasses, and mangroves strengthen coastlines against erosion and promote sediment production and retention (Christianen et al. 2013; Harris et al. 2018; Brown et al. 2020). They have a critical role as a physical barrier to the open ocean, protecting shores from storms and wave action. Tropical coastal ecosystems comprise biodiversity hotspots, provide unique habitat, and support livelihoods (Costanza et al. 1997; Moberg and Rönnbäck 2003). Coastal seascapes also drive local economies through touristic activities such as diving and snorkelling (Spalding et al. 2017). However, their true value in terms of ecosystems services, function and cultural wealth cannot be fully constrained by economics alone (Lau et al. 2019). In the tropical coastal zone, coral reefs and seagrasses are interconnected and interdependent (Guannel et al. 2016). The ecological processes taking place within these systems transcend habitat boundaries, to support healthy ecosystem function (Harborne et al. 2006). The unique habitat found in shallow coastal waters supports fisheries, critical for protein provision and livelihoods in the regions where coral reefs and seagrasses occur (Mehvar et al. 2018). Coastal communities depend upon small-scale local fisheries as a primary source of protein, at an estimated value of USD 6 million (Burke et al. 2011). Indigenous communities in coastal regions around the world have a higher dependence on seafood, and fewer alternatives (Woodhead et al. 2019).

Seagrasses are marine flowering plants which appear on shorelines around the world to form extensive meadows which provide a range of ecological functions and services. Seagrass organic material has been used for construction and agriculture for hundreds of years (Nordlund et al. 2018). Seagrass meadows are some of the most valuable blue carbon systems in existence. Their underground network of rhizomes protects and retains carbon-rich sediments (Duarte et al. 2013a). Seagrasses filter coastal waters, ensuring high light transmission (Short and Short 1984), and there is evidence that they buffer ocean acidification as their CO_2 uptake through high rates of primary production influence pCO_2

and pH of sea water (Hendriks et al. 2014; Kapsenberg and Cyronak 2019; Ricart et al. 2021) supporting healthy coral growth (Jury et al. 2013; Takeshita 2017). In turn, the structure formed by adult coral skeletons provides shelter and protection for seagrass meadows, demonstrating the positive feedback between these systems (Harris et al. 2018; Du et al. 2020). The small-scale buffering capacity of seagrass meadows has been identified as a potential management tool for coastal waters undergoing ocean acidification (OA) (Manzello et al. 2012). This could potentially mitigate the impact of OA for adjacent reefs (Cyronak et al. 2018; Ricart et al. 2021). However, the buffering potential of seagrasses are varied depending upon local hydrodynamics and environmental influences (Koweek et al. 2018; Dam et al. 2021). Seagrasses also show bioremediation qualities, and there is evidence to suggest that seagrass meadows may ameliorate seawater pollution from human-originated bacteria, protecting marine invertebrates and fish from potential pathogens (Lamb et al. 2017). Seagrass canopies attenuate wave action, support sediment generation, and mitigate coastal erosion (Fonseca and Fisher 1986; Enríquez et al. 2001; Christianen et al. 2013). Seagrass meadows also provide nursery habitat for fisheries, such as the ecologically important herbivorous parrotfish, which can undergo ontogenetic or diurnal migration across coral reef, seagrass, and mangrove root habitats (Nagelkerken et al. 2002; Mumby et al. 2004; Dorenbosch et al. 2005). Grazing by herbivores is a critically important process in the coastal ocean for sediment generation and maintaining healthy ecosystems and energy flow (Bainbridge et al. 2018; Brown et al. 2020). On coral reefs, herbivores are a fundamental component of nutrient and organic carbon cycling within the trophic system, and they maintain the reef substrate clean of algae for larval settlement and coral growth (Edmunds and Carpenter 2001; Idjadi et al. 2010).

Coral reefs host one of the most biodiverse communities on Earth, a capacity that has been the subject of scientific debate since 'the Darwin Paradox' 200 years ago, which highlighted the contradiction of a highly productive ecosystem in oligotrophic waters (Gove et al. 2016). Early research demonstrated that the success of coral reefs is largely due to high rates of light-dependant primary productivity and the ability of the benthic community to cycle nutrients within the ecosystem (e.g., Odum 1956, 1957). Reef-building corals are powered in part by symbiosis with zooxanthellae, dinoflagellates which provide carbon fixed by photosynthesis to the coral host to fuel calcification (Goreau and Goreau 1959; Roth 2014). The endosymbionts benefit from nutrients and protection provided by

the coral polyp, as well as ideal, sunlit habitat to facilitate photosynthesis (Roth 2014). This relationship maintains the metabolic needs of both the host and symbiont and supports coral reef success in oligotrophic waters. Only since the second half of the 20th century have technologies advanced enough to facilitate scientific field research on coral reefs (Moore et al. 2009), and access to reefs deeper than a few metres has only become widely available since the onset of recreational SCUBA diving in the 1950s (Lang 2012). Subsequent decades of research have explored the key processes driving coral reef ecological function, however, the urgent threat of climate change and the degradation already observed on the world's coral reefs (Woodhead et al. 2019; Eddy et al. 2021) has shifted research perspectives towards conservation and rapid intervention to protect the critical ecosystem services and survival of coral reefs (van Oppen et al. 2017; Bayraktarov et al. 2020).

Since the range of services derived from coral reefs are vast, they can be divided into subcategories such as those that; support other services, regulate the environment, provide natural goods, and offer cultural benefits (Woodhead et al. 2019). Coral reef habitat provision and subsequent biodiversity support all other ecological services derived from seagrass and coral reefs. The complex architecture of the coral reef provides habitat for diverse organisms, and up to a third of all marine organisms spend at least part of their life history on the coral reef (Knowlton et al. 2010; Brandl et al. 2019). Coral reefs regulate their environment through calcification (G), the process by which they grow calcium carbonate ($CaCO_3$) skeletons. Over millennia, the ($CaCO_3$) skeletons deposited by reef calcifiers physically protects, builds, and maintains coastlines, (Perry and Alvarez-Filip 2018) and plays a critical role in biogeochemical cycling of the coastal ocean (Chave et al. 1972; Gattuso et al. 1999a). Scleractinian corals, the ecological engineers of coral reefs, form a complex structure for countless functional groups and species to inhabit (Richardson et al. 2017). Coral polyps typically measure just a few millimetres in size, however, the skeletal structures produced by coral colonies create entire reef systems, large enough to be seen from space. The coral reef structural matrix forms over geological timescales and is strong enough to shield coastlines from storm and wave energy. A meta-analysis of studies covering Atlantic, Pacific, and Indian Oceans found that coral reefs absorb 97% of wave energy (Ferrario et al. 2014), providing a natural barrier for coastal communities. In the US, hazard risk reduction exceeds US$1.8 billion annually (Reguero

et al. 2021). Coastal defence by coral reefs also benefits other habitats such as seagrass meadows, and reduces erosion of sediments, thus protecting critical blue carbon stocks (Ferrario et al. 2014; Storlazzi et al. 2021).

1.3 Anthropogenic influences on coral reefs and seagrasses

Since the industrial evolution ~ 200 years ago, the concentration of CO_2 in the atmosphere has increased by over 40% to reach 410 µatm, a rate which is unprecedented in the past several million years (Gingerich 2019). Under a scenario of 'controlled warming' (representative concentration pathway, RCP 2.6) this is expected to reach 490 µatm or rise to 1370 µatm under a 'business as normal' scenario (RCP 8.5) (van Vuuren et al. 2011). The high atmospheric concentrations of CO_2 and other greenhouse gases are causing catastrophic changes to Earth's climate systems including warming, shifts in ocean currents, increased storm frequency and severity, and weather extremes such as prolonged and frequent drought (IPCC 2013). Global warming has increased the surface temperature of Earth by 1 °C in the past century, and it is likely that the 1.7 °C tipping point will be exceeded by 2100 with projected loss of key ecosystems and species as a result (He and Silliman 2019; Doney et al. 2020; Barnard et al. 2021).

Over the past 50 years, the ocean has absorbed over 90% of the global warming induced heat (Flato et al. 2013), associated with a rapid rise in sea surface temperature (SST). Coastal environments are disproportionately impacted by anthropogenic activity compared to the open ocean (Ver et al. 1999), and they are undergoing increasing pressured from human activities. Increasing SST is a major threat for coral reefs and seagrasses, where organisms living in these environments have adapted to exist at the thermal limit and are sensitive to change (Rodolfo-Metalpa et al. 2014; Camp et al. 2017). Coral bleaching occurs when sea water temperatures increase by 1 °C for at least 1 month, when corals pass the temperature 'tipping point' (Goreau and Hayes 2021). The unprecedented mass bleaching event in the 1980s was the first direct ecosystem crisis caused directly by climate change (Goreau and Hayes 2021), an occurrence which is now a near-annual event (Hughes et al. 2017a; Ainsworth and Brown 2021).

With the unprecedented rapid increase in atmospheric CO_2 due to fossil fuel carbon emissions, the ocean has absorbed around 41% of anthropogenic carbon (Sabine et al. 2004; Quéré et al. 2018), resulting in a 0.1 unit decrease in ocean pH, which is expected to decline by a further 0.3 – 0.4 pH by 2100 (Caldeira and Wickett 2003). Ocean acidification (OA) threatens the existence of coral reefs, as it increases dissolution of $CaCO_3$ structures, while at the same time impeding calcification. CO_2 absorbed into the ocean reacts with seawater, causing a decrease in the availability of carbonate ions (CO_3^{2-}) and reducing the saturation state of $CaCO_3$ minerals (Ω). OA has caused a 40% increase in ocean acidification and a reduction of carbonate ion concentrations by 11% in the ~200 years (Orr et al. 2005) (Fig. 1-1).
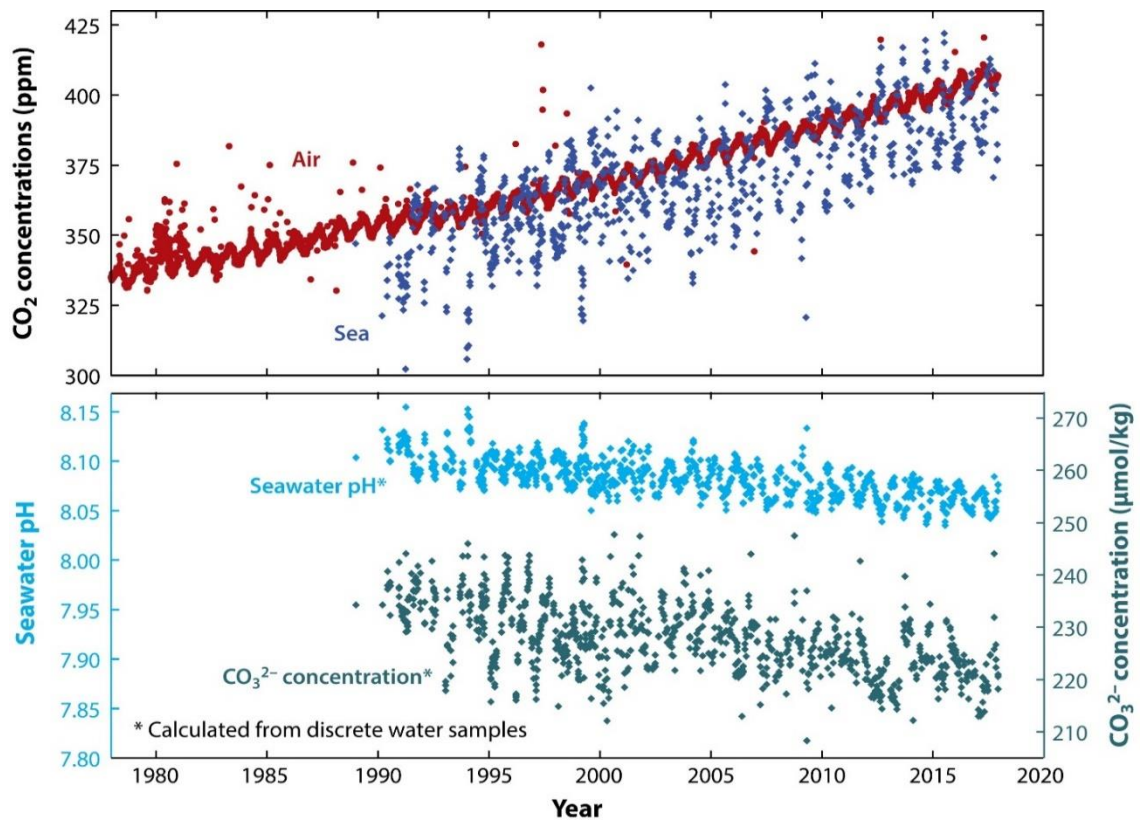
Figure 1-1: (top) Increasing CO_2 concentrations in the atmosphere, and (bottom) high CO2 influence on ocean sea water pH and carbonate concentration (μmol kg^{-1}). Figure from Doney et al. (2020).

Ocean deoxygenation has emerged as an additional major threat to the future of coral reefs (Altieri 2017; Johnson et al. 2021), and incidence of hypoxic events are accelerating (Earle et al. 2018; IUCN 2019). Deoxygenation is caused primarily by global climate change and eutrophication (Altieri and Gedan 2015; IUCN 2019). In tropical regions, warmer water temperatures have a reduced capacity to retain dissolved oxygen (DO), and high rates of aerobic metabolism deplete DO. Nutrient loading in sunny, warm coastal waters leads to rapid proliferation of algae in the water column. Through respiration, algae and microbes consume DO in the water column, which is further compounded by mortality of photosynthetic plants when light is blocked by algae in the water column. In the case of scleractinian corals, the impacts can be disastrous, resulting in mass mortality within days of exposure to low DO conditions (Johnson et al. 2021b). Deoxygenation in coastal waters is typically defined as a reduction in oxygen concentration to $< 2\text{mg L}^{-1}$, however some species are sensitive to more subtle changes in ocean oxygen concentration (Altieri et al. 2021). It is not uncommon for coral reef organisms to experience low oxygen conditions, as natural diel cycling of oxygen in the water column over coral reefs controlled by photosynthesis and respiration of benthic organisms can lead to low oxygen concentration conditions at night (Nelson and Altieri 2019). However, multi-day, extreme hypoxic events have been found to deplete the coral reef of oxygen and cause severe mass mortality of corals (Johnson et al. 2021a). The frequency, long term impacts, and recovery following short-term hypoxic events on coral reefs are relatively unknown, as the events generally last just a few days and reporting is scarce.

1.4 The decline of Caribbean coral reefs

Catastrophic losses of hard coral cover have been reported at sites across the Caribbean since the 1970's (Jackson et al. 2014; Estrada-Saldívar et al. 2019). In this region, global climate change exacerbates localised pressures on coral reefs caused by rapid coastal development in the area. Increasing construction and infrastructure development over recent decades are causing 'coastal squeeze' and loss of intertidal habitat (Unsworth et al. 2018). On Caribbean coral reefs, unprecedented changes to species composition and abundance are associated with local overdevelopment, disease, and pollution in addition to the global threats associated with climate change (Done 1992;

Williams and Graham 2019). Overfishing has also caused major degradation to the biodiversity of coral reefs and seagrass meadows (Hughes et al. 2003; Jackson et al. 2014). Since 2014, the compounding impact of Stony Coral Tissue Loss Disease has exacerbated this decline, causing near ecosystem collapse and extinction of some coral species (Estrada-Saldívar et al. 2019). As a result of these factors, the valuable coastal protection and habitat provision provided by these ecosystems is already reduced (Perry and Alvarez-Filip 2018).

With the functional extinction of scleractinian coral species fast becoming a reality in in the Caribbean region, loss of the structural complexity at the basis of all ecosystem services derived from coral reefs is a major risk. On the Florida Reef Tract (FRT), coral reef structure is being lost at a rate faster than it can be renewed (Eyre et al. 2018). As healthy corals are lost from coral reefs, proliferation of algae, soft corals, and resilient, weedier species of corals have overtaken the reef (Hughes et al. 2007; Williams et al. 2017). Eutrophication, algal overgrowth, and influx of invasive species, disrupt and impede ecosystem function (Kubicek et al. 2019). Overfishing of key herbivore species is linked to algal overgrowth and collapse of reef function in some areas of the Caribbean. In the 1980s, a marine pathogen decimated the populations of *Diadema antillarum*, the Caribbean black spined sea urchin (Lessios et al. 1984), which had previously maintained algal growth on coral reefs (Edmunds and Carpenter 2001; Idjadi et al. 2010). The lack of recovery in this population on Caribbean reefs is largely due to a lack of cryptic substrate where *Diadema* can be protected from predation (Bodmer et al. 2015, 2021). The lack of algae-free substrate on Caribbean coral reefs negatively impacts coral larval settlement, hindering the natural recovery of both the corals providing structural complexity, and the herbivores needed to maintain it (Lessios 2016) . Successful coral reproduction and recruitment of coral larvae is further hindered by ocean acidification (Albright et al. 2010; Doropoulos et al. 2012), disease (Piñón-González and Banaszak 2018), and changes to overall reef condition (Rinkevich and Loya 1985). The rapid decline of coral reef health and function in the Caribbean is useful as a model for understanding ecological and physiological response to multiple stressors, to predict and manage change in other regions (e.g., Crabbe et al. 2008; Blackwood et al. 2018). The study of Caribbean coral reefs has been integral in defining the sequential stages of degradation and has been possible to build a solid knowledge base documenting how environmental stressors and anthropogenic

influence can shift dynamics on coral reefs, disrupting ecological stable states through altering the benthic community, introducing invasive species, and ultimately changing the biogeochemistry and functional capacity of the coral reef ecosystem.

1.5 Reef restoration

The functional capacity of coastal ecosystems raises critical research questions for policy makers as governments around the world aim to transition to a sustainable blue economy (Brears 2021). The United Nations sustainable development goals recognise the health of the oceans as a priority, and the UN declaration of the 'decade of ecosystem restoration' indicates a shift in conservation practices from passive preservation toward active intervention (Waltham et al. 2020). To conserve the calcification potential of coral reefs, propagation and transplantation of scleractinian coral aims to restore natural rates of reef growth, with the ultimate goal of securing the ecosystem services that healthy coral reefs provide (Hein et al. 2017). Reef restoration is an active form of conservation intervention designed to support passive preservation efforts, such as the legal protection of endangered coral species and reef sites. Methods of reef restoration largely focus on the robust, reef-building Acropora genus of corals which are propagated in land and field nurseries and transplanted onto natural reefs (Lirman 2000; Young et al. 2012). This technique utilises the ability of fast-growing branching corals to asexually fragment and regenerate (Lirman 2000). Despite recent advances in the methods and technology to deploy such programs, the long-term outcomes are virtually unknown (Hein et al. 2017; Boström-Einarsson et al. 2020; Ferse et al. 2021). Tracking of restored populations is not standard practice and over half of restoration programs collect data on their restored coral populations for 1 year or less (Boström-Einarsson et al. 2020). Monitoring of coral reef restoration outcomes is essential for evaluating the impact of such efforts and for improving conservation strategy. However, traditional manual surveys conducted by SCUBA divers and snorkellers to measure the size of individual corals and estimate live coral cover of reef patches are labour intensive and costly. Reef restoration aims to re-establish ecological function, yet metrics of individual coral transplant survival do not capture this (Hein et al. 2020). Efficient and accurate methods are required to overcome the challenges of tracking changes to the fundamental processes driving ecosystem

function and carbon cycling in the coastal ocean. The biogeochemical approach offers a powerful tool to quantify these processes.

1.6 Benthic community metabolism

Seawater chemistry is influenced by a range of chemical, environmental, and physical forces within the coastal ocean. At the same time, biological activity drives daily and seasonal changes in seawater composition (e.g., Yates and Halley 2003; Koweek et al. 2015; Albright et al. 2015). Benthic metabolism refers to the balance of the fundamental biogeochemical processes taking place within the benthic community: calcification, $CaCO_3$ dissolution, photosynthesis, and respiration (Fig. 1-2). This balance of physiological processes controls the seawater chemistry and carbon cycling of tropical, coastal waters, as summarised in equations 1 and 2.

Eq. 1

$$CO_2 + H_2O \leftrightarrow CH_2O + O_2$$
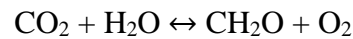
Photosynthesis $\leftrightarrow$ Respiration

Eq. 2

$$Ca^{2+} + CO_3^2 \leftrightarrow CaCO_3$$
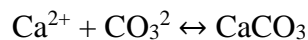
Calcification $\leftrightarrow$ Dissolution

As primary producers draw down carbon, they release O_2 through photosynthesis, and respiration reverses this process (Nelson and Altieri 2019). Therefore, it is possible to measure photosynthesis (P) from increases in dissolved oxygen (DO) and decreases in dissolved inorganic carbon (DIC). Conversely, decreasing DO or increasing DIC indicates net respiration (R). The overall balance of P to R within the ecosystem is known as net community production (NCP) and describes cycling of organic carbon within a benthic community (Fig. 1-2). Inorganic carbon cycling of benthic communities is defined as calcification (G) offset by dissolution (D), or net community calcification (NCC).

Inorganic carbon precipitation can be quantified using the total alkalinity anomaly technique (Smith and Kinsey 1976; Kinsey 1978; Chisholm and Gattuso 1991), to measure the change in total alkalinity (TA) of sea water. For each mole of $CaCO_3$ precipitated through calcification, 0.6 moles of CO_2 are released, corresponding with a reduction in seawater TA of 2 molar equivalents, and the reverse is true for carbonate dissolution. CO_2 is released at a lower rate than $CaCO_3$ is precipitated because of the buffering capacity of sea water, which is stable in standard pCO$_2$ (partial pressure of CO_2) of 350 µatm, salinity of 35 ppt, and temperature of 25 °C (Frankignoulle et al. 1994). However, the rate by which CO_2 is released by calcification changes under different seawater carbonate chemistry conditions. For example, in seawater with higher pCO$_2$ or lower total alkalinity, the amount of CO_2 release by calcification is higher. These processes also drive changes in sea water pH, which increases with net photosynthesis and dissolution, and decreases with net respiration and calcification. When NCC and NCP are equal (i.e., when changes in TA and DIC are close to 1) sea water pH remains stable (Cyronak et al. 2018). In warmer waters, the buffering capacity of sea water is also reduced. It is clear that the combined impacts of ocean warming, and ocean acidification will impact the biological carbon sequestration and cycling capacity of coral reefs and other calcifying ecosystems (Kleypas and Yates 2009; Veron 2011; Nakamura et al. 2017).

Biogeochemical measurements of community metabolism capture individual metabolic rates of functional groups and species, as well as the interactive physiological processes taking place within the benthic community, offering insight into relative composition of different functional groups and overall ecosystem function (Albright et al. 2015; Cyronak et al. 2018). These measurements are applicable across multidimensional scales from organisms to ecosystems, to quantify subtle, high-resolution changes in photosynthesis-respiration and calcification-dissolution over hours or days (e.g., Gattuso et al. 1999; Allemand et al. 2011; Smith et al. 2013; Page et al. 2017). Productivity measurements have been widely used for quantifying the carbon sequestration potential of seagrasses and other coastal ecosystems (e.g., Sargent and Austin 1949; McGillis et al. 2011; Long et al. 2015) and are particularly useful where growth measurements of benthic organisms do not always scale up to ecosystem-level processes. For example, metabolic rates measured from artificially constructed communities in ex-situ mesocosms to represent natural coral reefs benthos can provide some insight, but these experiments cannot account for the myriad of

environmental and biological influences driving metabolism in the natural (Page et al. 2017). Table 1-1 shows some of the common measurements of photosynthesis and calcification.

Table 1-1: Some of the different measurements of production and calcification measured from benthic communities and ecosystems.

	Abbreviation	Definition
Production	R_{DO}	dark oxygen flux
	R_{DIC}	-1(dark DIC flux – dark TA flux / 2)
	P_{DO}	light oxygen flux
	P_{DIC}	-1(light DIC flux- light TA flux / 2)
	P_{gross}	P_{DIC} - R_{DIC} or P_{DO} - R_{DO}
Calcification	G_{net}	-1(light TA flux / - 2)
	G_{dark}	-1(dark TA flux / - 2)
	G_{gross}	G_{net} - G_{dark}

1.7 Environmental drivers of benthic metabolism

At the ecosystem scale, the balance of net community calcification (NCC) to net community production (NCP) has been proposed as a metric for reef functional health (Cyronak et al. 2018). The ratio of NCP to NCC of an ecosystem reflects its carbon sink-source status, its capacity to alter sea water pH, and the composition of benthic communities (Gattuso et al. 1999a; Kleypas et al. 2011; Albright et al. 2015). This can be visualised using graphical vector analysis, or TA-DIC slopes, to quantify metabolic status of the benthos, and can provide inside into the composition and relative proportion of calcifying / photosynthesising functional groups (Albright et al. 2015; Cyronak et al. 2018). As these processes are heavily influenced by environmental conditions such as light, temperature and flow, development of methods and equipment for field-based measurements are essential for accurate and robust data collection. Field measurements of ecosystem metabolism using the biogeochemical approach offer insight into overall ecosystem function and can be used to determine diurnal and seasonal trends and to

recognise shifts over different temporal scales (Kinsey and Kinsey 1967; Jokiel et al. 2014). It is possible to link rates of NCC and NCP to the dominant functional groups of the benthos, and in this way, we can detect changes due to stressors and / or changes in benthic composition. In the case of coral reefs, the potential to quantify relative proportions of autotrophs and calcifying organisms from sea water samples offers a powerful and efficient tool for rapid assessment of reef functional health and can help identify reefs undergoing phase shift to algal dominance (Cyronak et al. 2018). These measurements can support research on reefs in geographically isolated areas or where limitations on manual sampling and surveys may impede more traditional methods.
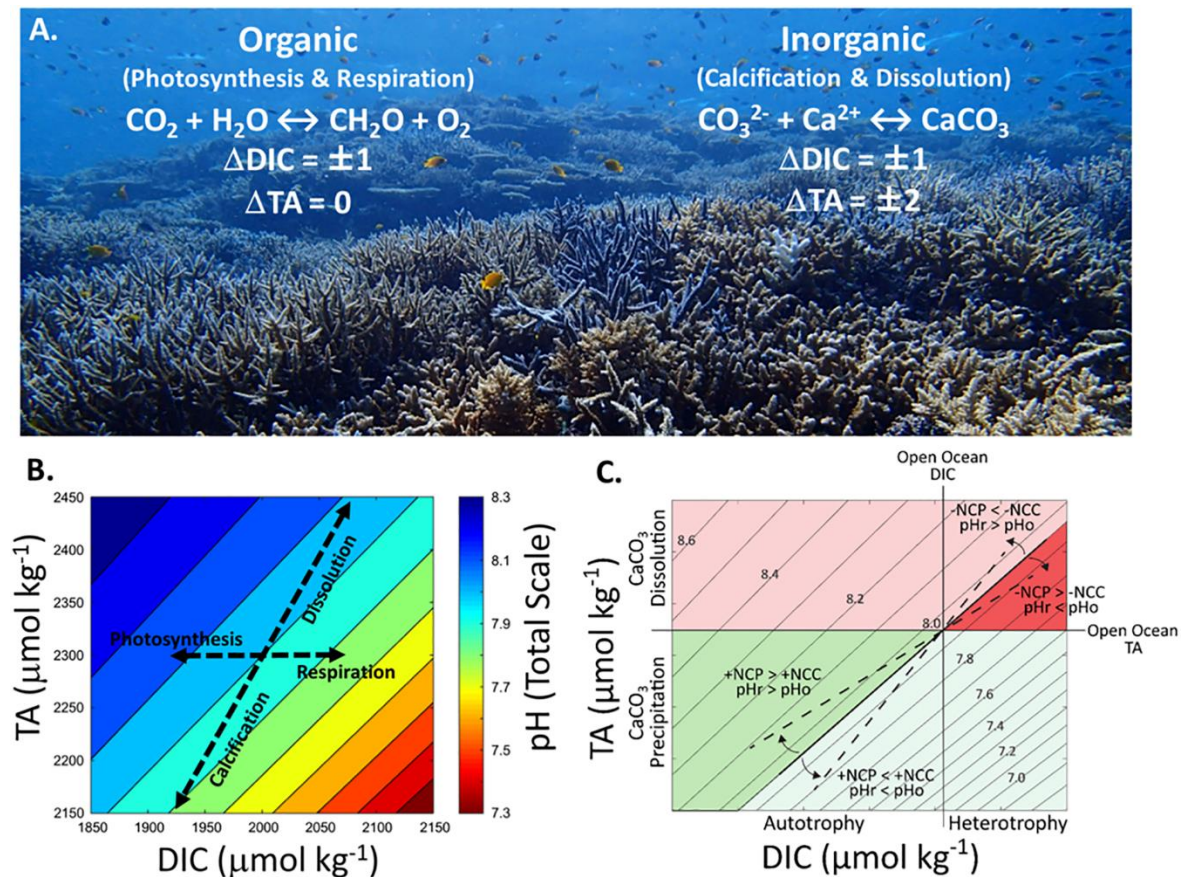
Figure 1-2: The dominant metabolic processes on coral reefs and their influence on seawater total alkalinity (TA), dissolved inorganic carbon (DIC), and pH. Figure from Cyronak et al. 2018.

1.8 Overview of methods for measuring benthic metabolism

Benthic O_2 fluxes have been used as a reliable measurement of productivity for decades. Early measurements of productivity tracked the trajectory of water flow across an ecosystem and measured changes in water chemistry as it passed over the benthos (Odum 1956; Kinsey and Kinsey 1967; Marsh and Smith 1978). This was originally done by watching a float traverse the ecosystem and taking samples at the start and end point, before floating sensor packages were used to travel with the body of water and log ΔDO across the transect (Kinsey and Kinsey 1967; Marsh and Smith 1978; Barnes and Devereux 1984). While these methods gave novel insight into the productivity of coastal ecosystems, primarily over coral reefs, they were limited in scope as they could only provide short-term rates of change (Kinsey 1983). These techniques were laborious and were often too difficult to conduct in the dark as visual tracking of the water flow was needed. Emerging technologies in autonomous sensing have broadened the application of biogeochemical measurements of community metabolism over larger areas and over timescales of minutes to months (Bushinsky et al. 2019). The aquatic eddy covariance (AEC) technique is advantageous because of its high temporal resolution (Berg et al. 2003; Attard et al. 2019; Berger et al. 2020). AEC uses the benthic boundary layer theory, which has been successfully applied to measure energy fluxes in physical oceanography studies, and more recently used to describe biogeochemical fluxes in coastal ecosystems. The AEC approach can be adapted to distinct benthos and ecosystems and is particularly useful for highly complex, variable systems (Attard et al. 2019).

Measuring calcification across ecosystem scales has its own set of logistical challenges. Biogenic calcification can be measured by quantifying the amount of $CaCO_3$ accreted, either using the buoyant weight technique for individual organisms, or by measuring skeletal growth in the field (Jokiel et al. 1978; Lewis et al. 2017; Lange et al. 2020). However, due to the slow timeframe over which organisms calcify, such changes take weeks to years to be detectable. Measurements of accretion give an integrated estimate of calcification over light and dark cycles; however, it is not possible to tease out shorter term fluctuations. Therefore, measuring instantaneous rates of calcification using the TA anomaly technique facilitates short term quantification of calcification rates in

response to light, diurnal cycles, or seasonal trends. In-situ measurements of calcification using the TA anomaly have been limited by a lack of technology to measure TA in the field. Most studies looking at NCC rely upon discrete water samples collected at start-end points of water trajectories. However, it is possible to estimate a TA gradient from simultaneous measurements of pH and DO (Barnes 1983), and recent advances in the sensors to measure these two parameters support this methodology for measuring in-situ calcification (Takeshita et al. 2016; McMahon et al. 2018; Platz et al. 2020). One such approach is the Benthic Ecosystem and Acidification Measurement System (BEAMS), which was developed to automate ecosystem metabolism measurements and facilitate long-term, high-resolution changes to calcification, photosynthesis, and respiration by benthic communities (Takeshita et al. 2016). BEAMS has been used to track changes to calcification after coral restoration (Platz et al. 2020), however this is the only study of its kind and biogeochemical analyses are not yet widely used for conservation purposes.

The community metabolism of coral reefs requires further research because of high variation between reef sites (Page et al., 2017), methodological discrepancies (Watanabe and Nakamura 2019), and lack of long-term monitoring of biogeochemical parameters (Yeakel et al. 2015). There is a need for studies which incorporate the relevant biomass of key functional groups of algae and coral and comparable methods (Watanabe and Nakamura 2019). In coastal ecosystems, daily fluctuations in pH and temperature occur on the same scale as long-term changes due to climate change. These daily fluctuations or 'ocean weather' have the potential to mask or confound measurements of seawater parameters when 24-hour variability is not considered (Cyronak et al. 2020), therefore longer term and higher resolution measurements are needed. Incubation methods overcome these fluctuations to some degree; by isolating organisms and the body of water surrounding them for a short time it is possible to measure changes to sea water chemistry controlled by the metabolic processes of the enclosed organisms. The primary method for such measurements is the benthic chamber, which isolates small areas of substrate of a given ecosystem to quantify changes in concentration of DO and other parameters. The incubation method has been widely used for decades to measure in-situ metabolism corals and seagrasses (e.g., Yates and Halley 2003; Olivé et al. 2016; Roth et al. 2019).

At the level of the individual organism, ex-situ incubations have been conducted to measure rates of productivity and calcification for a range of organisms at a much finer

resolution. These measurements have been scaled up using survey data of benthic compositions to define the carbon budget of ecosystems (Perry et al. 2012; Lange et al. 2020). Such measurements for individual organisms are conducted using the same seawater chemistry-based techniques in small, ex-situ incubation chambers. These methods provide insight into species-specific differences in metabolic rates, which can be used to assess organism health and to detect stress responses. Ex-situ incubations facilitate control of the parameters, which might drive or influence metabolic rates. For example, many studies have used controlled conditions to quantify the impact of light on coral metabolism (e.g., Sorek and Levy 2012; Iluz and Dubinsky 2015; Cohen et al. 2016)

1.9 Coral physiology and the link between calcification and photosynthesis

Scleractinian corals meet their nutritional needs through both heterotrophic and autotrophic processes. They have evolved a symbiosis with photosynthetic micro-algae, zooxanthellae, that have supported them to thrive in oligotrophic waters where nutrients are scarce. Many coral species derive a substantial portion of the energy required for calcification from photosynthetic by-products provided by endosymbionts (Hoogenboom et al.; Goreau et al. 1971; Brodersen et al. 2014). In some cases, photosynthesis provides 95% of a coral's metabolic energy (Muscatine 1973; Muscatine 1990). Calcification by scleractinian corals is one of the most important physiological processes to support the structural integrity and function of the coral reef and is therefore widely studied. However, the biological mechanisms by which corals form their $CaCO_3$ skeletons are not well-understood, and questions remain about the drivers of coral calcification.

Over 60 years ago, zooxanthellate corals were first observed to increase calcification rates with light (Goreau 1959). This phenomenon has since been widely observed and the term 'Light Enhanced Calcification' was developed. The discovery of LEC in zooxanthellate corals supported the hypothesis that photosynthesis is a driver of calcification in scleractinian corals (reviewed in Gattuso et al. 1999a; Cohen et al. 2016). It was proposed that LEC occurred due to photosynthetic removal of CO_2 (Goreau 1959), directly increasing pH around the site of calcification by removing aqueous CO_2. The link

between calcification and photosynthesis was further supported by a reduction in LEC in bleached corals (Goreau and Goreau 1959; Colombo-Pallotta et al. 2010). Biological controls of coral biomineralization are linked to the autoregulation of pH in the extracellular calcifying fluid (ECM). Higher pH in the ECM than in surrounding seawater leads to increased availability of CO_2 and therefore aragonite saturation. However, more recent work has demonstrated that the coral skeleton is entirely separated from seawater (Sun et al. 2020). Sun et al (2020) propose that the corals directly control the concentration of calcium and carbonate ions at the skeletal calcification site. Further research is needed to support a full understanding of the processes driving calcification and its relation to photosynthesis.

As the marine environment is undergoing dramatic change, it is critical to consider the physiology of corals under environmental stress. Ocean acidification influences the availability of aragonite, the primary mineral form of $CaCO_3$ used by corals for calcification, and therefore impacts the ability of corals to synthesise coral skeleton. Reductions in oceanic aragonite are correlated with lower rates of calcification on coral reefs, and some estimates predict that healthy coral reefs will cease to exist as ocean acidification increases (Hughes et al. 2007; Jokiel et al. 2016). There is evidence however for inconsistent response of calcification rates to OA and uncertainties about synergistic environmental stressors, methodological limitations, and questions about some of the fundamental assumptions used in OA modelling (Shamberger et al. 2011, 2018; Jokiel et al. 2016; Jokiel 2016).

1.10 Significance of this research

Defining ecosystem status and predicting future trajectories of coral reefs and seagrasses requires a thorough understanding of their ecological function and energetic processes. The overarching aim of this thesis is to contribute to the current knowledge of benthic metabolism from the organism to the ecosystem and evaluate the array of methods available to measure it. The role of light as the key environmental driver will be explored at each stage, and the results placed in the context of ecosystem function in a changing climate. The results will support academic enquiry into some of the long-standing questions of coral reef research while also providing novel insight, directly applicable to the current efforts for conserving and restoring coral reefs and seagrasses. These findings

will support enhanced monitoring and tracking of ecosystem degradation using biogeochemical methods that can be applied to coral reefs, seagrasses, and other marine benthic communities. This work is of particular significance given then rapidly escalating climate crisis, which threatens the ecosystems of the tropical coastal ocean and the ecosystem services they support.

1.11 Thesis outline

This thesis explores the metabolic processes of individual organisms (Chapter 2), small communities (Chapter 3), and across an ecosystem (Chapter 4) using a range of established and novel methods. Chapter 2 explores the relationships between calcification and photosynthesis of coral reef calcifiers in relation to light. The study involved ex-situ incubations to measure individual metabolic rates of key species of coral and calcifying algae used in reef restoration under different levels of natural light, carried out at the International Center for Reef Restoration Research (IC2R3) of Mote Marine Laboratory in the Florida Keys. The aims of this study were to; compare rates of calcification and photosynthesis of important calcifying coral reef organisms, quantify changes in their metabolic rates in response to light, and explore the balance of inorganic to organic carbon processes at different times of day. This chapter was published in Limnology and Oceanography (Mallon et al. 2022) and was presented at the International Coral Reef Society conference in 2021.

Chapter 3 presents my research with Operation Wallacea and the National Autonomous University of Mexico developing and trialling a low-cost benthic chamber designed to incubate benthic communities at a fraction of the cost of other benthic chambers currently available. Studying benthic metabolism in the field as opposed to the lab is critical for capturing true representations of the physiological processes of ecological communities. This can be achieved through in-situ incubations using chambers; however, these are often costly and inaccessible for conservation practitioners and scientists working in remote and / or low-income areas where coral reefs are situated. The aims in Chapter 3 were to; identify limitations of the benthic chambers available, define criteria for a novel chamber design, and to develop and trial a new benthic chamber. This chapter has been accepted for

publication in the journal PeerJ (*in press,* March 2022) and was presented at the Reef Futures Conference in Florida, 2018.

Scaling up from small community incubations to ecosystem-wide measurements of benthic metabolism is limited due to the lack of sensors capable of measuring in-situ calcification. Traditionally, this is measured through lab analysis of total alkalinity. However, the recently developed Benthic Ecosystem and Acidification system (BEAMS) measures calcification from other biogeochemical parameters. Chapter 4 reviews and compares established and ground-breaking methods for measuring benthic metabolism at the ecosystem scale and compares rates of net community calcification and photosynthesis measured by flow respirometry, control volume and benthic boundary techniques over a seagrass meadow. the aim was to review the methods available for measuring benthic metabolism at the ecosystem scale and compare rates of G and P collected with different methods. The data for this chapter was collected in collaboration with co-authors.

Figure 1-3: Methods for measuring calcification at different scales from the ecosystem to the individual**. Left:** a sample of crustose coralline algae attached to a cement 'puck' is placed inside an ex-situ incubation chamber to measure high resolution metabolic rates at different times of day (Chapter 2). **Middle:** The low-cost benthic chamber designed to incubate small communities in the field, deployed over a *Porites* coral in Akumal bay, Mexico in August 2019 (Chapter 3). **Right:** BEAMS apparatus deployed over a coral reef, one of the methods for measuring community or ecosystem-wide metabolism (Chapter 4).

2   Light-driven dynamics between calcification and production in functionally diverse coral reef calcifiers

 Declaration of authorship: The data in this chapter was collected and analysed by the author of the thesis. Co-authors reviewed paper drafts and provided supervision, feedback, and guidance.

2.1 Abstract

Coral reef metabolism, defined by the processes of photosynthesis, respiration, calcification, and calcium carbonate dissolution, underpins ecosystem function. However, the relationships between these physiological processes at the organismal level and their interactions with light remain unclear. We examined metabolic rates across a range of photosynthesising calcifiers in the Caribbean: the scleractinian corals *Acropora cervicornis, Orbicella faveolata, Porites astreoides,* and *Siderastrea siderea*, and crustose coralline algae under varying natural light. Net photosynthesis and calcification showed a parabolic response to light across all species, with distinctions between massive corals, branching corals, and crustose coralline algae, reflecting their relative functional roles on the reef. At night, all organisms were net respiring, and most were net calcifying, although some incubations demonstrated instances of net calcium carbonate dissolution. Peak metabolic rates at light-saturation and average dark rates (respiration and night calcification) were positively correlated across species. Interspecies relationships between photosynthesis, respiration, and calcification indicate that calcification rates are linked to energy production at the organismal level in calcifying reef organisms. The species-specific ratios of net calcification to photosynthesis varied with light over a diurnal cycle.

The dynamic nature of calcification / photosynthesis ratios over a diurnal cycle questions the use of this metric as an indicator for reef function and health at the ecosystem scale unless temporal variability is accounted for. The complex dynamics of metabolic processes with light in coral reef organisms indicate that a more comprehensive understanding of reef metabolism is needed for predicting the future impacts of global change.

2.2   Introduction

Coral reefs are highly productive ecosystems that build the largest living structures on Earth. The services obtained from the coral reef ecosystem include coastal protection, habitat provision, fisheries, and tourism (Hoegh-Guldberg et al. 2019). These services ultimately rely on biogenic calcification; the process by which a diverse community of framework-building corals, crustose coralline algae (CCA), and other calcifying organisms contribute to the calcium carbonate ($CaCO_3$) reef structure. Global climate change threatens the survival of important framework-building coral species, primarily through sea temperature rise and ocean acidification, which have been shown to directly impede coral growth and negatively impact coral reef-dwelling organisms and ecosystems (Kleypas and Yates 2009; Comeau et al. 2013). Exposed calcium carbonate structures and sediments are vulnerable to dissolution exacerbated by ocean acidification (Cyronak et al. 2013; Eyre et al. 2014), and it is expected that reef structure could be lost at a pace faster than it is constructed in the near future (Eyre et al. 2018).

A positive relationship between photosynthesis and calcification has been observed across cellular, organismal, and community scales in coral reefs (Gattuso et al. 1999a; Allemand et al. 2011). At the ecosystem scale, the balance of photosynthesis, respiration, calcification, and dissolution, collectively known as coral reef metabolism, controls the coral reef carbon cycle (Albright et al. 2015; Cyronak et al. 2018). Net ecosystem calcification is defined as the rate of calcium carbonate precipitation offset by dissolution, while net ecosystem production is defined as the difference between photosynthesis and respiration (Smith and Kinsey 1978). Reef metabolism is often measured through changes in the carbonate chemistry of sea water as it flows over a coral reef ecosystem, which requires detailed knowledge of the local hydrodynamics (Marsh and Smith 1978). The

ratio of net calcification to net production has been proposed as a proxy for monitoring reef function, which can be calculated from carbonate chemistry data (Cyronak et al. 2018; Takeshita et al. 2018). This metric provides useful insight into reef biogeochemistry as a simple, effective tool for monitoring change on coral reefs over space and time (Cyronak et al., 2018). However, this relies on a strong mechanistic understanding of how photosynthesis and calcification are linked from the organism to the ecosystem.

At the organismal level, connectivity between photosynthesis and calcification is reflected in the phenomena known as light-enhanced calcification, or the observation of increased calcification rates during the day compared to night (Goreau 1959; Gattuso et al. 1999a). Research into the mechanisms behind light-enhanced calcification have not yet reached a consensus, and it is possible that more than one process is taking place for the different species and functional groups exhibiting light-enhanced calcification, e.g., corals, calcifying algae, foraminifera (Cohen et al. 2016). One hypothesis is that higher rates of photosynthesis associated with optimal light conditions provide the coral with more energy for calcification (Chalker and Taylor 1975). Other studies show that metabolic carbon dioxide production through respiration is a major source of carbon for calcification (Furla et al. 2000). Another hypothesis is that photosynthesis influences carbonate chemistry equilibrium at the site of calcification through the uptake of carbon dioxide, which enhances calcium carbonate precipitation (McConnaughey and Whelan 1997; Allison et al. 2014), however, it is important to note that calcification and photosynthesis take place in different tissue layers. Cohen et al. (2016) recently demonstrated that calcification can be decoupled from photosynthesis by providing corals with different wavelengths of light, indicating that both processes are independently linked to sunlight. To make accurate predictions about the impact of climate change on coral reefs we must understand the mechanistic relationships between calcification and photosynthesis at the organismal scale before we can fully understand their interactions at community or ecosystem scales (Edmunds et al. 2016).

Shifting benthic community compositions are expected to alter the metabolism and carbon cycle of coral reef ecosystems (Hughes et al. 2018). In the Caribbean, coral reefs historically built by skeletal calcium carbonate of reef-building corals, primarily branching *Acropora* spp. and massive *Orbicella* spp., have experienced unprecedented losses of coral cover and proliferation of macroalgal cover in recent decades (Jackson et al, 2014).

Contemporary coral populations have lower species diversity and are dominated by resilient, weedy corals, such as *Porites astreoides* (Green et al. 2008), which lack reef-building life-history traits (Darling et al. 2012). As a result of these phase shifts, rugosity and carbonate accretion rates in the Caribbean have decreased over the past decades (Perry and Alvarez-Filip, 2018), impacting the maintenance of reef structure and habitat function (Muehllehner et al. 2016). Quantifying organismal metabolic rates and understanding the dynamic interactions between metabolic processes is critical for predicting the impact of changing coral reef ecosystems and the services they provide.

In this study, we measured the metabolic rates of key Caribbean coral reef calcifiers to determine the interaction between photosynthesis, respiration, and calcification over natural diurnal light cycles. We provide a comparison between species with distinct ecological functions, chosen to reflect past and present species dominance; (1) branching, rapid-growth *Acropora cervicornis*, (2) framework-building *Orbicella faveolata*, (3) resilient, weedy *Porites astreoides*, (4) framework-building, stress-tolerant *Siderastrea siderea*, and (5) abundant, low-profile, crustose coralline algae (CCA). We compared differences in metabolism across these calcifying organisms over a natural diurnal light-cycle and developed metabolism-irradiance curves to determine the relationships among photosynthesis, calcification, and irradiance at the organismal level.

2.3   Methods

Ex-situ incubations of four species of scleractinian coral and two crustose coralline algae (CCA) were conducted in the Climate and Acidification Ocean Simulator outdoor experimental facility at the Mote Marine Laboratory, Elizabeth Moore International Center for Coral Reef Research and Restoration, Summerland Key, Florida, in October and November of 2019. The Climate and Acidification Ocean Simulator facility is supplied with 20 µm particle filtered Atlantic seawater maintained by a dual heat exchanger system at 28.4 ± 0.2 °C (mean $\pm$ SD) in 3,800-litre header tanks. An automated controller system (Walchem W900, US) maintains ambient seawater at a pH of 8.04 ± 0.04.

2.3.1 Study organisms

Small colonies (mean surface area $13 \pm$ SD 3.54 cm^2) of *A. cervicornis* (n=6), *O. faveolata* (n=12), *P. astreoides* (n=12), and *S. siderea* (n=12) were randomly selected from the Mote Marine Laboratory land nursery of micro-fragmented corals (Fig. 2-1, Table 2-1). While small encrusting fragments do not represent the morphologies of larger, older colonies in the wild, using similarly fragmented corals with minimal differences in 'colony-wide' morphologies allows for better inter-specific comparisons. All corals originated from Mote's restoration nurseries, where they had been either sexually produced and / or micro-fragmented from field-collected colonies between 2010 - 2017 (Table 2-2). Additionally, crustose coralline algae growing on the base of two of the Mote restoration raceways were chiselled off and glued to clean ceramic tiles 3 weeks prior to the study. Due to morphological differences in colour and surface texture (Fig. 2-1), crustose coralline algae (CCA) were thought to be distinct species, however we were unable to identify them and are herein referred to as crustose coralline algae type 1 (CCA1) and type 2 (CCA2).
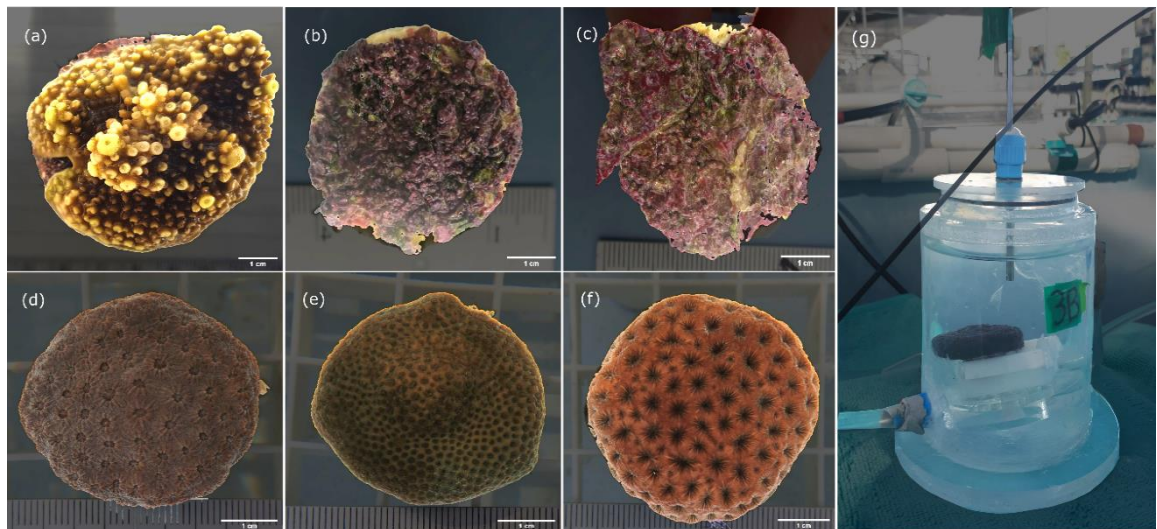
Figure 2-1: Examples of top-down photos used for surface area measurements on Image-J: (a) *A. cervicornis*, (b) crustose coralline algae type 1, (c) crustose coralline algae type 2, (d) *O. faveolata*, (e) *P. astreoides*, and (f) *S. siderea*, and (g) the incubation chambers used during this study showing the oxygen sensor inserted through the chamber lid, transparent water jacket, and the white plastic holder below coral with stir bar spinning underneath. Photos (a) through (f) show 1 cm scale bars.

Table 2-1: Summary of the mean (±SD) surface areas (cm^2) for each species calculated using Image-J software from top-down photographs. For branching coral *A. cervicornis*, a cylinder calculation was applied for the vertical portion of the coral.

Species	Surface area (cm, mean ± SD)	n
A. cervicornis	19.4 ± 2.79	6
CCA 1	10.2 ± 2.34	12
CCA 2	10.1 ±2.13	12
O. faveolata	11.2 ±1.55	12
P. astreoides	12.7± 1.54	12
S. siderea	14.4 ± 1.99	12

Table 2-2: Origins of sampled corals and crustose coralline algae (CCA1 and CCA2) used in this study. All organisms were sourced from Mote's International Center for Coral Reef Restoration and Research in Summerland Key.

Species	Origin	Year(s)
A. cervicornis	Key West field nurseries	2016-2017
CCA 1	Raceway cultivation (natural settlement)	2018 - 2019
CCA 2	Raceway cultivation (natural settlement)	2018 -2019
O. faveolata	Sexual recruits. Settled and reared in aquaria	2014 - 2017
P. astreoides	Sexual recruits. Settled and reared in aquaria	2014 - 2017
S. siderea	Micro-fragments from multiple field-collected donor colonies	2010 - 2017

Each specimen was randomly assigned to one of 12 holding tanks (19-litre volume, 40 x 20 x 25 cm, L x W x H) 2 weeks prior to the study. Each tank received 160 ml min-1 filtered natural seawater via a separate manifold and each tank was fitted with a circulation pump to maintain flow (Deluxe Submersible Water Pump 400GPH, China). While water flow has been shown to modulate coral metabolism and their response to environmental change (e.g., Comeau et al., 2014, 2019), the goal of this study was to maintain a constant flow in order to compare the metabolism between calcifying functional groups. Sea water parameters of pH (Seven2Go Pro S8, Mettler Toledo), temperature, and salinity (YSI Professional Plus) were monitored twice per day. For pH, electrodes were calibrated against National Bureau of Standards (NBS) scale buffers of 4.01, 7.00, and 10.00 at 25 °C and validated using other carbonate chemistry parameters (e.g., total alkalinity and dissolved inorganic carbon). Water temperature was controlled by an automated dual exchange heater and chiller, and, to maintain pH and salinity within each tank, water inflow was adjusted, and water changed as necessary. Table 2-3 provides an overview of the mean and standard deviation for all environmental parameters in the holding tanks.

A permanent shade cloth (30% attenuation) maintained natural light conditions (daytime = 321.38 ± 179.73, µmol m^{-2} s^{-1}, and peak = 494 ± 64.4 µmol m-2 s-1 photosynthetically active radiation (PAR) mean $\pm$ SD). The surface area of each fragment was measured from top-down photos, with additional cylinder calculations to incorporate the surface area of A. cervicornis branches. All size measurements were extracted from photos using Image-J (Schneider et al. 2012) with the SIOX plug-in (Simple Interactive Object Extraction, Wang, 2016) to identify live tissue cover and exclude any areas of cement plug not covered in tissue (Fig. 2-1, Table 2-1).

Table 2-3: Weekly and average seawater parameters of the raceways over the 4 weeks in which the experiment was conducted in 2019.

Week	Date	Temperature (°C)	Salinity (ppt)	pH NBS	TA (μmol/kg)	DIC (μmol/kg)	Arag_Ω	pCO2 (μatm)
1	14/10/2019	28.6	37.29	8.078	2313.81	2004.31	3.43	477.13
2	21/10/2019	28.6	38.08	7.963	2414.26	2088.26	3.62	492.9
3	28/10/2019	28.3	38.3	8.058	2306.39	1984.67	3.49	454.63
4	04/11/2019	28.5	38.4	8.051	2373.18	2074.64	3.31	541.55
5	11/11/2019	28.3	38.49	8.029	2346.88	2054.2	3.23	541.4
6	18/11/2019	28.3	38.45	n/a	2397.68	2107.26	3.24	570.26
Mean		**28.43**	**38.17**	**8.04**	**2358.70**	**2052.22**	**3.39**	**512.98**
Standard deviation		**±0.15**	**±0.45**	**0.04**	**44.06**	**±48.36**	**±0.15**	**±44.72**

2.3.2 Incubation Protocol

Incubations were conducted over 12 days between 31st October and 21st November 2019, with each day selected for consistency in wind, cloud cover, and rainfall. One fragment per species was randomly selected each day and placed into an incubation chamber for ~1 hour at the following times: 2 hours after sunrise (AM), during the solar peak (PEAK), and 2 hours after sunset (DARK). On 3 of the 12 days, an additional incubation between the solar peak and sunset was included (PM). Separate readings of photosynthetically active radiation (PAR) were taken for each chamber position at the start and end of incubations with Li-cor model LI-1500G and an underwater quantum sensor (LI-192SA), oriented horizontally. Average PAR light values (mean of start and end) were calculated for individual chambers and varied from 67 to 595 μmol m^{-2} s^{-2} between AM, PM, and PEAK incubation times (Fig. 2-2).

Incubation chambers were set up in a dry raceway tank adjacent to holding tanks for consistent light conditions. Incubations consisted of 4 double-walled transparent acrylic incubation chambers (300 ml) sealed with a transparent acrylic lid, with a rubber O-ring closure (Fig. 2-1g). A thermocycler (VWR MX7LR-20) recirculated water through the transparent cooling jackets of the incubators at 26.5 ± 0.5 °C to maintain water inside the chambers at 27.6 ± 1.5 °C. Incubation chambers were positioned on magnetic stirrers set at 600 revolutions per minute (RPM) and flow simulated using a 2 cm stir bar placed under the specimens with a plastic grid base to allow water movement without disturbing the organism. All incubations were run for 1 hour $\pm$ 3 minutes, with seawater samples taken at the start and end (see below for details).
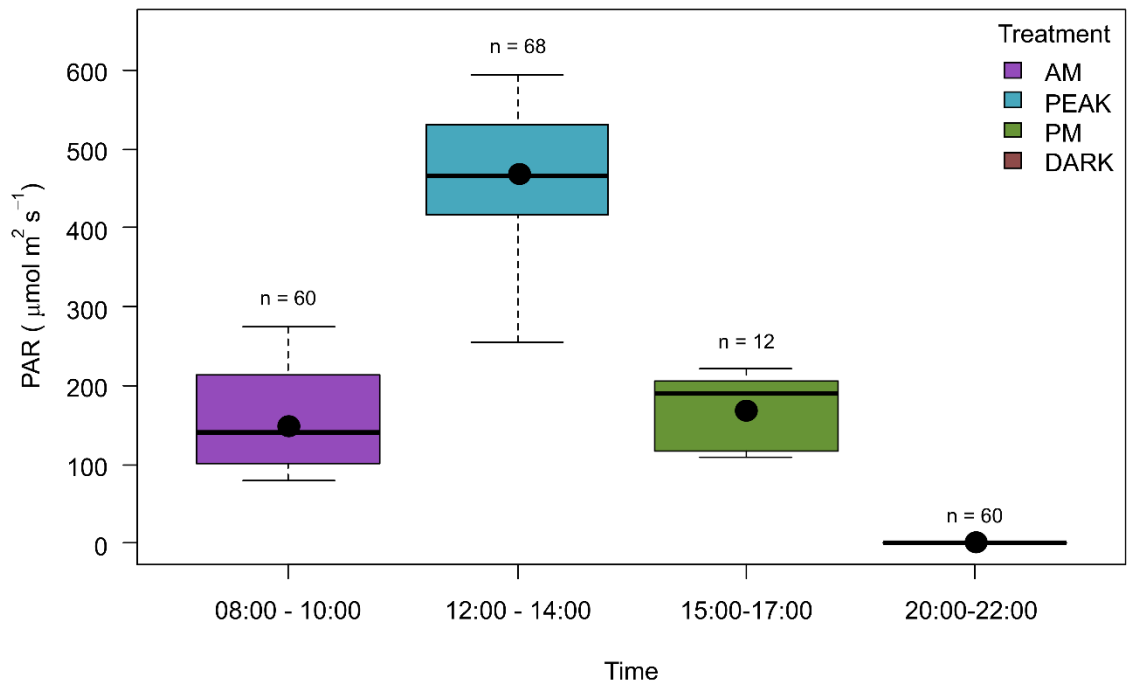
Figure 2-2: Photosynthetically Active Radiation (PAR) measured at incubation times. Boxplots show mean (circle), median (horizonal line), and IQR (box and whisker). The number of individual incubations carried out within the treatment time (n) including control incubations is shown above each box. Colours represent the time treatments: AM (2 hours after sunrise 8:00 to 10:00), peak (solar noon 12:00 to 14:00), PM (2 hours before sunset 15:00 to 17:00) and dark (2 hours after sunset 20:00 to 22:00). Average AM treatment PAR was $155 \pm 66.8 \, \mu mol \, m^{-2} \, s^{-1}$ (mean $\pm$ SD), for peak treatment incubations PAR averaged $494 \pm 64.4 \, \mu mol \, m^{-2} \, s^{-1}$ and late afternoon PM treatment PAR averaged $171 \pm 43.9 \, \mu mol \, m^{-2} \, s^{-1}$ PAR.

2.3.3 Measured Parameters

Dissolved oxygen (DO) fibre optic oxygen sensors (Firesting O_2, Pyroscience, Germany) were inserted in each chamber to ~1 cm above the coral 3 - 5 minutes prior to the incubation start time, to allow for acclimation of the sensor and adjustment of its position. The oxygen sensors were calibrated to 0 and 100% O_2 saturation using air-saturated water prior to each incubation. Real-time measurements of dissolved oxygen ($\mu mol/L$) were recorded each second during the incubation. To calculate oxygen fluxes, start and end values were calculated as the mean values over the first and last minute of the 1-hour incubations. The fluxes derived from the start and end values were similar to fluxes

derived from linear slopes between time and oxygen during each incubation. Start and end fluxes were used for a more direct comparison to fluxes derived from the carbonate chemistry data.

Water samples for carbonate chemistry analysis were taken at the start and end of incubations using a 100 ml plastic syringe, immediately filtered (0.45 µm), poisoned with 200 µl of saturated mercuric chloride, and stored in 250 ml amber borosilicate glass bottles at the Mote Ocean Acidification Laboratory, until they were processed. One sample was taken for the start conditions as all chambers were filled with the same water prior to beginning the incubations. Total alkalinity (TA) was measured by potentiometric titration using an automated titrator (Metrohm 905 Titrando), following the standard best practice (Dickson et al. 2007). Mean values for each sample were derived from 2 to 3 samples (40 mL) with a precision of $\pm$ 3.84 µmol kg^{-1}. Measurements were corrected to Dickson Certified Reference Material (CRM, batches 184, 187, 189) measured at the start and end of each day. Dissolved inorganic carbon (DIC) was analysed using an Apollo SciTech Analyzer (Model AS-C3). Mean values were derived from 2 to 3 replicates of 1 mL injections and corrected for drift with measurements of certified reference material at the start and end of the analysis. Precision of dissolved inorganic carbon measurements was 2.41 µmol kg^{-1}.

2.3.4 Calculations of Metabolic Processes

Metabolic rates were calculated from the difference between starting and ending concentrations of dissolved oxygen (ΔDO), total alkalinity (ΔTA), and dissolved inorganic carbon (ΔDIC). To calculate fluxes, all seawater chemistry measurements were normalised to individual incubation chamber volumes (259.69 $\pm$ 12.57 ml, mean $\pm$ SD) and coral surface areas (Table 2-1). Control incubations (e.g., empty ceramic tiles) showed negligible changes in seawater chemistry (ΔDO = 0.4 $\pm$ 6.8 µmol l^{-1}, ΔDIC = -7.24 $\pm$ 10.96 µmol kg^{-1}, ΔTA = -2.8 $\pm$ 8.7 µmol kg^{-1}, mean $\pm$ SD), and as such no corrections in seawater chemistry due to water column processes were made.

Net production (μmol cm^{-2} hr^{-1}) was calculated from changes in dissolved oxygen and dissolved inorganic carbon concentrations according to the following equations:

$$P_{DO} = \frac{\Delta DO \times V}{A \times t}$$

$$P_{DIC} = -\frac{\left(\Delta DIC - \frac{\Delta TA}{2}\right) \times V}{A \times t}$$

where, ΔDO, ΔDIC, and ΔTA represent the respective changes in dissolved oxygen, dissolved inorganic carbon, and total alkalinity concentrations in μmol L^{-1}. V is the volume of the incubation chamber in litres (L), A is the surface area of the sample (cm^2), and t is duration of the incubation in hours (1 hr).

Net calcification was calculated using the alkalinity anomaly technique according to the following equation:

$$G_{net} = \frac{\left(-\frac{\Delta TA}{2}\right) \times V}{A \times t}$$

The relationship between photosynthesis and calcification was modelled on gross metabolic rates (i.e., photosynthesis + respiration, and calcification + dark calcification) to light using the following hyperbolic tangent function from Jassby and Platt (1976):

$$P_{net} = P_{max} \times \tanh\left(\frac{\alpha \times E}{P_{max}}\right) + R$$

where P_{net} is the modelled net production rate, R is the average dark respiration rate, and E is irradiance (μmol m^{-2} s^{-1}). The coefficients derived from the model include: the initial slope between P_{net} and light (α) and the maximum gross photosynthetic rate (P_{max}).

For calcification, we adapted Eq. 4 to model calcification (G_{net}) as:

$$G_{net} = G_{max} \times \tanh\left(\frac{\alpha \times E}{G_{max}}\right) + G_{dark}$$

where G_{dark} is the average dark calcification rate for each species, representing the non-light enhanced portion of the measured calcification rates, G_{max} is the maximum gross calcification, and alpha (α) is the initial slope between calcification and irradiance.

The light saturation point (E_K) was calculated from model coefficients P_{max} or G_{max} and alpha for each model using the following equation:

$$E_K = \frac{P_{max}}{\alpha}$$

The absolute ratio of calcification to both calcification and production was calculated as follows:

$$G_{net}/M_{tot} = \frac{|G_{net}|}{|P_{net}| + |G_{net}|}$$

where M_{tot} (or the sum of both calcification and production) represents total carbon metabolism.

2.3.5   Statistical Analysis

All statistical analyses were conducted in the statistical environment R using RStudio version R.4.0.2 (R Core Team, 2020). The *RespR* package (Harianto et al. 2019) was used to extract and inspect oxygen data (Fig 2-11). The *Tidyverse* (Wickham 2019) was used for data organisation and synthesis, and data visualisation was conducted with base-R functions and *ggplot / ggpubr*.(Wickham 2016). Shapiro-Wilkes tests were combined with visual assessments of density and Q-Q plots to evaluate approximately normal distributions

for individual species. Repeated measures two-way ANOVA tests were used to test differences between treatments and pairwise comparisons. Post-hoc Bonferroni-corrected t-tests were used to compare differences between all possible pairs of species at each time of day and for each parameter. Models were fitted using R linear and non-linear least squares functions of the *Stats* package. Model fit was assessed by residuals plots generated using the *nlstools* package (Baty et al. 2015). Models were evaluated based on R^2, confidence intervals and standard error of the regression (sigma, σ).

Figure 2-3: Example outputs of plots generated using R package *RespR* to 'inspect' each incubation for anomalies. Plots in the top row show raw oxygen data and bottom row show the slope of a rolling linear regression during a 1 hour incubation of *A. cervicornis* in the light (left) and dark (right). Further examples in appendix A.

2.4 Results

Rates of metabolism were statistically different between treatment times for photosynthesis (P_{DO} repeated measures ANOVA $F_{3,155} = 336.05$, $p = <0.05$, and P_{DIC} repeated measures ANOVA $F_{3,143} = 331.37$, $p = <0.05$), and for calcification (G_{net} repeated measures ANOVA $F_{3,149} = 27.24$, $p = <0.05$) (Table 2-4, Fig. 2-4). During the day, photosynthesis (+P_{DO} and +P_{DIC}) and calcification (+G_{net}) occurred in all incubations. At night, respiration occurred in all incubations (-P_{DO} and -P_{DIC}) while calcification was still generally positive (+G_{net}), although net dissolution (-G_{net}) was detected. All metabolic rates for all species were highest during the peak treatment (Figs. 2-3, 2.4).

Metabolism was species specific, with *Orbicella faveolata*, *Porites astreoides*, and *Siderastrea siderea* having the highest average rates of calcification and photosynthesis, while both types of crustose coralline algae had the lowest (Pairwise comparisons using t-test, Fig. 2-3, Table 2-5). As *O. faveolata*, *P. astreoides*, and *S. siderea* had consistently similar rates, we refer to this grouping as the *'massive corals'* herein. We report rates as mean ± SD unless otherwise indicated. Overall, metabolic rates were higher in the massive corals than both *A. cervicornis* and crustose coralline algae over a diurnal cycle (Fig. 2-4). Night metabolism followed a similar grouping as the daytime measurements: respiration was greater in the massive corals ($R_{DO} = -0.75 \pm 0.23$ µmol cm^{-2} hr^{-1}, $R_{DIC} = -0.85 \pm 0.35$ µmol cm^{-2} hr^{-1}), than in *A. cervicornis* ($R_{DO} = -0.32 \pm 0.05$, $R_{DIC} = 0.38 \pm 0.08$ µmol cm^{-2} hr^{-1}) and crustose coralline algae ($R_{DO} = -0.31 \pm 0.14$ µmol cm^{-2} hr^{-1}, $R_{DIC} = -0.42 \pm 19$ µmol cm^{-2} hr^{-1}). Dark calcification (G_{dark}) was higher in the massive corals ($G_{dark} = 0.31 \pm 0.24$ µmol cm^{-2} hr^{-1}) than *A. cervicornis* ($G_{dark} = 0.03 \pm 0.08$ µmol cm^{-2} hr^{-1}) and crustose coralline algae ($G_{dark} = 0.06 \pm 0.18$ µmol cm^{-2} hr^{-1}), however, this difference was only significant for *S. siderea* (Table 2-5). Negative rates of dark calcification (i.e., -G_{dark}, net dissolution) were detected in 10 of the crustose coralline algae, one *A. cervicornis,* and two *O. faveolata* dark incubations, although dissolution rates were relatively low and close to 0.

Table 2-4: Output of repeated measures ANOVA two-way test between species and incubation times (time of day) for measured rates of photosynthesis (P_{DO}, P_{DIC}) and calcification (G_{net}).

	Effect	DFn	DFd	F	p	ges	
P_{DO}	Species	5	155	29.54	5.42×10^{-21}	0.49	*
	Treatment	3	155	336.05	1.36×10^{-67}	0.87	*
	Species: treatment	12	155	14.31	9.69×10^{-20}	0.53	*
P_{DIC}	Species	5	143	27.88	1.23×10^{-19}	0.49	*
	Treatment	3	143	331.37	3.72×10^{-64}	0.87	*
	Species: treatment	12	143	12.75	1.92×10^{-17}	0.51	*
G_{net}	Species	5	149	28.21	4.84×10^{-20}	0.49	*
	Treatment	3	149	27.24	4.21×10^{-14}	0.35	*
	Species: treatment	12	149	1.83	4.80×10^{-02}	0.13	*

Figure 2-4: Boxplots of metabolic rates at different times of day for each species. Y-axes show; photosynthesis from oxygen evolution (P_{DO}), photosynthesis by carbon assimilation (P_{DIC}), and calcification (G_{net}) rates, normalised to time and surface area (fluxes in μmol cm^2 hr^{-1}). Boxplots show median (horizontal bar) and IQR (box and whisker), and individual data points are depicted as hollow circles. Species are shown in colours and labelled above each plot. Time of day is shown on the x-axis: AM 08:00 to 10:00, peak 12:00 to 14:00, PM 15:00 to 17:00 and dark 20:00 to 22:00. Only three species were incubated during the PM treatment.
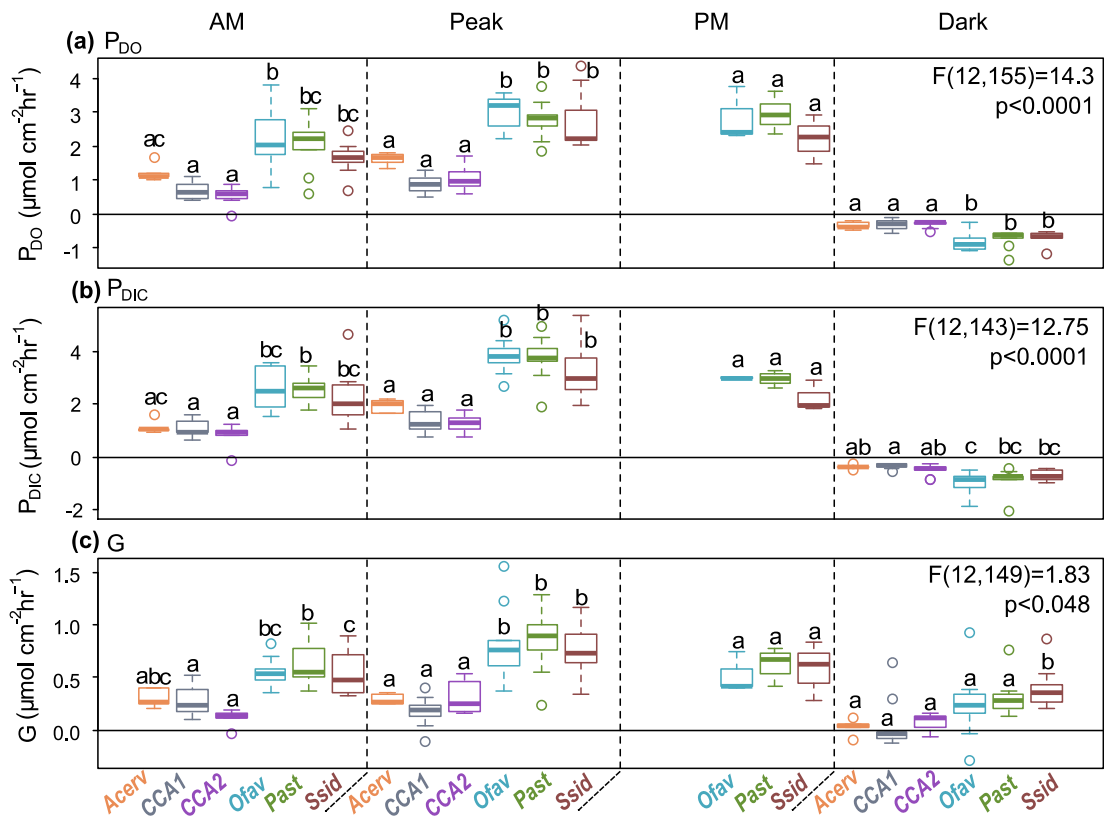
Figure 2-5: Boxplots of metabolic rates at different times of the day for each species, with ANOVA differences between different times of day and pairwise t-test ad-hoc comparison between species. Y-axes are P_{DO} (photosynthesis from oxygen evolution), P_{DIC} (photosynthesis by carbon assimilation), and G (calcification). All rates are normalised to time and surface area resulting in fluxes in the units μmol cm^2 hr^{-1}. Boxplots show median (horizonal bar) and IQR (box and whisker), outliers are depicted as hollow circles. Species are shown in colours and labelled on the bottom x-axis. Dotted vertical lines show the divisions between incubations done during different times of the day. Time periods are labelled at the top of the panels; AM 08:00 to 10:00, PEAK 12:00 to 14:00, PM 15:00 to 17:00 and DARK 20:00 to 22:00. Only three species were incubated during the PM treatment. Two-way repeated measures ANOVA for the effect of treatment time and species is displayed on top right of each plot. Letters above box plots show post-hoc pairwise comparisons using t-tests, where the matching letters represent no significant difference between species.

Table 2-5: Output of repeated measures ANOVA two-way test between species and incubation times (time of day) for measured rates of photosynthesis (P_{DO}, P_{DIC}) and calcification (G_{net}).

	Effect	DFn	DFd	F	p	ges	
P_{DO}	Species	5	155	29.54	5.42×10^{-21}	0.49	*
	Treatment	3	155	336.05	1.36×10^{-67}	0.87	*
	Species: treatment	12	155	14.31	9.69×10^{-20}	0.53	*
P_{DIC}	Species	5	143	27.88	1.23×10^{-19}	0.49	*
	Treatment	3	143	331.37	3.72×10^{-64}	0.87	*
	Species: treatment	12	143	12.75	1.92×10^{-17}	0.51	*
G_{net}	Species	5	149	28.21	4.84×10^{-20}	0.49	*
	Treatment	3	149	27.24	4.21×10^{-14}	0.35	*
	Species: treatment	12	149	1.83	4.80×10^{-02}	0.13	*

Table 2-6: Results of post hoc pairwise comparisons using t-test to identify significant difference between species for each of the 3 measured rates: photosynthesis from oxygen evolution (P_{DO}), photosynthesis by carbon assimilation (P_{DIC}), and calcification (G_{net}), at different treatment times (AM, PEAK, DARK).

Treatment	Group 1	Group 2	n1	n2	P – value	Adjusted P	
		P_{DO}					
AM	*A. cervicornis*	*O. faveolata*	5	11	0.00267	0.0401	*
	CCA 1	*O. faveolata*	7	11	2.09E-06	3.13E-05	****
	CCA 2	*O. faveolata*	8	11	1.48E-07	2.22E-06	****
	CCA 1	*P. astreoides*	7	11	9.01E-06	0.000135	***
	CCA 2	*P. astreoides*	8	11	6.99E-07	1.05E-05	****
	CCA 1	*S. siderea*	7	11	0.000994	0.0149	*
	CCA 2	*S. siderea*	8	11	0.000119	0.00178	**
PEAK	*A. cervicornis*	*O. faveolata*	5	12	3.51E-06	5.26E-05	****
	CCA 1	*O. faveolata*	11	12	5.58E-14	8.38E-13	****
	CCA 2	*O. faveolata*	8	12	1.59E-11	2.38E-10	****

	A. cervicornis	*P. astreoides*	5	12	6.03E-05	0.000905	***
	CCA 1	*P. astreoides*	11	12	2.35E-12	3.53E-11	****
	CCA 2	*P. astreoides*	8	12	5.45E-10	8.18E-09	****
	A. cervicornis	*S. siderea*	5	12	0.000197	0.00295	**
	CCA 1	*S. siderea*	11	12	1.24E-11	1.86E-10	****
	CCA 2	*S. siderea*	8	12	2.58E-09	3.87E-08	****
DARK	*A. cervicornis*	*O. faveolata*	5	10	3.96E-05	0.000594	***
	CCA 1	*O. faveolata*	10	10	6.11E-07	9.16E-06	****
	CCA 2	*O. faveolata*	9	10	4.96E-07	7.44E-06	****
	A. cervicornis	*P. astreoides*	5	10	0.000805	0.0121	*
	CCA 1	*P. astreoides*	10	10	3.27E-05	0.00049	***
	CCA 2	*P. astreoides*	9	10	2.42E-05	0.000363	***
	A. cervicornis	*S. siderea*	5	10	0.00171	0.0256	*
	CCA 1	*S. siderea*	10	10	9.10E-05	0.00137	**
	CCA 2	*S. siderea*	9	10	6.59E-05	0.000989	***

P_{DIC}							
AM	*A. cervicornis*	*O. faveolata*	5	11	0.000505	0.00757	**
	CCA 1	*O. faveolata*	7	11	0.000124	0.00185	**
	CCA 2	*O. faveolata*	8	11	1.41E-05	0.000211	***
	A. cervicornis	*P. astreoides*	5	11	0.000291	0.00436	**
	CCA 1	*P. astreoides*	7	11	6.54E-05	0.000981	***
	CCA 2	*P. astreoides*	8	11	7.50E-06	0.000113	***
	CCA 1	*S. siderea*	7	11	0.0025	0.0375	*
	CCA 2	*S. siderea*	8	11	0.000306	0.00459	**
PEAK	*A. cervicornis*	*O. faveolata*	5	12	2.23E-06	3.35E-05	****
	CCA 1	*O. faveolata*	11	12	1.57E-11	2.36E-10	****
	CCA 2	*O. faveolata*	8	12	4.81E-11	7.21E-10	****
	A. cervicornis	*P. astreoides*	5	12	5.56E-06	8.35E-05	****
	CCA 1	*P. astreoides*	11	12	4.93E-11	7.40E-10	****
	CCA 2	*P. astreoides*	8	12	1.42E-10	2.13E-09	****
	A. cervicornis	*S. siderea*	5	12	0.000776	0.0116	*
	CCA 1	*S. siderea*	11	12	3.05E-08	4.58E-07	****
	CCA 2	*S. siderea*	8	12	6.30E-08	9.45E-07	****
DARK	*A. cervicornis*	*O. faveolata*	5	10	0.000957	0.0144	*
	CCA 1	*O. faveolata*	10	10	4.99E-05	0.000748	***

	CCA 2	O. faveolata	9	10	0.00176	0.0264	*
	CCA 1	P. astreoides	10	10	0.000502	0.00753	**

			G_{net}				

AM	CCA 1	O. faveolata	7	11	0.00206	0.0309	*
	CCA 2	O. faveolata	8	11	4.00E-06	6.00E-05	****
	A. cervicornis	P. astreoides	5	11	0.00147	0.0221	*
	CCA 1	P. astreoides	7	11	0.00021	0.00315	**
	CCA 2	P. astreoides	8	11	3.07E-07	4.61E-06	****
	CCA 1	S. siderea	7	11	0.00163	0.0244	*
	CCA 2	S. siderea	8	11	3.03E-06	4.55E-05	****
PEAK	A. cervicornis	O. faveolata	5	12	0.000196	0.00295	**
	CCA 1	O. faveolata	11	12	5.93E-08	8.90E-07	****
	CCA 2	O. faveolata	8	12	3.52E-05	0.000528	***
	A. cervicornis	P. astreoides	5	12	5.13E-05	0.000769	***
	CCA 1	P. astreoides	11	12	1.14E-08	1.71E-07	****
	CCA 2	P. astreoides	8	12	7.37E-06	0.00011	***
	A. cervicornis	S. siderea	5	12	0.000805	0.0121	*
	CCA 1	S. siderea	11	12	4.80E-07	7.19E-06	****
	CCA 2	S. siderea	8	12	0.000199	0.00299	**
DARK	A. cervicornis	S. siderea	5	10	0.00245	0.0368	*
	CCA 1	S. siderea	10	10	0.000503	0.00754	**
	CCA 2	S. siderea	9	10	0.00169	0.0254	*

2.4.1 Relationships between Metabolism and Light

To elucidate species-specific relationships with light, metabolic-irradiance curves were modelled using a hyperbolic tangent equation (Eqs. 4, 5; Figs. 2-7 to 2-9). All photosynthesis-irradiance model evaluations showed a high R^2 (>0.80), and coefficients were significant (p < 0.001) for photosynthesis measured from changes to both dissolved oxygen (P_{DO}) and dissolved inorganic carbon (P_{DIC}). Calcification-light models generally had lower R^2 and higher sigma (σ) relative to calcification (G_{net}) values (Table 2-7) than photosynthesis-irradiance models, indicating a weaker model fit, and coefficient estimates

were not always significant (alpha (α) p > 0.1 for *A. cervicornis* and crustose coralline algae). Of the coral species, *A. cervicornis* had the lowest maximum photosynthesis and calcification (P_{max} and G_{max}). Initial photosynthesis-irradiance curve slopes (α) were highest for the massive corals. Photosynthetic-irradiance saturation (E_K) was highest in *A. cervicornis* (P_{DIC} E_K = 356), and in calcification-irradiance models light saturation (E_K) was highest for *P. astreoides* and *S. siderea* (G_{net} E_K = 448 and 544 µmol PAR, respectively).
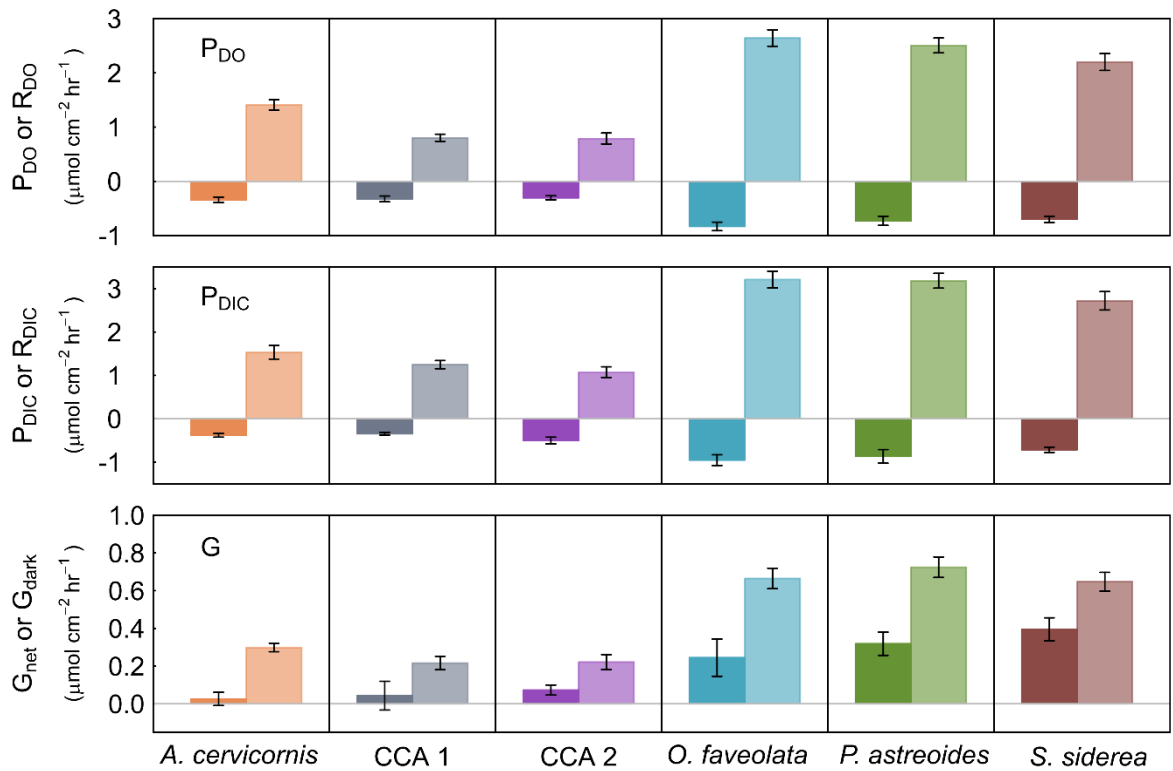
Figure 2-6: Panelled bar plots show species-specific average rates of dark (*left bar, darker shade*) and light (*right bar, lighter shade*) metabolism. The colour scheme is the same as in Figs. 2-5, 2-6 and species are labelled on the bottom x-axis. Rates shown are the mean light and dark rates across all days, and error bars represent standard error (SE).

2.4.2 Relationships between calcification and photosynthesis

The model coefficients P_{max} and G_{max} exhibited a positive linear relationship across all species ($R^2 = 0.88$, $p < 0.05$), while mean respiration (R) and dark calcification (G_{dark}) rates ($R^2 = 0.66$, $p = 0.05$) exhibited a negative linear correlation between all species (Fig. 2-10). This demonstrates that calcification increases with rates of net production across species during the day and with increased respiration in the dark. When the metabolic rates of all species were grouped together, linear correlations between P_{DIC} and G_{net} were weaker (light $R^2 = 0.39$, $p < 0.001$, dark $R^2 = 0.15$, $p = 0.04$) than correlation between model coefficients G_{max} - P_{max} and R - G_{dark} (Fig. 2-10). When the linear models were broken down by species, regression models of P_{DIC} and G_{net} were only significant in *P. astreoides* (light $R^2 = 0.39$, dark $R^2 = 0.78$, $p < 0.005$, Fig. 2-12). These relationships indicate tight coupling of photosynthesis, respiration, and calcification and show differences within and between different species of coral reef calcifiers.

Dissolved oxygen production (P_{DO}) was positively correlated with dissolved inorganic carbon assimilated (P_{DIC}), demonstrating a metabolic quotient (Q) value of 1.18 overall (Fig. 2-13) and individual differences in Q between species (Fig. 2-13, Table 2-8). The ratio of carbonate precipitation to organic production (G_{net}/M_{tot}) demonstrated shifts in the balance of calcification to photosynthesis over the day in relation to ambient light (Fig. 2-14.
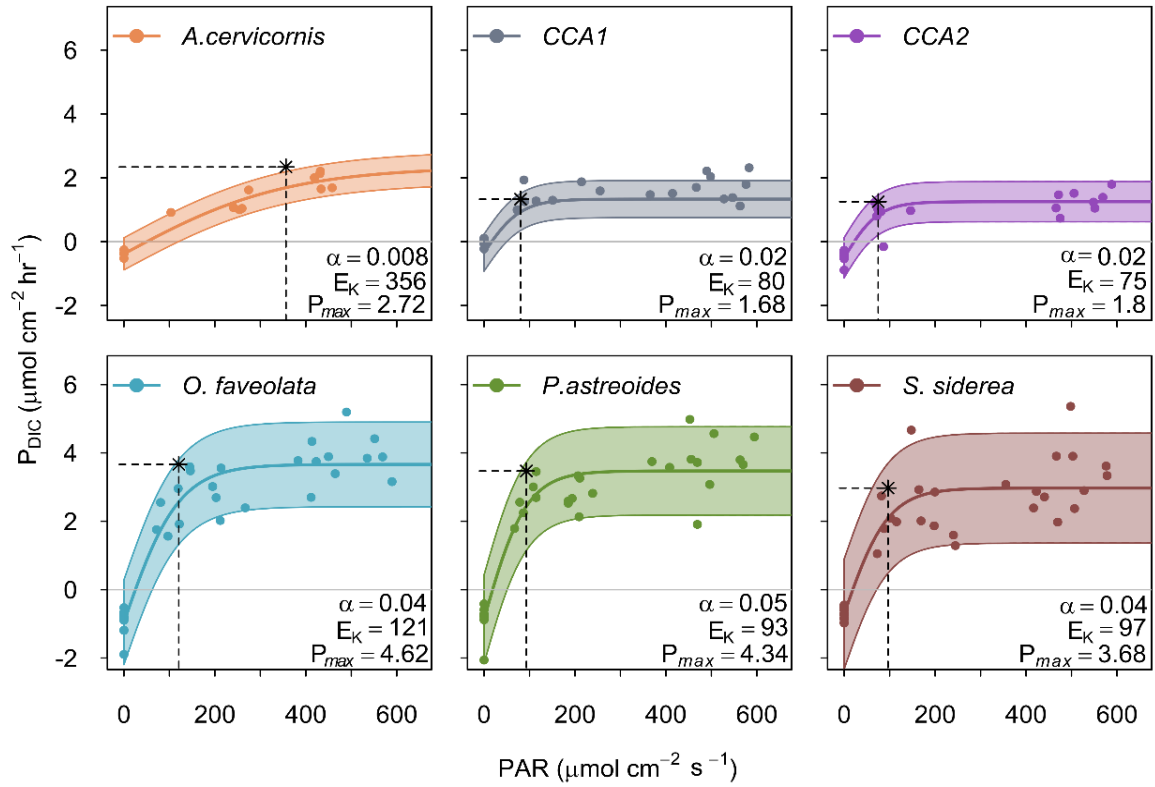
Figure 2-7: Photosynthesis-irradiance curves for; *A. cervicornis*, crustose coralline algae types 1 and 2 (CCA1, CCA2), *O. faveolata*, *P. astreoides,* and *S. siderea*, with photosynthesis measured from changes to dissolved inorganic carbon (P_{DIC}). Shaded areas show 95% confidence intervals around the modelled relationship and points show the measured values. Dashed horizontal/vertical lines show the model coeffients: net maximum photosynthesis (P_{max} - R in µmol cm^{-2} hr^{-1}) and light saturation (E_K, as photosynthetically active radiation (PAR) in µmol s^{-1} m^{-2}).
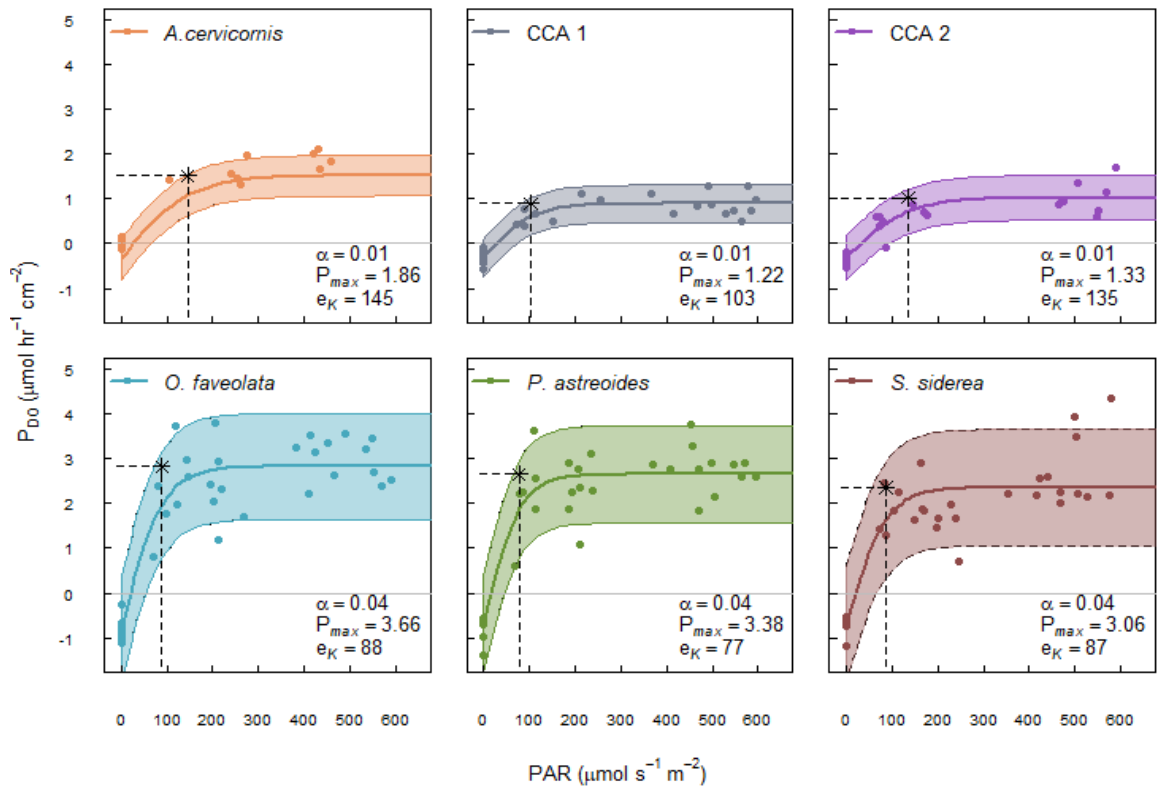
Figure 2-8: Photosynthesis-irradiance curves for; *A. cervicornis*, crustose coralline algae types 1 and 2 (CCA1, CCA2), *O. faveolata*, *P. astreoides,* and *S. siderea*, with photosynthesis measured from changes to dissolved oxygen (P_{DO}). Shaded areas show 95% confidence intervals around the modelled relationship and points show the measured values. Dashed horizontal/vertical lines show the model coeffients: net maximum photosynthesis (P_{max} - R in µmol cm^{-2} hr^{-1}) and light saturation (E_K, as photosynthetically active radiation (PAR) in µmol s^{-1} m^{-2}).
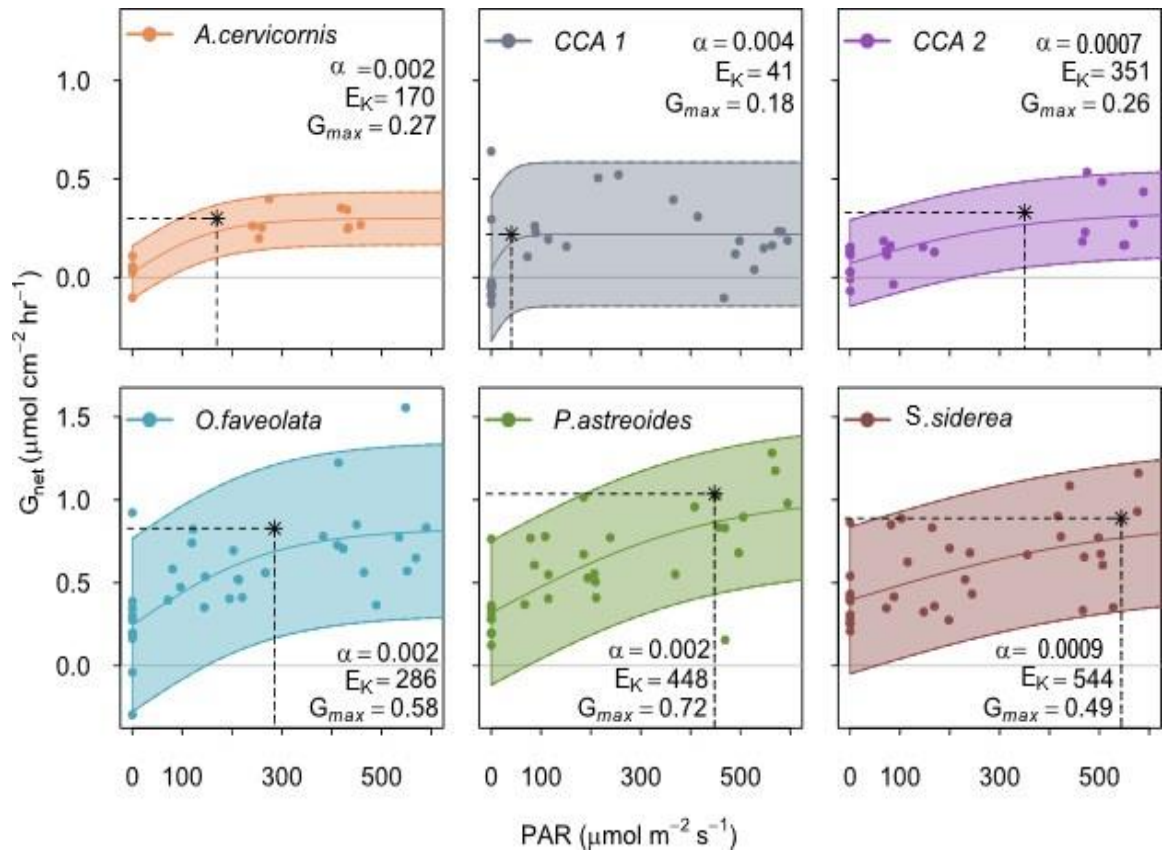
Figure 2-9: Calcification-irradiance curves for; *A. cervicornis*, crustose coralline algae types 1 and 2 (CCA1, CCA2), *O. faveolata*, *P. astreoides,* and *S. siderea.* Points show the measured net rates at distinct photosynthetically active radiation (PAR) light levels, and the solid, coloured lines show the modelled metabolic curve. Shaded areas represent 95% confidence intervals. Dotted vertical lines indicate E_K (light saturation point) and dashed horizonal lines depict maximum gross calcification (G_{max}).

Table 2-7: Metabolic-irradiance model coefficients: maximum photosynthesis (P_{max}), maximum calcification (G_{max}), and initial slope (α), presented with standard error ($\pm$SE) and confidence intervals (CI 2.5% and CI 97.5%). All coefficients were estimated from non-linear least squares fit of Eq. 4, where respiration (R) is the mean dark rate for P_{DO} and P_{DIC}, and G_{dark} is the mean dark calcification rate. Light saturation point (E_K) was calculated from Pmax and α according to Eq. 6.

P_{DO}	P_{max}	CI 2.5%	CI 97.5%	$\pm$SE	p	α	CI2.5%	CI 97.5%	$\pm$SE	p	R or	E_K	σ	RSS	R^2
A. cervicornis	1.86	0.19	0.36	0.10	<0.0001	0.013	-6.63E-04	3.90E-03	0.003	<0.001	-0.34	145	0.23	0.70	0.94
CCA (1)	1.22	0.08	0.27	0.06	<0.0001	0.012	-1.72E-02	2.59E-02	0.002	<0.001	-0.32	103	0.21	1.18	0.88
CCA (2)	1.33	0.05	0.47	0.09	<0.0001	0.010	-2.00E-04	1.67E-03	0.002	<0.001	-0.30	135	0.26	1.50	0.84
O. faveolata	3.66	0.32	0.85	0.15	<0.0001	0.042	5.74E-04	3.51E-03	0.008	<0.001	-0.83	88	0.60	12.40	0.88
P. astreoides	3.38	0.18	1.26	0.13	<0.0001	0.044	6.47E-04	2.55E-03	0.009	<0.001	-0.73	77	0.56	10.49	0.88
S. siderea	3.06	-0.41	1.40	0.16	<0.0001	0.035	1.23E-05	1.80E-03	0.008	<0.001	-0.70	87	0.66	14.91	0.81
P_{DIC}															
A. cervicornis	2.72	1.80	3.64	0.43	<0.0001	0.008	0.01	0.01	0.001	<0.001	-0.38	356	0.26	0.85	0.94
CCA (1)	1.68	1.50	1.85	0.09	<0.0001	0.021	0.01	0.03	0.005	0.0003	-0.35	80	0.30	2.10	0.88
CCA (2)	1.75	1.52	1.99	0.11	<0.0001	0.023	0.01	0.03	0.005	0.0003	-0.50	75	0.32	2.05	0.87
O. faveolata	4.62	4.25	4.98	0.18	<0.0001	0.038	0.03	0.05	0.005	<0.001	-0.95	121	0.63	12.40	0.91
P. astreoides	4.34	3.99	4.69	0.17	<0.0001	0.047	0.03	0.06	0.007	<0.001	-0.87	93	0.66	13.49	0.89
S. siderea	3.68	3.25	4.12	0.21	<0.0001	0.038	0.02	0.06	0.009	0.0001	-0.71	97	0.82	21.54	0.80
G	**G_{max}**										**G_{dark}**				
A. cervicornis	0.27	0.19	0.36	0.04	<0.0001	0.0016	-6.63E-04	3.90E-03	0.0010	**0.148**	0.03	170	0.07	0.06	0.80
CCA (1)	0.18	0.08	0.27	0.05	0.0009	0.0044	-1.72E-02	2.59E-02	0.0105	**0.681**	0.04	41	0.19	0.90	0.18
CCA (2)	0.26	0.05	0.47	0.10	0.0194	0.0007	-2.00E-04	1.67E-03	0.0005	**0.117**	0.07	351	0.11	0.27	0.46
O. faveolata	0.58	0.32	0.85	0.13	<0.0001	0.0020	5.74E-04	3.51E-03	0.0007	0.008	0.24	286	0.27	2.34	0.40
P. astreoides	0.72	0.18	1.26	0.27	0.011	0.0016	6.47E-04	2.55E-03	0.0005	0.002	0.32	448	0.22	1.52	0.49
S. siderea	0.49	-0.41	1.40	0.44	**0.274**	0.0009	1.23E-05	1.80E-03	0.0004	0.047	0.40	544	0.23	1.68	0.26
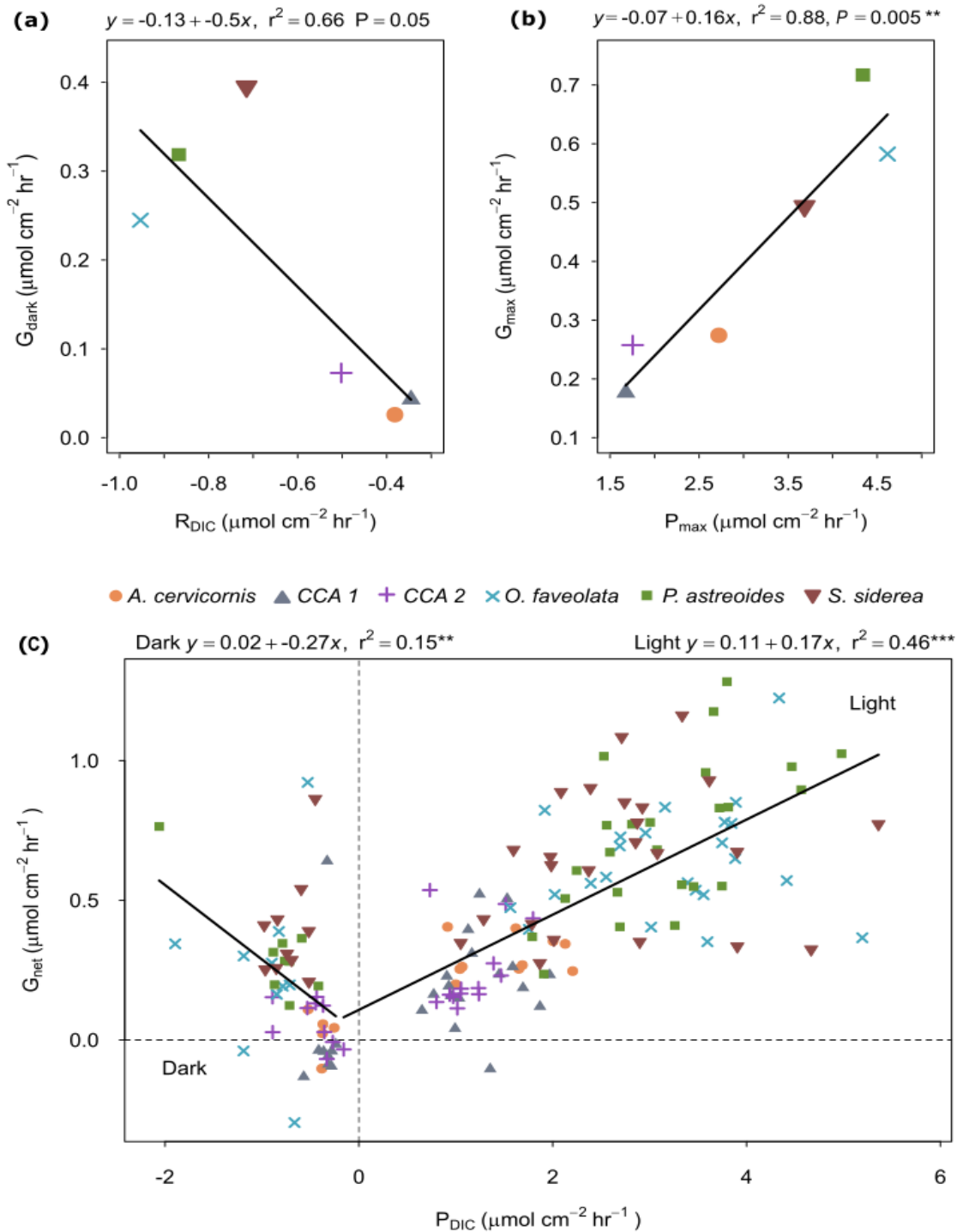
Figure 2-10: Linear relationships between; (a) maximum metabolic rates derived from model coefficients for photosynthesis- and calcification- irradiance curves (P_{max} and G_{max}), (b) mean average respiration (R_{DIC}) and dark calcification (G_{dark}) for each species, and (c) individual measured photosynthesis (P_{DIC}) and calcification (G) rates. Individual species; *A. cervicornis*, crustose coralline algae type 1 (CCA1), crustose coralline algae type 2 (CCA2), *O. faveolata*, *P. astreoides,* and *S. siderea,* are depicted as different colours and symbols (*see* legend).

(a)

(b)
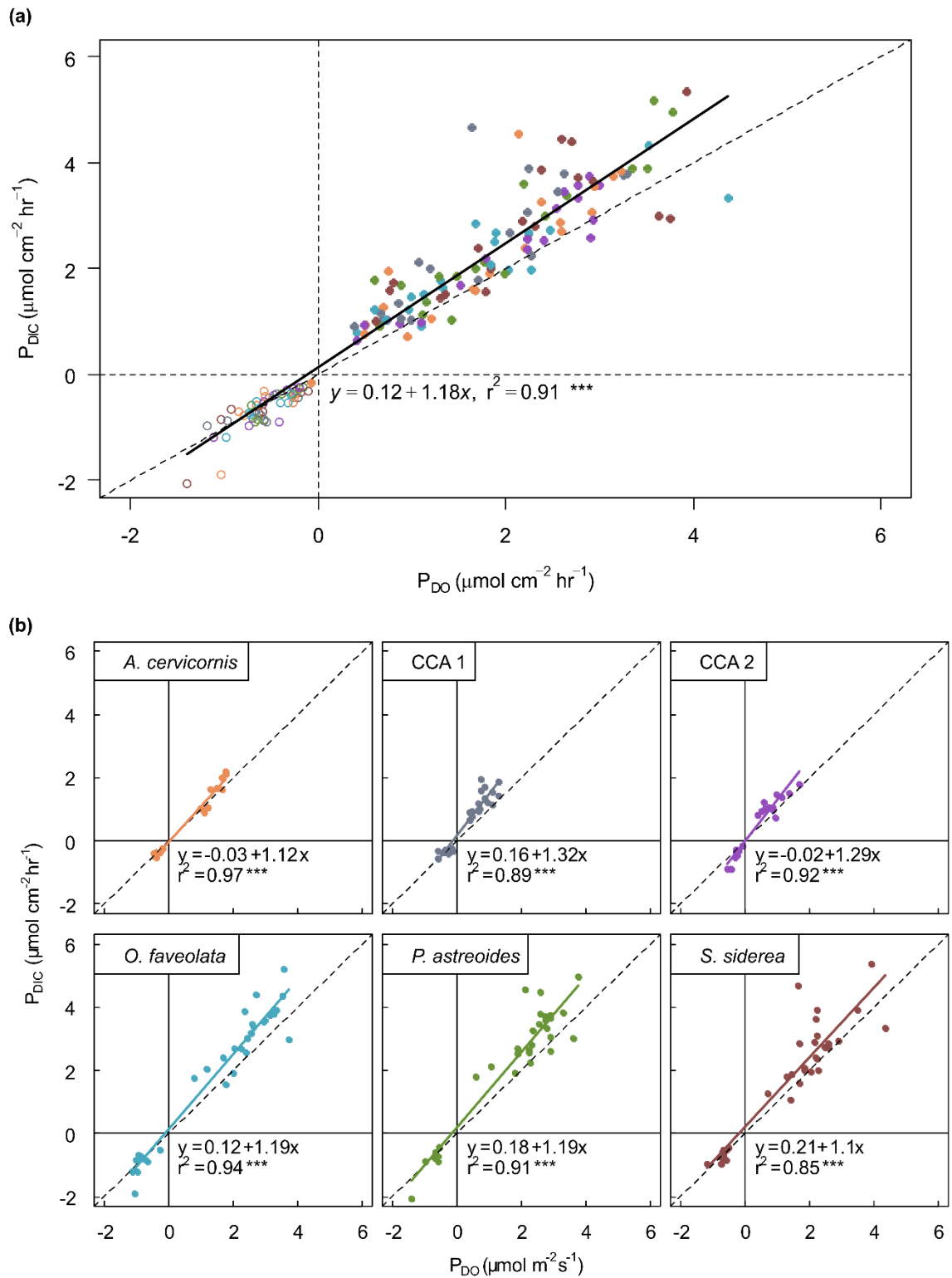
Figure 2-11: Linear models showing strong positive relationship between photosynthesis measured by carbon assimilation (P_{DIC}) and oxygen production (P_{DO}): (a) across species and functional groups, and (b) separated by species. All models were significant to the *p* < 0.001 level (denoted by ***). CCA1 and CCA2 refer to the two types of crustose coralline algae used in this study.
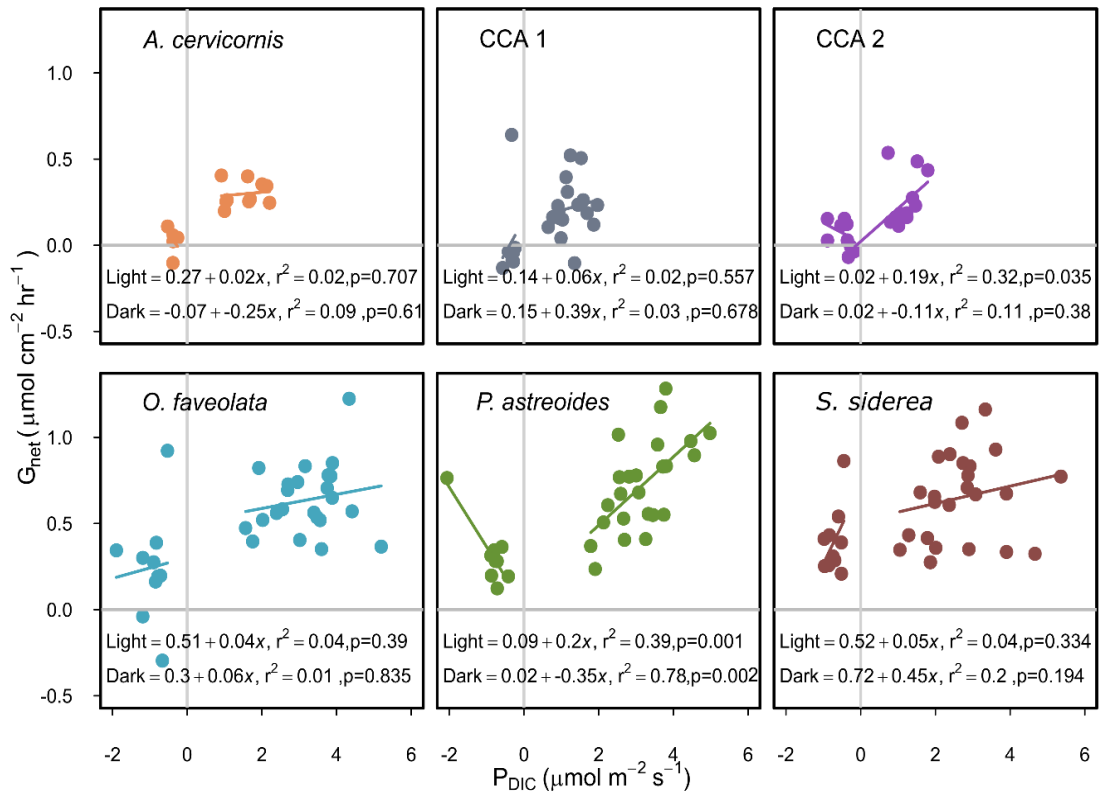
Figure 2-12: Linear relationships between photosynthesis (P_{DIC}) and calcification (G_{net}) for each species incubated in the study; *A. cervicornis*, crustose coralline algae type 1 (CCA1), crustose coralline algae type 2 (CCA2), *O. faveolata, P. astreoides*, and *S. siderea.* Linear equations, R^2 and significance are displayed on each plot. Vertical / horizontal grey lines highlight intercept =0, or night/day. Fitted lines are for dark (left hand side of each plot) and light (right hand side of each plot).

Table 2-8: Mean photosynthetic quotient (PQ), respiratory quotient (RQ), and net metabolic quotient (Q) of carbon to oxygen ratios (e.g., ΔDIC/ΔDO). Ratios presented for each species and for the groups two groups coral and crustose coralline algae (CCA).

Group	Q	±SD	PQ	±SD	RQ	±SD
A. cervicornis	1.10	0.19	1.07	0.16	1.17	0.26
CCA 1	1.55	0.56	1.65	0.43	1.35	0.74
CCA 2	1.55	0.40	1.50	0.44	1.63	0.35
O. faveolata	1.27	0.33	1.29	0.30	1.20	0.42
P. astreoides	1.31	0.43	1.38	0.46	1.14	0.26
S. siderea	1.20	0.41	1.28	0.45	1.03	0.24
Corals	1.24	0.38	1.28	0.39	1.13	0.31
CCA	1.55	0.49	1.58	0.43	1.49	0.58
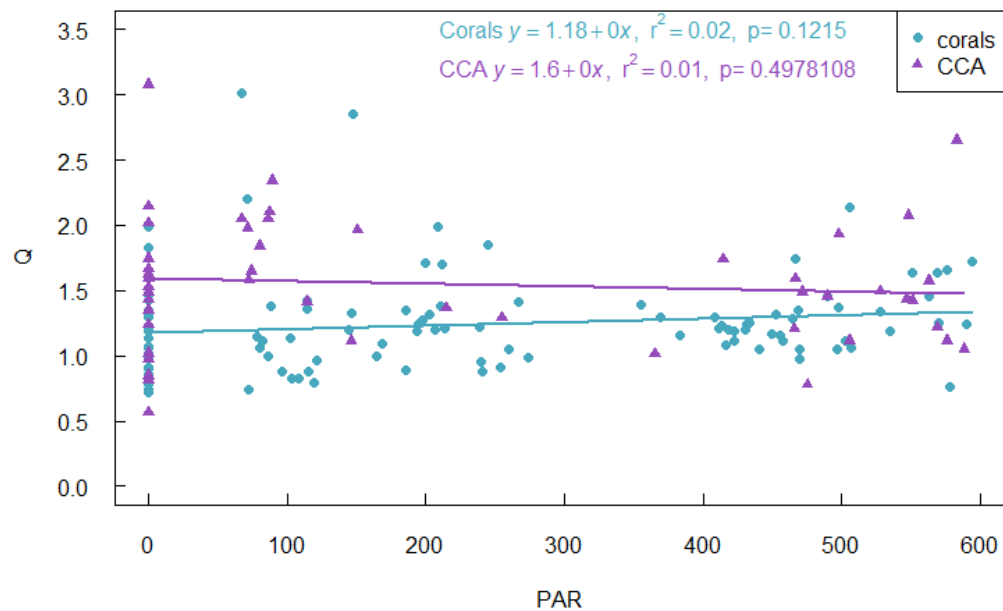
Figure 2-13: The relationship between metabolic quotient (Q) and light for corals and crustose coralline algae (CCA) grouped together. Linear models have low R2 and are nonsignificant, although there is a slight increase in Q with light in the corals.
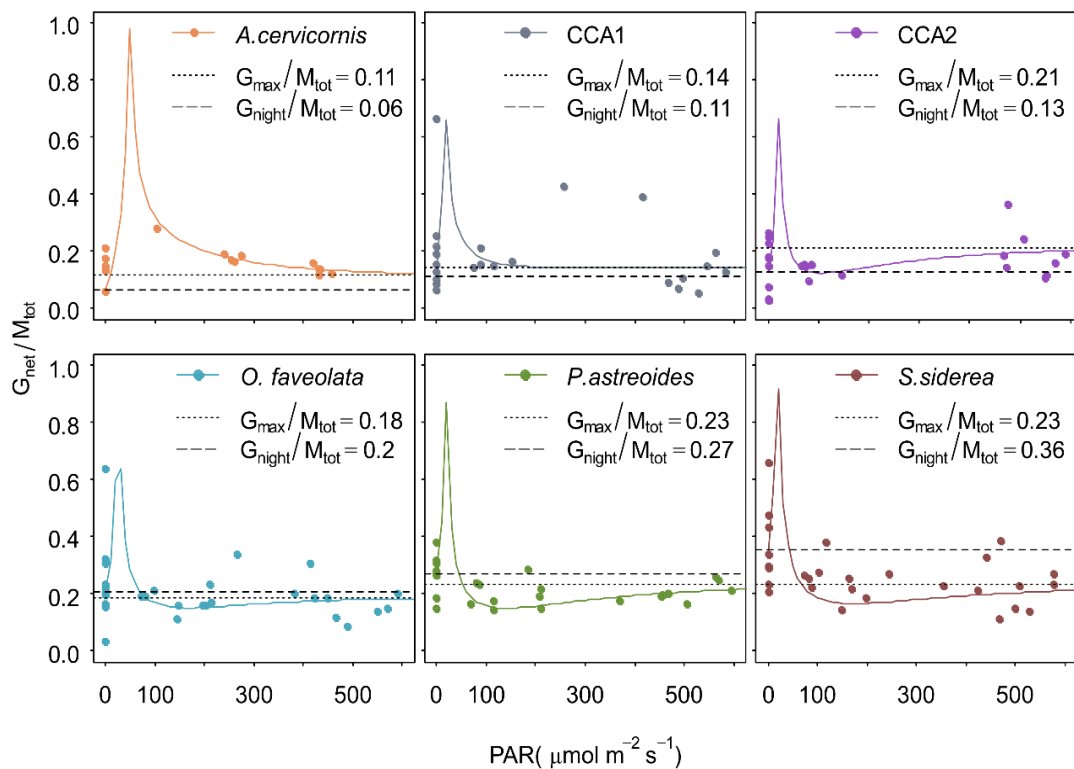
Figure 2-14: Ratios of calcification to total carbon metabolism (G_{net}/M_{tot}) calculated from each incubation (points) and metabolism-irradiance models (curves, coloured by species) plotted against light (PAR). Light and dark mean averages are depicted by dotted and dashed lines, respectively, and values are displayed in the top right of the plot for each species. CCA1 and CCA2 refer to the two types of crustose coralline algae used in this study.

2.5 Discussion

This study aimed to determine the relationships between production, calcification, and light in a variety of calcifying coral reef organisms from the Caribbean. Differences were found in metabolism between morning, afternoon, and night incubations and were species-specific, however linearity between metabolic-irradiance model coefficients demonstrated that photosynthesis and calcification are correlated across species (Fig. 2-10). The results from this study confirm that production and calcification rates of tropical benthic calcifiers exhibit a hyperbolic response to diurnal light cycles (Chalker and Taylor 1978; Cohen et al. 2016). Our analyses revisit the current understanding of relationships between organismal-level metabolism and irradiance in benthic coral reef calcifiers, and we interpret these findings in the context of ecosystem scale estimates of metabolism and predicted changes due to ongoing anthropogenic change.

2.5.1 Species-specific differences in metabolic rates

From the results of the incubations, three general groupings were apparent: (1) massive coral species *O. faveolata, P. astreoides* and *S. siderea*, (2) *A. cervicornis,* and (3) crustose coralline algae. The highest metabolic rates were observed in massive coral species under all conditions (Figs. 2-4, 2- 4). The metabolic rates of *A. cervicornis* and crustose coralline algae were relatively similar, but they were grouped separately due to distinctions between the mechanisms by which coralline algae and corals calcify, and to reflect differences in the ecosystem function they provide. We discuss differences and similarities between the three groups in relation to their ecological function below.

Metabolic rates were highest in the massive corals; demonstrating that per area of live tissue, they produce more oxygen and calcium carbonate. Despite their higher metabolic rates, it is unlikely that massive corals potentially have a stronger influence on community metabolism than branching *A. cervicornis* and encrusting crustose coralline algae because of the relative benthic cover and architectural complexity of each species. Given the distinct ecological function and life-history traits within the massive coral grouping (Darling et al. 2012), the similarity in their metabolic rates was unexpected. *P. astreoides* is considered a weedy species of the Caribbean due to its fast growth, low-relief morphology, and ability to thrive in suboptimal conditions, whereas

O. faveolata and *S. siderea* are key, framework-building corals (Darling et al. 2012). As Caribbean benthic communities undergo phase shifts, *P. astreoides* is colonising space once dominated by massive, framework building corals to become one of the most abundant scleractinian corals on Caribbean coral reefs (Green et al. 2008). Our results show that the contribution of *P. astreoides* to community reef metabolism is at the same scale as that of traditional reef-building corals, however, the similarity in biogeochemical signal does not confer the same ecological traits, as *P. astreoides* does not provide habitat or architectural complexity to the reef (Green et al., 2008). Therefore, while shifts toward weedy species dominance may not be detectable via changes in reef metabolism, the changes to benthic composition will still impact reef carbon cycles and accretion through changes in calcium carbonate morphology and composition (Perry and Alvarez-Filip, 2018). The third massive coral, *S. siderea*, is generally considered a slow-growing species. However, its calcification rates were also high, and the observed slow growth despite high calcification rates could be related to the high density of *S. siderea* skeletons (Hughes 1987).

Fast-growing *A. cervicornis* had the lowest calcification rates of the corals in this study, but they can also have relatively lower skeletal densities than the massive corals (Kuffner et al. 2017). Historically, *A. cervicornis* was a primary reef-building coral species and occupied more space on shallow water tropical reefs in the Caribbean than any other scleractinian coral (Rodríguez-Martínez et al. 2014; Toth et al. 2019), however, it and *Acropora palmata* have declined by over 80% over recent decades in the Caribbean (Jackson, 2014; Rodríguez-Martínez et al., 2014). It is possible that the lower rates of calcification observed in *A. cervicornis* were influenced by the relatively low flow induced within the mesocosm setting, as higher wave action may stimulate growth in this species (Jokiel 1978), however, our calcification rates agree with previous estimates (Chalker and Taylor 1975, 1978). Colonies of *A. cervicornis* have a complex, branching structure with high surface area and they contribute different ecosystem functions compared to massive corals (Alvarez-Filip et al. 2011; Darling et al. 2012), which is reflected in the lower metabolic rates observed in our study. In general, *A. cervicornis* has low calcification yet high accretion rates, although skeletal density shows plasticity based on growing conditions (Kuffner et al. 2017). The life-history trait of lower density skeletons could promote asexual reproduction when high energy wave action fragments branches of larger colonies, allowing for the rapid proliferation of *Acropora* spp. (Tunnicliffe 1981; Lirman 2000). Despite having lower calcification rates than the massive corals, *A. cervicornis* provides a unique habitat for

the biodiversity of species which reside in the dense thickets formed by this branching coral (Tunnicliffe 1981; Precht et al. 2002).

The lowest metabolic rates were recorded for crustose coralline algae; biogenic calcifiers which reinforce and strengthen the calcium carbonate matrix to cover otherwise exposed coral skeleton (Littler and Littler 2013). Additionally, they promote calcification by scleractinian corals (Chisholm 2000) via inducing larval settlement and providing substrate for juvenile corals to grow (Heyward and Negri 1999). Due to their encrusting morphology, crustose coralline algae are often overlooked in quantification of coral reef calcification and accretion. We report rates of calcification and photosynthesis in crustose coralline algae in line with framework building *A. cervicornis* (Figs. 2-4, 2-5). This demonstrates the important contribution that crustose coralline algae can play in coral reef ecosystem metabolism beyond their other ecological functions. The two crustose coralline algal types were the closest to displaying net dissolution, indicating calcification slows or stops at night within this functional group, potentially due to dependence on light. Crustose coralline algae are expected to be more heavily impacted by ocean acidification than corals due to the higher proportion of magnesium-calcite in their skeletons, which could disproportionately impact the role of these organisms as important benthic calcifiers (Diaz-Pulido et al. 2012).

2.5.2 Impact of Light on Species-specific Metabolism

Coral reefs encompass diverse and dynamic light environments over hourly, daily, and seasonal scales (Edmunds et al. 2018). However, most reef-wide estimates of community metabolism are conducted on timescales that do not incorporate instantaneous changes in light, even though community metabolism can change on sub-hourly timescales (Takeshita et al. 2016). Applying metabolic-light models to high-resolution time series of light could provide more complete estimates of community level metabolism. Studies have shown that scaling up to community and ecosystem levels from organismal studies can be complicated in coral reef ecosystems (e.g., Edmunds et al. 2016), however, the comparisons in our study add important insight into coral reef metabolism research. In this study, net metabolic rates (both photosynthesis and calcification) fit a commonly used hyperbolic function with light (Figs. 2-7 to 2-9)

(Jassby and Platt 1976), supporting the idea that both photosynthesis and calcification are driven by light (Falkowski et al. 1984; Cohen et al. 2016).

Photosynthesis-irradiance models fitted with both oxygen and carbon data sets (e.g., P_{DO} and P_{DIC}) demonstrated that photosynthetic efficiency (α), modelled maxima (P_{max}), and average respiration were greatest in the massive corals, highlighting that these species are drivers of coral reef production (Figs. 2-7, 2-8). Light saturation (E_K) was higher in *A. cervicornis* and crustose coralline algae, potentially reflecting their ability to thrive in the shallowest and most sunlit areas of the reef (i.e., lagoon and crest). For calcification-irradiance models, massive species had the highest maximum and night rates (G_{max} and G_{dark}), while estimates of photosynthetic efficiency (α) were mixed across species. The differences between metabolic-light models support previous work showing that photosynthesis and calcification have species-specific independent relationships with light (Gattuso et al. 2000; Sawall et al. 2018).

Relationships between photosynthesis, respiration, and calcification have been shown to exist across a wide range of marine calcifiers, and in the current study we demonstrate that a strong relationship exists across different species, genera, and functional groups (Fig. 2-10). The strong positive linear relationship between maximum calcification and photosynthesis indicates that maximum net daytime photosynthesis and calcification rates are linked (Fig. 2-10b). We also found a strong negative linear relationship between average respiration and dark calcification across all species at night, indicating that dark calcification is linked to energy produced from respiration (Fig. 2-10a). Linear relationships also existed during the day and night for measured values of calcification and photosynthesis across all species (light $R^2 = 0.47$, $p < 0.0005$, dark $R^2 = 0.15$, $p = 0.005$; Fig. 2-10c). However, relationships between calcification and photosynthesis were less clear for each individual species (Fig. 2-12). This could be due to lower replicates within each species and smaller ranges in dark rates that made it difficult to detect a clear relationship by species. While our study shows that photosynthesis and calcification are linked across benthic calcifiers, we also saw differences at the species level (Fig. 2-12), likely related to ecological function (González-Barrios and Álvarez-Filip 2018). For example, *P. astreoides* has a strong linear relationship between calcification and photosynthesis (light $R^2 = 0.39$, dark $R^2 = 0.78$, p=<005, Fig. 2-12), whereas other species such as *A. cervicornis* did not. Calcification of different species of corals have been shown to respond to global change differently (Kornder et al. 2018), which may reflect the interaction of these two

processes at the cellular or organismal level. Light modulates the response of calcification to ocean acidification (Suggett et al. 2013) therefore, developing species level metabolic irradiance curves is important for understanding future impacts of global change.

The functional relationship between light, photosynthesis, and calcification is complex and operates at multiple levels (Allemand et al. 2011). We demonstrate a positive linear relationship between modelled metabolic maxima (G_{max} and P_{max}), indicating that energy from photosynthesis and respiration drive calcification. It is clear that coral metabolic processes are tightly coupled (Gattuso et al., 1999). However, recent research indicates that photosynthesis and calcification are parallel but independent light-driven processes (Cohen et al., 2016). The link between photosynthesis and calcification (i.e., light-enhanced calcification) at the organismal scale may be related to these processes co-evolving to occur at similar times due to increased energy supply for calcification (Sorek et al. 2014). If that is the case, then the relationships between photosynthesis and calcification found at the organismal level may not be as intimately linked within cells. Further research is needed to define the functional relationships between light, photosynthesis, and calcification from the cell to the organism to better predict the impacts of global change on coral ecosystems.

Knowing instantaneous relationships between light and metabolism at the organismal scale (e.g., Figs. 2-7 to 2-9) could help scale metabolism rates up to the community and ecosystem at finer temporal scales. Direct measurements of coral reef net ecosystem metabolic rates are time consuming, expensive, and often require specific environmental conditions (Gattuso et al., 1999). Newer technology is being developed that can estimate community benthic metabolism rates over high-resolution temporal scales (<1hr) using boundary layer techniques (i.e., eddy correlation and BEAMS) that measure oxygen and pH (Barnes and Devereux 1984; Long et al. 2013; Takeshita et al. 2016). These techniques require that we know the ratio of carbon and oxygen uptake and removal during the processes of photosynthesis and respiration (e.g., $\Delta DIC / \Delta DO$). For an organism, these values are known as the net photosynthetic and respiratory quotients, or PQ and RQ respectively, and net metabolic quotient, Q, on a community or ecosystem wide scale (Barnes and Devereaux, 1984; Takeshita et al., 2016). By measuring both oxygen and carbon fluxes we were able to determine the net metabolic quotient for the different species in this study (Fig. 2-11). The metabolic quotient was higher for crustose coralline algae (1.55 ± 0.49) than coral species ($1.24 \pm$

0.38), which reflects elevated carbon assimilation to oxygen production. For corals, the metabolic quotient was similar across species (1.1-1.2), and closer to a 1:1 ratio, although the values still indicated a greater assimilation of dissolved inorganic carbon compared to dissolved oxygen production. Overall, the metabolic quotient Q was 1.18 for all species and incubations combined. Interestingly, there was a trend of increasing metabolic quotient with light when all corals were grouped together, indicating that the metabolic quotient may be more variable over short time scales than previously assumed (Fig. 2-13). Further understanding the influence of light on the balance of assimilation of dissolved inorganic carbon to dissolved oxygen production will help to build our understanding of the reef metabolic quotient and how it changes under distinct light levels. More estimates of species-specific metabolic quotients for coral reef organisms will help in efforts aimed at using readily available pH and oxygen sensors to monitor the metabolism of coral communities at a greater resolution in both space and time.

2.5.3 Ratios of Organic and Inorganic Carbon Cycling in Coral Reef Organisms

Ratios of net calcification to photosynthesis (G_{net}/P_{net}) quantify the relative balance between these two processes and have been proposed to be a useful metric for reef biogeochemical function and health (Cyronak et al., 2018). Previous studies have shown that calcification / photosynthesis ranges from -8 to 17 on the organismal scale and from 0 to 0.7 on an ecosystem scale (Gattuso et al., 1999; Cyronak et al., 2018). In this study, we calculated absolute ratios of net calcification to the sum of net calcification and net photosynthesis (G_{net}/M_{tot}) according to Eq. 7. We chose this metric because both calcification and production can be negative, which results in unreliable values as either the denominator or numerator approach 0. Also, G_{net}/M_{tot} is more intuitive than G_{net}/P_{net} as it represents the relative proportion of total carbon metabolism due to calcification and ranges between 0 to 1. Over the course of the incubations G_{net}/M_{tot} ranged from 0.03 to 0.66, which indicates that when both calcification and production are occurring production tends to dominate (Fig. 10). However, when the ratios were calculated using the metabolism-irradiance curves, G_{net}/M_{tot} ranged from 0 to 1 and all organisms exhibited a strong peak at the irradiance level where net photosynthesis crosses 0. This is because as net photosynthesis approaches 0 the

absolute ratio comes closer to $|G_{net}|/|G_{net}|$. Ratios calculated using the model coefficients for maximum calcification and photosynthesis (G_{max}/M_{tot}), i.e., G_{max} and P_{max} and night calcification to respiration (G_{dark}/M_{tot}) ranged from 0.11 to 0.23 and 0.06 to 0.36, respectively (Fig. 2-14). The daily changes in G_{net}/M_{tot} indicate that there is not one value that can readily describe the relative ratio of calcification and production for each calcifying organism, and that organisms can equilibrate to very different values during the day and night. In fact, the highly dynamic nature of G_{net}/M_{tot} related to light brings into question the use of G_{net}/P_{net} ratios as a single, determinant value of reef function and health at the ecosystem scale (Cyronak et al., 2018). If G_{net}/M_{tot} do not stabilize to one consistent value on an organismal scale, it is difficult to imagine that these ratios stabilize across reef communities and ecosystems made up of many calcifying and non-calcifying organisms. Future work into determining the importance of G_{net}/M_{tot} as a metric for reef biogeochemical cycling is needed.

2.5.4 Conclusions

We identified patterns in the metabolism of six Caribbean benthic calcifiers under natural diurnal light cycles. Our findings support previous work showing that photosynthesis and calcification are parallel processes driven by irradiance (Gattuso et al., 2000; Cohen et al., 2016), highlighting the importance of considering natural variations in light. Some metabolic rates of individual species could be generalized to larger categorical groupings such as the 'massive coral' species. However, both *A. cervicornis* and crustose coralline algae had similar metabolic rates despite occupying very different functional niches in coral reef accretion. While calcification and photosynthesis both fit traditional hyperbolic tangent functions with light, coefficients of the metabolism-irradiance models varied between species. Interestingly, the modelled metabolic maxima (G_{max} and P_{max}) and dark calcification / respiration (G_{dark} and R) were correlated across all photosynthesising calcifiers in this study. These correlations indicate that energy provided by photosynthesis and respiration may be an important control on organismal calcification, however, mechanistic studies are needed to further address this. Understanding the dynamic species-specific balance of calcification and production could provide useful insights into estimates of community- and reef-wide carbon cycles. For example, our results demonstrate that benthic surveys with simple groupings of calcifying and non-calcifying organisms could give important

insights into coral reef carbon cycles. Finally, we establish dynamic relationships between calcification and photosynthesis over diurnal light cycles that bring into question the application of calcification / photosynthesis ratios to monitor biogeochemical function on an ecosystem scale. Overall, the carbon cycle of coral reefs is highly dynamic at the organismal scale, driven by complex relationships between photosynthesis, respiration, calcification, and light. These relationships likely scale up and interact with local hydrodynamics to create the intense variations in carbon chemistry observed on coral reefs.

3   A low-cost benthic incubation chamber for in-situ community metabolism measurements

All data collected and analysed by thesis author.

3.1 Abstract

Benthic incubation chambers facilitate in-situ metabolism studies in shallow water environments. They are used to isolate the water surrounding a study organism or community so that changes in water chemistry can be quantified to characterise physiological processes such as photosynthesis, respiration, and calcification. Such field measurements capture the biological processes taking place within the benthic community while incorporating the influence of environmental variables that are often difficult to recreate in ex-situ settings. Variations in benthic chamber designs have evolved for a range of applications. In this study, we built upon current designs to create a novel chamber, which is (1) low-cost and assembled without specialised equipment, (2) easily reproducible, (3) minimally invasive, (4) adaptable to varied substrates, and (5) comparable with other available designs in performance. We tested the design in the laboratory and field and found that it achieved the outlined objectives. Using non-specialised materials, we were able to construct the chamber at a low cost (under $20 USD per unit), while maintaining similar performance and reproducibility with that of existing designs. Laboratory and field tests demonstrated minimal leakage (2.08 ± 0.78 % water exchange over 4 hours) and acceptable light transmission (86.9 ± 1.9 %), results comparable to those reported for other chambers. In the field, chambers were deployed in a shallow coastal environment in Akumal, Mexico, to measure productivity of (a) seagrass, and (b) coral-, algae-, and sand-dominated reef patches. In both case studies, production rates aligned with those of comparable benthic chamber deployments in the literature and followed established trends with light, the primary driver of benthic metabolism, indicating robust performance under field conditions. We demonstrate that our low-cost benthic chamber design uses locally accessible and minimal resources, is adaptable for a variety of field settings, and can be used to collect

reliable and repeatable benthic metabolism data. This chamber has the potential to broaden accessibility and applications of in-situ incubations for future studies.

3.2   Introduction

Quantifying the relative balance of autotrophic and heterotrophic processes taking place within a benthic community provides insight into ecosystem functioning and species composition (Albright et al. 2015; Cyronak et al. 2018). As coastal ecosystems undergo degradation, understanding ecosystem capacity for oxygen production and carbon cycling through photosynthesis is critical. For example, defining ecosystem productivity can support conservation of high 'blue carbon value' ecosystems (Duarte et al. 2010, 2013c) and characterisation of community metabolism facilitates geographical and temporal comparisons of ecological function, which otherwise might be logistically limited (Cyronak et al. 2018; Lange et al. 2020). Measurements of in-situ community metabolism capture individual rates of productivity for functional groups and species, as well as the interactive physiological processes taking place within the entire benthic community, rather than the simplified, reconstructed communities often used in ex-situ measurements. Such measures offer important insight into the critical role of coastal marine ecosystems for carbon capture and cycling.

Rates of photosynthesis and respiration can be measured directly from fluxes in dissolved oxygen concentrations to calculate the net community productivity (NCP) taking place within a benthic community. The development of in-situ gear to incubate benthic organisms and communities has been guided by distinct research applications. Ecosystem metabolism can be measured via three main approaches in the field; benthic boundary layer and eddy covariance (e.g., (Long et al. 2015b; Takeshita et al. 2016; Berg et al. 2022), flow respirometry using Lagrangian and Eularian adaptations (e.g., Barnes 1983; Falter et al. 2008; Shaw et al. 2014), and enclosed incubations (see examples in Table 1). This study focusses on the incubation method as a straightforward approach for deriving metabolic rates of single organisms or benthic communities in the field.

Benthic chambers can be deployed in the field to contain sediments, corals, seagrasses, and other biota, either as communities or as individual organisms, for

periods of hours to days to capture in-situ measurements of community or organismal metabolic rates (e.g. Huettel and Gust 1992; Yates and Halley 2003; Murphy et al. 2012; Camp et al. 2015; van Heuven et al. 2018; Roth et al. 2019). Standard benthic chamber designs consist of a tent or dome made from a rigid, transparent container with a circulation pump (to mimic natural water flow), and a sampling port (e.g., Roth et al., 2019, Table 1). Some chambers can only be deployed in areas where substrate is suitable for the chamber base to be inserted, for example, often the base must be buried in sand or sediments to create an effective seal (e.g., Olivé et al. 2016). However, the technology has evolved to encompass a range of applications from smaller, single organism chambers to larger community enclosures (Table 1). For example, high precision, real-time, in-situ metabolism measurements of small surface areas of coral have been made possible by the development of a high-tech adaptation of the benthic chamber concept: the Coral In Situ Metabolism and Energetics (CISME) system, described in Murphy et al. (2012). CISME is a specialised underwater respirometer that incubates small areas (~ 24.5 cm^2) of live coral to measure pH, dissolved oxygen, and temperature changes. The electronic housing has waterproof cables supplying power, a recirculation pump, and LED control, while a water sample loop holds incubation samples so that total alkalinity can be used to derive calcification rates.

At the opposite end of the size-spectrum, large tent-like structures have been developed to incubate entire patches of benthic communities (surface areas of several m^2). For example, the Submersible Habitat for Analysing Reef Quality (SHARQ) developed by Yates and Halley (2003) and other large tent enclosures such as the one described by van Heuven et al. (2018), allow for measurements of seawater chemistry and can even be adapted for in-situ experiments adding CO_2 or other treatments, e.g., Kline et al., (2012). The SHARQ and similar chamber designs (e.g., van Heuven et al. 2018) incorporate a submersible circulation pump to ensure turbulent flow within the incubated area. Flow is a primary driver of benthic metabolism and regulates organism response to environmental effects such as ocean acidification (Comeau et al. 2014, 2019). The costs of building such chambers are moderate to high, and multiple replicate chambers for parallel incubations further raise the costs, while specialised materials may be difficult to source in some parts of the world where coral reefs and seagrasses are most abundant. Submersible pumps, bespoke parts, and other expensive materials create an economic barrier to the in-situ incubation chamber technique. To address these limitations, the Flexi-chamber, developed by Camp et al. (2015), requires minimal specialised materials and can be constructed at a low cost (< USD $20). The

Flexi-chamber is made of a flexible plastic bag with a sampling valve installed, which is attached to the base of the study organism with a cable tie. Both the bag and valve were sourced from a medical supply store. The Flexi-chamber can be used to measure metabolism for single organisms, and it is ideal for branching corals, or organisms with complex morphological formations. The Flexi-chamber was robustly tested in the laboratory and field and performed in line with other incubation chamber designs (Camp et al. 2015). However, the chamber can only be used on substrates suitable for a cable tie attachment. For flatter substrates, a domed benthic chamber design is more effective. The medium size chamber by Roth et al. (2019) can be placed over the substrate and was successfully produced at a lower cost (~ $250 USD) than previous designs, while maintaining the efficiency and precision of more expensive equipment. However, the design requires a bespoke rigid acrylic cylinder and a circulation pump to recreate water movement inside the chamber, incurring a higher cost.

To contribute to the array of chambers currently available for field incubations, we designed a chamber prototype, which was both low cost and suitable for deployment on complex substrates incorporating small benthic communities to accurately measure community metabolism. Our objectives were to design a benthic chamber that is; (1) low cost and easily constructed without specialised equipment, (2) reproducible for scientific soundness, (3) minimally invasive to reduce any impact on incubated organisms, (4) adaptable for use in a range of substrate types and underwater environments, and (5) comparable with other chamber designs such as those described in Table 1.

Table 3-1: Summary of selected designs of in situ benthic chambers for measuring coral reef metabolism, since 2000

	Name	Scale	Cost USD	Leakage	Light	Strengths	Limitations
	Coral In-Situ Metabolism and Energetics (CISME) (e.g., Romanó de Orte et al. 2021)	< 1 individual	$32,000	Unreported, expected minimal	0% (Artificial light)	High accuracy and precision. Instantaneous measurements	Expensive and specialised. Very small areas can be incubated (24.5 cm^2).
	Flexi-Chamber (Camp et al. 2015)	Single	< $20	None-to-minimal	84%	Low-cost and easily sourced materials. Flexible material maintains water movement.	Cable tie closure around the base is not suitable for all benthic organisms.
	Flexi-community benthic chamber for remote locations, *this study*	Single small community	<$20	2% over 4 hours	89%	Low-cost, easily sourced materials. Adaptable design. Flexible material maintains water movement.	Under some conditions seal is not as reliable as other methods.
	In-situ chambers for measuring biogeochemical fluxes (E.g., Roth et al. 2019)	Single small community	~$250	5.3% within 6 hr (reef sands) 12.4% within 6 hr (rocky)	92%	Can be deployed on hard substrate or sediments.	Requires circulation pump. Bespoke design requires specific materials.
	Submersible Habitat for Analyzing Reef Quality (SHARQ) (Yates & Halley 2003)	Larger communities (~12 m^2 planar surface area)	Not reported	Variable depending on substrate type	>71%	Can incubate entire communities.	Requires circulation pump. Bespoke design requires specific materials.

3.3 Materials and Methods

3.3.1 Study location

Experiments were carried out in the School of Geographical and Earth Sciences Laboratory at the University of Glasgow, the Scottish Centre for Ecology and the Natural Environment (SCENE) fieldwork site, and in Akumal Bay Natural Refuge Area, Mexico. SCENE is located on the eastern shore of Loch Lomond in west central Scotland (56°07'41.1" N, 4°36'48.4" W). Akumal is a small coastal town on the Caribbean coast of the Yucatan peninsula, with relatively limited access to specialised materials. The Natural Refuge of Akumal Bay (20°23'42.2" N, 87°18'49.8" W) is a protected area within the Mexican Caribbean Biosphere Reserve and consists of a semi-enclosed lagoon with patches of seagrass and coral ecosystems (Fig 3-1a). Field experiments in Akumal were approved by the Comisión Nacional de Áreas Naturales Protegidas (CONANP F009.DRBCM/240/2019).

3.3.2 Chamber design, materials, construction, and costs

The benthic chamber design consists of three key components: (1) a water-tight polyethylene tent, (2) a sampling valve, and (3) a heavy yet malleable circular base for maintaining the tent enclosure seal against the substrate (Fig. 3-1, Table 3-2). The tent is made from a polyethylene plastic bag. It is possible to keep the shape of the plastic bag intact, by simply cutting in a straight line at the bottom of the bag for the desired height, allowing an extra 10 – 15 cm at the bottom to allow the circular malleable base to sit on top. Alternatively, a polyethylene bag or sheet can be cut and re-sealed using a heat sealer into any desired enclosure shape, e.g., dome or pyramid. For case study 1 the bottom of the bag was folded to create a 'skirt' for the base to sit on. In case study 2 a dome shaped benthic chamber was used (Fig 3-1b, e), which was made by cutting the polyethylene bag into panels and re-sealing using a heat sealer. We used a food packaging heat sealer to join the panels. The valve was inserted by creating a small incision in the enclosure tent and inserting one valve on the inside and securing it with the Luer lock connector of a second valve on the inside. A small bicycle tube repair patch was used to create a solid base for the valve to be inserted through. For the base, bicycle inner tubes were filled with sand and fishing weights to create a heavy,

malleable base, and re-sealed using bicycle tyre repair kits found at a local hardware store. All materials to build the chamber were sourced locally. Transparent polyethylene for the tent enclosure was bought from a local food packaging company, Luer-lock valves were sourced in the local pharmacy and pre-used bicycle tyre inner tubes were donated by the local community. The materials used and their associated costs are summarised in Table 3-2.
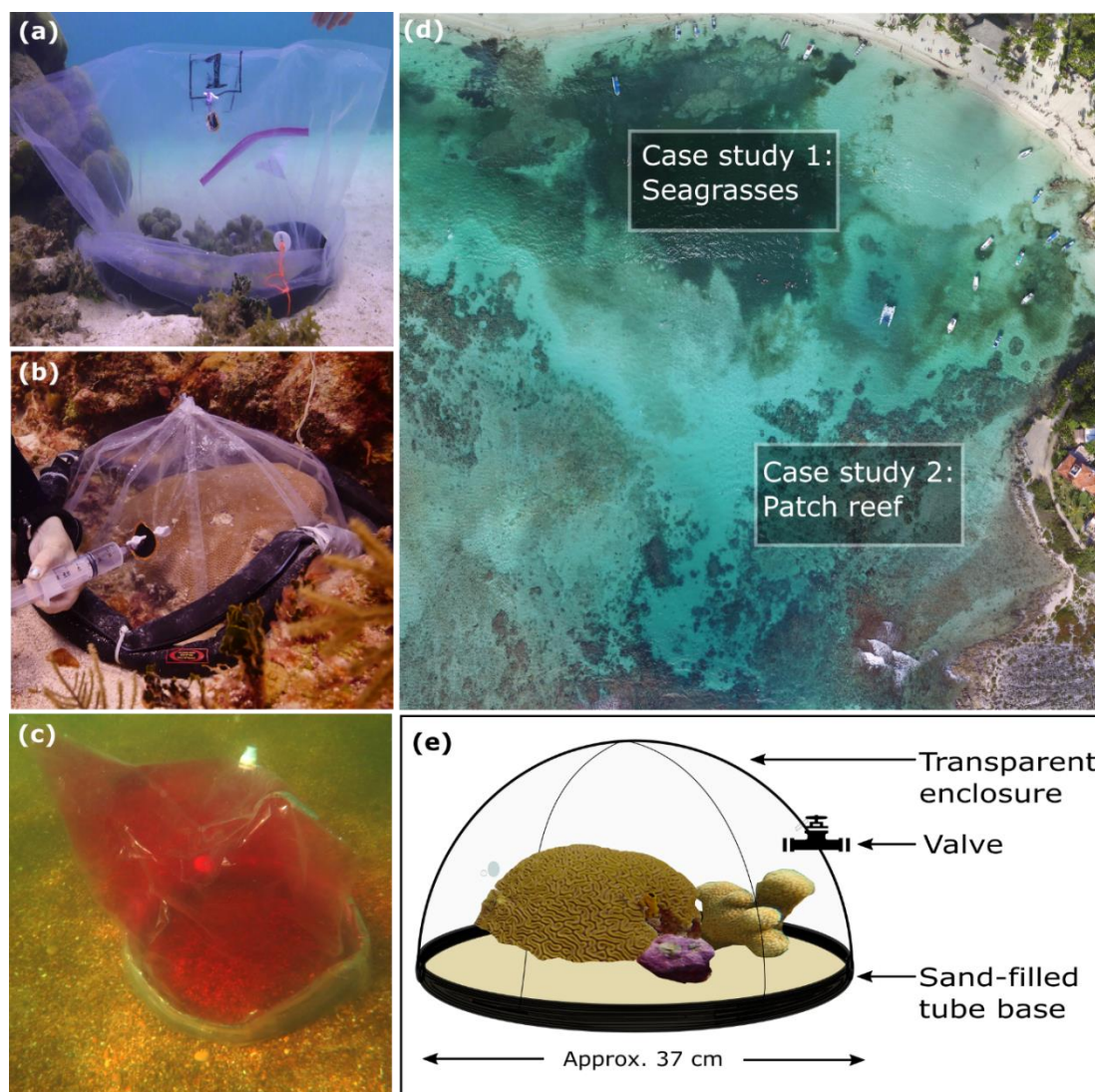
Figure 3-1 : Visual summary of field deployed benthic chambers for case studies 1 and 2. Photographs depicting: **(a)** tall version of the chamber constructed using the unchanged plastic bag; **(b)** low-profile chamber created by cutting the plastic bag into panels and heat sealing in a dome form, for use in high-energy environments**; (c)** visual assessment of leakage and mixing from the chamber using dispersal of red food dye injected into the chamber; **(d)** aerial image taken above Akumal Bay showing the sites where chambers were deployed for case studies, photo credit: Edgar Escalante Mancera and Miguel Ángel Gómez Reali; and **(e)** a schematic diagram of the chamber prototype developed.

Table 3-2: Summary of key chamber design components.

	Key features	Materials and costs (USD)	Adaptations
Enclosure	Plastic retains upright structure due to neutrally buoyancy, while its flexibility allows movement with water, facilitating mixing and flow. If needed, watertight glue or silicone can be used along the vertical seams to provide a more rigid upright structure.	Transparent polyethylene bags were sourced from local food packaging and grocery stores for $0.25 per unit in Mexico, and for approx. $1.80 per unit in the UK. Glue and silicone for re-sealing were sourced at local hardware stores for <$5, with an estimated cost of $0.50 per chamber.	Size of plastic bag can be changed to incubate different volumes of water or surface areas of substrate Enclosure transparency or colour filtration can be achieved with different plastics. The shape of chamber can be adapted for high-energy settings.
Sampling valve	A valve was installed into each chamber for the extraction of water samples with syringes. Installation involved a pinprick hole in the plastic, with a valve Luer-lock inserted and attached to a second Luer-lock valve on the inside of the chamber.	The valves tested in this study were 3-way Luer-lock valves, priced at $1.12 per unit. In lieu of valves, sports bottle caps can be implemented at a similar cost.	A sampling port of any size can be installed, depending on study requirements. 3-way valves can facilitate the addition of experimental treatments. Tubing can be added to the interior valve to achieve sampling from the centre of the incubated area.
Base	The heavy chamber base is placed on top of the plastic enclosure skirt to create a seal with the substrate. The base is malleable so that it can be moulded to the complexity of solid substrates, and in the case of soft substrata, buried as needed.	Bicycle inner tubes were cut to size and filled with sand and small fishing weights. After filling, the tubes were sealed using bicycle tyre patches and glue. As the used bicycle tubes were donated there was no cost. New inner tubes cost ~$4 each. Fishing weights $3 per kg.	Base weight can be adjusted as needed, depending on the environmental conditions. Stones can be used in lieu of fishing weights.

3.3.3 Design validation

Three key characteristics were investigated to validate the reproducibility and correct functioning of the chambers: (1) leakage of water from / to the chamber, (2) light transmission across the plastic membrane, and (3) temperature stability within the chamber.

1. Leakage

To test for leaks, non-toxic red food dye was inserted using a syringe (20ml) into a chamber deployed over sediments in shallow water at each of our field sites. Visual surveys were conducted by two snorkellers who monitored the water outside of the chamber for any obvious visible leaks of red-dyed water for 30 minutes (Fig. 3-1c). An underwater camera (Canon Powershot S120) was attached to a dive weight and placed on the substrate outside the chamber for the duration of the 30-minute deployments, and the video was reviewed for any red dye leakage around the base of the chamber. This process was repeated 3 times before case studies and before lab testing. Following this initial coarse assessment, a 90-litre aquarium tank was filled with artificial salt water (tap water prepared with Marine salts at a salinity of 21.5 ± 4.7 ppt.) and field water movement was simulated using 4 circulation pumps (Reef Tide 4000s 12v DC Wavemaker Pump, UK) positioned on the sides of the tank to create a zig-zag water motion across the tank. A prototype of the benthic chamber was placed in the tank and a super-saturated saline solution was inserted using a plastic syringe connected to the valve of the benthic chamber so that the water inside the chamber reached a salinity of 38.3 ± 5.7 ppt. Salinity was measured once per minute during the 4-hour incubation, inside and outside the benthic chamber using two cross-calibrated salinity loggers (Onset Hobo U24-002-C Saltwater Conductivity / Salinity Data Logger). The leakage test was repeated 3 times, and for each repeat a different chamber was used.

2. Light attenuation

A chamber was deployed over sediments in Akumal Bay at a depth of 2 m for 3 days between 07:00 and 19:00 hours in August 2019. A different chamber was used for each day of the experiment (n=3). Photosynthetically active radiation (PAR) was measured simultaneously inside and outside the chamber with two submersible sensors (Odyssey Submersible PAR Logger) attached to a 4 kg dive weight and positioned inside and outside of each chamber to log light each minute (μmol photons m^{-2} s^{-1}). The

sensors were calibrated against a recently calibrated Licor quantum sensor (LI-190, LI-COR Biosciences, US). Additionally, light transmission (%) between the photosynthetically relevant wavelengths of 300 nm – 800 nm was measured through the plastic membrane (Shimadzu UV-3600 UV-Vis).

3. Temperature

Changes to the temperature of water inside the chamber were measured to demonstrate accumulation of heat, which we would expect to see if the water is not mixing well. Temperature inside the chambers was collected using a handheld probe (Pro DSS multiparameter, YSI, US) at the start and end of field deployments of 9 chambers in tropical conditions over 4 days in case study 2. A separate 4-hour deployment in cold water conditions, at the SCENE fieldwork site in Loch Lomond was also conducted in August 2021 and temperature was continuously logged for the duration of the incubation (per minute) inside and outside of the chamber using temperature loggers (Onset HOBO UA-002-08 Pendant 8K Light and Temperature) with an accuracy of $\pm 0.5°C$.

3.3.4 Field operation of the benthic chamber

Field deployments over benthic communities were conducted to validate the reproducibility and adaptability of the chambers. Two case studies were conducted in Akumal Bay (Fig. 1d), one with incubations of seagrass patches and the other over coral reef communities (total of 41 deployments). Chambers were installed by divers and snorkellers. For all field incubations, water samples were extracted at the start and end of 1.5 to 3.5-hour long incubations using 100 ml plastic syringes with a Luer-lock connection to the chamber valve. Dissolved oxygen, pH, temperature, and salinity were measured using a handheld non-submergible multiparameter sensor (ProDSS equipped with ODO Optical Dissolved Oxygen and EXO pH Smart Sensors, YSI, US) attached to a kayak for analysis of samples within 1 minute of extraction. Chambers were flushed between incubations times by lifting them from the substrate and releasing the incubated water. A few minutes were allowed for any stirred-up sediments to re-settle before reassembling the chamber. Repeated measurements (n=15) of chamber volume were conducted in shallow (<1 meters) of Akumal Bay by filling chambers using a 100 ml syringe and recording variability between volumes to estimate error in volume measurements.

3.3.5 Adaptations of the chamber

A more streamlined, low-profile, dome-shaped chamber (Fig. 3-1b) was used due to higher surge at the coral reef site, nearer to the reef crest than the protected seagrass area (Fig. 1d). This was also an adaptation for the lower profile of reef patches (~15 cm height) compared to seagrasses (~ 30 cm height). The panels were cut as curved triangles (29 x 16 cm, H x W) with arching sides and each dome was constructed of 8 panels and two 8 cm skirts were added at the base. These skirts were added due to higher wave action at this site, to prevent leakage around the seal. All plastic seams were sealed with a double seal 1 cm apart on each joint, using a generic, locally available heat sealer. For the high-energy environment (case study 2) a heavier base was created by adding 8 kg of fishing weights into the bicycle tyre tube to total ~10 kg per base. Chambers were randomised over the substrate types for each incubation; algae-, coral-, and sand- dominated. Incubations lasted 3.5 hours. PAR was measured as described above in both case studies.

3.3.6 Case study 1: Seagrass production

Benthic chambers (n=5) were assembled and deployed over seagrasses and sediment substrate at 1.5 to 2 m depth. Seagrass surveys were conducted using the methods outlined in (Hernández and Tussenbroek (2014) to estimate seagrass abundance in Akumal Bay (Fig. 1d). Sampling was conducted at the start and end of incubations at midday, late afternoon, and after dark. Each incubation lasted 1.5 to 2.5 hours. The chamber constructed for the seagrasses (Fig. 3-1c) was taller and narrower than the chamber used in case study 2 (Fig. 3-1b) to accommodate the height of the seagrasses.

3.3.7 Case study 2: Production rates of distinct coral reef communities

Benthic chambers (n=9) were deployed by SCUBA divers at 2-3 m depth over four days for multiple incubations during solar noon and after dark over small patches of reef. Using swim patterns from a central point ('Case study 2' label on Fig. 3-1d),

small patches of mixed coral (*Porites spp.*), algae, crustose coralline algae, and sand/sediment were identified (n=21), of which 9 were randomly selected for incubation. Surface area and volume of the incubated reef patches were measured using photogrammetry. 3D models of incubated reef patches were constructed from ~100 photographs of each patch using Agisoft Metashape and compared following the methods outlined in Lange and Perry (2020). Surface areas (m^2) and volume (m^3) were extracted from the 3D models. We converted the volume to litres and deducted it from the chamber volume to calculate the individual sea water volume for each incubation and used this, with the surface area measurement to normalise metabolic rates. All areas of flat sediment were measured from top-down photos using ImageJ (Schneider et al. 2012).

3.3.8 Metabolism calculations

Net community production (NCP, mmol m^{-2} hr^{-1}) was calculated from changes to dissolved oxygen (DO) using the following equation:

(Eq. 1)

$$NCP = \frac{\Delta DO \times V}{SA \times T}$$

where ΔDO is the change in dissolved oxygen (mmol L^{-1}), which is normalised to the chamber volume (V) of water in litres, the surface area (SA) of the incubated sample in m^2, and the incubation duration time (T) in hours. Surface area was measured from 3D models using the program Agisoft following the protocol outlined in Lange and Perry (2020). Individual chamber seawater volumes (V) were calculated by converting the estimated organism volume extracted from 3D models (m^3) into litres (L) and subtracting this from the empty chamber seawater volume. Dissolved oxygen fluxes were normalised to individual chamber water volumes and organism surface areas.

3.3.9 Photosynthesis-Irradiance models

Rates of productivity (NCP) were modelled to light using the hyperbolic tangent equation of Jassby and Platt (1976):

$$P_{net} = P_{max} \times \tanh\left(\frac{\alpha \times E}{P_{max}}\right) + R$$

where P_{net} is the modelled net production rate (mmol m^{-2} hr^{-1}), R is the average dark respiration rate (mmol m^{-2} hr^{-1}), and E is irradiance in PAR (μmol photons m^{-2} s^{-1}). The coefficients derived from the model include: the initial slope (α) between NCP and light and the maximum gross photosynthetic rate (P_{max}).

3.3.10   Statistical analysis

Statistical analyses were carried out using RStudio version 1.4.1717 (R Core Team 2019) with the package *Tidyverse* (Wickham 2019). Each data set was assessed for parametric assumptions using Shapiro Wilkes, Q-Q plots, and histograms. Data did not always meet the assumptions of normality; therefore, nonparametric statistical tests were selected for the analyses. For testing of chamber parameters (light, pH, temperature, leakage), paired sign tests and Wilcoxon rank sum tests with continuity correction were used, and for the case studies Kruskal Wallace tests were used to compare mean rates of NCP at different times of day and between different benthic communities. Linear regressions of seagrass NCP with light were modelled using *ggplot* with *ggpmisc* extension on R (Wickham 2016; Aphalo 2021). Photosynthesis - irradiance curves were modelled using R nonlinear least squares estimation and coefficients / model fit were evaluated based on R^2, confidence intervals, and standard error of the regression (sigma, σ).

3.4 Results

3.4.1 Construction of benthic chambers for field deployment

Benthic chambers (*n=6*) were successfully constructed and deployed by citizen scientists in the seagrass meadow of Akumal Bay in July 2019. Materials were sourced locally and the cost per chamber was USD $17.62. Details on costs for the items are included in Table 2. The time taken to fill rubber tubes with sand and weights, cut the plastic bag, and install a valve ranged from 15 to 30 minutes for 2 people and 45 minutes for 1 person. The chambers were deployed without difficulty by a range of users of varying experience.

3.4.2 Leakage

Salinity inside the chamber at the start of the incubations (38.9 ± 0.3 ppt; mean $\pm$ SD) was reduced by 0.8 ± 0.3 ppt over the course of the 4-hour incubations. Overall, the difference in salinity was -2.1 ± 0.8 % between the start and end values of 3 replicate incubations during 4-hour incubations. The salinity of the water outside the chamber remained stable throughout the incubations (26.1 ± 0.1 ppt.).

3.4.3 Transparency

Laboratory testing found that light transmission through the polyethylene plastic was 74.4 % at 750 nm and 61.1 % at 400 nm (Fig. 3-2a). In the field, the difference between PAR measured simultaneously inside and outside the chamber over 3 field deployments was 13.0 % $\pm$ 1.9 (mean $\pm$ SD) and the difference was only found to be significant over 2 hours at peak sun on 2 days (Wilcoxon signed rank test with continuity correction, Table 3-3).

3.4.4 Temperature

Seawater temperatures measured inside (30.7 ± 0.7 °C, median ± SD) and outside chambers (30.7 ± 0.8 °C, $n = 9$) at the end of 3-hour incubations in peak sun were not significantly different (Sign test statistic = 18, df = 28, p =0.185).

Table 3-3: Wilcoxon rank sum test with continuity correction to test differences between photosynthetically active radiation (PAR in µmol photons m^{-2} s^{-1}) inside vs. outside chambers during deployments over 3 days in August 2019.

	Date measured	PAR (mean ±SD in µmol m^{-2} s^{-1})		W statistic	p-value
		inside	outside		
Full day (0700 to 1900)	01/08/19	258 ±238	289 ±267	2322	0.3305
	03/08/19	269 ±239	300 ±268	2151	0.418
	07/08/19	216 ±255	242 ±285	2882	0.2474
Solar peak only (1200 to 1400)	01/08/19	461 ±195	515 ±218	86	0.4428
	03/08/19	622 ±116	696 ±130	109	0.03324
	07/08/19	611 ±22	684 ±25	144	7.396 x 10^{-07}
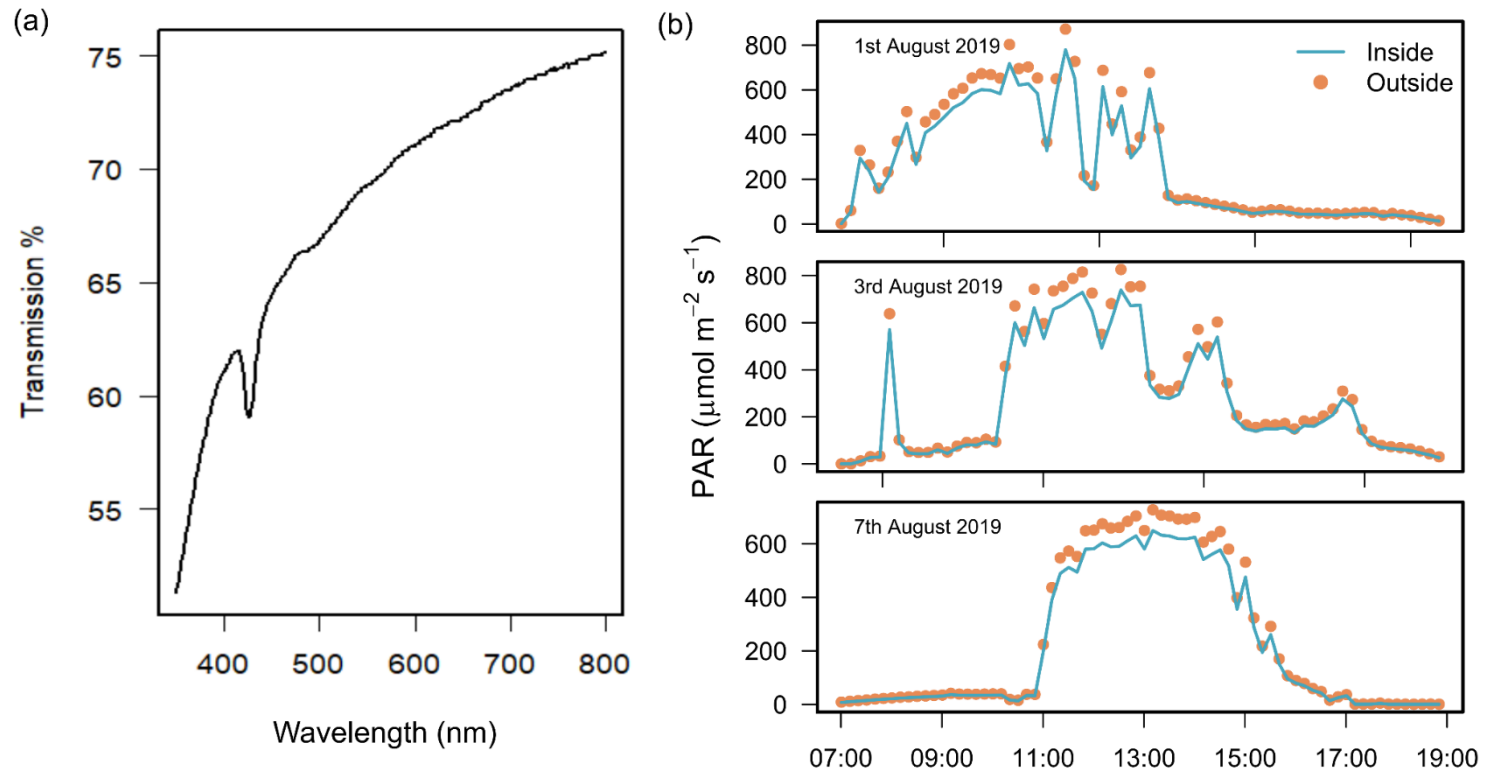
Figure 3-2: Light transmission of the benthic chamber. Chamber transparency measured with (a) a spectrophotometer to quantify percentage (%) transmission of light between 400 – 750 nm, and (b) light sensors during the field deployment of chambers (n=3) to measure PAR (μmol m^{-2} s^{-1}) inside (blue line) and outside (orange dots) of the chamber over 3 days of exposure to natural solar radiation between 07:00 to 19:00 hours.

3.4.5 Case Study 1: Seagrass productivity rates increase with peak sunlight

Six benthic chambers were deployed over a seagrass-sediment substrate in Akumal Bay. Seagrass coverage was composed of three species: *Thalassia testudinum, Syringodium filiforme,* and *Halodule wrightii*, and visual surveys indicated 50% areal coverage within the incubation area. Increases in DO concentration demonstrated positive net community productivity (NCP) during daylight incubations, while negative NCP after sunset indicated net respiration for all seagrass incubations (Fig. 3-3). All values presented as mean ±SD. The difference in dissolved oxygen (ΔDO) was 78.5 ± 7.5 µmol L^{-1} at solar noon when concentrations of 272.5 ±7.5 µmol L^{-1} DO were reached and during night incubations fell to 186.8 ±12.7 µmol L^{-1} DO with an average ΔDO of -45.2 ±12.7 µmol L^{-1}. NCP was significantly different during different times of the day (KW = 13.3, df = 2, p = 0.00126). Average NCP was highest at solar noon (6.7 ±1.3 mmol m^{-2} hr^{-1}), lower in the late afternoon (2.4 ± 0.6 mmol m^{-2} hr^{-1}) and negative after sunset (-3.3 ± 0.4 mmol m^{-2} hr^{-1}). Seagrass NCP had a strong linear relationship with PAR (R^2 = 0.93, p = <0.0001) (Fig. 3-4). One incubation done over sediments (n=1) also had the highest NCP rate at solar noon (2.6 mmol m^{-2} hr^{-1}) and was negative at night (-0.6 mmol m^{-2} hr^{-1}).
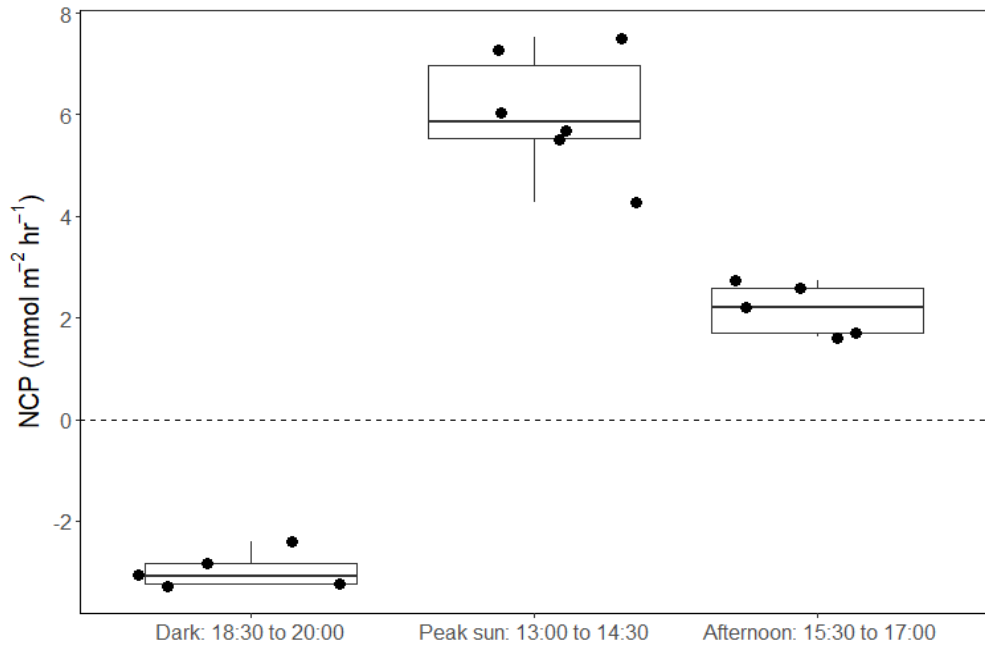
Figure 3-4 : <u>Net community productivity (NCP) of incubated seagrass patches measured from benthic incubations.</u> NCP was calculated from the change in dissolved oxygen (ΔDO) normalised to chamber volume and incubation time (mmol m-2 hr^{-1}). Incubation chambers were deployed simultaneously over seagrasses in the dark (n=5), at solar noon when PAR = mean 757 $\pm$SD, 88 µmol m^{-2} s^{-1} (n=6), and in the late afternoon, PAR = mean 463 $\pm$SD 75 µmol m^{-2} s^{-1} (n=5)

$$y = -2.92 + 0.0112\,x,\ R^2 = 0.93$$
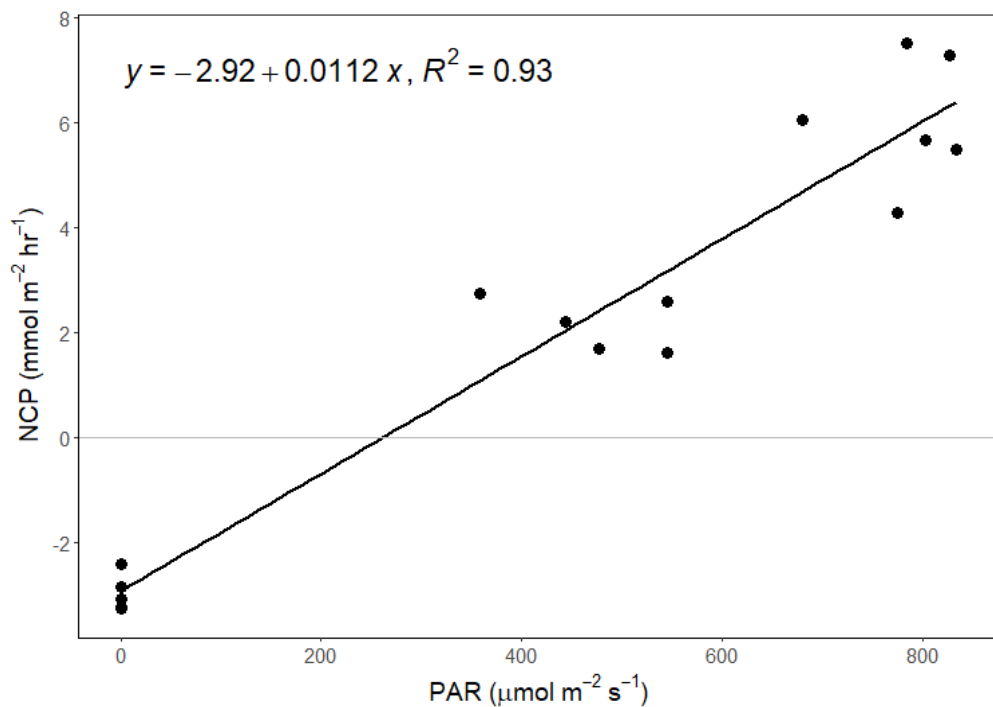
Figure 3-3 : Linear regression of net community production (NCP in mmol m^{-2} hr^{-1}) of seagrass incubations with light (PAR in µmol m^{-2} s^{-1}).

3.4.6 Case Study 2: Measuring productivity of coral-algae reef patches

Compositions of 9 small patches of reef (planar surface area = 1075.2 cm^2) were described by relative proportions of functional groups such as coral, macroalgae, crustose coralline algae, and sediment measured from 3D models (Figs. 3-5 & 3-6). Two patches consisted of sediments only, 3 were algae-dominated, and 4 were coral-dominated. One of the coral-dominated patches consisted of a coral, which had begun to bleach. Surface areas calculated from 3D models were 2.86 ± 1.04 m^2. Chamber seawater volumes averaged (mean ±SD) 15.72 ± 2.86 L (Table 3-4). NCP was generally positive during daytime incubations and negative at night for all substate types (Kruskal-Wallace statistic = 49.9, df = 1, p = 1.61 x 10^{-12}). NCP rates measured from the 9 distinct patches were different during the daytime (Kruskal-Wallace statistic = 25.0, df =8, p = 0.002) and at night (Kruskal-Wallace statistic = 19.2, df =8, p = 0.014). When the patches were categorised into algae-, coral-, and sand-dominated groups, pairwise comparisons revealed that NCP was different between sand - algae and coral – algae, but algae and coral did not have significantly different NCP during the day or at night (Table 3-4). Photosynthesis-irradiance data fit a hyperbolic relationship with PAR for all substrates (Fig. 3-7). Photosynthetic maximum (P$_{max}$) was highest in the algae-dominated substrate type (11.6 ± 0.9 mmol m^{-2} hr^{-1}) and lowest for sand/sediments (4.2 ± 0.6 mmol m^{-2} hr^{-1}). All model coefficients were significant (Table 5).

Table 3-4: <u>Surface areas in square metres (m^2) and sea water volume in litres (L) of incubated reef patches.</u> Estimates from 3D models following the protocol outlined by Lange and Perry (2020).

Patch	Substrate type	Replicate	Surface area (m^2)	Seawater volume (L)
1	Sand	1	1.14	20.00
2	Sand	2	1.22	20.00
3	Algae	1	2.24	13.26
4	Algae	2	2.43	15.55
5	Algae	3	3.20	12.82
6	Coral	1	1.77	15.41
7	Coral	2	2.73	16.20
8	Coral	3	1.03	17.27
9	Bleached coral	4	4.39	11.769
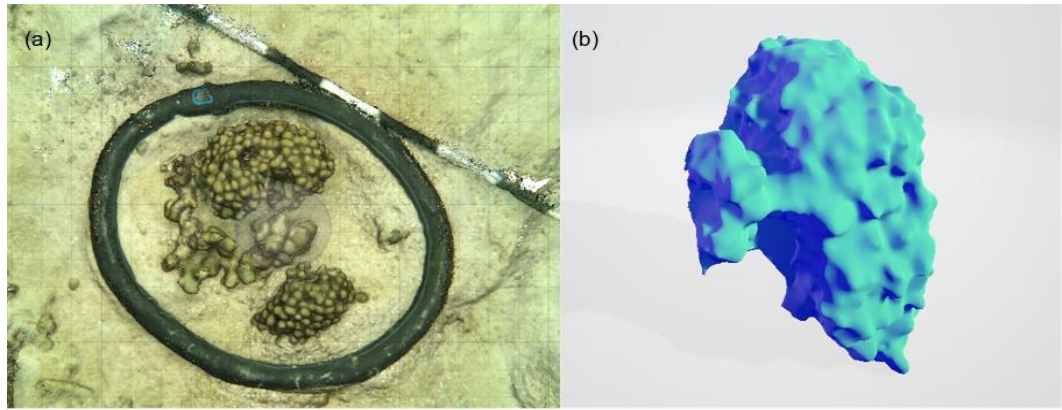
Figure 3-5: An example of the 3D model generated for each of the incubated patches to measure surface area of complex structures and to estimate the volume occupied by the organism. 3D models were built from photographs taken in-situ to estimate the composition, and measure volume and surface area of each patch: **(a)** screenshot of 3D model built from photographs used for visual assessment of the relative cover. **(b)** 3D profile of a coral colony from which volume and surface areas were derived. The surface area of the base of the colony was removed from the overall surface area calculated.
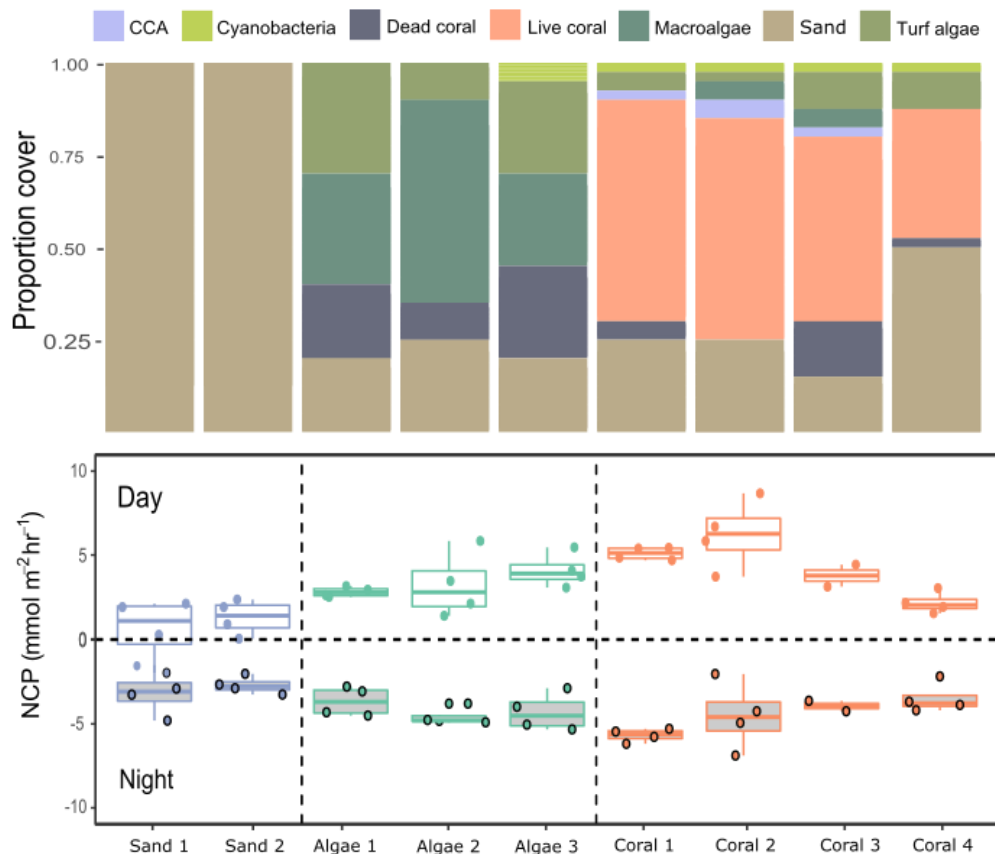
Figure 3-6: Net community productivity (NCP) per incubated patch over 4 days and nights. Stacked bar plots **(top)** show the proportional cover for each category of functional group and the boxplot **(bottom)** show the rates of NCP (mmol m^{-2} hr^{-1}) measured from differences in dissolved oxygen (ΔDO) normalised to chamber volume and organism surface area (m^2) per hour following equation 1.

3.5 Discussion

We designed and tested a novel benthic incubation chamber, drawing together key principles from existing designs (e.g., Yates and Halley 2003; Camp et al. 2015; Roth et al. 2019). The benthic chamber was designed to incubate small communities, single organisms, or sediments. The equipment created was low cost, reproducible, minimally invasive, and adaptable, with comparable features and capabilities to other in-situ benthic incubation chambers (*see* Table 1). The chambers were successfully assembled and deployed for fieldwork by citizen scientists and students. Construction of a single benthic chamber took between 15 to 30 minutes for two people, including the time taken to measure the volume of the chamber and to fill the tube base with sand. In the water, deployment over complex substrate took 5 minutes or less by two qualified divers. The performance of the chambers was evaluated by conducting productivity measurements using field deployments of the chambers over as a seagrass bed (case study 1), as well as algae, coral, and sand dominated reef patches (case study 2). The results obtained using this method were comparable to those obtained in previous studies using established chambers designs, demonstrating the effectiveness and feasibility of the chamber design as a low-cost alternative for benthic incubations. Lowering the costs of in-situ incubation apparatus broadens the accessibility and scope for measurements of benthic metabolism for conservation monitoring purposes.

3.5.1 Evaluating the chamber design

The benthic chamber design presented in this study is novel in its accessibility and scope for implementation with limited resources. Benthic incubations allow for direct measurements of benthic metabolism and are an important tool for quantifying carbon fluxes from physiological processes within benthic communities. However, the most inexpensive chambers currently available for in-situ community incubations cost around USD \$200 to build and require bespoke parts and a submersible pump for operation (Roth et al. 2019), while the economical 'flexi-chamber' (Camp et al. 2015) is limited to individual coral colonies, rather than benthic communities. The chamber presented in the current study incubates communities or individuals and it costs < USD \$20 to construct. At such low costs, multiple replicates are feasible. The training required to build, deploy, and collect data using most chamber designs is not yet widely

available. We demonstrated that the flux measurements can be normalised to surface area and volume data either using more traditional estimates of planar area and percentage cover in case study 1 or using a 3D modelling approach as in case study 2. This demonstrates the adaptability of our chamber design for example when the software and computational power required for the latter technique may not be available. The benthic chamber itself does not require any specialised equipment or training to deploy as materials were locally sourced and citizen scientists were able to make and deploy the chambers with minimal training.

We demonstrated that the novel chambers can be constructed from locally sourced materials without the need for any specialised parts. Plastic bags, bicycle inner tubes, fishing weights, and SCUBA gear for underwater transport were all easily sourced on site. We purchased Luer-lock valves from a local medical supply store, however, we also trialled the chamber construction and deployment with a plastic sports bottle cap instead of the valve (Fig. 1c). The chamber in this study was constructed for less than USD $20, however it should be noted that the sensors used to measure dissolved oxygen, pH, and salinity inside the chambers should be considered as an additional cost. This is true of all but one of the selected chambers in Table 1 and would be dependent on the individual experiment being conducted with the benthic chamber and the precision and accuracy required.

To verify the reproducibility of the chamber design for determining photosynthesis, we conducted net community productivity measurements. First, we measured light attenuation of the polyethylene tent and found a reduction of 13% $\pm$ 1.9 between inside and outside the chamber (Fig. 3-2b). These results aligned with the transparency of comparable chambers, such as the 9% reduction in light reported in Roth et al. (2019) and 16% in Camp et al. (2015). Our results support previous findings that transparent plastic polyethylene or vinyl materials sourced at food packaging, hardware, or medical supply stores are effective for incubations of photosynthetic organisms (Yates and Halley 2003; Camp et al. 2015). As the chamber is adaptable for distinct locations, uses, and resources, light attenuation should be measured given the variability in light transmission by different plastics.

One of the unique features of the novel chamber design is the malleable base, which facilitates deployment over hard, uneven substrate without using destructive methods to fix the chamber in place. This is particularly useful for incubations in

managed or protected areas, where attachment by digging the chamber base into sediments or pinning the chamber to a coral reef using nails or cable tie attachments might not be feasible. The rubber tubing base was weighted with easily available materials to create a seal with the substrate, which could be adapted to 3D structure on the reef incurring minimal damage. Given that the malleable base could be a potential source of leakage, laboratory testing was conducted, and we demonstrated that the rate of water exchange was 2% over 4 hours. We consider the novel benthic chamber to be a reproducible method and effective for accurate measurement, based on the results of laboratory testing and case studies. Water exchange during field deployments may vary, depending on the local conditions, for example surge, currents, and substrate type, therefore it is advisable that users of the chamber incorporate a testing phase to adjust the weight of the base to ensure that it is sufficient to create a seal. Users could replicate the salinity method by adding hypersaline solution to the chamber and measuring salinity at the start and end of the incubation time (Webb et al. 2021), or an alternative if refractometers are not available would be the visual assessment of leakage using non-toxic food dye. It is also possible to visually assess water mixing and movement using dye. We injected red food dye into field-deployed chambers and observed full dispersal within one minute (Fig. 3-1c).

Water movement over the reef is a driver of metabolic fluxes (Comeau et al. 2014; 2019) and maintaining natural water movement without the restriction of a solid chamber wall sustains ambient in-situ conditions throughout the sampling period. The flexibility of the plastic bag material used for the tent enclosure also has the benefit of reducing costs compared to rigid chambers by encouraging natural water movement and mitigating the need for a submersible pump inside the chamber. The concept of using a flexible plastic enclosure was demonstrated with the Flexi-chamber design (Camp et al. 2015). While the flexibility of the tent enclosure promotes natural water movement and mixing, any benthic chamber will disrupt natural water movement, which should be considered when interpreting data collected with benthic chambers in general. The NCP rates measured in our case studies also demonstrate that water movement is maintained by the flexible walls, as supported by the NCP rates measured (discussed below).

The benthic chamber used in this study is adaptable to different substrate types, environmental conditions, and research applications. The simple and flexible design enables easy adjustment of size and volume, and additional valves or sampling ports

can be easily installed. The chamber can be used to measure additional parameters to those measured in this study, for example, to collect sea water samples for carbonate chemistry to measure calcification rates. This may add to the expertise and costs of using the chamber. The weight of the base can be altered for high or low energy systems, and the height of the dome can also be changed to accommodate different samples sizes and heights. It can also be adjusted to enhance or minimise hydrodynamic mixing by naturally occurring currents or wave action. As the base is malleable, it can be used on hard substrate or soft sediments as demonstrated in our case studies over reef communities and seagrass beds. The two case studies demonstrated the adaptability of the chamber.

3.5.2 Seagrass productivity measured with the benthic chambers

Incubations over seagrass and sand demonstrated a typical diel trend of NCP increasing with sunlight and switching to net respiration at night. Seagrass productivity rates were in line with those of previous studies measuring seagrass NCP, however, variability does exist (Duarte et al. 2010). The average solar noon NCP rate measured in this study (6.7 ± 1.3 mmol m^{-2} hr^{-1}) was lower than NCP measured in Florida with the SHARQ chamber (12.3 ± 1.0 mmol m^{-2} hr^{-1}, Turk et al. (2015). However, our rates were higher than the average NCP for tropical Western Atlantic seagrass meadows described in a meta-analysis by Duarte et al. (2010) in which daily NCP averaged 23.7 ± 7.8 mmol m^{-2} day^{-1} over 155 seagrass studies, which would equate to an hourly rate of approximately 2.2 mmol m^{-2} hr^{-1}. Seagrasses in Akumal Bay are colonised by epiphytes and cyanobacteria (Hernández and Tussenbroek 2014), associated with high nutrient load in the bay, which may have influenced our NCP measurements (Coleman and Burkholder 1994; Borowitzka et al. 2007). Productivity increased linearly with light and did not reach photosynthetic saturation. Therefore, it was not possible to fit the hyperbolic tangent equation, possibly due to the limited light conditions in the study design (i.e., there were only 2 light levels).

3.5.3 Measuring productivity of coral -algae reef patches

Net production rates measured for all reef patches were positive during light incubations and negative for dark incubations in line with previous studies of in-situ coral reef metabolism measured with benthic chambers. For example, light NCP measured with the SHARQ enclosure at a reef site in Florida averaged 8.6 ± 1.0 mmol $m^{-2} hr^{-1}$ (Turk et al. 2015), a rate that also aligned with NCP measured estimated by CROSS (McGillis et al. 2011), and previous SHARQ deployments within the Caribbean region (Turk et al. 2015). Our night respiration rates, measured from around dusk until 21:00 – 22:00 hours, were also in agreement with the values measured in the early evening using SHARQ deployments in Turk et al. (2015). The highest rates of NCP were measured in coral patch 3, which was the only replicate containing *P. astreoides* as well as *P. porites.* Net community production was lowest in patch containing a bleached *P. porites* colony ('Coral 4'on Fig. 5), which had been subjected to heavy sedimentation and algal overgrowth. The lower rates of NCP measured in the incubations of this colony most likely reflect lower metabolic rates due to environmental stress. Coral patches 1 and 2 were very similar in terms of the health, size, and structure of the *P. porites* colonies incubated and they had minimal (<10%) algae within the chambers, as reflected by the similar rates measured in these incubations. We modelled reef NCP data to light and found a hyperbolic relationship between PAR and NCP as have other studies (Berg et al. 2013a; Turk et al. 2015; Takeshita et al. 2016). However, our modelling approach was somewhat limited by the range of light levels and number of incubations. Future research should aim to include more incubations at different times of day. The low costs of the chamber we present in this study supports such research.

3.5.4 Conclusions

Monitoring of coastal ecosystem health is of critical importance for tracking and predicting ecological response to global climate change and other localised threats. This study presents a novel benthic chamber design, which reduces the cost of in-situ incubations of benthic organisms in shallow coastal ecosystems, while maintaining reproducibility. The chamber was designed to be minimally invasive and adaptable, which we demonstrate through successful field deployment. We measured productivity

rates for seagrasses and reef patches in line with previous studies and provide a comparison of rates. Further studies are needed for quantification of coastal carbon cycling and efficient methods to enhance conservation monitoring, and the low-cost benthic chamber we describe overcomes some of the limitations of other designs. It is a potential tool for diverse users to employ in such research endeavours.

4 Ecosystem-scale measurements of benthic metabolism

The data for this chapter were collected in 2015 as part of a collaborative project by Dr Tyler Cyronak, Nova Southeastern University, Dr Yuichiro Takeshita, Monterey Bay Aquarium Research Institute, and Dr Andreas Andersson, Scripps Institution of Oceanography, and provided to me for my thesis when my planned field and international lab visits were cancelled in 2020/1 due to COVID-19.

4.1 Introduction

Coastal marine ecosystems provide valuable services to humanity, are critical components of the global carbon cycle and are where most humans interact with the sea (Barbier et al., 2011; Gattuso et al., 1998; Mehvar et al., 2018; Smith & Hollibaugh, 1993). However, the future of coastal systems such as inshore coral reefs, seagrasses, mangroves, and salt marshes is under threat from local and global anthropogenic change. Efficient monitoring of coastal ecosystem ecological function is of critical importance for understanding and predicting the effects of environmental degradation. New technologies designed to monitor biogeochemical fluxes within coastal waters could provide important insights into changing ecosystem dynamics over time and space (Bushinsky et al., 2019). Benthic metabolism is an important driver of ecosystem function and supports the goods and services that these ecosystems provide. For example, the balance of photosynthesis and respiration in seagrass beds is linked to the ability of these ecosystems to sequester and store C and can potentially act as ocean acidification refugia (Berg et al., 2019; Kapsenberg & Cyronak, 2019; Ricart et al., 2021). On coral reefs, the ability to calcify, or produce a calcium carbonate framework, underpins their most critical ecosystem service linked to habitat construction (Allemand et al., 2011; Perry & Alvarez-Felipe, 2018). Therefore, measuring community and ecosystem metabolism could provide an effective tool for long-term and high-resolution monitoring of ecosystem functional change.

In shallow marine ecosystems, metrics of benthic metabolism are divided into: (1) net community production (NCP), defined as the combined processes of photosynthesis and respiration, and (2) net community calcification (NCC), which describes the balance of biogenic carbonate precipitation by calcifying organisms offset by carbonate

dissolution. NCP can be measured from changes in dissolved oxygen (DO) or dissolved inorganic carbon (DIC) concentrations, although changes in DIC usually need to be corrected for any changes due to processes that impact alkalinity (Kinsey, 1979; Smith, 1973). Calcification can be measured using the total alkalinity (TA) anomaly based on the stoichiometry of changes in alkalinity for each mole of $CaCO_3$ produced or consumed (Smith and Kinsey 1976; Gattuso et al. 1999). Other techniques have also been used to measure benthic calcification rates, including measuring changes in calcium (Gattuso et al., 1999; Gómez Batista et al., 2020) and monitoring concurrent changes in oxygen and pH (Barnes & Devereux, 1984; Takeshita et al., 2016b).

Measuring benthic metabolism can help determine whether ecosystems are net autotrophic or heterotrophic and net calcifying or dissolving. By linking these metrics back to ecosystem function, we can directly measure the function and health of benthic coastal systems. Measurements of benthic in-situ metabolism present unique challenges due to the complex dynamics and variable environmental conditions found in shallow coastal waters. Metabolic rates are significantly influenced by flow, ambient light, and nutrient input, along with fluctuations in temperature, pH, and salinity (Courtney et al., 2017; Cyronak et al., 2020; Kinsey, 1983; Silbiger & Sorte, 2018; Takeshita, 2017). Considering the diverse array of processes that control benthic metabolism, it is difficult to replicate the myriad of important environmental influences in ex-situ mesocosm settings. Because of this complexity, in-situ measurements are considered a critical component for refining characterisation and understanding of coastal ecosystem metabolism (Berg et al., 2019; Takeshita et al., 2016b).

A range of approaches have been developed to quantify benthic fluxes since the 1950's (Figure 1). The earliest studies relied upon on natural hydrodynamics to track changes in dissolved oxygen as water parcels flowed over the benthos (Odum, 1956, 1957; Smith & Marsh, 1973) or during natural periods of tidal isolation. The 'slack water approach' measures changes in seawater oxygen concentrations occurring in bodies of water, which are isolated at certain times of day due to slack tide (Kinsey, 1978; Shaw et al., 2014). Where natural hydrodynamics do not present such an opportunity, artificial isolation can be achieved with in-situ incubation chambers, which enable water parcels to be isolated over a benthic community (e.g., Yates and Halley 2003; Roth et al. 2019). Despite the convenience of these methods that allows one to ignore physics for their mass balance, the isolation approach does not generally represent the range of natural conditions that the benthic communities can experience.

For example, interruption to natural water flow has been shown to decrease oxygen production by benthic organisms (Camillini et al., 2021; Comeau et al., 2014; Patterson et al., 1991; Shaw et al., 2014).

Flow respirometry overcomes some of the limitations of enclosure and slack water techniques by measuring changes in seawater chemistry as it traverses the benthos. As water passes from point A to B of an ecosystem, changes to dissolved oxygen concentrations are measured to calculate production or respiration. The Lagrangian approach relies upon tracing water parcels using dyes or floats to approximate speed and direction as water travels between upstream and downstream sampling points (Barnes, 1983; Gattuso et al., 1993; Marsh & Smith, 1978). Conversely, the Eulerian approach implements fixed moorings where chemical sensors record measurements at static points along a known current trajectory (Frankignoulle et al., 1996). One limitation of the flow respirometry technique is that measurements are taken at one fixed depth, where water may not be fully mixed. The Eulerian approach was modified in the control volume approach, which overcomes this limitation by sampling at multiple depths within a theoretical control volume. With advancing technologies, the Lagrangian method was adapted to incorporate floating sensors to track dissolved oxygen and pH in-situ, as the water passed across the benthic community, allowing estimations of NCC (Barnes and Devereux 1984; McMahon et al. 2018). However, the method is only feasible in areas of consistent current direction and often requires intensive sampling or long-term sensor deployments to achieve adequate measurement resolution (Gattuso et al., 1993; McGillis et al., 2011). Because these types of community metabolic measurements are sporadic, the data are often assembled into a composite diurnal curve based on the time of day that each measurement was made (e.g., Cyronak et al. 2013; Shaw et al. 2014). While useful, these composite day analyses can miss critical short-term fluctuations and drivers of benthic metabolism.

As our understanding of the interconnected and dynamic processes defining coastal ecosystem metabolism has evolved, so has the technology we use to measure it. In-situ measurements of benthic metabolism depend upon a variety of factors such as depth, light, hydrodynamics, as well as the precision and stability of the sensing equipment (Silveira et al., 2019). Technological advances over recent decades mean that measuring dissolved oxygen in ocean systems is now precise and stable for autonomous sensors, which can be deployed for months or even years (Bushinsky et al., 2019). Modern dissolved oxygen optodes are stable once deployed, facilitating long

term deployment and have been used to measure changes in P and R over distinct time scales within ecosystems (Moore et al. 2009). The advances in dissolved oxygen sensing have enabled longer term and higher resolution measurements of productivity in coastal marine ecosystems. For example, aquatic eddy covariance (AEC) uses dissolved oxygen microelectrodes to measure instantaneous changes in DO, which are correlated with vertical velocity gradients to calculate oxygen exchange between benthic communities and overlying seawater. The AEC method was first applied to the coastal ocean by Berg et al. (2003) and has since been used to measure benthic metabolism of seagrasses and coral reefs (Long et al. 2013; Berg et al. 2013b, 2019; Attard et al. 2019).

Despite these advances in oxygen sensing over recent decades, technologies for in-situ measurements of total alkalinity are not yet available. Therefore, quantification of community calcification and dissolution requires lab analyses of discrete water samples, limiting the scope of calcification measurements in terms of resolution, timeframe, and location. However, Barnes (1983) demonstrated that it is possible to estimate changes in TA from measurements of pH and DO. Applications of the method were limited by the available technology for measuring pH and DO in-situ. However, improvements in the longevity and calibration of modern autonomous sensors can now support the application of this method. The Benthic Ecosystem and Acidification Measurement System (BEAMS) utilizes the gradient flux approach with autonomous sensing of changes in DO and pH to calculate in-situ calcification rates. BEAMS is the first method to record long-term and high resolution (10 min interval) simultaneous NCC and NCP.

In this study, we compare approaches for measuring net community calcification (NCC) and production (NCP) in a calcium carbonate dominated seagrass bed (Bailey's Bay, Bermuda; Fig.4-1). We deployed autonomous sensors to determine metabolic rates using (1) Lagrangian, (2) 1D control volume, and (3) BEAMS approaches, alongside static deployments of (4) advective benthic chambers and (5) discrete water sampling. The unique flow characteristics within the bay allowed us to compare a range of techniques over the same benthic community. We also compared estimates of the ratio of calcification to total metabolism (NCC + NCP) using direct measurements of metabolism and assumptions based on discrete chemistry measurements across the bay.
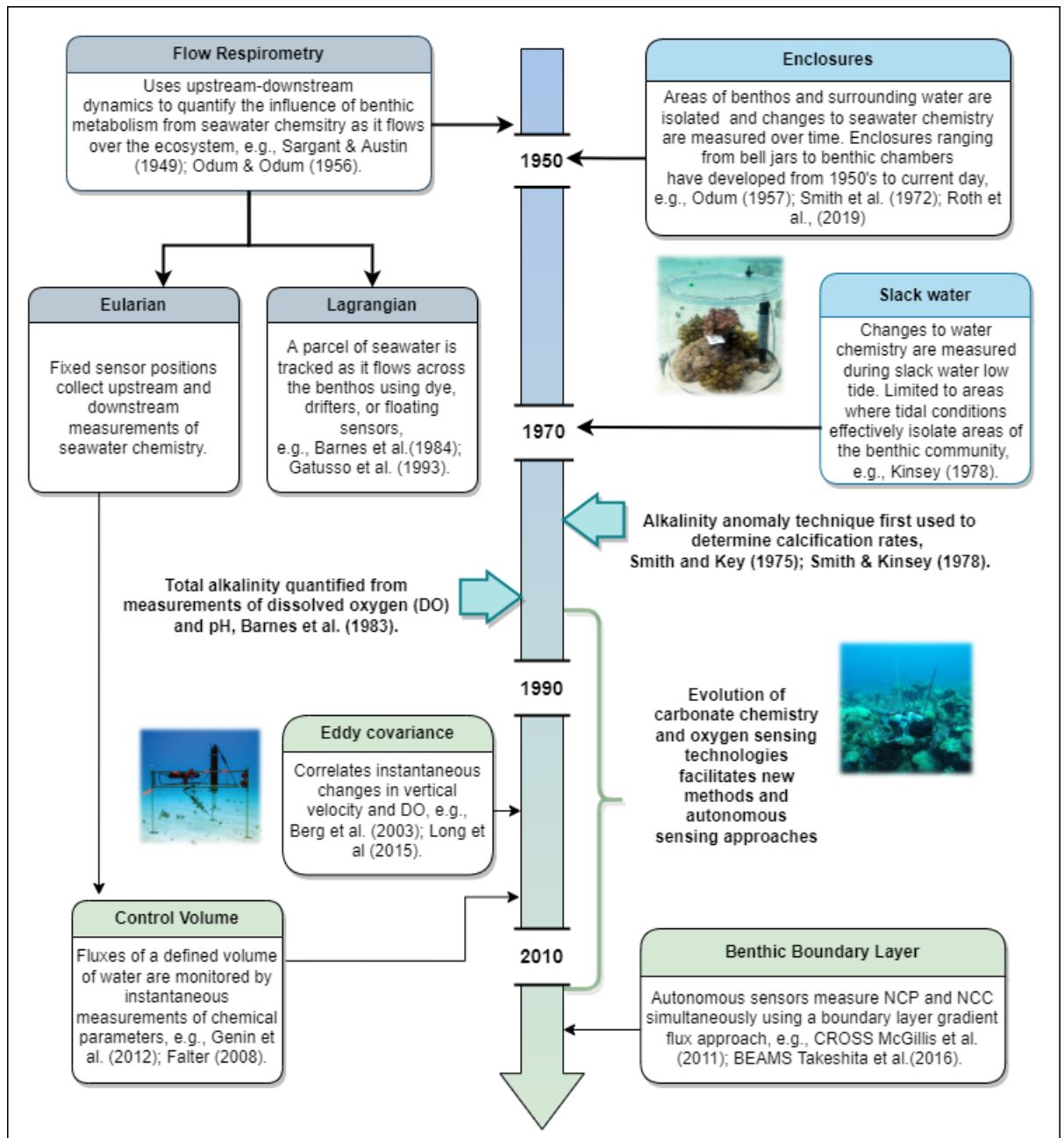
Figure 4-1: Timeline of the key method developments for measuring benthic metabolism in coastal ecosystems with an emphasis on coral reefs since ~1950. The methods are grouped into three broad categories, top left shows some of the key methods using **flow respirometry** to track changes in seawater chemistry as it traverses the benthic community. Top right methods are based on **isolating** the water around a benthic community to measure changes in chemistry. The lower section of the timeline shows some of the more recent methods for measuring ecosystem metabolism using **autonomous technologies**. Boxes with dotted outlines highlight the methods compared in the current study. Text without boxes describe the key scientific advancements.

4.2 Methods

4.2.1 Study Site

Data were collected in Bailey's Bay, a shallow, semi-enclosed lagoon located ~ 3 km west of the Bermuda Institute of Ocean Sciences (BIOS) research station (32.350°N, 64.725°W) (Fig.4-2a) from the 21st to the 25th July 2015. Benthic cover in Bailey's Bay consists of carbonate sediments and seagrasses: primarily *Thalassia testudinum*, interspersed with sparse patches of *Syringodium filiforme,* and *Halodule wrightii* (Holzer and McGlathery 2016). Seagrass cover was denser in the north-eastern region of the bay and became sparser to carbonate-dominated substrate in the south-west of the bay (Cyronak et al., 2018). Data were collected at the same area for each of the methods, between SP1 and SP2 positions, except for the discrete samples which were collected at sites across the entire bay (Fig. 4-2a)

4.2.2 Autonomous sensor array

Two autonomous sensor packages were deployed 320 m apart at upstream (32° 20.8656' N, 64° 43.7748' W), and downstream (32° 20.9736' N, 64° 43.6135' W) points of the dominant current direction over 4 days in July 2015. The positions of the sensor packages, referred to as SP1 and SP2 herein, and the current speed and direction are shown in Figure 4-2a. Both autonomous sensing stations were equipped with a SeapHOx package (Bresnahan et al. 2014) to measure dissolved oxygen, pH (total scale), pressure, salinity, temperature, and PAR (Q100 Apogee) every 30 seconds, and a Nortek 1MHz acoustic doppler profiler to measure current direction and speed. Depth of the sensor packages was determined from the SeapHOx inbuilt pressure gauge. One point calibration was carried out with water samples collected at the site of sensor deployment. Currents were measured at 0.5Hz and averaged to 10 min intervals prior to analysis. The data collected by SP1 and SP2 were used in calculations of benthic metabolism using BEAMS, flow respirometry, and control volume approaches.
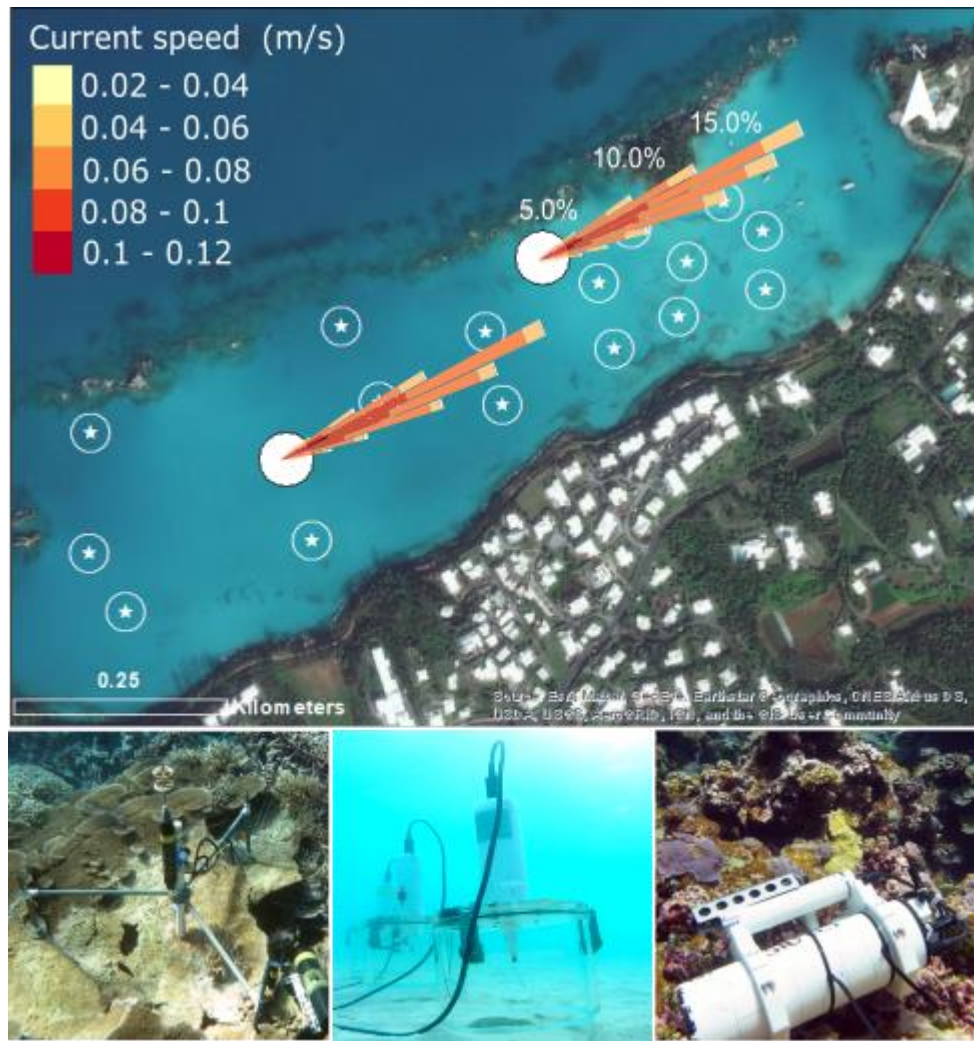
Figure 4-2: (a) Satellite image of Bailey's Bay, Bermuda generated using ArcGIS to show discrete sampling points (white circles / stars), position of autonomous sensor packages (large white circles); and current profiles (current roses with colour gradient for speed shown in the legend), **(b)** photographs of BEAMS apparatus, **(c)** advective benthic chamber enclosures deployed over sediments close to the upstream autonomous sensing packages, and **(d)** photograph of a SeapHox sensor, which was deployed at upstream and downstream positions shown in 4-2(a) as filled white circles.

4.2.3 Approaches for measuring net community metabolism

Net community metabolism (production and calcification) was measured using a range of distinct approaches: (1) Lagrangian, (2) control volume, (3) BEAMS, (4) advective benthic chamber enclosures, and (5) discrete samples (Fig. 2). Data for the BEAMS, Lagrangian, and control volume approaches were collected with autonomous sensors over 4 consecutive days of sensor deployment in July 2015. Chambers were deployed over the first 2 days only, and discrete samples were collected on days 1 and 2 of the study period.

(1) Lagrangian

Upstream-downstream measurement (SP1 and SP2) and the speed and direction of water traversing the benthos were tracked so that changes to sea water chemistry could be calculated as water traversed the seagrass-sediment benthos could be calculated. Time was tracked using a quasi-Lagrangian framework following DeCarlo et al. 2017. The trajectory and speed of the water travelling across the bay was used to back-track the time at which a parcel of water was sampled by each sensor. Differences in dissolved oxygen (ΔDO) between upstream and downstream sensors were used to calculate net production. The rates were normalised to depth (d) and time (t) as show in Equation 1:

Eq. 1

$$NCP = \frac{\Delta\text{DO } dp}{t}$$

Where ΔDO is the measured change in dissolved oxygen, *d* is depth in metres, *p* is the density of seawater, and *t* is the time it took for the water to move from SP1 to SP2 in minutes.

(2) 1D control volume

The 1D control volume is a modified Eularian approach which relies upon defining a 1D volume and measuring benthic fluxes at within that area. We defined the 1D control volume between SP1 and SP2 and changes in dissolved oxygen within the control volume were used to calculate net community productivity as follows:

Eq.2

$$NCP = 0.5 * \left(\frac{\partial C_1}{\partial t} d_1 + \frac{\partial C_2}{\partial t} d_2 \right) + (C_1 - C_2) \frac{Ud}{L}$$

where ∂C_1 and ∂C_2 are the derivatives of the SeapHOx DO data series (1 hour rolling mean), divided by travel time (∂t) between SeapHOx 1 and 2, U is the velocity of water flow between the two sensors (m/s), and L is the length they travel in metres.

(3) Benthic Ecosystem and Acidification Measurement System (BEAMS)

The BEAMS approach, outlined in detail in Takeshita et al. (2016), measures NCC and NCP from gradients in the benthic boundary layer (BBL) driven by benthic activity. BEAMS measures change in NCP from direct measurements of dissolved oxygen concentration along a vertical gradient from 0.2 m to 0.7 m depth. At the same location as the SeapHOx sensors, two Benthic Ecosystem and Acidification Measurement System (BEAMS) were installed on the seabed to measure gradients of DO, salinity, pH, and temperature at 3 depths every 10 minutes.

(4) Advective benthic chamber enclosures

Benthic chambers (n=8) were deployed over sediments close to SP1 in duplicates for 48 hours from the 21st to the 25th of July, and discrete samples of seawater were collected at 1, 3, 5, 12, and 24 hours. Chambers were custom made from Plexiglass with a volume of approximately 4 litres. The base of the chamber was inserted around 15cm into the sediment. To ensure homogeneous distribution of solutes within the chamber, a rotating disc inside the chamber was set to 40 RPM and switched between clockwise – anticlockwise direction on each rotation. The rotation also simulated advection. Water samples were extracted from the chambers using a syringe and DO, salinity and pH were measured in-situ. Samples were stored in borosilicate glass bottles and fixed with mercuric chloride following standard protocol (Dickson et al., 2007) for carbonate analysis. NCP was calculated from the difference between start /end DO following equation 3, and NCC measured from changes in TA over the duration of the incubation.

(5) Discrete samples

Using standard methods (e.g., Dickson et al. 2007), discrete waters samples were collected across the bay at 18 locations (Fig 4-1a, white stars) as described in Takeshita et al., (2018).

4.2.4 Calculating net community calcification

NCC was calculated using the alkalinity anomaly (Kinsey 1978) following the standard equation:

Eq. 3

$$NCC = \frac{-0.5\Delta\text{TA}\ dp}{t}$$

Where ΔTA refers to the difference in TA measured at 'start' and 'end' points of benthic chamber incubations, sampling transects, and flow approaches. The rate is normalised to depth (d), and water pressure (p), and time in hours (t). For BEAMS and CV approaches ΔTA was estimated from ΔDO and ΔpH following the equation (Barnes, 1983):

Eq.4

$$-\Delta TA = \frac{\Delta DO \times Q + (K_1 - K_2)TA_2 - K_1(B_1 + OH_1) + K_2(B_2 + OH_2)}{(K_1 - 0.5)}$$

Where ΔDO is the difference in dissolved oxygen concentration between downstream and upstream measurements, Q is the photosynthetic quotient, or the relative change in dissolved inorganic carbon to oxygen (ΔDIC / ΔDO), K is the ratio of carbonate alkalinity to DIC, B is borate concentration, and OH is the hydroxide concentration, calculated using pH and K_W. TA_2 was assumed to be 2306 µmol kg and DIC 1990 µmol. We calculated K from salinity, pH, and temperature using the K1 and K2 functions of the SeaCarb package on R with the Waters et al., (2014) constant. The temperature measurements at each timepoint were incorporated into the relevant calculation of K. B was calculated from from salinity and equilibrium constants also on SeaCarb.

4.2.5 Analyses

NCC and NCP were modelled with light with a hyperbolic tangent function (Jassby and Platt 1976):

<div align="right">Eq. 5</div>

$$net\ community\ metabolism\ =\ P_{max} \times \tanh\left(\frac{\alpha \times E}{P_{max}}\right) + R$$

where net community metabolism refers to the measured P or G rate, R is the average dark respiration rate, and E is irradiance (μmol m^{-2} s^{-1}). The coefficients derived from the model include: the initial slope between metabolism and light (α) and the maximum gross photosynthetic rate, P_{max}, or maximum calcification, G_{max}.

Ratios of organic carbon production to inorganic carbon precipitation and dissolution were calculated using the following equation:

<div align="right">Eq. 6</div>

$$G_{net}/M_{tot}\ =\ \frac{|G_{net}|}{|P_{net}|\ +\ |G_{net}|}$$

4.2.6 Statistics

All data were compiled and analysed in R studio Version 1.4.1717 (R Core Team, 2021), with the help of the Tidyverse (Wickham, 2019) and ggplot (Wickham, 2016) packages for data handling and visualisation. Data collected at the SeapHOx stations after 7pm on the 24th of July were removed due to a shift in current speed / direction that interrupted the measurements (Fig 4-3). We plotted the data as time series comparisons, binning the data per hour to create composite measurements incorporating the remaining two days of data. Integrated rates were calculated using the trapezoidal integration with the *PRACMA* package on R (Borchers 2021). Metabolism-irradiance curves were plotted with nonlinear least squares with the hyperbolic tangent

equation (Jassby & Platt, 1976) and the model fit was evaluated from visual assessment, confidence intervals for each of the coefficients, and standard error of the regression (sigma, σ). Linear regressions of TA:DIC models were calculated and plotted using the *ggmisc* package (Aphalo, 2021).

4.3 Results

The autonomous sensor packages were deployed over 4 consecutive days, however due to unstable weather conditions, which affected the current direction and other parameters, only 48 hours of data have been included in the analysis. Figure 4-3 shows the raw data collected with the SeapHOx. Data after 19:00 h on the 24th were removed from the analysis (red line on Fig. 4-3 shows cut off point). Despite the stormy weather conditions, environmental parameters measured at the autonomous sensor stations (before the 25th July) remained relatively constant throughout the sampling period: temperature (28.42 °C ± 0.23), salinity (36.82 ppt. ± 0.16 ppt), and pH (7.97 ± 0.008). PAR was low due to cloud cover ($185.9 \pm 197.54 \, \mu mol \, m^{-2} \, s^{-1}$, mean ± SD). There was slight variability of these parameters at different times of day / night (Table 4-1).

Measurements of ecosystem metabolism using Lagrangian, control volume, BEAMS, and benthic chamber apparatus revealed small but important differences between the techniques. For all methods, NCP was positive during daytime hours and negative (i.e., net respiration) at night (Figs 4-4 & 4-5). NCC generally showed a similar trend of positive rates during the day and negative (i.e., net dissolution) at night, however the signal was likely below the threshold for BEAMs to detect (Fig 4-7). Advective benthic chambers placed over sediments confirmed positive day and negative night NCC and NCP, which were similar in magnitude to the other methods (Fig. 4-8). Rate integration over 12- and 24-hour periods highlighted agreement between Lagrangian and control volume measurements, while differences between BEAMS 1 and 2 demonstrated their sensitivity to the slightly distinct benthos in the two areas of the bay (Fig. 4-9). Community metabolism increased with light levels according to traditional light-metabolism dynamics, however coefficients between metabolism– irradiance models revealed further differences between the methods (Fig 4-12).
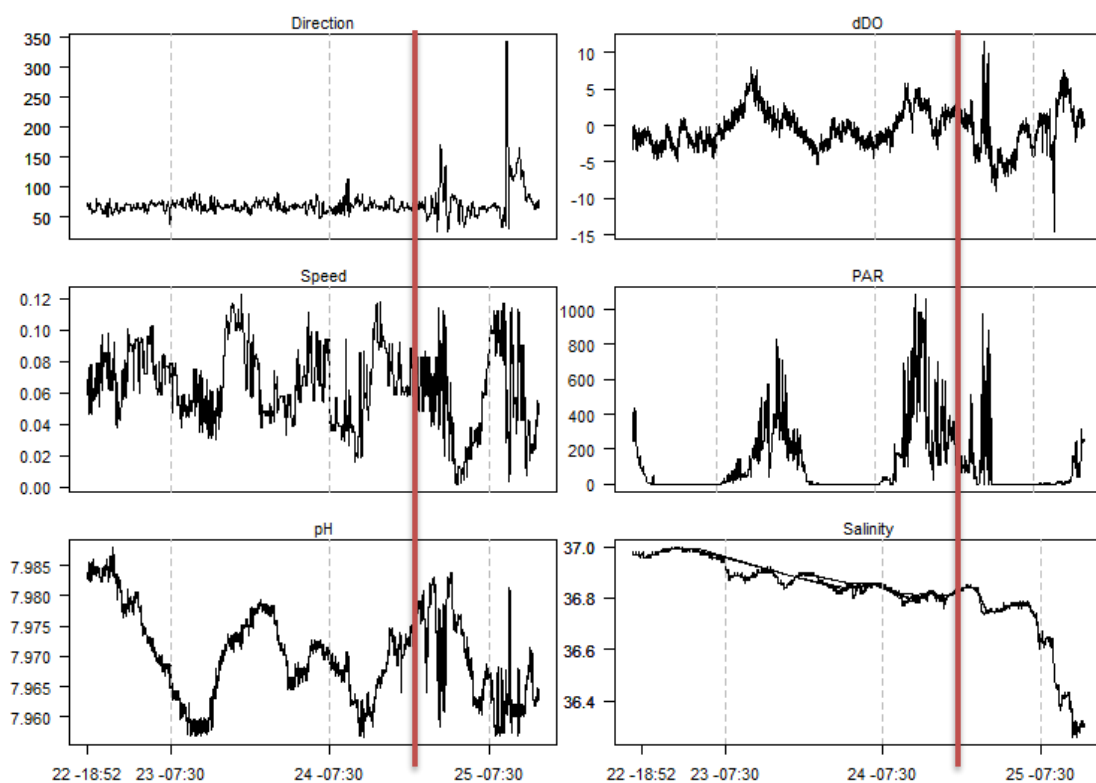
Figure 4-3: Raw data collected by the SeapHOx autonomous sensor at the end station of the transect (SP2). Vertical red line shows where the data were cut off due to stormy weather conditions, data beyond this line (after 19:00 hrs on the 24th) were removed for the analysis.

Table 4-1: Environmental parameters at different times of day (mean±SD).

	PAR	Depth (m)	Temp (C)	pH	Salinity (ppt.)	Speed (m/s)	DO (umol/l)
07:00 –	237.66	2.58	28.31	7.96	36.85	0.05	178.96
12:00	±195.26	±0.17	±0.09	±0.00	0.05	±0.01	±2.68
12:00 -	393.71	2.91	28.47	7.97	36.84	0.09	187.36
1400	±257.73	±0.05	±0.04	±0.00	0.04	±0.02	±2.02
14:00 –	188.11	2.62	28.55	7.98	36.87	0.07	190.06
1900	±178.47	±0.18	±0.13	±0.00	0.05	±0.02	±1.18
19:00 -	12.95	2.64	28.49	7.97	36.90	0.06	181.87
07:00	±38.55	±0.19	±0.20	±0.01	0.07	±0.02	±4.05

4.3.1 Autonomous measurements of net community metabolism

Diel cycles for NCP were consistent between all measurements using the autonomous sensors (Lagrangian, control volume, and BEAMS), with positive NCP increasing with daylight and negative NCP indicating net respiration at night (Figs. 4-4 & 4-5a). Lagrangian and control volume NCP trends were similar over the 24-hour cycle, whereas there was greater variability both within and between BEAMS 1 and 2 NCP data series (Figs 4-4 & 4-5). Overall, NCP was highest in BEAMS 2 over the 48-hour period, potentially reflecting the higher cover of seagrass at the location of SP2 in Bailey's Bay. Peak NCP rates occurred around solar noon for Lagrangian and control volume, while BEAMS detected greater variability in NCP around peak sun between the two sampling locations. Lower NCP at BEAMS 1 was observed, likely due to its positioning over sediments compared to higher seagrass cover at BEAMS 2. NCC rates also followed a diel cycle with positive NCC during light hours, and some dissolution at night. Calcification rates were relatively low, and the fluctuations in the BEAMS measurements (Fig. 4-4 & 4-5) indicated that the NCC signal may have been below BEAMS detection limits. NCC is calculated using Q which was assumed to be 1.1, based on previous work (Cyronak et al., 2018; Takeshita et al., 2016). However, Figure 4-6 demonstrates how different Q values used in the NCC calculation from BEAMS measurements can influence the calculated rate, and subsequent analysis of NCC-NCP ratios. 24-hour composite plots of hourly binned NCP and NCC data showed strongest similarity between Lagrangian and control volume trends, whereas greater variability was observed in hourly rates measured by BEAMS (Fig. 4-7).
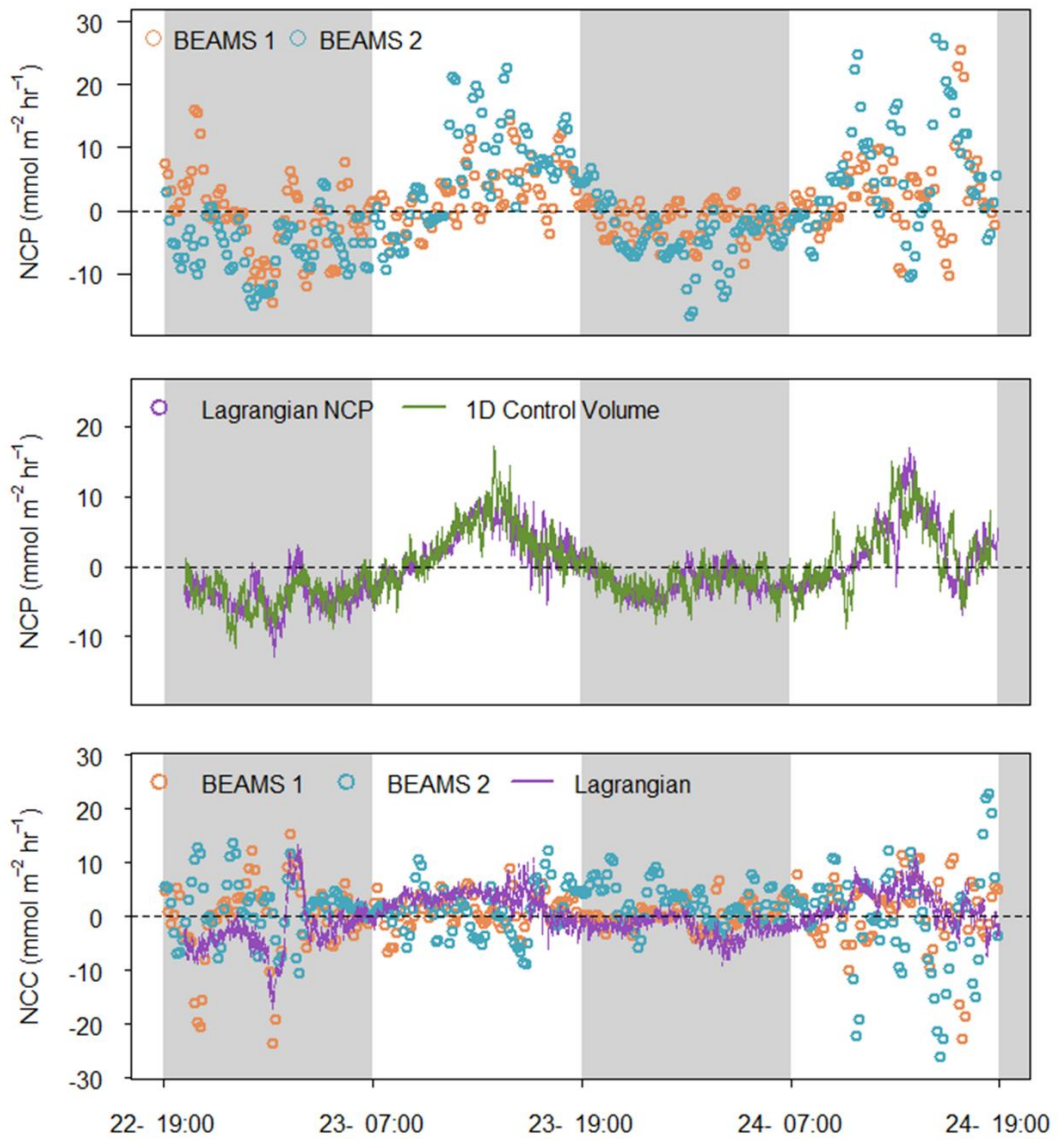
Figure 4-4: Net community production (NCP) measured with autonomous sensors using the BEAMS (top), Lagrangian and control volume (middle) approaches, and for net community calcification (NCC) (bottom). BEAMS data were collected every 10 minutes at the location of the SeapHOx equipment packages (SP1 and SP2), while Lagrangian and control volume were calculated from measurements taken every 1 to 2 minutes (as dictated by the flow rate between SP1 and SP2). Dark and light background indicate hours of daylight.
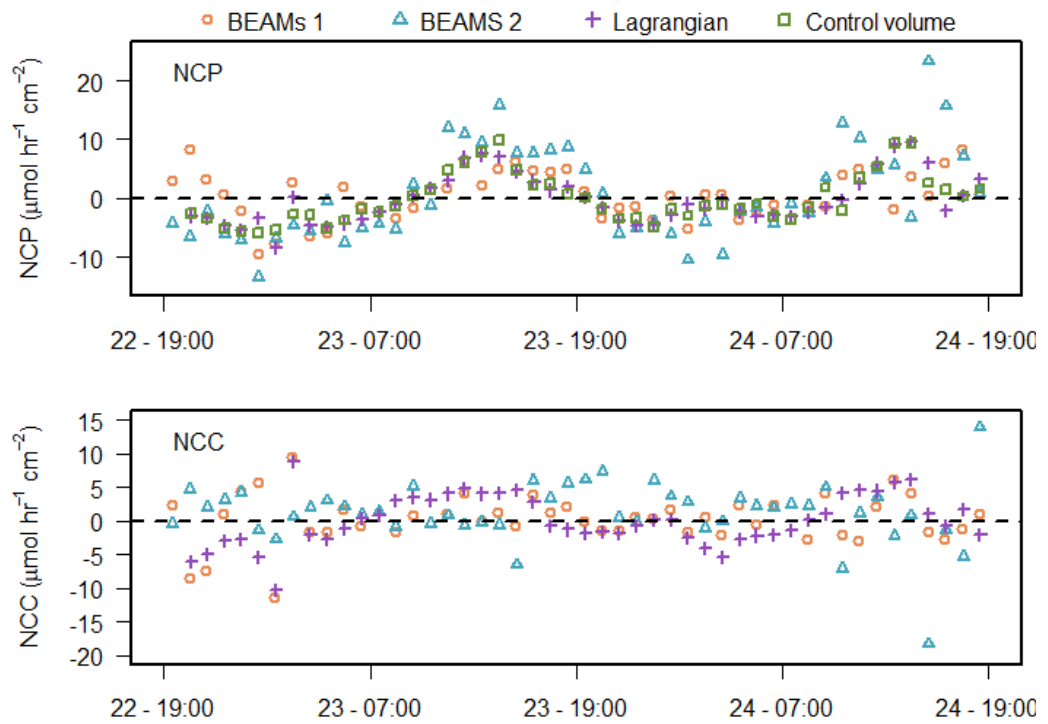
Figure 4-5: Hourly binned mean average for each autonomous sensing method. Top: Met community production (NCP), bottom: net community calcification (NCC). Different methods shown with colours and symbols.
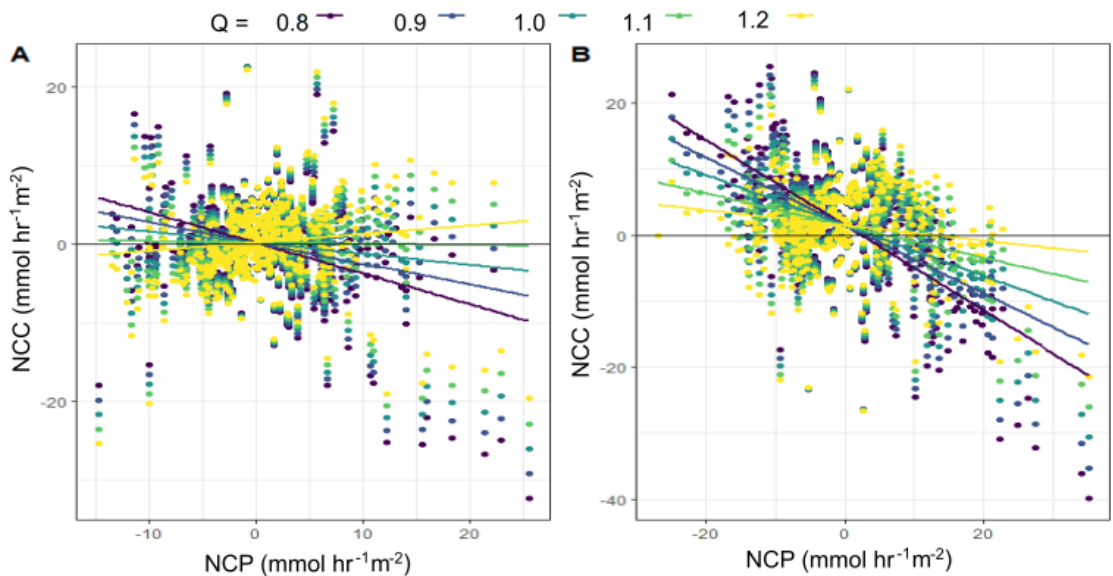
Figure 4-6: Net community calcification (y-axis) to net community production (x-axis) with NCC calculated using metabolic quotient (Q) values ranging from 0.8 to 1.2 using the BEAMS approach. Plot A shows BEAMS 1, plot B is BEAMS 2.

(a) Net community production (NCP)
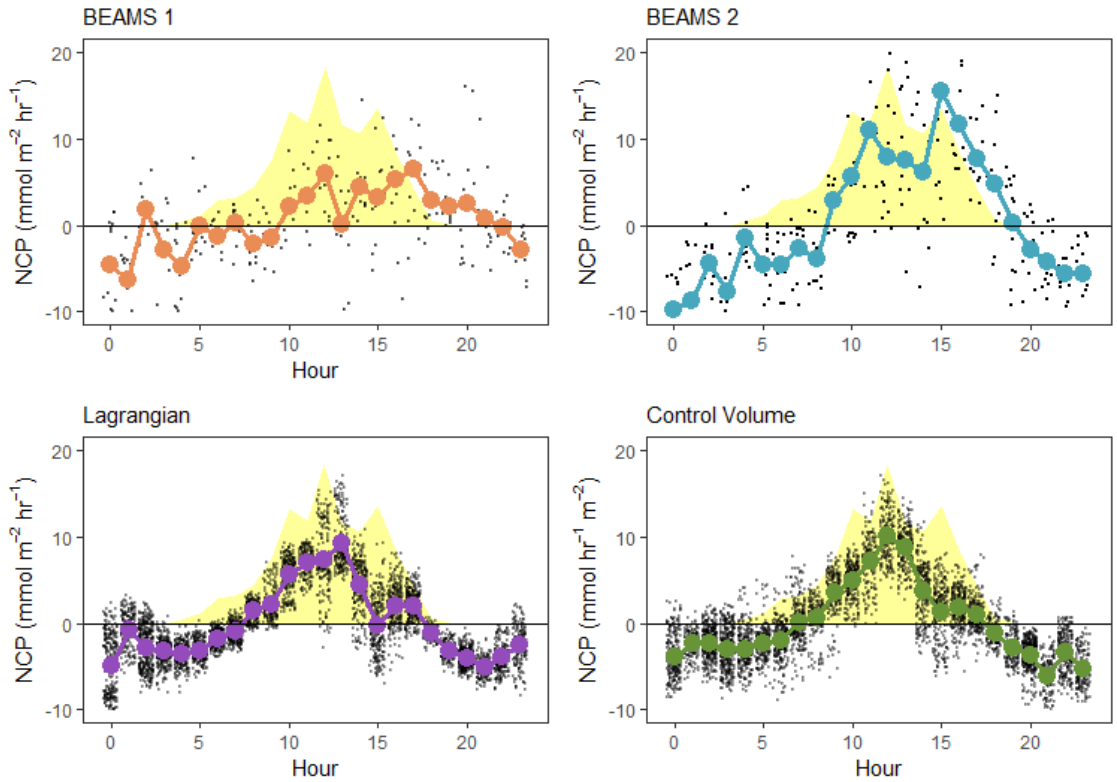
(b) Net community calcification (NCC)
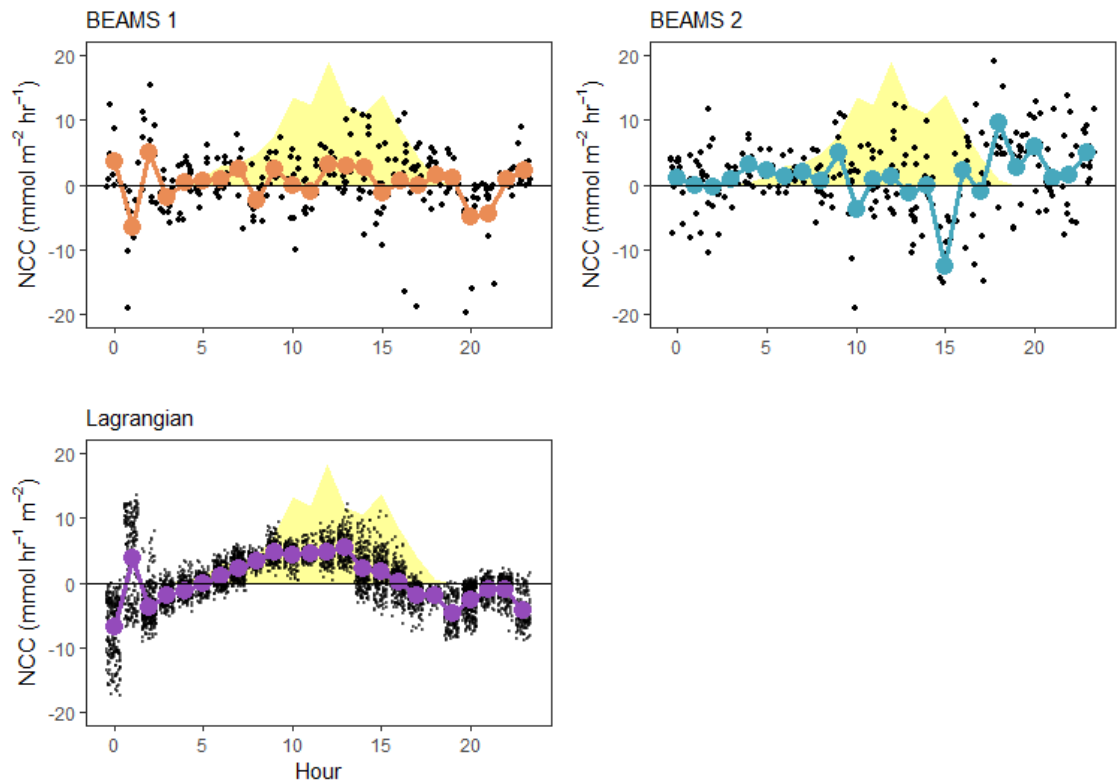
Figure 4-7: Composite time series of **(a)** net community production (NCP) and **(b)** net community calcification (NCC). Shaded yellow area shows PAR measured, small black dots are individual data points. Large, coloured dots are hourly mean values.

4.3.2 Advective benthic chamber incubations

Hourly rates of metabolism measured in the benthic chambers were lower than values measured by autonomous sensors. Twelve-hour incubations had positive rates of metabolism during the day and negative rates (net respiration and dissolution) at night (Fig. 4-8). Shorter incubations (2 to 5 hours) measured rates of NCC and NCP that were highest during solar noon incubations (NCP= 4.52 ± 0.68 mmol m^{-2} hr^{-1}, NCC $=1.45 \pm 0.37$ mmol m^{-2} hr^{-1}, mean $\pm$ SD), however, they were lower compared to the other methods.
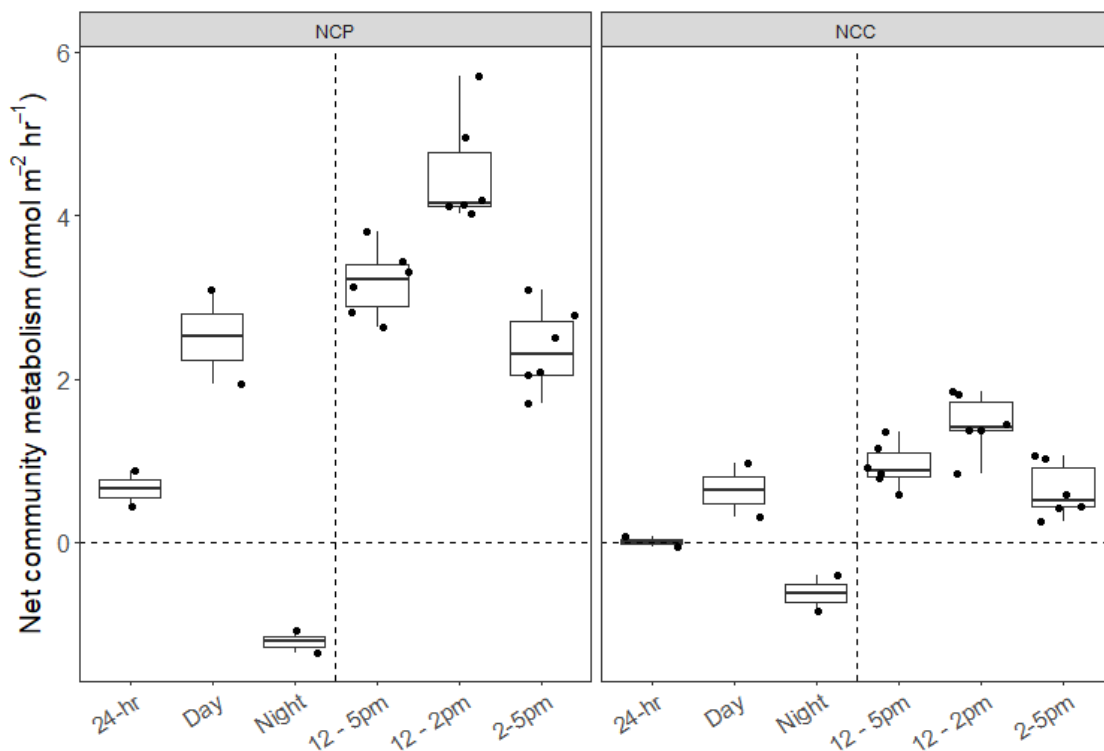
Figure 4-8: Metabolic rates measured in chamber deployments. Day and night are between 7.30 am and 7.30 pm respectively. Dotted vertical lines separate 24 and 12-hour incubations and shorter incubations for NCP **(left)** and NCC **(right)**.

Daytime (12-hour) and 24-hour incubations had NCP rates aligned with the equivalent integrated rates from autonomous measurements. However, night-time chamber incubations had lower rates of negative NCP (net respiration) when compared to the integrated night rates measured with autonomous sensors (Table 4-2, Fig 4-9). Similarity was apparent between metabolism measured by chambers and BEAMS 1 (integrated rates, Fig 4-9), as both BEAMS 1 and chambers measured metabolism over the sediments rather than seagrasses.
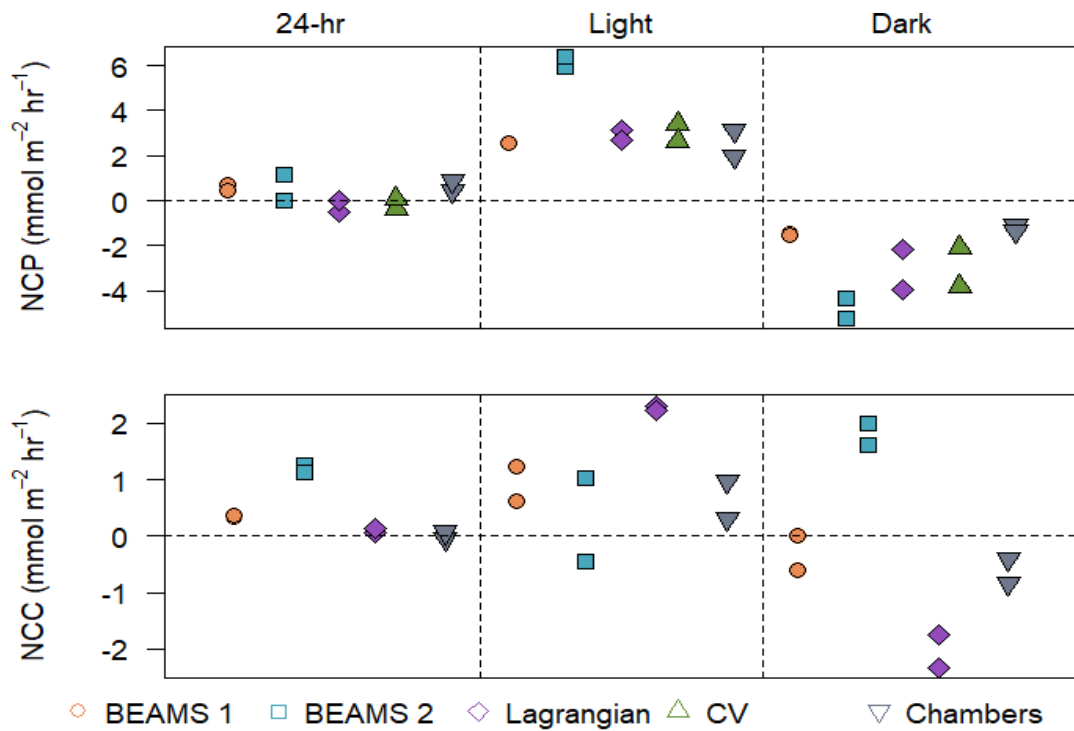
Figure 4-9: Integrated rates for each of the methods over 24 hours **(left)**, during light hours only **(middle)** and overnight **(right)**. Light and dark hours were between 7.30 am and 7.30 pm respectively. Top: Net community production (NCP) and bottom: net community calcification (NCC). The different methods are defined by shapes and colours.

Table 4-2: Summary of integrated rates calculated over 24 hours and day / night (NCP and NCC in mmol m^{-2} hr$^{-1)}$. The number of 24-hour period of data collection is indicated by *n.*

		n	24-hour		night		day	
NCP (mean ±SD)	BEAMS 1	2	0.60	±0.17	-1.34	±0.28	2.54	±0.02
	BEAMS2	2	0.61	±0.82	-4.92	±1.30	6.17	±0.32
	Lagrangian	2	-0.25	±0.37	-3.14	±0.89	2.57	±0.41
	Chambers	2	0.65	±0.31	-3.37	±1.36	2.72	±0.55
	Control volume	2	-0.11	±0.32	-1.21	±0.19	2.52	±0.81
NCC (mean ±SD)	BEAMS 1	2	0.35	±0.02	-0.27	±0.45	0.92	±0.42
	BEAMS2	2	1.19	±0.09	2.05	±0.84	0.29	±1.06
	Lagrangian	2	0.10	±0.06	-2.13	±0.32	2.33	±0.36
	Chambers	2	0.01	±0.08	-0.63	±0.30	0.64	±0.47

4.3.3 The relationship between net community calcification and production

Regression analysis of net community calcification to production (NCC: NCP) is a useful tool for understanding ecological function of an ecosystem (Cyronak et al., 2018; Muehllehner et al. 2016), with the slope and direction indicative of the relative balance of organic to inorganic carbon fluxes taking place between the benthos and surrounding seawater. For this analysis, we plotted NCC: NCP linear regressions using data collected with the Lagrangian, BEAMS and benthic chambers (Fig. 4-10) and found that regression gradients and R^2 were variable between methods and between night and day data. Additionally, TA: DIC regressions of discrete samples collected parallel to sensor deployments showed differences between morning, peak sun, and afternoon (Fig 4-11). The control volume approach only measured NCP, therefore was not included.
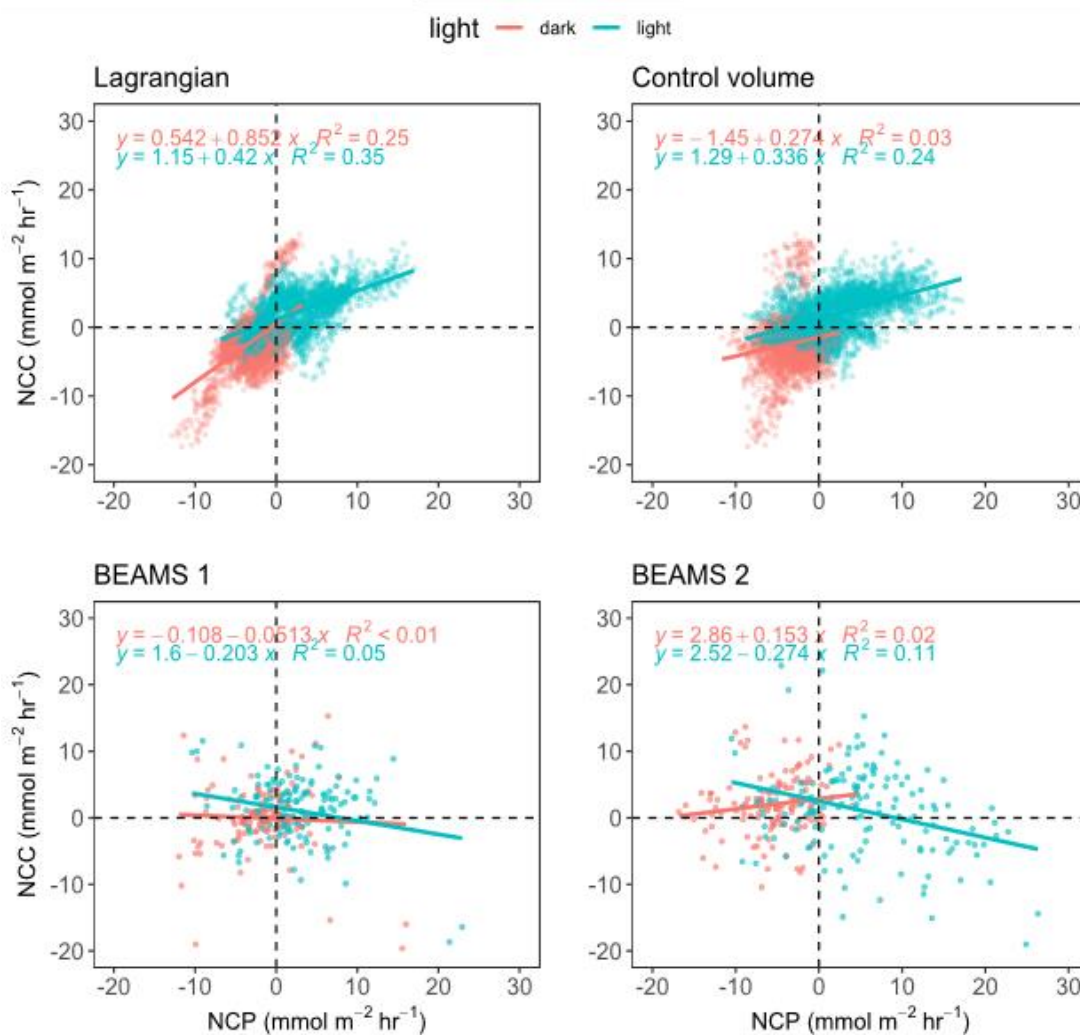
Figure 4-10: Scatterplots and linear regressions show the relationship between NCP vs. NCC during light (blue) and dark (red) observations for each of the methods: **(a)** Lagrangian, **(b)** Control Volume, and **(c)** BEAMS 1 **(d)** BEAMS 2.
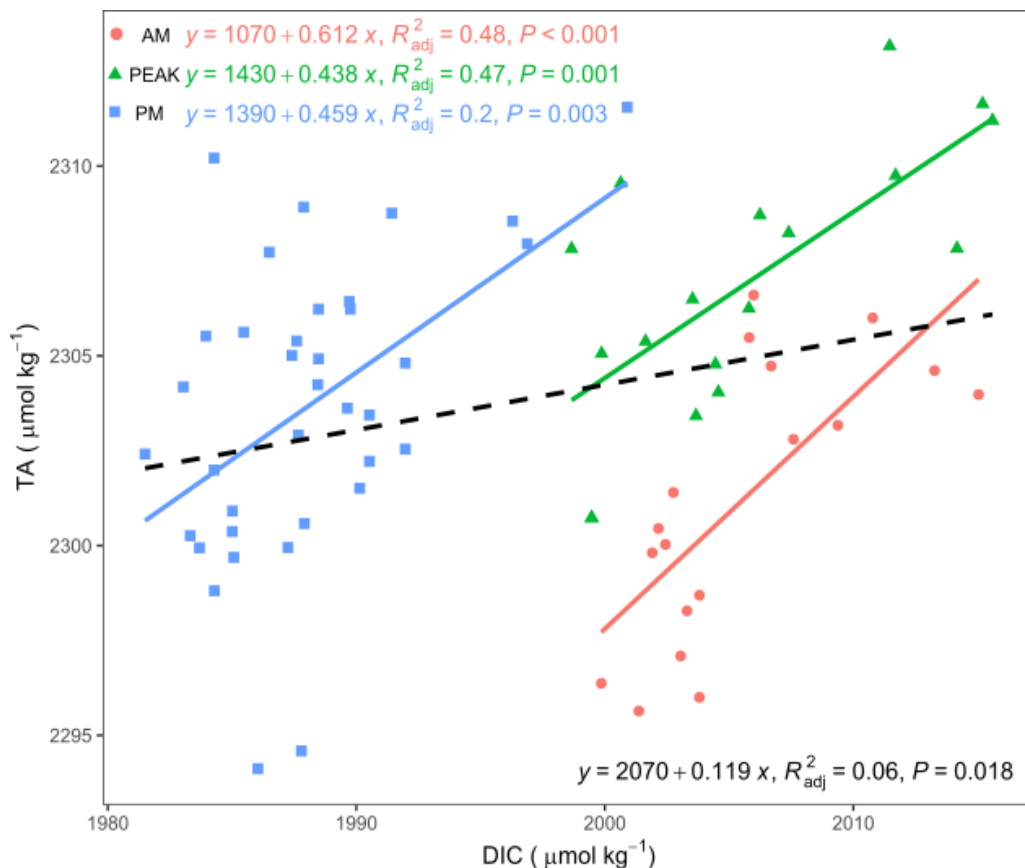
Figure 4-11: Regressions of total alkalinity concentration to dissolved inorganic carbon (TA:DIC) measured from seawater samples collected using the 'discrete sampling' method at different time surveys across the bay: AM (07:00-08:00), PEAK (noon to 14:00), PM (16:00 to 18:00), represented with different colours and shapes. Black dotted line and black writing show the linear regression for all data grouped together.

4.3.4 Light influence on metabolism

While NCP values varied between methods, the influence of light was apparent for all measurements with a similar trend of NCP increasing with light until peak solar irradiance. Metabolism-irradiance models demonstrated a hyperbolic relationship between light and NCP (Fig. 4-12), and the model coefficients demonstrated that BEAMS 2 had the highest maximum NCP (P_{max} 16.55 ± SE 1.23) and BEAMS 1 the lowest (P_{max} 6.0 ± SE 0.74 mmol hr^{-1}). Model coefficients for Lagrangian and control volumes were almost identical (Table 4-3). NCC collected by BEAMS did not fit the model (Fig. 4-13, Table 4-3).
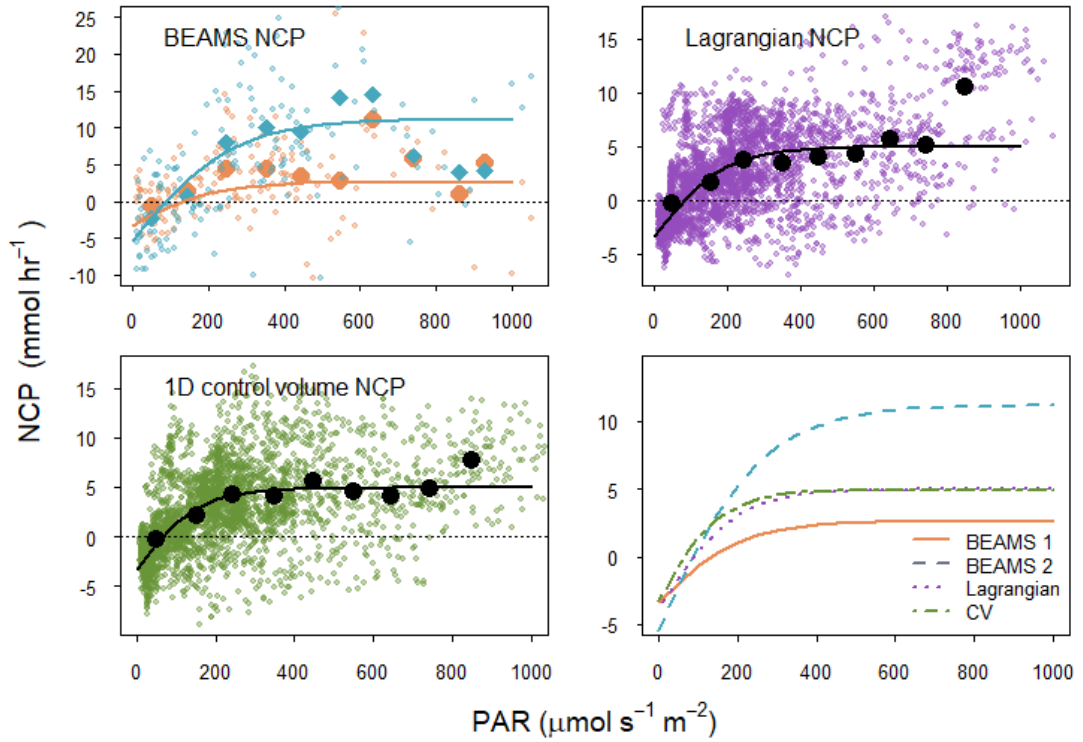
Figure 4-82: Photosynthesis-irradiance models for autonomous sensing methods used to measure net community production from changes to dissolved oxygen. Models were fit using a hyperbolic tangent function. Black dots show the mean for each 100 µmol m^{-2} s^{-1} PAR interval, while small, coloured dots show individual data points.
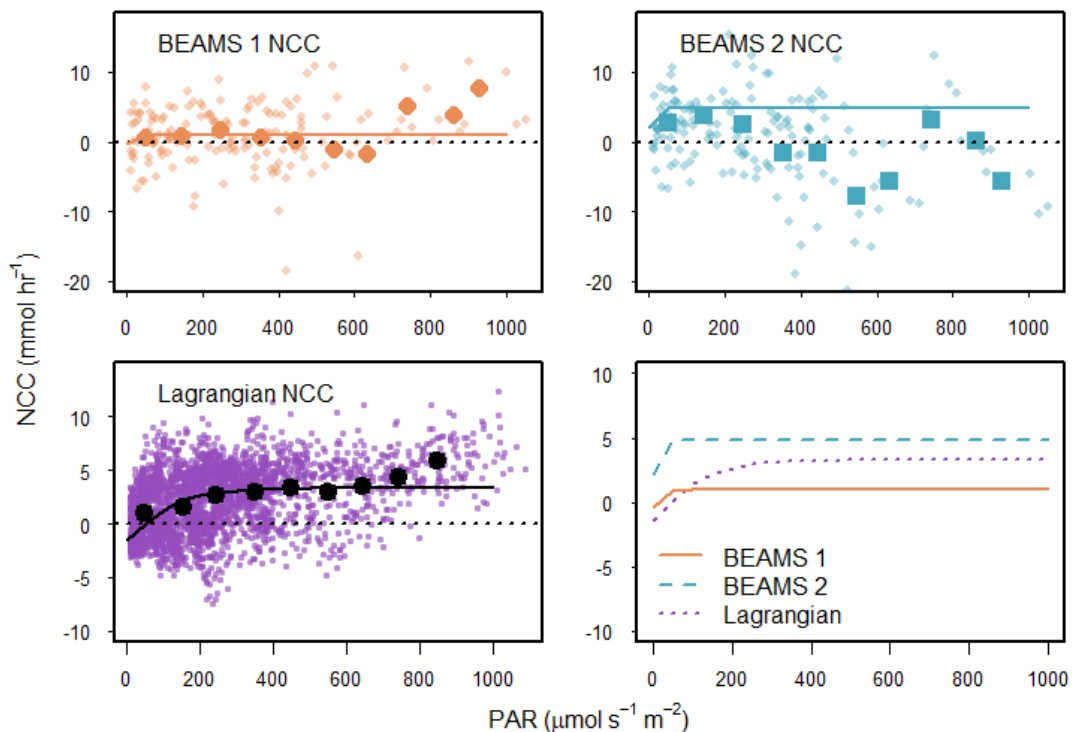
Figure 4-13: Calcification – irradiance models for each of the methods used to measure net community calcification (NCC) calculated from changes in total alkalinity (ΔTA) derived from pH and DO measurements. Small dots show the individual data points, larger points show binned averages (100 µmol m^{-2} s^{-1} PAR intervals).

Table 4-3: Results of the metabolism-irradiance model fitting using the hyperbolic tangent function. Model coefficients P_{max} and G_{max} are the modelled maximum values, alpha α is the initial slope gradient, and E_K is the irradiance saturation point calculated from the metabolic maxima and alpha values. Coefficients derived from the models are presented with standard error (SE) and 2.5 % and 97.5 % confidence intervals. R and G_{dark} refer to the mean average night / dark values, which were input into the models. The model fit was defined by sigma σ, the residual standard error and the residual sum of squares (RSS).

NCP	P_{max}	$\pm SE$	CI 2.5%	CI 97.5%	α	$\pm SE$	CI 2.5%	CI 97.5%	R	E_K	σ	RSS
BEAMS1	**6.00**	0.74	4.54	7.45	**0.03**	0.01	0.01	0.04	-1.76	209.04	4.96	3916.66
BEAMS2	**16.55**	1.26	14.06	19.04	**0.06**	0.01	0.05	0.08	-5.41	261.73	7.05	8055.74
Lagrangian	**8.36**	0.13	8.10	8.63	**0.05**	0.001	0.04	0.05	-3.39	185.53	3.53	38076.75
CV	**8.31**	0.13	8.06	8.57	**0.05**	0.002	0.05	0.05	-3.28	170.53	3.64	40487.82

NCC	G_{max}	$\pm SE$	CI 2.5%	CI 97.5%	α	$\pm SE$	CI 2.5%	CI 97.5%	G_{dark}	E_K	σ	RSS
BEAMS 1	1.33	0.42	0.51	2.15	0.04	0.09	-0.14	0.23	-0.34	29.95	4.85	3738.29
BEAMS 2	2.64	0.59	1.47	3.82	0.33	2.11	-3.83	4.50	2.13	7.93	7.43	8955.05
Lagrangian	4.75	0.09	4.57	4.93	0.03	0.00	0.03	0.03	-1.46	148.89	2.81	24241.60

4.3.5 Shifting ratios of organic and inorganic carbon cycling in response to light

Quantifying the ratio of calcification to production for benthic communities in coastal ecosystems is considered a metric of overall ecosystem function and health. The calcification / photosynthesis ratio (G_{net} / P_{net}) has been successfully implemented to quantify the carbon metabolism of seagrasses and coral reefs; however, estimates are often made based on individual measurements at peak light or dark conditions and generalised to the 24-hour period. We found that the balance of organic production to inorganic carbon precipitation and dissolution shifts over the course of a 24-hour cycle, and that different methods of measuring NCC and NCP gave distinct ratios when modelled to light (Fig.4-14). Lagrangian and control volume had similar total metabolism (M_{tot}) ratios, however they were different from BEAMS.
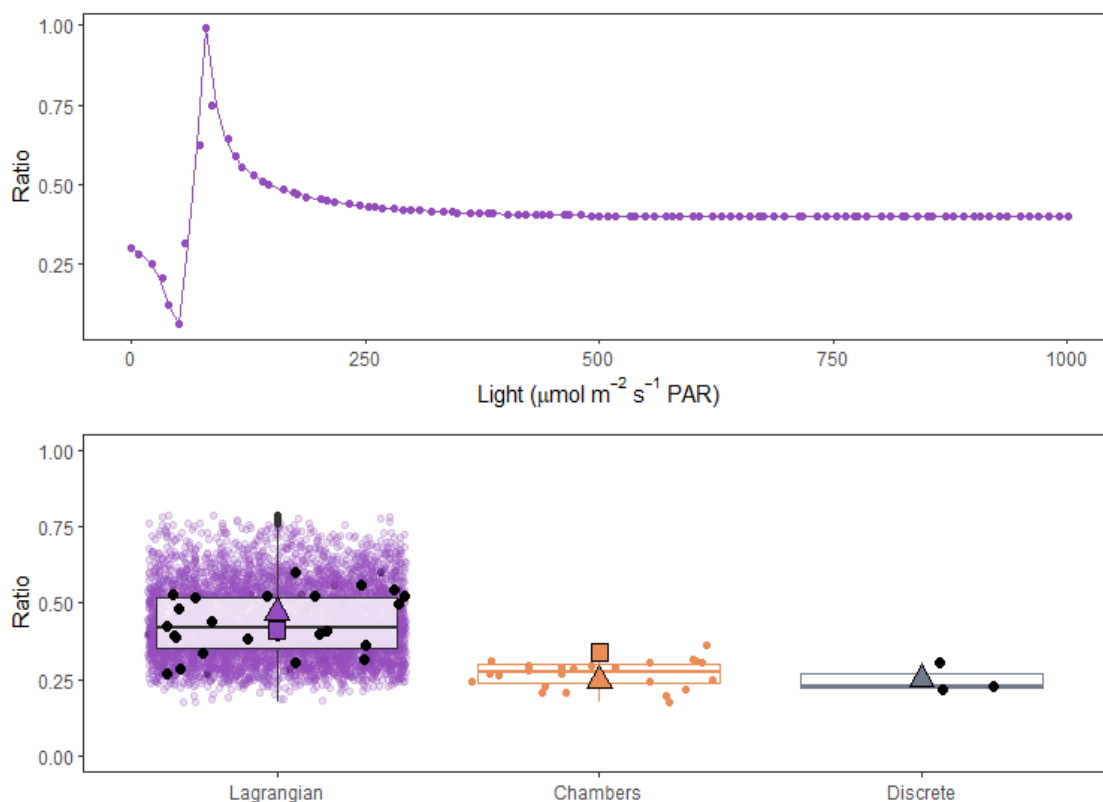
Figure 4-14: Total metabolism ratios (M_{tot}, the sum of both calcification and production) for the distinct methods used to measure NCP and NCC. Top: Lagrangian M_{tot} calculated from the photosynthesis- and calcification-irradiance curves and plotted against light. Bottom: Boxplots showing the spread of M_{tot} for the different methods. Triangles are daily mean averages; squares are night means. Lagrangian shows the individual data points as purple dots and hourly means as black dots.

4.4 Discussion

This study compared measurements of benthic community metabolism collected with a range of well-established and emerging techniques in a shallow seagrass and CaCO$_3$ sediment bay. Autonomous sensors were deployed to directly measure changes in NCP using Lagrangian flow respirometry, control volume, and BEAMS approaches. Net community calcification was indirectly calculated from BEAMS and Lagrangian measurements of DO and pH using the equation of Barnes et al (1983). Traditional discrete samples were also collected during surveys and in-situ chamber incubations. Differences were found between the methods, highlighting strengths and limitations of each approach, with important implications for field measurements of benthic metabolism.

4.4.1 Comparing Methods to Measure Net Community Production

Autonomous measurements of NCP were positive during daytime and negative at night over the 48-hour deployment, following the expected trend with PAR for all methods. NCP measured by Lagrangian flow respirometry and 1D control volume approaches showed almost identical time series trends (Figs. 4-4, 4.5). Flow respirometry measures changes to water as it traverses the ecosystem, whereas the 1D control volume approach incorporates vertical gradients for higher precision measurements (Teneva et al. 2013). Both methods used the same sensing packages, however, the calculations for each were distinct (see methods section). While the results from these two methods were similar, the logistics for a 1D control volume measurement require specific hydrodynamic conditions that may not exist in certain habitats or ecosystems (Falter et al. 2008). The Lagrangian flow method requires 2 sensor packages, and knowledge of the current conditions at the study site. One strength of the flow respirometry method is that it incorporates natural currents, a key influence on metabolic rates as reflected in higher community metabolism reported by previous studies (Shaw et al. 2014). Lagrangian and control volume NCP measurements were similar to BEAMS, despite the fact that BEAMS only measures benthic metabolism while the other two methods incorporate water column metabolism (Long et al. 2019). This indicates that benthic metabolism dominated the overall

metabolic fluxes in Bailey's Bay. However, more studies are needed to confirm this, especially considering that Long et al. (2019) reported that water column fluxes accounted for 58% of the total oxygen flux at an offshore Bermuda reef.

Another constraint of flow respirometry studies is that they have historically required repeated measurements over multiple days to compile sufficient data for a 24-hour ecosystem metabolism rate calculation, however, as we conducted flow respirometry using high resolution autonomous sensors (30 second intervals) the data collected are essentially real-time. Similarly, the BEAMS approach facilitates high resolution, accurate, and instantaneous measurements of community metabolism. As the method focusses on vertical gradients, it is not subject to some of the limitations of flow respirometry, which cannot be conducted if direction of flow changes, and measurements are generalised over the transect area, which may be hundreds of metres. BEAMS has shown agreement with benthic chamber measurements in previous research (McGillis et al. 2011), demonstrating that BBL-based technologies such as BEAMS can provide accurate metabolic rate measurements for coastal ecosystems. The higher hourly variability of BEAMS NCP measurements (Fig 4-7) likely represents real-time fluctuations that were not detected by the other methods. BEAMS measurements of NCP do not rely on flow, similar to the control volume technique they require vertical pumping of seawater only. Their smaller footprint shows in the low NCP observed by BEAMS 1, which was deployed over sediments compared to BEAMS 2, which was deployed over seagrass and had a higher rate of NCP.

Benthic incubation chambers had the lowest metabolic rates when compared to hourly composite rates, supporting previous studies showing that the reduced flow is associated with lower metabolic rates (Dennison and Barnes 1988; Comeau et al. 2019). The chambers were fitted with circulation discs; however, this does not constitute an accurate simulation of environmental turbulence and flow rates. Chamber incubations have been used to successfully measure rates of metabolism across a range of scales, from the single organism to the community (Fig. 4-1). While the results from such chamber deployments have provided useful insight, comparisons between studies are limited due to the lack of method standardisation. Discrepancies between measurements are often accredited to environmental and geographical heterogeneity, however, relatively few direct comparisons have been conducted. Integration of rates over 24 hours showed comparable values for NCC and NCP between the chambers and autonomous methods, with the closest agreement between BEAMS 1 and chambers,

likely due to the apparatus for both being deployed over the same substrate (carbonate sediments).

4.4.2 In-situ Calcification Measurements

A major challenge in measuring ecosystem metabolism is the technological limitations of measuring total alkalinity. Currently, in-situ apparatus to directly measure changes in TA is not currently available, therefore measurements of NCC typically require laboratory analysis of discrete water samples. However, it is possible to approximate a total alkalinity gradient from simultaneous measurements of DO and pH, a method that has been successfully implemented for quantifying coral reef and seagrass NCC (Barnes 1983; Barnes and Devereux 1984; Takeshita et al. 2016). With advances in autonomous sensing of DO and pH, this method for measuring NCC has the potential to improve the scope of ecosystem-wide measurements of NCC. In this study, NCC was calculated from pH and DO for Lagrangian flow and BBL approaches, with different results. Instantaneous measurements of NCC are dependent on the assumption of the quotient Q, which in our study was 1.1, based on previous studies. We also explored the NCC: NCP relationship with Q values ranging from 0.8 to 1.2 (Fig. 4-6) and found that lowering the Q value in our equation decreased NCC during daylight hours and increased night NCC (i.e., lowering dissolution rate estimates). This finding highlights that site-specific Q will impact NCC measurements and needs to be incorporated into future studies.

4.4.3 Light as a driver of ecosystem metabolism

Production is controlled by ambient light conditions driving photosynthesis in shallow coastal ecosystems. A similar relationship between NCC and light has also been reported (Shaw et al. 2012; Cyronak and Eyre 2016) although it is unclear if this is due to the influence of NCP or if calcification is directly stimulated by light. Light-enhanced Calcification (LEC) occurs in corals and reef calcifiers, however the influence of light on carbonate sediments is relatively unknown. At night, respiration and dissolution became the predominant processes taking place in Bailey's Bay. It appears the switch from net calcification to dissolution was not picked up by BEAMS, most likely due to the low signal. Regression analysis of night data revealed that the relationship between NCC to NCP differs between night and day, with steeper slopes

observed during daytime hours, reflecting stronger correlation between NCP and NCC during daylight hours, highlighting the importance of light as a driver of benthic metabolism.

4.4.4 Quantifying carbon cycling in coastal ecosystems

Coastal ecosystems are significant for global carbon cycling, oxygen production and carbonate lockdown, however, their geographic heterogeneity and temporal variability have limited observation, so that for many coastal ecosystems net ecosystem metabolism over space and time is not fully constrained. Autonomous sensing technology has the potential to update and facilitate longer term and ecosystem-wide metabolism measurements at scale. Seagrass carbon is stored primarily underground in the $CaCO_3$ sand-sediments. Measuring calcium carbonate sediment accretion and dissolution is critical for understanding and predicting their potential as a globally significant carbon store. These processes are controlled by advection and environmental conditions as well as the NCC and NCP of surrounding coral reefs and seagrass meadows. Two of the methods used in this study provided sediment-specific rates; BEAMS 1 and chambers as they were deployed over carbonate sediments, however NCC measured by chambers was low, and BEAMS 1 may not have detected any trend in NCC over the course of the deployment. BEAMS have successfully constrained reef calcification rates in previous studies (Takeshita et al. 2016; Platz et al. 2020), and it is likely that the lower rates of NCC in the current study were not strong enough for BEAMS. We found that ratios of NCC to NCP were different between methods, and between night and day (Figs. 4-10 & 4-14).

4.4.5 Implications for ecosystem monitoring and conservation

Seagrasses are blue carbon ecosystems, referring to their photosynthetic capacity to sequester atmospheric CO_2. Blue carbon estimates typically focus on quantification of organic carbon stock within the ecosystem; however, the role of inorganic carbon precipitation and dissolution is a critical component of long-term carbon storage capacity (Macreadie et al. 2017). Seagrass meadows are diverse communities of autotrophic and heterotrophic organisms, therefore, simply measuring the biomass of

seagrass to estimate their carbon value does not fully incorporate the interactive dynamics of the community as a whole (Long et al. 2015b). Therefore, the balance of calcification to photosynthesis of coastal ecosystems is essential for quantifying accurate blue carbon budgets and predicting the response of these ecosystem to climate change. Coral reefs and seagrasses are considered interdependent and connected ecosystems, supporting nutrient transfer and biogeochemical function across the tropical coastal ocean. These ecosystems of the coastal ocean are some of the most vulnerable to climate change and anthropogenic impacts. Logistical limitations have presented a challenge for long-term monitoring of change on these ecosystems, and this study explored some of the biogeochemical methods available to measure high-resolution metabolism to support and enhance coastal monitoring and quantification of coastal carbon cycling.

Based on the findings of this study, future research should aim to further compare these methods in a range of environments, for example, over a coral reef where the calcification signal would likely be higher and therefore easier to detect patterns within the diel cycle. The methods compared in Chapter 4 demonstrated agreement and discrepancies depending on the parameter measured and time frame of the measurement, for example, lower rates of calcification were reported from longer 12-hour chamber deployments than shorter 2-hour deployments or Lagrangian measurements of NCC. Studies to quantify metabolism of a smaller subsection of an ecosystem should incorporate BEAMS (i.e., approx. 10 m^2 footprint) or chambers (approx. 1 m^2 planar area), while broader ecosystem-wide estimates of metabolism would benefit from using the Lagrangian flow method. As there have been limited direct comparisons of methods to determine which should be used for distinct applications, it is worthwhile at this stage to incorporate more than one method for measuring ecosystem metabolism into future studies. Another key recommendation for applications of these methods arising from the current study is to encourage longer term deployments of autonomous sensors to provide greater insight into diurnal, weekly and monthly shifts in metabolism. This is critical as changing marine conditions such as warming, acidification and deoxygenation may become additional challenges for accurate quantification of seawater parameters and metabolism estimates.

5   Conclusions

As coastal ecosystems are heavily impacted by the changing climate, quantifying benthic metabolism is increasingly important as a metric for ecological function and for understanding coastal carbon cycling. Measurements of benthic metabolism can be used to track changes to ecosystem function and species compositions, to predict benthic community trajectories and future ecosystem response to climate change and environmental degradation. In this thesis, the balance of calcification to dissolution, and photosynthesis to respiration were evaluated at three distinct scales: individual organism, small community, and the broader ecosystem, using an array of established techniques and novel equipment. This final chapter presents the key findings of the thesis, highlights their significance, and discusses future research directions.

The first key findings of this research were the species-specific differences in metabolic rates of coral reef calcifiers. Chapter 2 measured calcification (G_{net}), dissolution (G_{dark}), photosynthesis (P_{net}), and respiration (R) in small individual replicates of scleractinian coral and calcifying algae. The organisms chosen for this study represented key functional groups on the reef: *Acropora cervicornis* is a branching, rapid-growth coral, *Orbicella annularis* and *Siderastrea Siderea* are slower growing reef builders, *Porites astreoides* is an opportunistic 'weedy' species, and crustose coralline algae (CCA) is a low-profile, encrusting calcifier which cements reef substrate in place and provides critical substrate for juvenile coral recruitment (Fig. 2-1). In general, metabolic rates were different between species of coral, and between coral and CCA (Figs. 2-4 to 2-6). However, there was unexpected similarity of calcification rates between *A. cervicornis*, a key reef-builder and one of the fastest growing corals, with CCA, an organism which does not contribute to building large coral reef structures in the same way as reef-building corals.

Quantification of calcification and production rates in different coral species is important for coral reef conservation and restoration efforts that are currently underway. In the Caribbean region, *A. cervicornis* is widely regarded as one of three key, rapid-growth, reef-building corals (Lirman, 2000). Along with *A. palmata*, it has been a major focus of reef restoration programs for its ability to fragment and regenerate, rapidly producing high quantities of live coral for transplantation onto the reef (Young et al. 2012; Schopmeyer et al. 2017; Bayraktarov et al. 2020). However, the results of Chapter 2 showed lower rates of calcification in this species compared

with the other corals in this study. The lower rates of calcification measured in the massive corals could be due to slower $CaCO_3$ precipitation resulting in denser skeletal structures, compared to *A. cervicornis* which has faster skeletal extension but a weaker skeletal structure (Kuffner et al., 2017). The fragments of coral used in this study were sourced from Mote Marine Laboratory restoration program in the Florida Keys, where micro-fragmentation is used to create thousands of small coral colonies reared in outdoor aquaria and in-situ nurseries before transplantation onto local restoration sites (Forsman et al. 2015). Measuring and comparing the metabolic rates of the coral species used in this program has broad significance for restoration programs in the Caribbean region, as the findings could guide future restoration decisions. For example, this research may make it more feasible to choose species with higher rates of calcification for outplanting at sites with low structural complexity. It is also important to consider how the micro-fragmentation process may impact calcification rates. Faster growth of coral tissue and skeleton has been reported in recently fragmented corals (Page et al. 2018; Schlecker et al. 2022). While the fragments used in this study had been grown out in tanks and were not recently fragmented, future replication of this study should aim to use field collected colonies, and ideally in-situ measurements of physiological processes.

Census surveys such as the Reef Budget method are used to quantify carbonate accretion on coral reefs by surveying benthic cover to scale up using species-specific calcification rates derived from the literature (Perry et al. 2012; Lange et al. 2020). Further research is needed to better understand the link between calcification rates measured using the biogeochemical approach as in the current study, versus measurements of carbonate accretion in the field using census methods. The corals and algae used in chapter were all a similar size and age (i.e., surface area ~ 15cm^2; 2-3 years since micro fragmentation in the aquaria), and little is known about how metabolic rates change with age in scleractinian corals. Future studies are needed to quantify differences in metabolic rates for corals at different life stages, for example, to define rates of production and calcification in juvenile corals vs. larger adult corals. Quantification of the differences in calcification rate between species and life stages will enhance and update research using protocols such as the Reef Budget, which currently relies upon genera-wide and / or single data points for calcification rates which are then extrapolated to ecosystem-level calcification budgets.

The metabolic rates analysed in Chapter 2 were measured from small ex-situ chambers under natural light at different times of day (Fig. 2-2). The findings demonstrated that at the individual level, metabolism in these organisms shifts with light over a diurnal cycle (Figs. 2-4, 2-5). Metabolic rates changed depending on the time of day and natural light level, and differences between morning, noon, and late afternoon were significantly different for both calcification and photosynthesis (Fig. 2-5). These findings provide insight into the relationship between light, calcification, and photosynthesis in corals and CCA. The incubations in Chapter 2 also demonstrated that photosynthesis and calcification are coupled biological processes (Figs 2-7 to 2-9). When rates were modelled with light, calcification and photosynthesis were linked across functional groups (Fig. 2-10). This relationship was stronger in some calcifiers than others, indicating that distinct mechanisms may be controlling the metabolism in different species and functional groups (Fig. 2-12). These findings contribute to the light-enhanced calcification debate (Cohen et al., 2016). The correlation between G_{net} and P_{net} showed that these processes are coupled (Gattuso et al. 1999a; Albright et al. 2015), supporting the hypothesis that photosynthesis fuels calcification, as shown in previous work (e.g., Gattuso et al. 1999a). However, it is possible that G_{net} and P_{net} rates are parallel yet independently driven by light. It was beyond the scope of the study to separate the independent influence of light as a direct control on calcification. Future experiments should incorporate different light regimes to further test the role of light as a direct driver of calcification. Understanding the drivers of metabolisms facilitated predictions of organism response to environmental stressors. For example, reduced light due to eutrophication and algal overgrowth may negatively impact calcification rates on coral reefs (Chalker et al. 1988; Suggett et al. 2013). Additionally, as sea levels rise, less light may reach coral reefs and, since this study shows that metabolism is a light-driven process in coral reef calcifiers, reduced light will directly impact the calcification potential of coral reefs.

Analysis of light-driven shifts in metabolism over the course of 24-hour cycles brought into question the use of the static G_{net}/P_{net} metric which has been used to quantify carbon cycling in coastal ecosystems (Cyronak et al., 2018). By using data collected under different light levels to create a 24-hour G/P ratio using the absolute values of G and P, it was possible to see that the balance of organic to inorganic carbon cycling shifts throughout the diurnal light cycle. The metabolism-irradiance models in this study were used to develop a novel metric for carbon cycling: total metabolism (M_{tot}) (Fig. 2-13), building upon the typical G_{net} / P_{net} ratio, which is commonly used to

describe the balance of organic production to inorganic carbon precipitation on coral reefs (Albright et al., 2015; Cyronak et al., 2018). The metric usually relies upon discrete measurements of G_{net} and P_{net} at one time of day. The new metric of total metabolism (M_{tot}) incorporates measurements collected over a diurnal cycle rather than a 'snapshot' estimate of one point on the diurnal cycle, in contrast to previous research aiming to define ecosystem carbon cycling with a single ratio of G/P (Cyronak et al. 2018; Gattuso et al., 1999a; *and references within*). This finding, that the balance of inorganic to organic carbon processes in coral reef calcifiers fluctuates over the diurnal cycle, is a substantial advancement on the current understanding and metrics used to quantify the relative balance of G_{net} to P_{net} and can immediately by applied to studies measuring carbon metabolism either at the individual scale or for larger ecological communities.

The small-scale, ex-situ incubations in Chapter 2 allowed for high resolution measurements of species-specific metabolism of individual samples. However, ex-situ incubation methods are limited in their scope due to confounding effects introduced in a controlled setting (e.g., handling of the organisms) and the artificial circumstance of single isolated organism, excluding surrounding benthic communities, sediments, and natural fluctuations in seawater parameters (e.g., Patterson et al. 1991; Lesser et al. 1994; Mass et al. 2010). Incubation chambers have been used for decades to measure benthic metabolism in the field (e.g., Camp et al., 2015; Roth et al., 2019; Yates & Halley 2003), and Chapter 3 included a review of the key designs in benthic chamber technology since 2000 (Table 3-1). The aim was to identify and address the research gap for a community-sized chamber that can be field constructed at a low cost and deployed over varied substrates. I developed a novel chamber design and trialled it over 2 field seasons on coral reefs and seagrasses in Akumal Bay, Mexico, and over sediments in Loch Lomond, Scotland, to demonstrate its performance and feasibility as a useful, low-cost equipment for field measurements of benthic metabolism (Fig. 3-1). The key findings of Chapter 3 were the results of experiments through which I validated the benthic chamber design. The 5 aims were met as follows: (1) the chamber was assembled at a low-cost and without specialised equipment in the field for two case studies; (2) the construction of the chamber, and the experiments carried out with it were easily reproducible; and (3) through incubation of delicate corals and other organisms the chambers was found to be minimally invasive, (4) adaptable to varied substrates, and (5) comparable with other available designs in terms of its field performance.

The chamber was developed with students and citizen scientists to trial field construction and deployment. The design cost less than USD $20 to build in the field and did not require specialised parts (Table 3-2). The only other chamber available at such a low cost is the Flexi-chamber, however, this is specialised for single coral head incubations and can only be used where coral morphology permits a cable-tie attachment (Camp et al., 2015). The novel design presented in Chapter 3 incorporated the plastic bag type enclosure of the Flexi-chamber, while being suitable for diverse benthic communities. In terms of size, the chamber by Roth et al (2019) is the most similar and is also suitable for incubating small communities. However, the chamber requires bespoke parts and costs over 200 Euros to construct. Therefore, providing a low-cost alternative with similar utility and no loss in performance (i.e., light transmission, leakage etc), will be a powerful tool for future measurements of benthic metabolism and increases accessibility for researchers with limited funding and resources.

It was critical to show that despite the low cost, this chamber performs similarly to other chambers available. Controlled testing in the lab demonstrated that chamber leakage and light transmission aligned with the other chambers reviewed (Fig 3-2, Table 3-3). These tests demonstrated that the chamber provides a comparable utility with the established chamber equipment available. The results of NCP measurements from field deployments over seagrasses and coral reef patches aligned well with those of other studies. In case study 1, there was a difference between productivity of seagrasses incubated at different times of day, showing the importance of light as a driver of productivity in seagrass meadows (Figs 3-3 & 3-4). In the second case study, the chambers were deployed over coral reef patches (Fig 3-5). The incubated patches were of a similar size, but dominated either by coral, algae, or sediments (Fig. 3-6). Differences in NCP were apparent between substrate types, although not all differences were significant. However, the measured reef NCP fit the hyperbolic tangent model (Fig. 3-7), in agreement with the results of individual coral reef organisms in Chapter 2. These results validated the chamber design and showcased the usability of the benthic chamber for studies investigating productivity of benthic communities.

Productivity measurements provide insight into the carbon sequestration potential for blue carbon budgeting purposes, to quantify how much photosynthesis is taking place and therefore how much CO_2 is drawn down. The benthic chamber in Chapter 3 can be used to measure photosynthesis in areas where other chambers cannot be

deployed, for example, some chamber designs require that the base is dug into sediments (e.g., Olivé et al. 2016), which would not have been feasible in a protected area such as Akumal Bay. The chambers can be incorporated into studies measuring parameters other than DO, for example, water samples can be collected from the valve over the course of an incubation and analysed in the lab for carbonate chemistry to measure calcification. For blue carbon budgeting purposes, this can indicate how much of the carbon drawn down by photosynthesis is then locked into sediments or $CaCO_3$ deposits (Macreadie et al., 2017). Quantification of calcification-dissolution is useful for understanding the functional status of ecosystems such as coral reefs and tracking shifts in benthic composition which in turn drive changes to metabolism (Lantz et al. 2021; Davis et al. 2021). As calcification rates on coral reefs are declining and the ability of the reef to maintain its structure and function is threatened (Eyre et al. 2018), methods to track calcification are increasingly important. The novel chamber design contributes to the equipment available to support direct field measurements of calcification. Indeed, carbonate chemistry water samples were collected from the benthic chambers in the Chapter 3 case studies, but due to an error in sample storage, the results could not be included in this study. In future work, water samples should be collected at the start and end of incubations over coral reef patches over a gradient of degradation and analysed for changes in TA and DIC to fully constrain the carbon metabolism of the incubated areas. Understanding shifts in metabolism of phase-shifted coral reefs is important for understanding the ecological function of contemporary coral reefs (Perry and Alvarez-Filip 2018; Romanó de Orte et al. 2021). The chamber is also adaptable for other experiments. For example, measurements of metabolism under stressful conditions, can be conducted by injecting pollutants or high pCO_2 seawater into the chamber and measuring the impact on benthic metabolism (e.g., adapting the methods of Kline et al., 2012).

The benthic chamber developed and trialled in Chapter 3 provides a significant contribution to field equipment for conducting in-situ incubations with minimal resources. The chamber is low-cost, and the work has been published in an open access journal so that the list of materials, construction, and example deployment over corals, sediment and seagrasses is widely available. Future studies could be conducted to test the ability of the chamber for field experiments simulating different conditions such as OA or nutrient input. Using the benthic chamber, future field incubations of corals and CCA should be conducted and compared with the results of the ex-situ incubations in chapter 2 and expanded to include all corals used in restoration programs. Since the

coral fragments are destined for outplant onto the reef, it would be possible to measure metabolic rates for all restoration species in ex-situ chambers as well as in-situ incubations. Additionally, the in-situ measurements should be repeated over time to track shifts in metabolic rates of corals transplanted onto the reef. This would be important for tracking the success and longevity of coral restoration efforts. The chamber can be adapted to incubate large adult colonies in the field. Chapter 3 demonstrated this on coral-dominated reef patches, but it would be possible to adapt the chamber to have a larger enclosure and base, for incubations of large, freestanding coral colonies in the field, to measure their rates of P_{net} and G_{net}, to provide novel insight into the metabolism of these organism. This data could be added to the Reef Budget database, to support accurate upscaling of reef-wide carbonate production estimates, which is currently limited by the data available. For example, some of the rates used in the Reef Budget are not species-specific, and as Chapter 2 shows, there are significant differences between species of coral reef calcifiers.

Scaling up biogeochemical flux measurements to constrain carbon cycling of large communities and entire ecosystems is increasingly important as coastal ecosystems undergo climate-induced change. In Chapter 4, the predominant biogeochemical methods used for ecosystem-wide field measurements were reviewed (Fig. 4-1) and a selection were used to measure net community metabolism (NCC and NCP) over a seagrass-sediment dominated bay in Bermuda. Autonomous sensors were deployed for continuous measurements of DO, pH, salinity and temperature, alongside parallel deployments of benthic chambers and collection of discrete water samples (Fig. 4-2). Several different approaches were used to collect data for ecosystem-wide metabolism (calcification and productivity). Metabolism was calculated from changes in DO and pH using BEAMS, 1D control volume, and Lagrangian approaches. Water samples were collected from discrete transects and benthic chambers and analysed in the lab for changes in total alkalinity. The results found typical patterns of positive NCP and NCC during the day and net negative at night (i.e., net respiration and dissolution) with strongest agreement between Lagrangian and 1D control volume NCP (Fig. 4-4). The BEAMS method was effective for measuring high resolution NCP data. BEAMS deployed over seagrass-dominated benthos had higher NCP than BEAMS deployed over sediments, a difference not shown by the other autonomous sensing methods (Figs 4-4 to 4-6).

Lower NCP was observed in the benthic chambers, likely because they were deployed over areas with lower density of seagrass (fig 4-7). In this experiment, NCC was calculated from Lagrangian DO and pH, a method first proposed by Barnes in 1983, and more recently propelled by advances in DO and pH sensing technology. The Lagrangian-derived NCC rates demonstrated the expected trend with light. However, NCC measured by BEAMS was not representative, most likely because the change in seawater chemistry did not give a strong enough signal for BEAMS, which has shown more accurate results over coral reefs where the calcification signal is stronger (Platz et al., 2020; Takeshita et al., 2016c). The daily integrated rates (i.e., when rates were standardised to night, day, or 24-hours) showed strong agreements between all methods for NCP, with the exception of BEAMS 2 which had higher NCP during the day and net R at night due to its position over the seagrasses (Fig. 4-8). NCC showed discrepancies between all measurements, including the chambers, demonstrating that method selection for measurements of NCC has a strong influence on the results. As with the experiment in Chapter 2, a linear correlation between NCC and NCP was apparent, however, the R^2 values were low. This is not uncommon in open water biogeochemical measurements due to the array for environmental influences. NCP measurements were modelled with light and showed a good fit to the hyperbolic tangent equation, but this was not true of NCC, again most likely due to low NCC signal. Finally, the M_{tot} ratio was calculated for the different methods and demonstrated that both the method and light influence the ratio of inorganic to organic carbon cycling taking place within the ecosystem.

Measuring coastal carbon cycling is critical for tracking climate-induced ecosystem degradation and predicting future change. Chapter 4 compares distinct approaches to measuring NCP and NCC at larger scales using autonomous sensing, benthic chamber deployments, and discrete water samples. The significance of this research is important for blue carbon accounting in coastal ecosystems. This research demonstrates that autonomous sensors provide reliable measurements of NCP and NCC, and support future sensor deployments over longer time frames. The results show that the Lagrangian approach for measuring NCC is the most reliable over an ecosystem with relatively low calcification rates and provides guidance that BEAMS should be used for NCC only where the calcification signal is strong, for example over coral reefs as in previous work (Takeshita et al. 2016; Platz et al. 2020). The differences in benthic chamber and autonomous sensing measurements are important for studies which use benthic chamber measurements to scale up to the ecosystem

level. Building upon these studies, the implementation of ecosystem-wide measurements with autonomous sensors for reef restoration monitoring requires further research to trial and fine-tune methods. Quantifying calcification rates at restoration sites can provide insight into the ecological function of the ecosystem and highlight changes in their carbonate accretion capacity (Platz et al., 2020). For example, using the wide-scale measurements of calcification in Chapter 4 it would be possible to improve efficiency of ground truthing and scoping for restoration sites. Some sites are dominated by net dissolution, which could be detected using BEAMS or flow respirometry as a quick and efficient alternative to traditional census surveys. This was trialled successfully with BEAMS by Platz et al. (2020) at one of Mote's restoration sites in the Florida Keys, however this is the only example found in the literature and therefore there is considerable scope to build upon the results of this research by trialling novel methods of restoration tracking. The relative balance of NCP to NCC can be used to estimate benthic composition, however the data used for calculating TA:DIC slope is often limited to single sampling points throughout a 24-hour cycle. In this thesis, the role of light has been the common theme at each of the scales explored. The difference in M_{tot} over 24-hours of light for individual corals and CCA in Chapter 2 and for the seagrass meadow in Chapter 4 demonstrates that future work should incorporate the diurnal cycle when quantifying the balance of organic production – inorganic carbon precipitation. Scaling up of metabolic measurements from the scale of the organisms to the ecosystem is a major challenge. One of the key findings was that light is primary driver of metabolism across scales from the individual to the ecosystem, and therefore any future attempts to scale measurements should incorporate light. Autonomous sensing supports such endeavours, as they can be deployed over days, weeks, or even years, and as the designs for autonomous sensors area advancing, they require less maintenance and are more economical. Future deployments of autonomous sensors should be conducted over longer time frames to incorporate seasonal variation, for example multi-year or decadal deployments will be critical for understanding the coastal carbon cycle as both global climate and ecosystems change.

5.1 Concluding remarks

The research presented in this thesis contributes novel insight into the metabolic processes driving coastal carbon cycling in coral reefs and seagrasses, and the methods for measuring benthic metabolism. Measuring benthic metabolism from biogeochemical signals in seawater (e.g., ΔDO, ΔTA, ΔDIC), is an effective proxy for

ecosystem status and ecological function. In this thesis, measurements of photosynthesis-respiration and calcification-dissolution were collected at three scales: individual organisms (Chapter 1), small benthic communities (Chapter 2), and ecosystem-wide levels (Chapter 3) for key benthic organisms and communities of coral reefs and seagrass meadows. Through a combination of lab and field measurements, light was identified as a key driver of benthic metabolism. Data were collected with novel and established methods for quantifying metabolism, demonstrating the range of approaches, and providing a comparison to support future research efforts. Modelling biological activity in response to a diurnal light cycle at each of these scales revealed novel insight into the link between light, productivity, and calcification. This work highlights the importance of incorporating light into measurements of metabolism regardless of scale and provides an alternative metric for quantifying balance of organic- inorganic carbon production of coral reefs and seagrasses. The findings have important implications for coastal ecosystem monitoring, conservation, and restoration, with specific methodological applications to guide future research. The results support future endeavours to further constrain the role of light in biogenic calcification and the application of benthic metabolism measurements as a tool for conservation and restoration tracking.

6 Appendices

6.1 Appendix A: Published work

Light-driven dynamics between calcification and production in functionally diverse coral reef calcifiers

Jennifer Mallon [1,2*], Tyler Cyronak [3], Emily R. Hall [4], Anastazia T. Banaszak [2*], Dan A. Exton [5], Adrian M. Bass [1*]

[1]School of Geographical and Earth Sciences, University of Glasgow, Glasgow, Scotland
[2]Unidad Académica de Sistemas Arrecifales, Universidad Nacional Autónoma de México, Puerto Morelos, Mexico
[3]Department of Marine and Environmental Sciences, Halmos College of Natural Sciences and Oceanography, Nova Southeastern University, Dania Beach, Florida
[4]Ocean Acidification Program, Mote Marine Laboratory, Sarasota, Florida
[5]Operation Wallacea, Spilsby, Lincolnshire, UK

Abstract

Coral reef metabolism underpins ecosystem function and is defined by the processes of photosynthesis, respiration, calcification, and calcium carbonate dissolution. However, the relationships between these physiological processes at the organismal level and their interactions with light remain unclear. We examined metabolic rates across a range of photosynthesising calcifiers in the Caribbean: the scleractinian corals *Acropora cervicornis*, *Orbicella faveolata*, *Porites astreoides*, and *Siderastrea siderea*, and crustose coralline algae (CCA) under varying natural light conditions. Net photosynthesis and calcification showed a parabolic response to light across all species, with differences among massive corals, branching corals, and CCA that reflect their relative functional roles on the reef. At night, all organisms were net respiring, and most were net calcifying, although some incubations demonstrated instances of net calcium carbonate ($CaCO_3$) dissolution. Peak metabolic rates at light-saturation (maximum photosynthesis and calcification) and average dark rates (respiration and dark calcification) were positively correlated across species. Interspecies relationships among photosynthesis, respiration, and calcification indicate that calcification rates are linked to energy production at the organismal level in calcifying reef organisms. The species-specific ratios of net calcification to photosynthesis varied with light over a diurnal cycle. The dynamic nature of calcification/photosynthesis ratios over a diurnal cycle questions the use of this metric as an indicator for reef function and health at the ecosystem scale unless temporal variability is accounted for, and a new metric is proposed. The complex light-driven dynamics of metabolic processes in coral reef organisms indicate that a more comprehensive understanding of reef metabolism is needed for predicting the future impacts of global change.

Coral reefs are highly productive ecosystems that build some of the largest living structures on Earth. The services obtained from the coral reef ecosystem include coastal protection, habitat provision, fisheries, and tourism (Hoegh-Guldberg et al. 2019). These services ultimately rely on biogenic calcification; the process by which a diverse community of framework-building corals, crustose coralline algae

(CCA), and other calcifying organisms contribute to the calcium carbonate ($CaCO_3$) reef structure. Global climate change threatens the survival of important framework-building coral species, primarily through increasing seawater temperature and ocean acidification, both of which have been shown to directly impede coral growth and negatively impact coral reef-dwelling organisms and ecosystems (Kleypas and Yates 2009; Comeau et al. 2013). Exposed $CaCO_3$ structures and sediments are vulnerable to dissolution exacerbated by ocean acidification (Cyronak et al. 2013; Eyre et al. 2014), and it is expected that reef structure could be lost at a pace faster than it is constructed in the near future (Eyre et al. 2018).

A positive relationship between photosynthesis and calcification has been observed across cellular, organismal, and community scales in coral reefs (Gattuso et al. 1999; Allemand et al. 2011). At the ecosystem scale, the balance of

*Correspondence: jmallon967@gmail.com, banaszak@cmarl.unam.mx, adrian.bass@glasgow.ac.uk

Additional Supporting Information may be found in the online version of this article.

photosynthesis, respiration, calcification, and dissolution, collectively known as coral reef metabolism, controls the coral reef carbon cycle (Albright et al. 2015; Cyronak et al. 2018). Net ecosystem calcification is defined as the rate of $CaCO_3$ precipitation offset by dissolution, while net ecosystem production is defined as the difference between photosynthesis and respiration (Smith and Kinsey 1978). Reef metabolism is often measured through changes in the carbonate chemistry of sea water as it flows over a coral reef ecosystem, which requires detailed knowledge of the local hydrodynamics (Marsh and Smith 1978). The ratio of net calcification to net production has been proposed as a proxy for monitoring reef function, which can be calculated from carbonate chemistry data (Cyronak et al. 2018; Takeshita et al. 2018). This metric provides useful insight into reef biogeochemistry as a simple, effective tool for monitoring change in coral reef metabolism over space and time (Cyronak et al. 2018). However, the success of the calcification/production ratio metric depends on a strong mechanistic understanding of how photosynthesis and calcification are linked from the organism to the ecosystem.

At the organismal level, connectivity between photosynthesis and calcification is reflected in the phenomena known as light-enhanced calcification, or the observation of increased calcification rates during the day compared to night (Goreau 1959; Gattuso et al. 1999). Research into the mechanisms behind light-enhanced calcification have not yet reached a consensus, and it is possible that more than one process is taking place for the different species and functional groups exhibiting light-enhanced calcification, for example, corals, calcifying algae, foraminifera (Cohen et al. 2016). One hypothesis is that higher rates of photosynthesis associated with optimal light conditions provide the coral with more energy for calcification (Chalker and Taylor 1975). Other studies show that metabolic CO_2 production through respiration is an important source of carbon for calcification (Furla et al. 2000). Another hypothesis is that photosynthesis influences carbonate chemistry equilibrium at the site of calcification through the uptake of CO_2, which enhances $CaCO_3$ precipitation (McConnaughey and Whelan 1997; Allison et al. 2014). However, it is important to note that calcification and photosynthesis take place in different tissue layers (Jokiel 1978). Cohen et al. (2016) demonstrated that calcification can be decoupled from photosynthesis by providing corals with different wavelengths of light, indicating that both processes are independently linked to sunlight. To make accurate predictions about the impact of climate change on coral reefs, we must understand the mechanistic relationships between calcification and photosynthesis at the organismal scale before we can fully understand their interactions at community or ecosystem scales (Edmunds et al. 2016).

Shifting benthic community compositions are expected to alter the metabolism and carbon cycle of coral reef ecosystems (Hughes et al. 2018). In the Caribbean, coral reefs historically built by the skeletal calcium carbonate of reef-building corals, primarily branching *Acropora* spp. and massive *Orbicella* spp., have experienced unprecedented losses of coral cover and proliferation of macroalgal cover in recent decades (Jackson et al. 2014; Toth et al. 2019). Contemporary coral populations have lower species diversity and are dominated by resilient, weedy corals, such as *Porites astreoides* (Green et al. 2008), which lack reef-building life-history traits (Darling et al. 2012). As a result of these phase shifts, rugosity and carbonate accretion rates in the Caribbean have decreased over the past decades (Perry and Alvarez-Filip 2018), impacting the maintenance of reef structure and habitat function (Muehllehner et al. 2016; Yates et al. 2017; Kuffner et al. 2019). Quantifying organismal metabolic rates and understanding the dynamic interactions between metabolic processes is critical for predicting the impact of changing coral reef ecosystems and the ecosystem services they provide.

In this study, we measured the metabolic rates of key Caribbean coral reef calcifiers to determine the interaction among photosynthesis, respiration, and calcification over natural diurnal light cycles. We provide a comparison between species with distinct ecological functions, chosen to reflect past and present species dominance: (1) branching, rapid-growth *Acropora cervicornis*; (2) framework-building *Orbicella faveolata*; (3) resilient, weedy *Porites astreoides*; (4) framework-building, stress-tolerant *Siderastrea siderea*; and (5) abundant, low-profile, crustose coralline algae (CCA). We compared differences in metabolism across these calcifying organisms over a natural diurnal light cycle and developed metabolism–irradiance curves to determine the relationships among photosynthesis, calcification, and irradiance at the organismal level.

Methods

Ex situ incubations of four species of scleractinian coral and two crustose coralline algae (CCA) were conducted in the Climate and Acidification Ocean Simulator outdoor experimental facility at the Mote Marine Laboratory, Elizabeth Moore International Center for Coral Reef Research and Restoration, Summerland Key, Florida, in October and November of 2019. The Climate and Acidification Ocean Simulator facility is supplied with 20-μm particle-filtered Atlantic seawater maintained by a dual heat exchanger system at 28.4°C $\pm$ 0.2°C (mean $\pm$ SD) in 3800-liter header tanks. An automated controller system (Walchem W900) maintains ambient seawater at a pH of 8.04 $\pm$ 0.04.

Study organisms

Small colonies (mean surface area $13 \pm$ SD 3.54 cm^2) of *A. cervicornis* ($n = 6$), *O. faveolata* ($n = 12$), *P. astreoides* ($n = 12$), and *S. siderea* ($n = 12$) were randomly selected from the Mote Marine Laboratory land nursery of micro-fragmented corals (Fig. 1a–f; Supporting Information Table S1). While small encrusting fragments do not represent the morphologies of larger, older colonies in the wild, using similarly

2
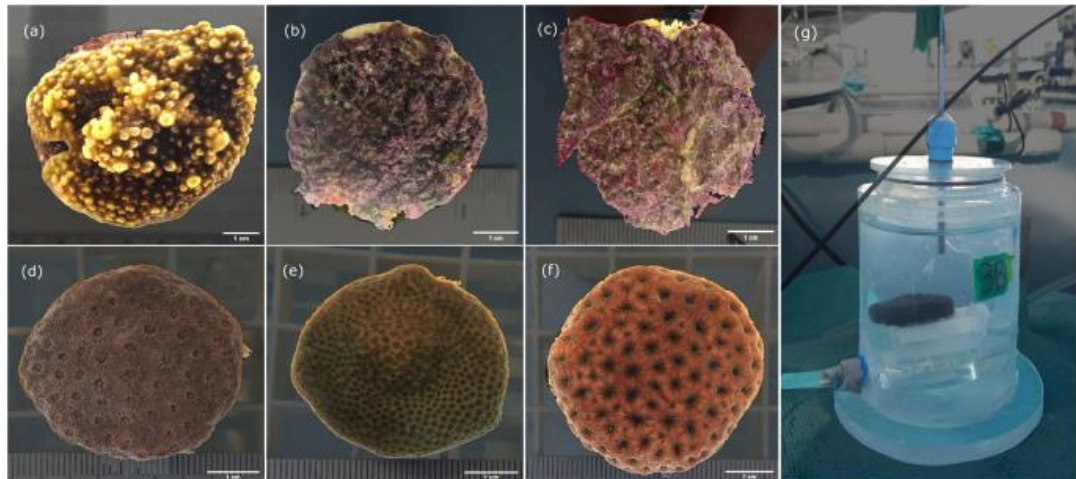
Fig 1. Examples of top-down photos used for surface area measurements on Image-J: (**a**) *Acropora cervicornis*, (**b**) crustose coralline algae type 1 (CCA1), (**c**) crustose coralline algae type 2 (CCA2), (**d**) *Orbicella faveolata*, (**e**) *Porites astreoides*, and (**f**) *Siderastrea siderea*, (**g**) the incubation chambers used during this study showing the oxygen sensor inserted through the chamber lid, transparent water jacket, and the white plastic holder below coral with stir bar spinning underneath. Photos (**a**) through (**f**) show 1 cm scale bars.

fragmented corals with minimal differences in "colony-wide" morphologies allows for better interspecific comparisons. All corals originated from Mote's restoration nurseries, where they had been either sexually produced and/or micro-fragmented from field-collected colonies between 2010 and 2017 (Supporting Information Table S2). In addition, crustose coralline algae growing on the base of two of the Mote restoration raceways were chiseled off and glued to clean ceramic tiles 3 weeks prior to the study. Due to morphological differences in color and surface texture (Fig. 1), CCA were thought to be distinct species; however, we were unable to identify them and are herein referred to as CCA type 1 (CCA1) and CCA type 2 (CCA2).

Each specimen was randomly assigned to one of 12 holding tanks (19-liter volume, $40 \times 20 \times 25$ cm, $L \times W \times H$) 2 weeks prior to the study. Each tank received 160 mL min^{-1} filtered natural seawater via a separate manifold and each tank was fitted with a circulation pump to maintain flow (Deluxe Submersible Water Pump 400GPH). While water flow has been shown to modulate coral metabolism and their response to environmental change (Comeau et al. 2014, 2019), the goal of this study was to maintain a constant flow to compare the metabolism between calcifying functional groups. Sea water parameters of pH (Seven2Go Pro S8, Mettler Toledo), temperature, and salinity (YSI Professional Plus) were monitored twice per day. For pH, electrodes were calibrated against National Bureau of Standards scale buffers of 4.01, 7.00, and 10.00 at 25°C and validated using other carbonate chemistry parameters (e.g., total alkalinity [TA] and dissolved inorganic carbon

[DIC]). Water temperature was controlled by an automated dual exchange heater and chiller, and, to maintain pH and salinity within each tank, water inflow was adjusted and changed as necessary. Supporting Information Table S3 provides an overview of the mean and standard deviation for all environmental parameters in the holding tanks. A permanent shade cloth (30% attenuation) maintained natural light conditions (daytime $= 321.38 \pm 179.73$, μmol m^{-2} s^{-1}, and peak $= 494 \pm 64.4$ μmol m^{-2} s^{-1} photosynthetically active radiation [PAR] mean $\pm$ SD). The surface area of each fragment was measured from top-down photos, with additional cylinder calculations to incorporate the surface area of *A. cervicornis* branches. All size measurements were extracted from photos using Image-J (Schneider et al. 2012) with the Simple Interactive Object Extraction plug-in (Wang 2016) to identify live tissue cover and exclude any areas of cement plug not covered in tissue (Fig. 1; Supporting Information Table S1).

Incubation protocol

Incubations were conducted over 12 d between 31 October 2019 and 21 November 2019, with each day selected for consistency in wind, cloud cover, and rainfall. One fragment per species was randomly selected each day and placed into an incubation chamber for ~ 1 h at the following times: 2 h after sunrise (AM), during the solar peak (PEAK), and 2 h after sunset (DARK). On 3 of the 12 d, an additional incubation between the solar peak and the sunset was included (PM). Separate readings of PAR were taken for each chamber position at

3
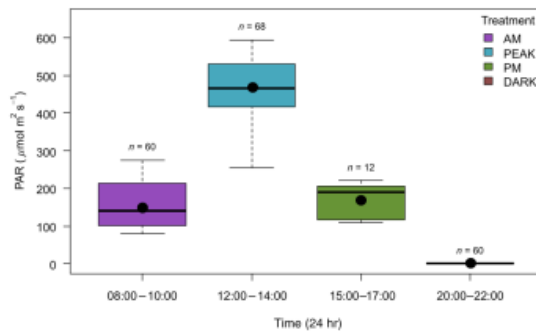
Fig 2. PAR measured during the different incubation time periods. Boxplots show mean (circle), median (horizonal line), and IQR (box and whisker). The number of individual incubations carried out within each time period (*n*) including control incubations is shown above each box. Colors represent the time periods: AM (2 h after sunrise 8 : 00 to 10 : 00), PEAK (solar noon 12 : 00 to 14 : 00), PM (2 h before sunset 15 : 00 to 17 : 00) and DARK (2 h after sunset 20 : 00 to 22 : 00). Average AM PAR was 155 ± 66.8 μmol m^{-2} s^{-1} (mean ± SD), PEAK 494 ± 64.4 μmol m^{-2} s^{-1}, and PM 171 ± 43.9 μmol m^{-2} s^{-1} PAR.

the start and end of incubations with Li-cor model LI-1500G and an underwater quantum sensor (LI-192SA), oriented horizontally. Average PAR light values (mean of start and end) were calculated for individual chambers and varied from 67 to 595 μmol m^{-2} s^{-2} between the three daylight incubation periods (8:00–10:00, 12:00–14:00, and 15:00–17:00; Fig. 2).

Incubation chambers were set up in a dry raceway tank adjacent to holding tanks for consistent light conditions. Incubations consisted of four double-walled transparent acrylic incubation chambers (300 mL) sealed with a transparent acrylic lid, with a rubber O-ring closure (Fig. 1g). A thermocycler (VWR MX7LR-20) recirculated water through the transparent cooling jackets of the incubators at 26.5°C ± 0.5°C to maintain water inside the chambers at 27.6°C ± 1.5°C. Incubation chambers were positioned on magnetic stirrers set at 600 revolutions per minute and flow simulated using a 2-cm stir bar placed under the specimens with a plastic grid base to allow water movement without disturbing the organism. All incubations were run for 1 h ± 3 min, with seawater samples taken at the start and end (see below for details).

Environmental parameters

Dissolved oxygen (DO) fiber-optic oxygen sensors (Firesting O$_2$, Pyroscience) were inserted in each chamber to $\sim$ 1 cm above the coral 3–5 min prior to the incubation start time, to allow for acclimation of the sensor and adjustment of its position. The oxygen sensors were calibrated to 0% and 100% O$_2$ saturation using air-saturated water prior to each incubation. Real-time measurements of DO (μmol l^{-1}) were recorded each second during the incubation. To calculate oxygen fluxes, start

and end values were calculated as the mean values over the first and last minute of the 1-h incubations. The fluxes derived from the start and end values were similar to fluxes derived from linear slopes between time and DO during each incubation (Supporting Information Figs. S1–S6). Start and end fluxes were used for a more direct comparison to fluxes derived from the carbonate chemistry data.

Water samples for carbonate chemistry analysis were taken at the start and end of incubations using a 100-mL plastic syringe; immediately filtered (0.45 μm), poisoned with 200 μL of saturated mercuric chloride, and stored in 250-mL amber borosilicate glass bottles at the Mote Ocean Acidification Laboratory until they were processed. One sample was collected at the start as all chambers were filled with the same water prior to beginning the incubations. TA was measured by potentiometric titration using an automated titrator (Metrohm 905 Titrando), following the standard best practice (Dickson et al. 2007). Mean values for each sample were derived from two to three samples (40 mL) with a precision of ± 3.8 μmol kg^{-1}. Measurements were corrected to Dickson Certified Reference Material (Batches 184, 187, and 189) measured at the start and end of each day. DIC was analyzed using an Apollo SciTech Analyzer (Model AS-C3). Mean values were derived from two to three replicates of 1 mL injections and corrected for drift with measurements of certified reference material at the start and end of the analysis. Precision of DIC measurements was 2.4 μmol kg^{-1}.

Calculations of metabolic processes

Metabolic rates were calculated from the difference between measurements taken at the end of the incubation minus the starting values (end – start) of DO (ΔDO), TA (ΔTA), and DIC (ΔDIC) concentrations. To calculate fluxes, all seawater chemistry measurements were normalized to individual incubation chamber volumes (259.69 ± 12.57 mL, mean ± SD) and coral surface areas (Supporting Information Table S1). Control incubations (e.g., empty ceramic tiles) showed negligible changes in seawater chemistry (ΔDO = 0.4 ± 6.8 μmol l^{-1}, ΔDIC = -7.2 ± 11.0 μmol kg^{-1}, ΔTA = -2.8 ± 8.7 μmol kg^{-1}, mean ± SD), and as such no corrections in seawater chemistry due to water column processes were made.

Net production (μmol cm^{-2} h^{-1}) for light incubations was calculated from changes in DO (P_{DO}) and DIC (P_{DIC}) concentrations according to the following equations:

$$P_{DO} = \frac{\Delta DO \times V}{A \times t} \tag{1}$$

$$P_{DIC} = -\frac{\left(\Delta DIC - \frac{\Delta TA}{2}\right) \times V}{A \times t} \tag{2}$$

where ΔDO, ΔDIC, and ΔTA represent the respective changes in DO, DIC, and TA concentrations in μmol L^{-1}. The volume of the incubation chamber in liters is represented as *V*, while

4

A is the surface area of the sample (cm^2), and t is duration of the incubation in hours (1 h). To calculate respiration (R_{DO} and R_{DIC}), the same equations were used with dark incubation data.

Net calcification (G_{net}) for light incubations was calculated using the alkalinity anomaly technique according to the following equation:

$$G_{net} = \frac{\left(-\frac{\Delta TA}{2}\right) \times V}{A \times t} \qquad (3)$$

For dark calcification rates (G_{dark}) the same equation was used with data collected from dark incubations only.

The relationship between light and photosynthesis and calcification was modeled using gross metabolic rates (i.e., photosynthesis + respiration and calcification + dark calcification) using the following hyperbolic tangent function from Jassby and Platt (1976):

$$P_{net} = P_{max} \times \tanh\left(\frac{\alpha \times E}{P_{max}}\right) + R, \qquad (4)$$

where P_{net} is the modeled net production rate, R is the average dark respiration rate, and E is the irradiance (μmol m^{-2} s^{-1}). The coefficients derived from the model include: the initial slope between P_{net} and light (α) and the maximum gross photosynthetic rate (P_{max}).

For calcification, we adapted Eq. 4 to model calcification (G_{net}) as:

$$G_{net} = G_{max} \times \tanh\left(\frac{\alpha \times E}{G_{max}}\right) + G_{dark} \qquad (5)$$

where G_{dark} is the average dark calcification rate for each species, representing the non-light-enhanced portion of the measured calcification rates, G_{max} is the maximum gross calcification, and alpha (α) is the initial slope between calcification and irradiance.

The light saturation point (E_K) was calculated from model coefficients P_{max} or G_{max} and alpha for each model using the following equation:

$$E_K = \frac{P_{max}}{\alpha} \qquad (6)$$

The absolute ratio of calcification to both calcification and production was calculated as follows:

$$G_{net}/M_{tot} = \frac{|G_{net}|}{|P_{net}| + |G_{net}|}$$

where M_{tot} (or the sum of both calcification and production) represents total carbon metabolism (see Discussion section for more details about this metric).

Statistical analysis

All statistical analyses were conducted in the statistical environment R using RStudio version R.4.0.2 (R Core Team, 2020). The *RespR* package (Harianto et al. 2019) was used to extract and inspect oxygen data (Supporting Information Figs. S1–S6). The *Tidyverse* (Wickham 2019) was used for data organization and synthesis, and data visualization was conducted with base-R functions and *ggplot/ggpubr* (Wickham 2016). Shapiro–Wilkes tests were combined with visual assessments of density and Q–Q plots to evaluate approximately normal distributions for individual species. Repeated measures two-way ANOVA tests were used to test differences between treatments and pairwise comparisons. Post hoc Bonferroni-corrected t tests were used to compare differences between all possible pairs of species at each time of day and for each parameter. Models were fitted using R linear and nonlinear least squares functions of the *Stats* package. Model fit was assessed by residuals plots generated using the *nlstools* package (Baty et al. 2015). Models were evaluated based on R^2, confidence intervals, and standard error of the regression (sigma, σ).

Results

Rates of metabolism were statistically different between treatment times for photosynthesis (repeated measures ANOVA for P_{DO} $F_{3,155} = 336.05$, $p = <0.05$, and P_{DIC} $F_{3,143} = 331.37$, $p = <0.05$), and for calcification (G_{net} repeated measures ANOVA $F_{3,149} = 27.24$, $p = <0.05$) (Supporting Information Table S4; Fig. S7). During the day, photosynthesis (+P_{DO} and +P_{DIC}) and calcification (+G_{net}) occurred in all incubations (Fig. 2). At night, respiration occurred in all incubations (−P_{DO} and −P_{DIC}) while calcification was still generally positive (+G_{net}), although some net dissolution (−G_{net}) was detected (Fig. 3). Metabolic rates for all species were highest during the peak treatment (Fig. 3).

Metabolism was species specific, with *O. faveolata*, *P. astreoides*, and *S. siderea* having the highest average rates of calcification and photosynthesis, while both types of CCA had the lowest (pairwise comparisons using t test; Supporting Information Table S5). As *O. faveolata*, *P. astreoides*, and *S. siderea* had consistently similar rates, we refer to this grouping as the "massive corals" herein. We report rates as mean ± SD unless otherwise indicated. Overall, metabolic rates were higher in the massive corals than both *A. cervicornis* and CCA over a diurnal cycle (Fig. 4). Night metabolism followed a similar grouping as the daytime measurements: respiration was greater in the massive corals ($R_{DO} = -0.75 \pm 0.23$ μmol cm^{-2} h^{-1}, $R_{DIC} = -0.85 \pm 0.35$ μmol cm^{-2} h^{-1}), than in *A. cervicornis* ($R_{DO} = -0.32 \pm 0.05$, $R_{DIC} = 0.38 \pm 0.08$ μmol cm^{-2} h^{-1}) and CCA ($R_{DO} = -0.31 \pm 0.14$ μmol cm^{-2} h^{-1}, $R_{DIC} = -0.42 \pm 19$ μmol cm^{-2} h^{-1}). Dark calcification (G_{dark}) was higher in the massive corals ($G_{dark} = 0.31 \pm 0.24$ μmol cm^{-2} h^{-1}) than *A. cervicornis* ($G_{dark} = 0.03 \pm 0.08$ μmol cm^{-2} h^{-1}) and CCA ($G_{dark} = 0.06 \pm 0.18$ μmol cm^{-2} h^{-1}); however, this difference
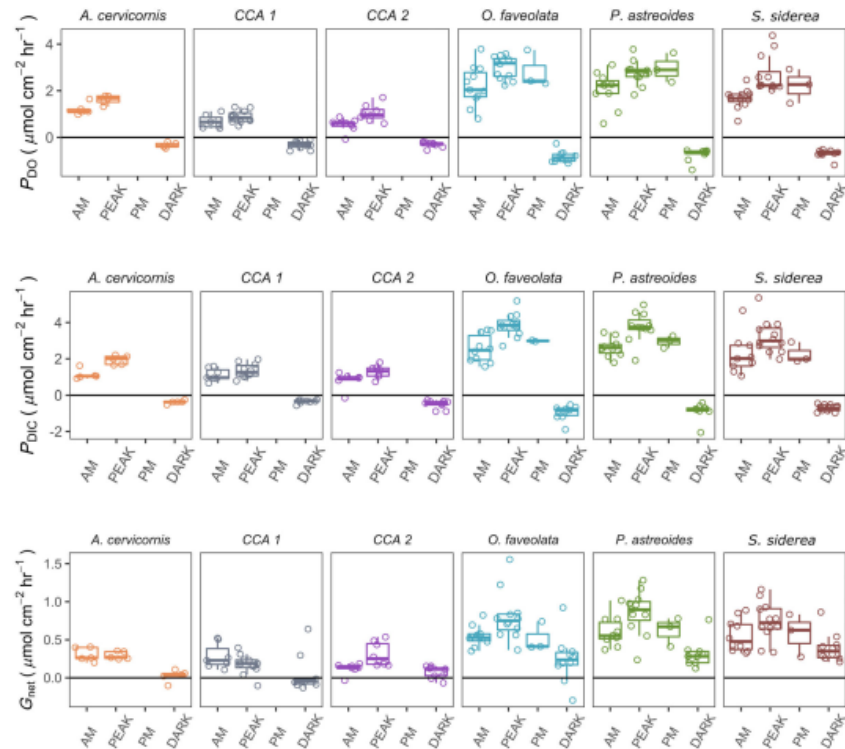
Fig 3. Boxplots of metabolic rates at different times of day for each species. *Y*-axes show; photosynthesis from oxygen evolution (P_{DO}), photosynthesis by carbon assimilation (P_{DIC}), and calcification (G_{net}) rates, normalized to time and surface area (fluxes in μmol cm^{-2} hr^{-1}). Boxplots show median (horizonal bar) and IQR (box and whisker), and individual data points are depicted as empty circles. Species are shown in colors and labeled above each plot. CCA1 and CCA2 are two types of crustose coralline algae. Time of day is shown on the *x*-axis: AM 08 : 00 to 10 : 00, PEAK 12 : 00 to 14 : 00, PM 15 : 00 to 17 : 00, and DARK 20 : 00 to 22 : 00. Only three species were incubated during the PM treatment.

was only significant for *S. siderea* (Supporting Information Table S5). Negative rates of dark calcification (i.e., $-G_{dark}$, net dissolution) were detected in 10 of the CCA, 1 of *A. cervicornis*, and 2 of *O. faveolata* dark incubations, although dissolution rates were relatively low and close to zero.

Relationships between metabolism and light

To elucidate species-specific relationships with light, metabolic–irradiance curves were modeled using a hyperbolic tangent equation (Eqs. 4, 5; Figs. 5, 6; Supporting Information Fig. S8). All photosynthesis–irradiance model evaluations had a high R^2 (> 0.80), and coefficients were significant ($p < 0.001$) for photosynthesis measured from changes to both DO (P_{DO}) and DIC (P_{DIC}). Calcification-light models generally had lower R^2 and higher sigma (σ) relative to calcification (G_{net}) values (Supporting Information Table S6) than photosynthesis–irradiance models, indicating a weaker model fit, and coefficient estimates were not always significant (alpha [α], $p > 0.1$

for *A. cervicornis* and crustose coralline algae). Of the coral species, *A. cervicornis* had the lowest maximum photosynthesis and calcification (P_{max} and G_{max}). The initial slope (α) of the photosynthesis–irradiance curves was highest for the massive corals. Photosynthetic–irradiance saturation (E_K) was highest in *A. cervicornis* (P_{DIC} $E_K = 356$), and in calcification–irradiance models light saturation (E_K) was highest for *P. astreoides* (G_{net} $E_K = 448$ μmol s^{-1} m^{-2}) and *S. siderea* (G_{net} $E_K = 544$ μmol s^{-1} m^{-2}).

Relationships between calcification and photosynthesis

The model coefficients P_{max} and G_{max} exhibited a positive linear relationship (Fig. 7) across all species ($R^2 = 0.88$, $p < 0.05$), while mean respiration (R) and dark calcification (G_{dark}) rates exhibited a negative linear correlation between all species ($R^2 = 0.66$, $p = 0.05$). This across-species relationship demonstrates that calcification increases with rates of net production during the day and with increased respiration in the
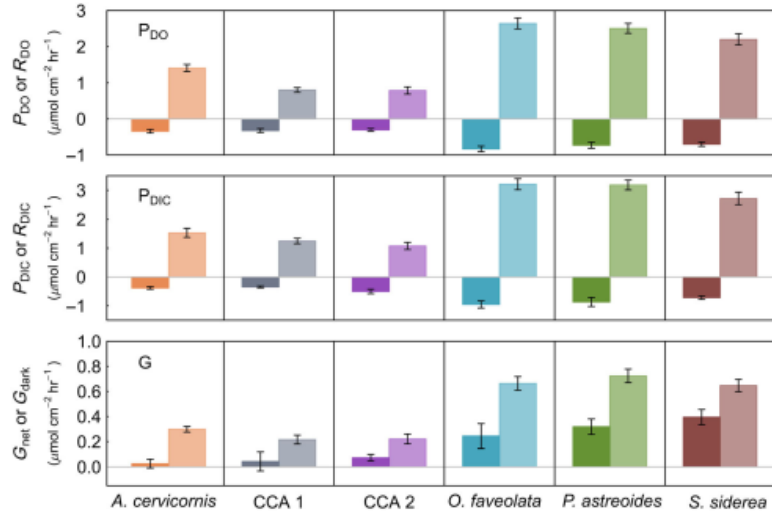
6

Fig 4. Paneled bar plots show species-specific average rates of dark (*left bar, darker shade*) and light (*right bar, lighter shade*) metabolism. Photosynthesis and respiration were calculated from both DO (P_{DO} and R_{DO}, *top*) and dissolved inorganic carbon (P_{DIC} and R_{DIC}, *middle*) fluxes. Light and dark calcification was calculated from changes in total alkalinity during light and dark incubations (G_{net} and G_{dark}, *bottom*). The color scheme is the same as in Fig. 3 and species are labeled on the bottom *x*-axis. CCA1 and CCA2 refer to the two types of crustose coralline algae used in this study. Rates shown are the mean light and dark rates across all days, and error bars represent standard error (SE).
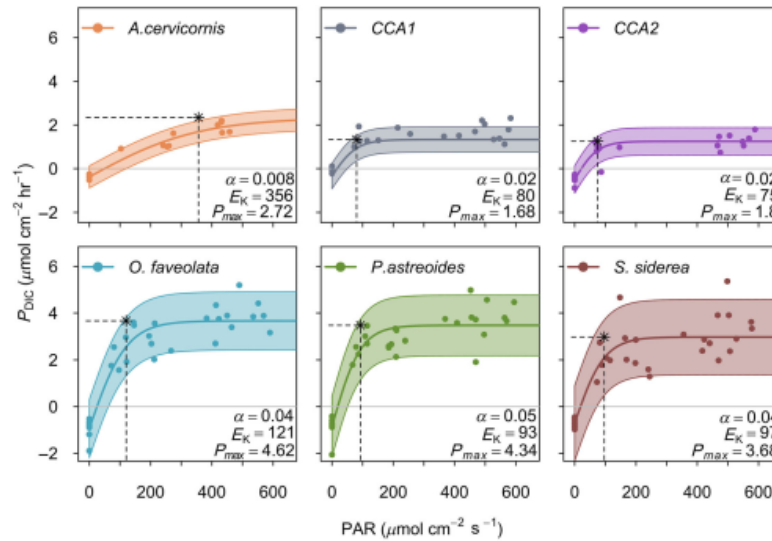
Fig 5. Photosynthesis–irradiance curves for *Acropora cervicornis*, crustose coralline algae (CCA1 and CCA2), *Orbicella faveolata*, *Porites astreoides*, and *Siderastrea siderea*, with photosynthesis measured from changes in dissolved inorganic carbon (P_{DIC}). Points show the measured net rates at distinct PAR light levels, and the solid, colored lines show the modeled metabolic curve. Shaded areas represent 95% confidence intervals. Dotted vertical lines indicate E_K (light saturation point) and dashed horizontal lines depict maximum net photosynthesis (P_{max} + R). Species-specific coefficients for the photosynthesis–irradiance models are displayed on each plot and full statistics provided in Supporting Information Table S6.
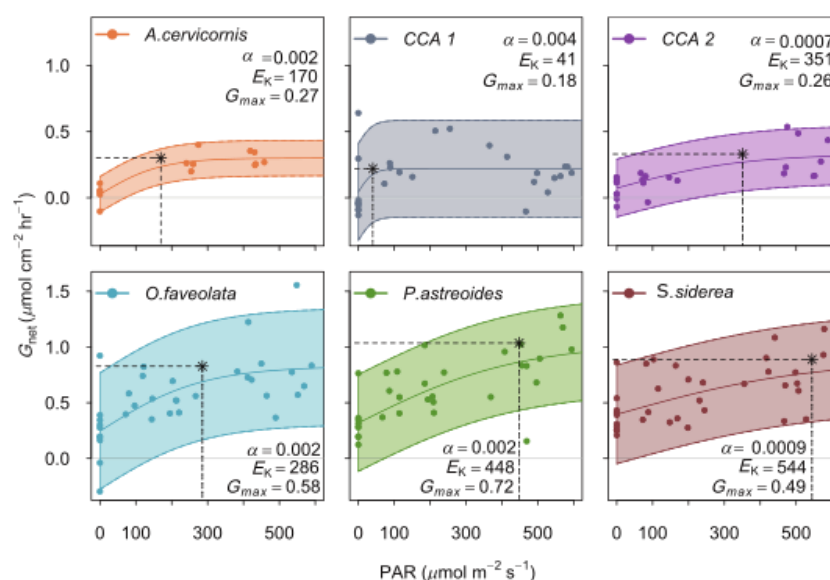
Fig 6. Species-specific calcification–irradiance models fitted to a hyperbolic tangent as described in the methods for *Acropora cervicornis*, crustose coralline algae (CCA1 and CCA2), *Orbicella faveolata*, *Porites astreoides*, and *Siderastrea siderea*. Shaded areas indicate the 95% confidence interval around the modeled curve. Modeled maximum net calcification (G_{max} + G_{dark}) and light saturation (E_k) points are depicted by dashed horizontal and vertical lines. Species-specific coefficients are displayed on each plot and full statistics provided in Supporting Information Table S6.

dark. When the metabolic rates of all species were grouped together, linear correlations between P_{DIC} and G_{net} were weaker (light $R^2 = 0.39$, $p < 0.001$, dark $R^2 = 0.15$, $p = 0.04$) than correlations between the model coefficients $G_{max} - P_{max}$ and $R - G_{dark}$ (Fig. 7c). When the linear models were broken down by species, regression models of P_{DIC} and G_{net} were only significant in *P. astreoides* (light $R^2 = 0.39$, dark $R^2 = 0.78$, $p < 0.005$; Fig. 8). These relationships indicate tight coupling of photosynthesis, respiration, and calcification, and show differences within and between different species of coral reef calcifiers.

DO production (P_{DO}) was positively correlated with DIC assimilation (P_{DIC}), indicating an overall metabolic quotient (Q) of 1.18 (Fig. 9a) with individual differences in Q between species (Fig. 9b; Supporting Information Table S7). The ratio of carbonate precipitation to organic production (G_{net}/M_{tot}) indicated that shifts in the balance of calcification to photosynthesis occur during the day in relation to irradiance (Fig. 10).

Discussion

This study aimed to determine the relationships among production, calcification, and light in a variety of calcifying coral reef organisms from the Caribbean. Differences were found in metabolism among morning, afternoon, and night

incubations and were species specific; however, linearity between metabolic–irradiance model coefficients demonstrated that photosynthesis and calcification are correlated across species (Fig. 7). The results from this study confirm that photosynthesis and calcification rates of tropical benthic calcifiers exhibit a hyperbolic response to diurnal light cycles (Chalker and Taylor 1978; Cohen et al. 2016). Our analyses revisit the current understanding of relationships between organismal-level metabolism and irradiance in benthic coral reef calcifiers, and we interpret these findings in the context of ecosystem scale estimates of metabolism and predicted changes due to ongoing anthropogenic change.

Species-specific differences in metabolic rates

From the results of the incubations, three general groupings were apparent: (1) massive coral species *O. faveolata*, *P. astreoides*, and *S. siderea*; (2) *A. cervicornis*; and (3) crustose coralline algae. The highest metabolic rates were observed in massive coral species under all conditions (Figs. 3, 4). The metabolic rates of *A. cervicornis* and CCA were relatively similar, but they were grouped separately due to distinctions between the mechanisms by which coralline algae and corals calcify, and to reflect differences in the ecosystem function they provide. We discuss differences and similarities between the three groups in relation to their ecological function below.
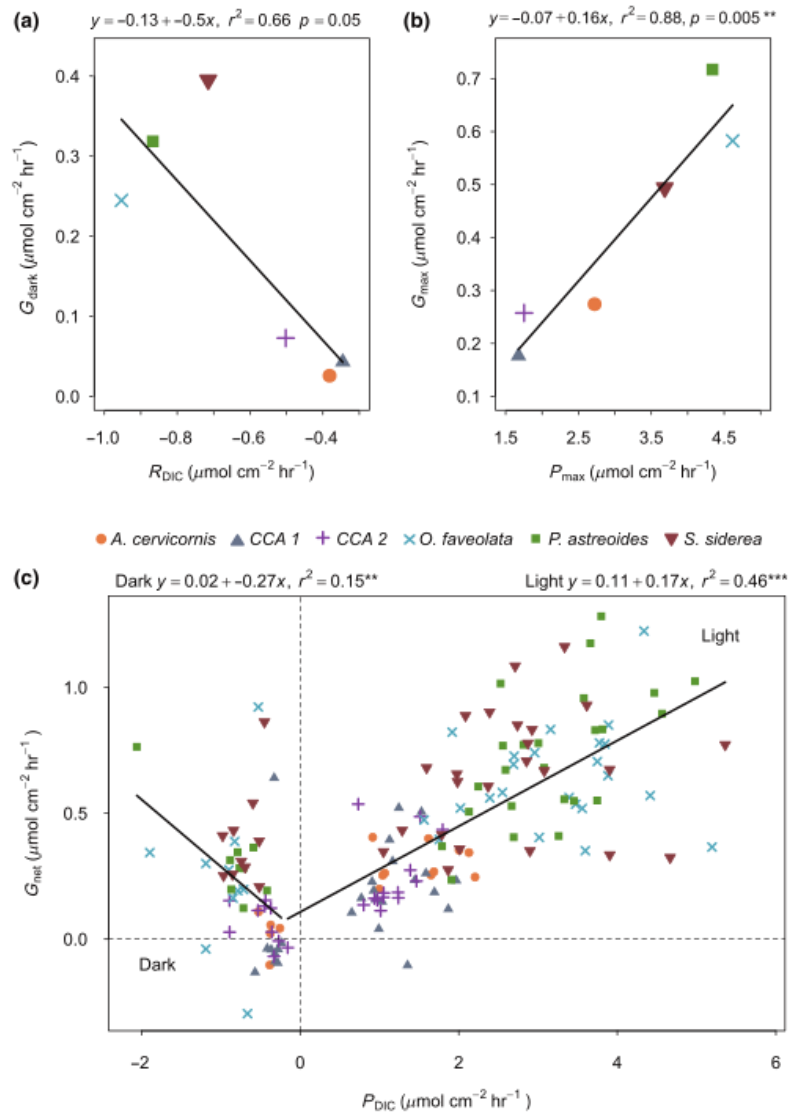
Fig. 7. Linear relationships between (**a**) mean average respiration (R_{DIC}) and dark calcification (G_{dark}) for each species, (**b**) maximum metabolic rates derived from model coefficients for photosynthesis– and calcification–irradiance curves (P_{max} and G_{max}) and (**c**) individually measured photosynthesis (P_{DIC}) and calcification (G_{net}) rates. Individual species, *Acropora cervicornis*, crustose coralline algae (CCA1 and CCA2), *Orbicella faveolata*, *Porites astreoides*, and *Siderastrea siderea*, are depicted as different colors and symbols (*see* legend).

Metabolic rates were highest in the massive corals demonstrating that per area of live tissue, they produce more oxygen and calcium carbonate. Despite their higher metabolic rates, it is unlikely that massive corals have a stronger influence on community metabolism than branching *A. cervicornis* and encrusting CCA because of the relative benthic cover and architectural complexity of each species found in nature. Given the distinct ecological function and life-history traits within the massive coral grouping (Darling et al. 2012), the similarity in their metabolic rates was unexpected (Fig. 4). *P. astreoides* is
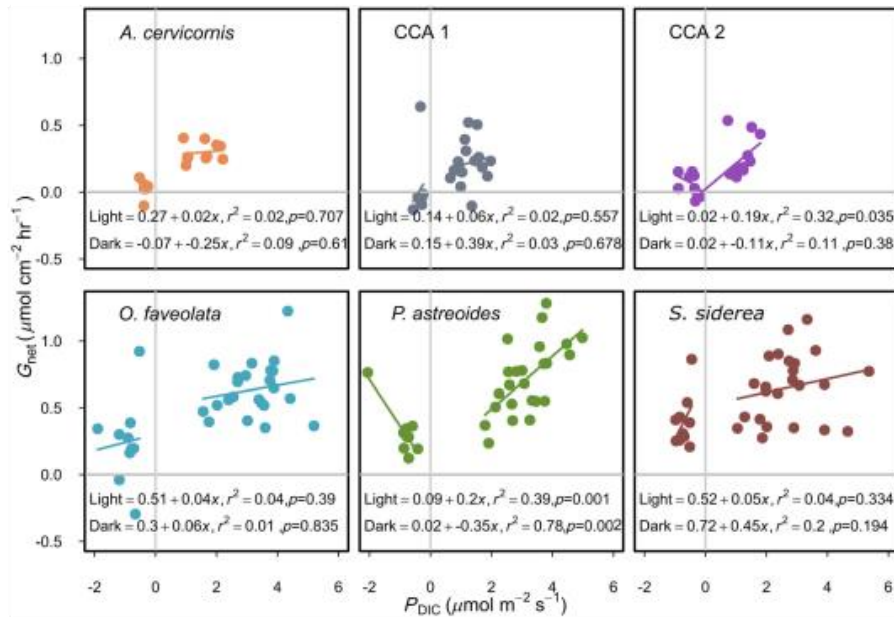
Fig. 8. Linear relationships between photosynthesis (P_{DIC}) and calcification (G_{net}) for each species incubated in this study. CCA1 and CCA2 refer to crustose coralline algae types 1 and 2. Linear regression equations, R^2, and p values are displayed on each plot. Fitted regression lines are for dark (left-hand side of each plot) and light (right-hand side of each plot) incubations.

considered a weedy species of the Caribbean due to its fast growth, low-relief morphology, and ability to thrive in suboptimal conditions, whereas *O. faveolata* and *S. siderea* are key, framework-building corals (Darling et al. 2012). As Caribbean benthic communities undergo phase shifts, *P. astreoides* is colonizing space once dominated by massive, framework building corals to become one of the most abundant scleractinian corals on Caribbean coral reefs (Green et al. 2008). Our results show that the contribution of *P. astreoides* to community reef metabolism is at the same scale as that of traditional reef-building corals; however, the similarity in biogeochemical signal does not confer the same ecological traits, as *P. astreoides* does not provide habitat or architectural complexity to the reef (Green et al. 2008). Therefore, while shifts toward weedy species dominance may not be detectable via changes in reef metabolism, the changes in benthic composition will still impact reef carbon cycles and accretion through changes in calcium carbonate morphology and composition (Perry and Alvarez-Filip 2018). The third massive coral, *S. siderea*, is generally considered a slow-growing species. However, its calcification rates were also high, and the observed slow growth despite high calcification rates could be related to the high density of *S. siderea* skeletons (Hughes 1987).

Fast-growing *A. cervicornis* had the lowest calcification rates of the corals in this study, but they can also have relatively lower skeletal densities than the massive corals (Kuffner et al. 2017). Historically, *A. cervicornis* was a primary reef-

building coral species and occupied more space on shallow water tropical reefs in the Caribbean than any other scleractinian coral (Rodríguez-Martínez et al. 2014; Toth et al. 2019); however, it and *Acropora palmata* have declined by over 80% over recent decades in the Caribbean (Jackson et al. 2014; Rodríguez-Martínez et al. 2014). It is possible that the lower rates of calcification observed in *A. cervicornis* were influenced by the relatively low flow induced within the mesocosm setting, as higher wave action may stimulate growth in this species (Jokiel 1978); however, our calcification rates agree with previous estimates (Chalker and Taylor 1975; Chalker and Taylor 1978). Colonies of *A. cervicornis* have a complex, branching structure with high surface area and they contribute different ecosystem functions compared to massive corals (Alvarez-Filip et al. 2011; Darling et al. 2012), which is reflected in the lower metabolic rates observed in our study. In general, *A. cervicornis* has low calcification yet high accretion rates, although skeletal density shows plasticity based on growing conditions (Kuffner et al. 2017). The life-history trait of lower density skeletons could promote asexual reproduction when high energy wave action fragments branches of larger colonies, allowing for the rapid proliferation of *Acropora* spp. (Tunnicliffe 1981; Lirman 2000). Despite having lower calcification rates than the massive corals, *A. cervicornis* provides a unique habitat for the biodiversity of species which reside in the dense thickets formed by this branching coral (Tunnicliffe 1981; Precht et al. 2002).

Fig. 9. Linear models showing strong positive relationship between photosynthesis measured by carbon assimilation (P_{DIC}) and oxygen production (P_{DO}) (**a**) across species and functional groups, and (**b**) separated by species. All linear models were significant to the $p < 0.001$ level (denoted by ***). CCA1 and CCA2 refer to the two types of crustose coralline algae used in this study.

The lowest metabolic rates were recorded for crustose coralline algae; biogenic calcifiers which reinforce and strengthen the calcium carbonate matrix to cover otherwise exposed coral skeleton (Littler and Littler 2013). In addition, they promote calcification by scleractinian corals (Chisholm 2000) via inducing larval settlement and providing substrate for juvenile corals to grow (Heyward and Negri 1999). Due to their encrusting morphology, crustose coralline algae are often overlooked in quantification of coral reef calcification and accretion based on visual surveys. We report rates of calcification and photosynthesis in CCA in line with framework building *A. cervicornis* (Figs. 3, 4).

This demonstrates the important contribution that crustose coralline algae can play in coral reef ecosystem metabolism beyond their other ecological functions. The two crustose coralline algal types were the closest to displaying net dissolution, indicating calcification slows or stops at night within this functional group, potentially due to dependence on light. Crustose coralline algae are expected to be more heavily impacted by ocean acidification than corals due to the higher proportion of high magnesium calcite in their skeletons, which could disproportionately impact the role of these organisms as important benthic calcifiers (Diaz-Pulido et al. 2012).

444

159
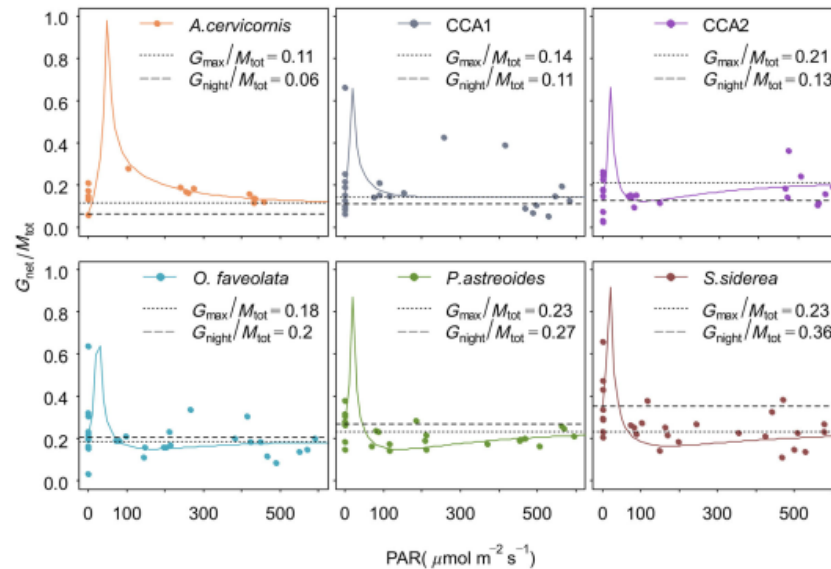
Fig. 10. Ratios of calcification to total carbon metabolism (G_{net}/M_{tot}) calculated from each incubation (points) and metabolism–irradiance models (lines) plotted against PAR. Ratios calculated using the model coefficients (i.e., net P_{max} and netG_{max}; R and G_{night}) are depicted by dotted and dashed lines and values are displayed in the top right of the plot for each species. CCA1 and CCA2 refer to the two types of crustose coralline algae used in this study.

Impact of light on species-specific metabolism

Coral reefs encompass diverse and dynamic light environments over hourly, daily, and seasonal scales (Edmunds et al. 2018). However, most reef-wide estimates of community metabolism are conducted on timescales that do not incorporate instantaneous changes in light, even though community metabolism can change on sub-hourly timescales (Takeshita et al. 2016). Applying metabolic-light models to high-resolution time series of light could provide more complete estimates of community level metabolism. Studies have shown that scaling up to community and ecosystem levels from organismal studies can be complicated in coral reef ecosystems (Edmunds et al. 2016); however, the comparisons in our study add important insight into coral reef metabolism research. In this study, net metabolic rates (both photosynthesis and calcification) fit a commonly used hyperbolic function with light (Figs. 5, 6) (Jassby and Platt 1976), supporting the idea that both photosynthesis and calcification are driven by light (Falkowski et al. 1984; Cohen et al. 2016).

Photosynthesis–irradiance models fitted with both oxygen and carbon data sets (e.g., P_{DO} and P_{DIC}) demonstrated that photosynthetic efficiency (α), modeled maxima (P_{max}), and average respiration were greatest in the massive corals, highlighting that these species are drivers of coral reef production (Fig. 5; Supporting Information Fig. S8). Light saturation (E_K) was higher in *A. cervicornis* and CCA, potentially reflecting

their ability to thrive in the shallowest and most sunlit areas of the reef (i.e., lagoon and crest). For calcification–irradiance models, the massive species group had the highest maximum and dark rates (G_{max} and G_{dark}), while estimates of calcification efficiency (α) were mixed across species. The differences between metabolic-light models support previous work showing that photosynthesis and calcification have species-specific and independent relationships with light (Gattuso et al. 2000; Sawall et al. 2018).

Relationships among photosynthesis, respiration, and calcification have been shown to exist across a wide range of marine calcifiers, and in the current study, we demonstrate that a strong relationship exists across different species, genera, and functional groups (Fig. 7). The strong positive linear relationship between G_{max} and P_{max} indicates that maximum net daytime photosynthesis and calcification rates are linked (Fig. 7b). We also found a strong negative linear relationship between average respiration and dark calcification across all species at night, indicating that dark calcification is linked to energy produced from respiration (Fig. 7a). Linear relationships also existed during the day and night for measured values of calcification and photosynthesis across all species (light $R^2 = 0.46$, $p < 0.0005$, dark $R^2 = 0.15$, $p = 0.005$; Fig. 7c). However, relationships between calcification and photosynthesis were less clear within each individual species (Fig. 8). This could be due to lower replicates within each

160

species and smaller ranges in dark rates that made it difficult to detect a clear relationship by species. While our study shows that photosynthesis and calcification are linked across benthic calcifiers, we also saw differences at the species level (Fig. 8), likely related to ecological function (González-Barrios and Álvarez-Filip 2018). For example, *P. astreoides* has a strong linear relationship between calcification and photosynthesis (light $R^2 = 0.39$, dark $R^2 = 0.78$, $p \leq 0.005$, Fig. 8), whereas other species such as *A. cervicornis* did not. Calcification of different species of corals has been shown to respond to global change differently (Kornder et al. 2018), which may reflect the interaction of these two processes at the cellular or organismal level. Light has also been shown to modulate the response of calcification to ocean acidification (Suggett et al. 2013). Therefore, developing species level metabolic irradiance curves under current and predicted ocean chemistry is important for understanding future impacts of global change.

The functional relationship among light, photosynthesis, and calcification is complex and operates at multiple levels (Allemand et al. 2011). We demonstrate a positive linear relationship between modeled metabolic maxima (G_{max} and P_{max}), indicating that energy from photosynthesis and respiration drive calcification. It is clear that coral metabolic processes are tightly coupled (Gattuso et al. 1999). However, recent research indicates that photosynthesis and calcification are parallel but independent light-driven processes (Cohen et al. 2016). The link between photosynthesis and calcification (i.e., light-enhanced calcification) at the organismal scale may be related to these processes co-evolving to occur at similar times due to increased energy supply for calcification (Sorek et al. 2014). If that is the case, then the relationships between photosynthesis and calcification found at the organismal level may not be as intimately linked within cells as previously thought. Further research is needed to define the functional relationships among light, photosynthesis, and calcification from the cell to the organism to better predict the impacts of global change on coral ecosystems.

Knowing instantaneous relationships between light and metabolism at the organismal scale (Figs. 5, 6; Supporting Information Fig. S8) could help scale metabolism rates up to the community and ecosystem at finer temporal scales. Direct measurements of coral reef net ecosystem metabolic rates are time consuming, expensive, and often require specific environmental conditions (Gattuso et al. 1999). Newer technology is being developed that can estimate community benthic metabolism rates over high-resolution temporal scales (< 1 h) using boundary layer techniques (i.e., eddy correlation and BEAMS) that measure oxygen and pH (Barnes and Devereux 1984; Long et al. 2013; Takeshita et al. 2016). These techniques require that we know the ratio of carbon and oxygen uptake and removal during the processes of photosynthesis and respiration (e.g., $\Delta DIC/\Delta DO$). For an organism, these values are usually seperated between day and night and known as the gross photosynthetic (PQ) and respiratory

quotients (RQ), respectively. However, over daily cycles across organisms, communities, and ecosystems, the net metabolic quotient (Q) is needed for calculating metabolic rates from oxygen and pH measurements (Barnes and Devereux 1984; Takeshita et al. 2016). By measuring both oxygen and carbon fluxes, we were able to determine the net metabolic quotient for the different species in this study (Fig. 9). The net metabolic quotient (Q) was higher for crustose coralline algae (1.55 ± 0.49) than coral species (1.24 ± 0.38), which reflects elevated carbon assimilation compared to oxygen production. For corals, the metabolic quotient was similar across species (1.1–1.2), and closer to a 1 : 1 ratio, although the values still indicated a greater assimilation of carbon compared to DO production. Overall, the net metabolic quotient (Q) was 1.18 for all species and incubations combined. Interestingly, there was a trend of increasing Q with light when all corals were grouped together, indicating that the metabolic quotient may be more variable over short time scales than previously assumed (Supporting Information Fig. S10). Further understanding the influence of light on the balance of carbon assimilation to dissolved oxygen production will help to build our understanding of the reef net metabolic quotient and how it changes with light variability over hourly, daily, and seasonal cycles. More estimates of species-specific metabolic quotients for coral reef organisms will help in efforts aimed at using readily available pH and oxygen sensors to monitor the metabolism of coral communities at a greater resolution in both space and time.

Ratios of organic and inorganic carbon cycling in coral reef organisms

Ratios of net calcification to photosynthesis (G_{net}/P_{net}) quantify the relative balance between these two processes and have been proposed to be a useful metric for reef biogeochemical function and health (Cyronak et al. 2018). Previous studies have shown that G_{net} to P_{net} ratios range from −8 to 17 on the organismal scale and from 0 to 0.7 on an ecosystem scale (Gattuso et al. 1999; Cyronak et al. 2018). In this study, we calculated absolute ratios of net calcification to the sum of net calcification and net photosynthesis (G_{net}/M_{tot}) according to Eq. 7. We chose this metric because both calcification and production can be negative, which results in unreliable values as either the denominator or numerator approach 0. Also, we believe that G_{net}/M_{tot} is more intuitive than G_{net}/P_{net} as it represents the relative proportion of total carbon metabolism due to calcification and ranges between 0 and 1. In all of the incubations, G_{net}/M_{tot} ranged from 0.03 to 0.66, which indicates that when both calcification and production are occurring production tends to dominate (Fig. 10). However, when the ratios were calculated using the metabolism–irradiance curves, G_{net}/M_{tot} ranged from 0 to 1 and all organisms exhibited a strong peak at the irradiance level where net photosynthesis crosses 0. This is because as net photosynthesis approaches 0 the absolute ratio comes closer to $|G_{net}|/|G_{net}|$. Ratios

calculated using the model coefficients for maximum calcification (i.e., *net* G_{max} and *net* P_{max}) and night calcification to respiration (i.e., G_{dark} and R) ranged from 0.11 to 0.23 and 0.06 to 0.36, respectively (Fig. 10).

The light-induced changes in G_{net}/M_{tot} indicate that there is not one value that can readily describe the relative ratio of calcification and production for each calcifying organism, and that organisms can "equilibrate" to very different values during the day and night. In fact, the highly dynamic nature of G_{net}/M_{tot} related to light brings into question the use of G_{net} to P_{net} ratios as a single, determinant value of reef function and health at the ecosystem scale (Cyronak et al. 2018). If G_{net}/M_{tot} do not stabilize to one consistent value on an organismal scale, it is difficult to imagine that these ratios stabilize over varying light regimes across reef communities and ecosystems made up of many calcifying and non-calcifying organisms. Future work into determining the importance and usefulness of G_{net}/M_{tot} as a metric for reef biogeochemical cycling is needed.

Conclusions

We identified patterns in the metabolism of six Caribbean benthic calcifiers under natural diurnal light cycles. Our findings support previous work showing that photosynthesis and calcification are parallel processes driven by irradiance (Gattuso et al. 2000; Cohen et al. 2016), highlighting the importance of considering natural variations in light for all reef metabolism studies. Some metabolic rates of individual species could be generalized to larger categorical groupings such as the "massive coral" species. However, both *A. cervicornis* and crustose coralline algae had similar metabolic rates despite occupying very different functional niches in coral reef accretion. While calcification and photosynthesis both fit traditional hyperbolic tangent functions with light, coefficients of the metabolism–irradiance models varied between species. Interestingly, the modeled metabolic maxima (G_{max} and P_{max}) and dark calcification and respiration (G_{dark} and R) were correlated across all photosynthesising calcifiers in this study. These correlations support the idea that energy provided by photosynthesis and respiration may be an important control on organismal calcification across different calcifying functional groups. However, mechanistic studies are needed to further address this. Understanding the dynamic species-specific balance of calcification and production could provide useful insights into estimates of community- and reef-wide carbon cycles. For example, our results demonstrate that benthic surveys with simple groupings of calcifying and non-calcifying organisms could give important insights into coral reef carbon cycles. Finally, we established dynamic relationships between calcification and photosynthesis over diurnal light cycles that bring into question the application of calcification to photosynthesis ratios to monitor biogeochemical function on an ecosystem scale. Overall, the carbon cycle of coral reefs is highly dynamic at the organismal scale, driven by complex relationships between photosynthesis, respiration, calcification, and light. These relationships likely scale up and interact with other biogeochemical and hydrodynamic processes to create the intense variations in carbon chemistry observed on modern coral reefs.

References

Albright, R., J. Benthuysen, N. Cantin, K. Caldeira, and K. Anthony. 2015. Coral reef metabolism and carbon chemistry dynamics of a coral reef flat. Geophys. Res. Lett. **42**: 3980–3988. doi:10.1002/2015GL063488

Allemand, D., É. Tambutté, D. Zoccola, and S. Tambutté. 2011. Coral calcification, cells to reefs, p. 119–150. *In* Coral reefs: An ecosystem in transition. Springer.

Allison, N., and others. 2014. Corals concentrate dissolved inorganic carbon to facilitate calcification. Nat. Commun. **5**: 5741. doi:10.1038/ncomms6741

Alvarez-Filip, L., N. K. Dulvy, I. M. Côteé, A. R. Watkinson, and J. A. Gill. 2011. Coral identity underpins architectural complexity on Caribbean reefs. Ecol. Appl. **21**: 2223–2231. doi:10.1890/10-1563.1

Barnes, D. J., and M. J. Devereux. 1984. Productivity and calcification on a coral reef: A survey using pH and oxygen electrode techniques. J. Exp. Mar. Biol. Ecol. **79**: 213–231. doi:10.1016/0022-0981(84)90196-5

Baty, F., C. Ritz, S. Charles, M. Brutsche, M.-L. Flandrois, and J.-P. Delignette-Muller. 2015. A toolbox for nonlinear regression in {R}: The package {nlstools}. J. Stat. Softw. **66**: 1–21.

Chalker, B. E., and D. L. Taylor. 1975. Light-enhanced calcification, and the role of oxidative phosphorylation in calcification of the coral *Acropora cervicornis*. Proc. R. Soc. Lond. B Biol. Sci. **190**: 323–331. doi:10.1098/rspb.1975.0096

Chalker, B. E., and D. L. Taylor. 1978. Rhythmic variations in calcification and photosynthesis associated with the coral *Acropora cervicornis* (Lamarck). Proc. R. Soc. Lond. B Biol. Sci. **201**: 179–189. doi:10.1098/rspb.1978.0039

Chisholm, J. R. 2000. Calcification by crustose coralline algae on the northern Great Barrier Reef, Australia. Limnol. Oceanogr. **45**: 1476–1484. doi:10.4319/lo.2000.45.7.1476

Cohen, I., Z. Dubinsky, and J. Erez. 2016. Light enhanced calcification in hermatypic corals: New insights from light spectral responses. Front. Mar. Sci. **2**: 122. doi:10.3389/fmars.2015.00122

Comeau, S., P. J. Edmunds, N. B. Spindel, and R. C. Carpenter. 2013. The responses of eight coral reef calcifiers to increasing partial pressure of CO_2 do not exhibit a tipping point. Limnol. Oceanogr. **58**: 388–398. doi:10.4319/lo.2013.58.1.0388

Comeau, S., P. J. Edmunds, C. A. Lantz, and R. C. Carpenter. 2014. Water flow modulates the response of coral reef

communities to ocean acidification. Sci. Rep. **4**: 1–6. doi:10.1038/srep06681

Comeau, S., C. E. Cornwall, C. A. Pupier, T. M. DeCarlo, C. Alessi, R. Trehern, and M. T. McCulloch. 2019. Flow-driven micro-scale pH variability affects the physiology of corals and coralline algae under ocean acidification. Sci. Rep. **9**: 1–12. doi:10.1038/s41598-019-49044-w

Cyronak, T., I. R. Santos, and B. D. Eyre. 2013. Permeable coral reef sediment dissolution driven by elevated pCO_2 and pore water advection. Geophys. Res. Lett. **40**: 4876–4881. doi:10.1002/grl.50948

Cyronak, T., and others. 2018. Taking the metabolic pulse of the world's coral reefs. PLoS One **13**: e0190872. doi:10.1371/journal.pone.0190872

Darling, E. S., L. Alvarez-Filip, T. A. Oliver, T. R. Mcclanahan, and I. M. Côté. 2012. Evaluating life-history strategies of reef corals from species traits. Ecol. Lett. **15**: 1378–1386. doi:10.1111/j.1461-0248.2012.01861.x

Diaz-Pulido, G., K. R. N. Anthony, D. I. Kline, S. Dove, and O. Hoegh-Guldberg. 2012. Interactions between ocean acidification and warming on the mortality and dissolution of coralline algae. J. Phycol. **48**: 32–39. doi:10.1111/j.1529-8817.2011.01084.x

Dickson, A. G., C. L. Sabine, and J. R. Christian. 2007. Guide to best practices for ocean CO_2 measurements. Publ, p. 3.

Edmunds, P. J., and others. 2016. Integrating the effects of ocean acidification across functional scales on tropical coral reefs. Bioscience **66**: 350–362. doi:10.1093/biosci/biw023

Edmunds, P. J., G. Tsounis, R. Boulon, and L. Bramanti. 2018. Long-term variation in light intensity on a coral reef. Coral Reefs **37**: 955–965. doi:10.1007/s00338-018-1721-y

Eyre, B. D., A. J. Andersson, and T. Cyronak. 2014. Benthic coral reef calcium carbonate dissolution in an acidifying ocean. Nat. Clim. Chang. **4**: 969–976. doi:10.1038/nclimate2380

Eyre, B. D., T. Cyronak, P. Drupp, E. H. De Carlo, J. P. Sachs, and A. J. Andersson. 2018. Coral reefs will transition to net dissolving before end of century. Science **359**: 908–911. doi:10.1126/science.aao1118

Falkowski, P. G., Z. Dubinsky, L. Muscatine, and J. W. Porter. 1984. Light and the bioenergetics of a symbiotic coral. Bioscience **34**: 705–709. doi:10.2307/1309663

Furla, P., I. Galgani, I. Durand, and D. Allemand. 2000. Sources and mechanisms of inorganic carbon transport for coral calcification and photosynthesis. J. Exp. Biol. **203**: 3445–3457.

Gattuso, J.-P., D. Allemand, and M. Frankignoulle. 1999. Photosynthesis and calcification at cellular, organismal and community levels in coral reefs: a review on interactions and control by carbonate chemistry. American Zoologist **39**(1): 160–183. [Correction added on 27 January 2022, after first online publication: The reference Gattuso et al. (1999) has been updated with the correct author names, title, and details.]

Gattuso, J.-P., S. Reynaud-Vaganay, P. Furla, S. Romaine-Lioud, J. Jaubert, I. Bourge, and M. Frankignoulle. 2000.

Calcification does not stimulate photosynthesis in the zooxanthellate scleractinian coral Stylophora pistillata. Limnol. Oceanogr. **45**: 246–250. doi:10.4319/lo.2000.45.1.0246

González-Barrios, F. J., and L. Álvarez-Filip. 2018. A framework for measuring coral species-specific contribution to reef functioning in the Caribbean. Ecol. Indic. **95**: 877–886. doi:10.1016/J.ECOLIND.2018.08.038

Goreau, T. F. 1959. The physiology of skeleton formation in corals. A method for measuring the rate of calcium deposition by corals under different conditions. Biol. Bull. **116**: 59–75. doi:10.2307/1539156

Green, D. H. D., P. P. J. Edmunds, and R. R. C. Carpenter. 2008. Increasing relative abundance of *Porites astreoides* on Caribbean reefs mediated by an overall decline in coral cover. Mar. Ecol. Prog. Ser. **359**: 1–10. doi:10.3354/meps07454

Harianto, J., N. Carey, and M. Byrne. 2019. respR—An R package for the manipulation and analysis of respirometry data. Methods Ecol. Evol. **10**: 912–920. doi:10.1111/2041-210X.13162

Heyward, A. J., and A. P. Negri. 1999. Natural inducers for coral larval metamorphosis. Coral Reefs **18**: 273–279. doi:10.1007/s003380050193

Hoegh-Guldberg, O., L. Pendleton, and A. Kaup. 2019. People and the changing nature of coral reefs. Reg. Stud. Mar. Sci. **30**: 100699. doi:10.1016/j.rsma.2019.100699

Hughes, T. P. 1987. Skeletal density and growth form of corals.

Hughes, T. P., and others. 2018. Global warming transforms coral reef assemblages. Nature **556**: 492–496. doi:10.1038/s41586-018-0041-2

Jackson, J., M. Donovan, K. Cramer, and V. Lam. 2014. Status and trends of Caribbean coral reefs: 1970–2012, Global Coral Reef Monitoring Network. IUCN.

Jassby, A. D., and T. Platt. 1976. Mathematical formulation of the relationship between photosynthesis and light for phytoplankton. Limnol. Oceanogr. **21**: 540–547. doi:10.4319/lo.1976.21.4.0540

Jokiel, P. L. 1978. Effects of water motion on reef corals. **35**: 87–97. doi:10.1016/0022-0981(78)90092-8

Kleypas, J., and K. Yates. 2009. Coral reefs and ocean acidification. Oceanography **22**: 108–117. doi:10.5670/oceanog.2009.101

Kornder, N. A., B. M. Riegl, and J. Figueiredo. 2018. Thresholds and drivers of coral calcification responses to climate change. Glob. Chang. Biol. **24**: 5084–5095. doi:10.1111/gcb.14431

Kuffner, I. B., E. Bartels, A. Stathakopoulos, I. C. Enochs, G. Kolodziej, L. T. Toth, and D. P. Manzello. 2017. Plasticity in skeletal characteristics of nursery-raised staghorn coral, *Acropora cervicornis*. Coral Reefs **36**: 679–684. doi:10.1007/s00338-017-1560-2

Kuffner, I. B., L. T. Toth, J. H. Hudson, W. B. Goodwin, A. Stathakopoulos, L. A. Bartlett, and E. M. Whitcher. 2019.

Lirman, D. 2000. Fragmentation in the branching coral *Acropora palmata* (Lamarck): Growth, survivorship, and reproduction of colonies and fragments. J. Exp. Mar. Biol. Ecol. **251**: 41–57. doi:10.1016/S0022-0981(00)00205-7

Littler, M. M., and D. S. Littler. 2013. The nature of crustose coralline algae and their interactions on reefs. Research and discoveries: the revolution of science through SCUBA. Smithsonian Institution, Washington, District of Columbia 20013- 7012, USA.

Long, M. H., P. Berg, D. de Beer, J. C. Zieman, D. de Beer, and J. C. Zieman. 2013. In situ coral reef oxygen metabolism: An Eddy correlation study. PLoS One **8**: e58581. doi:10.1371/journal.pone.0058581

Marsh, J. A., and S. V. Smith. 1978. Productivity measurements of coral reefs in flowing water. 361–377.

McConnaughey, T. A., and J. F. Whelan. 1997. Calcification generates protons for nutrient and bicarbonate uptake. Earth Sci. Rev. **42**: 95–117. doi:10.1016/S0012-8252(96)00036-0

Muehllehner, N., C. Langdon, A. Venti, and D. Kadko. 2016. Dynamics of carbonate chemistry, production, and calcification of the Florida Reef Tract (2009-2010): Evidence for seasonal dissolution. Global Biogeochem. Cycles **30**: 661–688. doi:10.1002/2015GB005327

Perry, C. T., and L. Alvarez-Filip. 2018. Changing geo-ecological functions of coral reefs in the Anthropocene. Blackwell Publishing Ltd.

Precht, W. F., A. W. Bruckner, R. B. Aronson, and R. J. Bruckner. 2002. Endangered acroporid corals of the Caribbean. Coral Reefs **21**: 41–42. doi:10.1007/s00338-001-0209-2

Rodríguez-Martínez, R. E., A. T. Banaszak, M. D. McField, A. U. Beltrán-Torres, and L. Álvarez-Filip. 2014. Assessment of *Acropora palmata* in the mesoamerican reef system. PLoS One **9**: 1–7. doi:10.1371/journal.pone.0096140

R Core Team. 2019. R: A language and environment for statistical computing.

Sawall, Y., E. J. Hochberg, Y. Sawall Id, and E. J. Hochberg. 2018. Diel versus time-integrated (daily) photosynthesis and irradiance relationships of coral reef organisms and communities. PLoS One **13**: e0208607. doi:10.1371/journal.pone.0208607

Schneider, C. A., W. S. Rasband, and K. W. Eliceiri. 2012. NIH image to ImageJ: 25 years of image analysis. Nat. Methods **9**: 671–675. doi:10.1038/nmeth.2089

Smith, S. V., and D. W. Kinsey. 1978. Calcification and organic carbon metabolism as indicated by carbon dioxide, p. 469–484. *In* D. R. Stoddart and R. E. Johannes [eds.]. Coral Reefs: Research Methods. UNESCO.

Sorek, M., E. M. Díaz-Almeyda, M. Medina, and O. Levy. 2014. Circadian clocks in symbiotic corals: The duet between Symbiodinium algae and their coral host. Mar. Genomics **14**: 47–57. doi:10.1016/j.margen.2014.01.003

Suggett, D. J., L. F. Dong, T. Lawson, E. Lawrenz, L. Torres, and D. J. Smith. 2013. Light availability determines susceptibility of reef building corals to ocean acidification. Coral Reefs **32**: 327–337. doi:10.1007/s00338-012-0996-7

Takeshita, Y., T. Cyronak, T. R. Martz, T. Kindeberg, and A. J. Andersson. 2018. Coral reef carbonate chemistry variability at different functional scales. Front. Mar. Sci. **5**: 175. doi:10.3389/fmars.2018.00175

Takeshita, Y., W. McGillis, E. M. Briggs, A. L. Carter, E. M. Donham, T. R. Martz, N. N. Price, and J. E. Smith. 2016. Assessment of net community production and calcification of a coral reef using a boundary layer approach. J. Geophys. Res. Ocean **121**: 5655–5671. doi:10.1002/2016JC011886

Toth, L. T., A. Stathakopoulos, I. B. Kuffner, R. R. Ruzicka, M. A. Colella, and E. A. Shinn. 2019. The unprecedented loss of Florida's reef-building corals and the emergence of a novel coral-reef assemblage. Ecology **100**: e02781. doi:10.1002/ECY.2781

Tunnicliffe, V. 1981. Breakage and propagation of the stony coral *Acropora cervicornis*. Proc. Natl. Acad. Sci. **78**: 2427–2431. doi:10.1073/pnas.78.4.2427

Wang, F. 2016. Tutorial SIOX plugin in ImageJ: Area measurement made easy. UV4Plants Bull. **2016**: 37–44. doi:10.19232/uv4pb.2016.2.11

Wickham, H. 2016. ggplot2: Elegant graphics for data analysis. Springer International Publishing,

Wickham, H. 2019. Welcome to the tidyverse. J. Open Source Softw. **4**: 1686.

Yates, K. K., D. G. Zawada, N. A. Smiley, and G. Tiling-Range. 2017. Divergence of seafloor elevation and sea level rise in coral reef ecosystems. Biogeosciences **14**: 1739–1772. doi:10.5194/BG-14-1739-2017

Conflict of Interest

None.

16

6.2 Appendix B: Examples of dissolved oxygen data output from coral incubations.
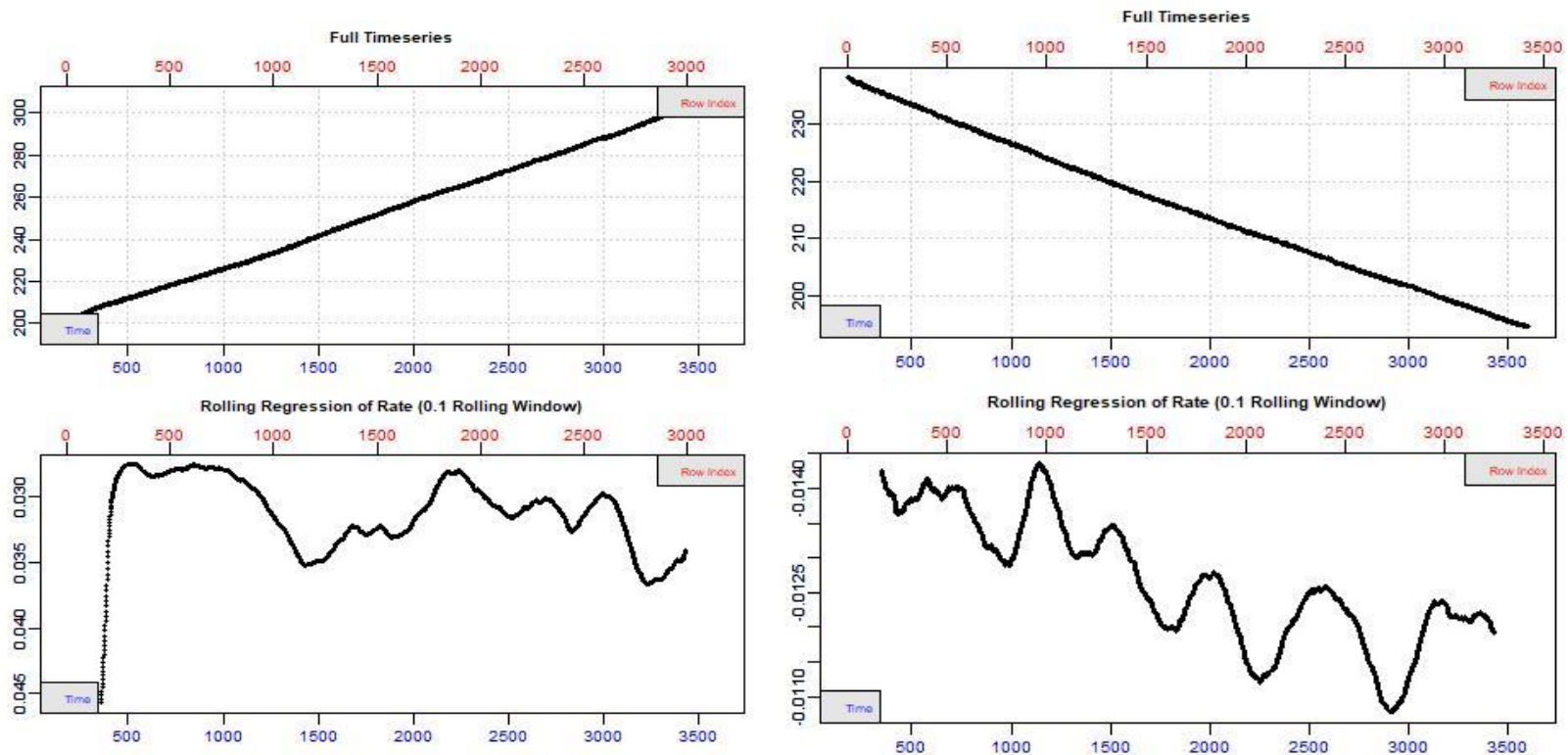
Figure 6-1: Plots generated using R package *RespR* to 'inspect' each incubation for anomalies. Plots in the top row show raw oxygen data and bottom row show the slope of a rolling linear regression during a 1 hour incubation of *O. faveolata* in the light (left) and dark (right).
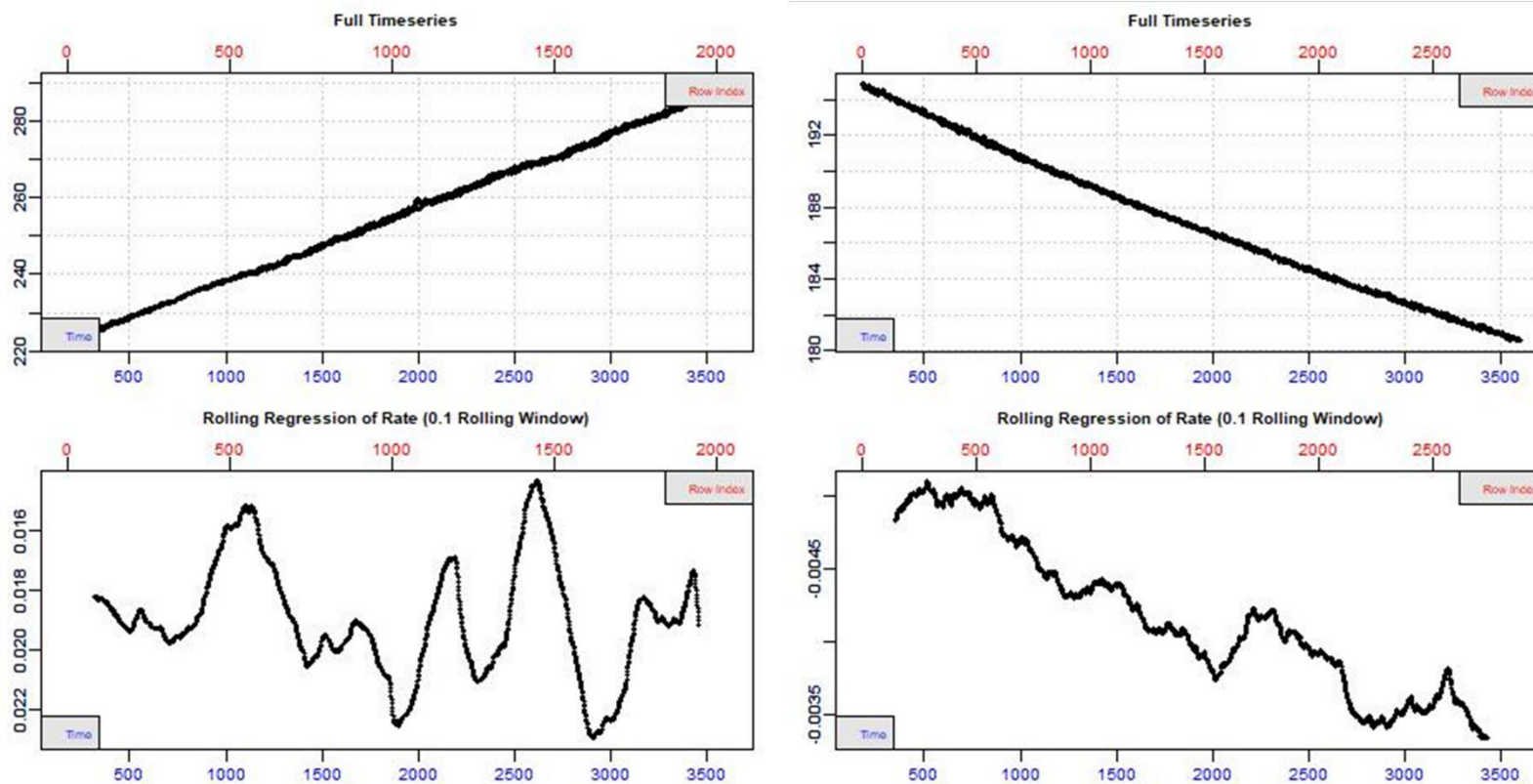
Figure 6-2: Examples of inspection plots of raw change in dissolved oxygen (ΔDO) during 1 hour incubations of crustose coralline algae type 1 (CCA1) during light (left) and dark (right) incubations.

Full Timeseries (top left)

Full Timeseries (top right)

Rolling Regression of Rate (0.1 Rolling Window) (bottom left)

Rolling Regression of Rate (0.1 Rolling Window) (bottom right)

167
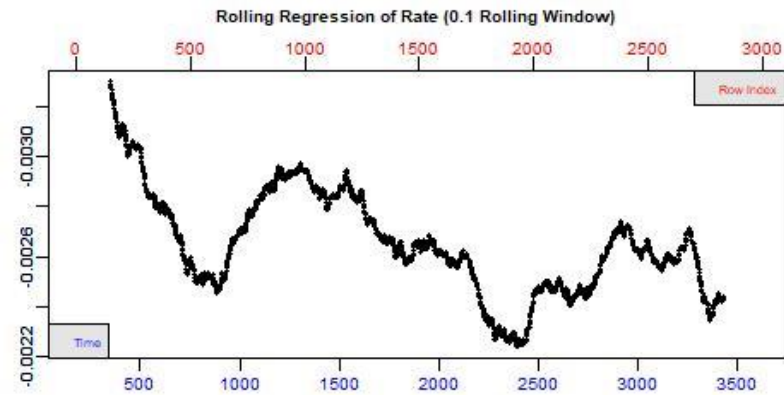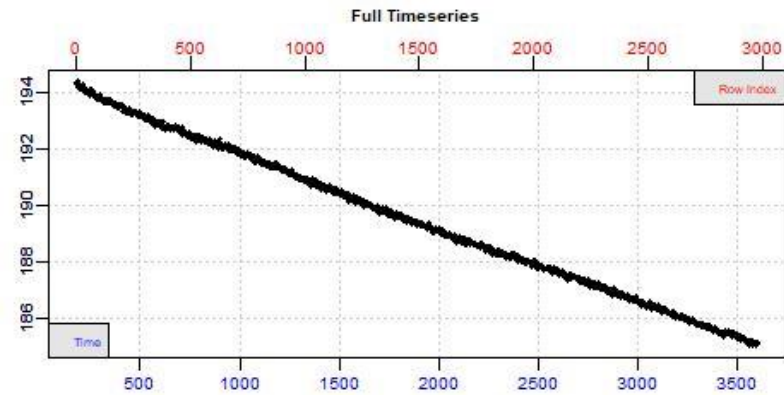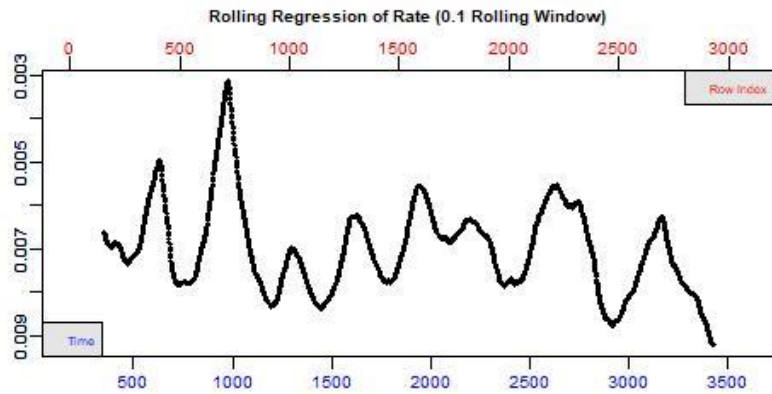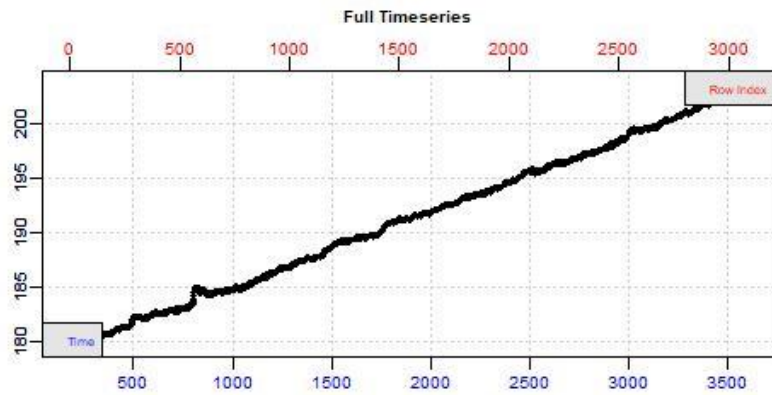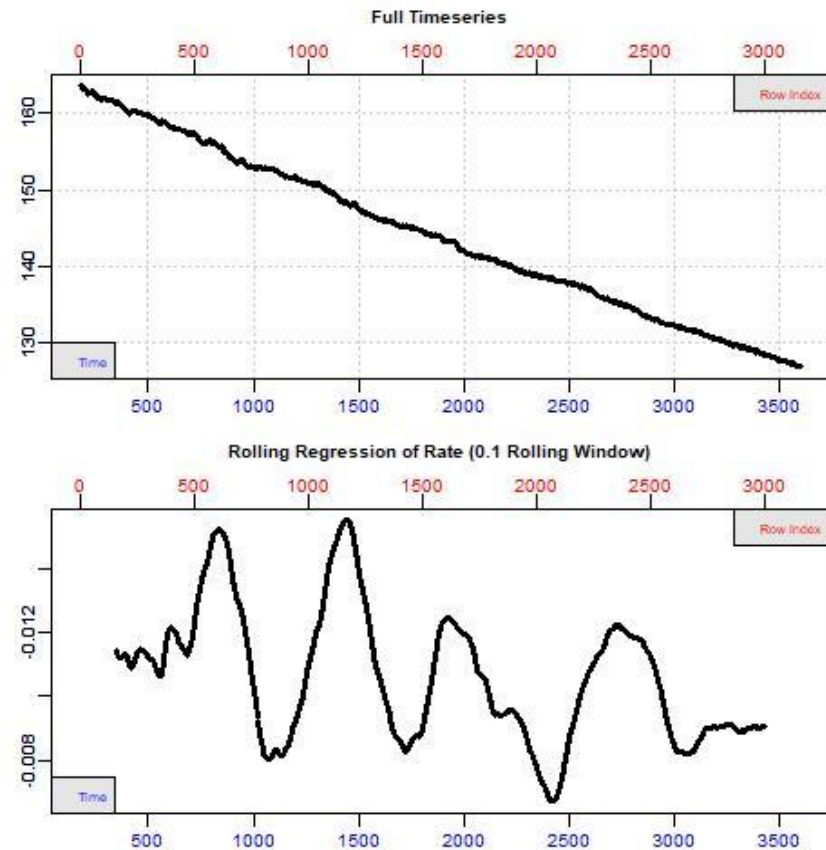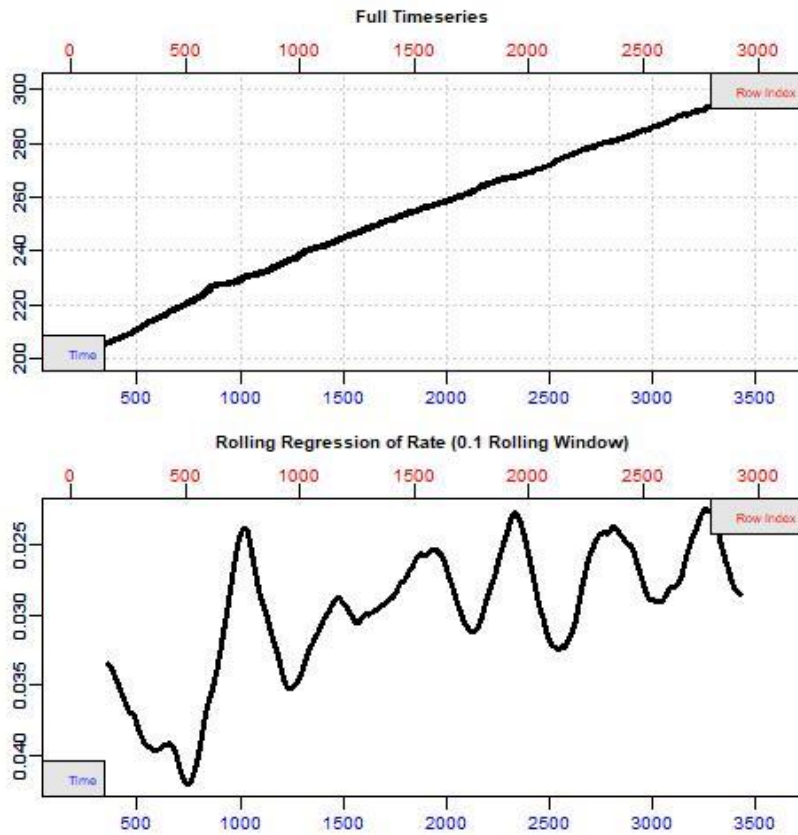
Figure 6-3: Examples of inspection plots of raw change in dissolved oxygen (ΔDO) during 1-hour incubations of *P. astreoides* during light (left) and dark (right) incubations.

Figure 6-4: Plots generated using R package *RespR* to 'inspect' each incubation for anomalies. Plots in the top row show raw oxygen data and bottom row show the slope of a rolling linear regression during a 1 hour incubation of *S.siderea* in the light (left) and dark (right).**Figure 6-5:** Examples of
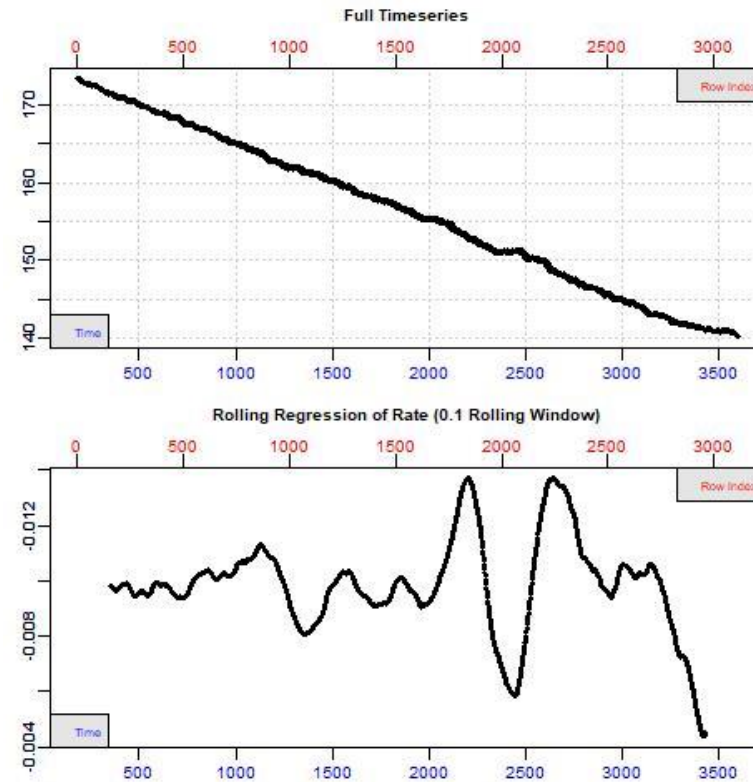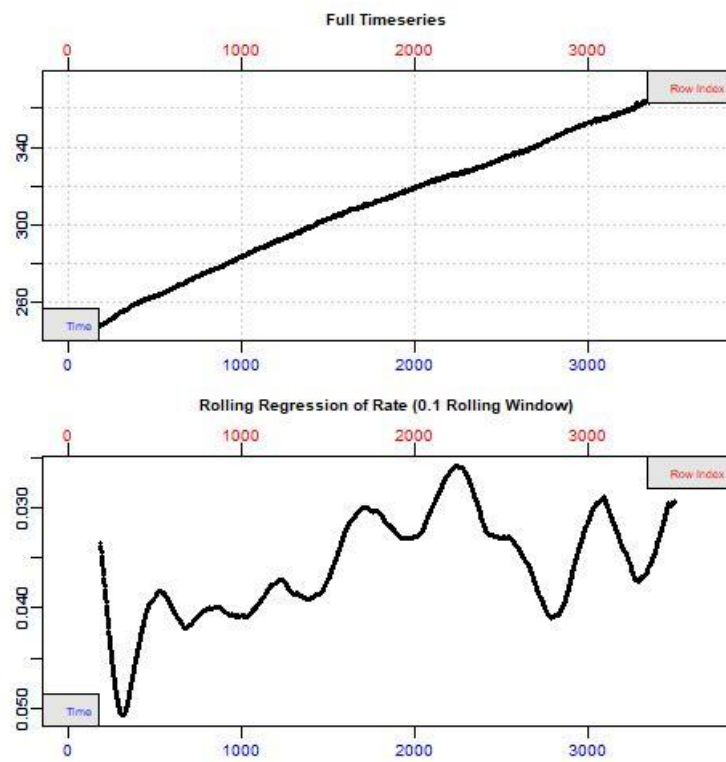
Figure 6-6: Plots generated using R package *RespR* to 'inspect' each incubation for anomalies. Plots in the top row show raw oxygen data and bottom row show the slope of a rolling linear regression during a 1 hour incubation of *S.siderea* in the light (left) and dark (right).

References

Ainsworth, T. D., and B. E. Brown. 2021. Coral bleaching. Curr Biol **31**: R5–R6. doi:10.1016/J.CUB.2020.10.048

Albright, R., J. Benthuysen, N. Cantin, K. Caldeira, and K. Anthony. 2015. Coral reef metabolism and carbon chemistry dynamics of a coral reef flat. Geophysical Research Letters **42**: 3980–3988. doi:10.1002/2015GL063488

Albright, R., B. Mason, M. Miller, and C. Langdon. 2010. Ocean acidification compromises recruitment success of the threatened Caribbean coral Acropora palmata. Proc Natl Acad Sci U S A **107**: 20400–4. doi:10.1073/pnas.1007273107

Alldredge, A., C. Carlson, and R. Carpenter. 2013. Sources of Organic Carbon to Coral Reef Flats. Oceanography **26**: 108–113. doi:10.5670/oceanog.2013.52

Allemand, D., É. Tambutté, D. Zoccola, and S. Tambutté. 2011. Coral calcification, cells to reefs, p. 119–150. *In* Coral Reefs: An Ecosystem in Transition. Springer Netherlands.

Allison, N., I. Cohen, A. A. Finch, and others. 2014. Corals concentrate dissolved inorganic carbon to facilitate calcification. Nature Communications **5**: 5741. doi:10.1038/ncomms6741

Altieri, A. H., and K. B. Gedan. 2015. Climate change and dead zones. Global Change Biology **21**: 1395–1406. doi:10.1111/GCB.12754

Altieri, A. H., M. D. Johnson, S. D. Swaminathan, H. R. Nelson, and K. B. Gedan. 2021. Resilience of Tropical Ecosystems to Ocean Deoxygenation. Trends in Ecology & Evolution **36**: 227–238. doi:10.1016/J.TREE.2020.11.003

Alvarez-Filip, L., N. K. Dulvy, I. M. Côteé, A. R. Watkinson, and J. A. Gill. 2011. Coral identity underpins architectural complexity on Caribbean reefs. Ecological Applications **21**: 2223–2231. doi:10.1890/10-1563.1

Aphalo, P. J. 2021. ggpmisc: Miscellaneous Extensions to "ggplot2".

Attard, K. M., I. F. Rodil, R. N. Glud, P. Berg, J. Norkko, and A. Norkko. 2019. Seasonal ecosystem metabolism across shallow benthic habitats measured by aquatic eddy covariance. Limnology and Oceanography Letters **4**: 79–86. doi:10.1002/LOL2.10107

Bainbridge, Z., S. Lewis, R. Bartley, and others. 2018. Fine sediment and particulate organic matter: A review and case study on ridge-to-reef transport, transformations, fates, and impacts on marine ecosystems. Marine Pollution Bulletin **135**: 1205–1220. doi:10.1016/J.MARPOLBUL.2018.08.002

Barnard, P. L., J. E. Dugan, H. M. Page, and others. 2021. Multiple climate change-driven tipping points for coastal systems. Scientific Reports 2021 11:1 **11**: 1–13. doi:10.1038/s41598-021-94942-7

Barnes, D. J., and M. J. Devereux. 1984. Productivity and calcification on a coral reef: A survey using pH and oxygen electrode techniques. Journal of Experimental Marine Biology and Ecology **79**: 213–231. doi:10.1016/0022-0981(84)90196-5

Barnes, D. J. J. 1983. Profiling coral reef productivity and calcification using pH and oxygen electrodes. Journal of Experimental Marine Biology and Ecology **66**: 149–161. doi:10.1016/0022-0981(83)90036-9

Baty, F., C. Ritz, S. Charles, M. Brutsche, and M.-L. Flandrois , Jean-Pierre Delignette-Muller. 2015. A Toolbox for Nonlinear Regression in {R}: The Package {nlstools}. Journal of Statistical Software **66**: 1–21.

Bauer, J. E., W. J. Cai, P. A. Raymond, T. S. Bianchi, C. S. Hopkinson, and P. A. G. Regnier. 2013. The changing carbon cycle of the coastal ocean, Nature Publishing Group.

Bayraktarov, E., A. T. Banaszak, P. Montoya Maya, and others. 2020. Coral reef restoration efforts in Latin American countries and territories. PLoS ONE **15**. doi:10.1371/journal.pone.0228477

Bellwood, D. R., T. P. Hughes, C. Folke, and M. Nyström. 2004. Confronting the coral reef crisis. Nature **429**: 827–833. doi:10.1038/nature02691

Berg, P., M. L. Delgard, P. Polsenaere, K. J. McGlathery, S. C. Doney, and A. C. Berger. 2019. Dynamics of benthic metabolism, O2, and pCO2 in a temperate seagrass meadow. Limnology and Oceanography **64**: 2586–2604. doi:10.1002/LNO.11236

Berg, P., M. Huettel, R. N. Glud, C. E. Reimers, and K. M. Attard. 2022. Aquatic Eddy Covariance: The Method and Its Contributions to Defining Oxygen and Carbon Fluxes in Marine Environments. Annual Review of Marine Science **14**: 431–455. doi:10.1146/ANNUREV-MARINE-042121-012329

Berg, P., M. H. Long, M. Huettel, and others. 2013b. Eddy correlation measurements of oxygen fluxes in permeable sediments exposed to varying current flow and light. Limnology and Oceanography **58**: 1329–1343. doi:10.4319/LO.2013.58.4.1329

Berg, P., H. Røy, F. Janssen, V. Meyer, B. B. Jørgensen, M. Huettel, and D. de Beer. 2003. Oxygen uptake by aquatic sediments measured with a novel non-invasive eddy-correlation technique. Marine Ecology Progress Series **261**: 75–83. doi:10.3354/MEPS261075

Berger, A. C., P. Berg, K. J. McGlathery, and M. L. Delgard. 2020. Long-term trends and resilience of seagrass metabolism: A decadal aquatic eddy covariance study. Limnology and Oceanography **65**: 1423–1438. doi:10.1002/lno.11397

Blackwood, J. C., C. Okasaki, A. Archer, E. W. Matt, E. Sherman, and K. Montovan. 2018. Modeling alternative stable states in Caribbean coral reefs. Natural Resource Modeling **31**: e12157. doi:10.1111/nrm.12157

Bodmer, M. D. v., A. D. Rogers, M. R. Speight, N. Lubbock, and D. A. Exton. 2015. Using an isolated population boom to explore barriers to recovery in the keystone Caribbean coral reef herbivore Diadema antillarum. Coral Reefs **34**: 1011–1021. doi:10.1007/s00338-015-1329-4

Bodmer, M. D. V., P. M. Wheeler, P. Anand, S. E. Cameron, S. Hintikka, W. Cai, A. O. Borcsok, and D. A. Exton. 2021. The ecological importance of habitat complexity to the Caribbean coral reef herbivore Diadema antillarum: three lines of evidence. Scientific Reports 2021 11:1 **11**: 1–13. doi:10.1038/s41598-021-87232-9

Borchers, H. 2021. pracma: Practical Numerical Math Functions.

Borowitzka, M. A., P. S. Lavery, and M. van Keulen. 2007. Epiphytes of Seagrasses, p. 441–461. *In* Seagrasses: Biology, Ecology and Conservation. Springer, Dordrecht.

Boström-Einarsson, L., R. C. Babcock, E. Bayraktarov, and others. 2020. Coral restoration – A systematic review of current methods, successes, failures and future directions. PLOS ONE **15**: e0226631. doi:10.1371/JOURNAL.PONE.0226631

Boysen-Jensen, P. 1914. Studies concerning the organic matter of the sea bottom. Rep. Dan. Biol. **Stn 22, 1-**.

Brandl, S. J., D. B. Rasher, I. M. Côté, J. M. Casey, E. S. Darling, J. S. Lefcheck, and J. E. Duffy. 2019. Coral reef ecosystem functioning: eight core processes and the role of biodiversity, Wiley Blackwell.

Brears, R. C. 2021. Blue Carbon Ecosystems and Ecosystem-Based Adaptation. Developing the Blue Economy 247–285. doi:10.1007/978-3-030-84216-1_9

Bresnahan, P. J., T. R. Martz, Y. Takeshita, K. S. Johnson, and M. LaShomb. 2014. Best practices for autonomous measurement of seawater pH with the Honeywell Durafet. Methods in Oceanography **9**: 44–60. doi:10.1016/J.MIO.2014.08.003

Brodersen, K. E., M. Lichtenberg, P. J. Ralph, M. Kühl, and D. Wangpraseurt. 2014. Radiative energy budget reveals high photosynthetic efficiency in symbiont-bearing corals. Journal of the Royal Society Interface **11**. doi:10.1098/rsif.2013.0997

Brown, K. T., D. Bender-Champ, M. Achlatis, and others. 2020. Habitat-specific biogenic production and erosion influences net framework and sediment coral reef carbonate budgets. Limnology and Oceanography lno.11609. doi:10.1002/lno.11609

Burke, L., K. Reytar, M. Spalding, and A. Perry. 2011. Reefs at Risk Revisited.

Bushinsky, S. M., Y. Takeshita, and N. L. Williams. 2019. Observing Changes in Ocean Carbonate Chemistry: Our Autonomous Future. Current Climate Change Reports **5**: 207–220. doi:10.1007/s40641-019-00129-8

Caldeira, K., and M. E. Wickett. 2003. Anthropogenic carbon and ocean pH. Nature 2003 425:6956 **425**: 365–365. doi:10.1038/425365a

Camp, E. F., S.-L. Krause, L. M. F. Santos, M. S. Naumann, R. K. P. Kikuchi, D. J. Smith, C. Wild, and D. J. Suggett. 2015. The "Flexi-Chamber": A Novel Cost-Effective In Situ Respirometry Chamber for Coral Physiological Measurements J.L. Rummer [ed.]. PLOS ONE **10**: e0138800. doi:10.1371/journal.pone.0138800

Camp, E. F., M. R. Nitschke, R. Rodolfo-Metalpa, F. Houlbreque, S. G. Gardner, D. J. Smith, M. Zampighi, and D. J. Suggett. 2017. Reef-building corals thrive within hot-acidified and deoxygenated waters. Scientific Reports 2017 7:1 **7**: 1–9. doi:10.1038/s41598-017-02383-y

Chalker, B. E., D. J. Barnes, W. C. Dunlap, and P. L. Jokiel. 1988. Light and reef-building corals. Interdisciplinary Science Reviews **13**: 222–237. doi:10.1179/isr.1988.13.3.222

Chalker, B. E., and D. L. Taylor. 1975. Light-enhanced calcification, and the role of oxidative phosphorylation in calcification of the coral Acropora cervicornis. **190**: 323–331. doi:10.1098/rspb.1975.0096

Chalker, B. E., and D. L. Taylor. 1978. Rhythmic variations in calcification and photosynthesis associated with the coral Acropora cervicornis (Lamarck). Proceedings of the Royal Society of London - Biological Sciences **201**: 179–189. doi:10.1098/rspb.1978.0039

Chave, K. E., S. v. Smith, and K. J. Roy. 1972. Carbonate production by coral reefs. Marine Geology **12**: 123–140. doi:10.1016/0025-3227(72)90024-2

Chisholm, J. 2000. Calcification by crustose coralline algae on the northern Great Barrier Reef, Australia. Limnology and Oceanography **45**: 1476–1484. doi:10.4319/lo.2000.45.7.1476

Chisholm, J. R. M. M., and J.-P. J. -P Gattuso. 1991. Validation of the alkalinity anomaly technique for investigating calcification of photosynthesis in coral reef communities. Limnology and Oceanography **36**: 1232–1239. doi:10.4319/lo.1991.36.6.1232

Christianen, M. J. A., J. van Belzen, P. M. J. Herman, M. M. van Katwijk, L. P. M. Lamers, P. J. M. van Leent, and T. J. Bouma. 2013. Low-Canopy Seagrass Beds Still Provide Important Coastal Protection Services. PLoS ONE **8**. doi:10.1371/journal.pone.0062413

Cohen, I., Z. Dubinsky, and J. Erez. 2016. Light Enhanced Calcification in Hermatypic Corals: New Insights from Light Spectral Responses. Front Mar Sci **2**: 122. doi:10.3389/fmars.2015.00122

Coleman, V. L., and J. A. M. Burkholder. 1994. Community structure and productivity of epiphytic microalgae on eelgrass (Zostera marina L.) under water-column nitrate enrichment. Journal of Experimental Marine Biology and Ecology **179**: 29–48. doi:10.1016/0022-0981(94)90015-9

Colombo-Pallotta, M. F., A. Rodríguez-Román, and R. Iglesias-Prieto. 2010. Calcification in bleached and unbleached Montastraea faveolata: Evaluating the role of oxygen and glycerol. Coral Reefs **29**: 899–907. doi:10.1007/s00338-010-0638-x

Comeau, S., C. E. Cornwall, C. A. Pupier, T. M. DeCarlo, C. Alessi, R. Trehern, and M. T. McCulloch. 2019. Flow-driven micro-scale pH variability affects the physiology of corals and coralline algae under ocean acidification. Scientific Reports **9**: 1–12. doi:10.1038/s41598-019-49044-w

Comeau, S., P. J. Edmunds, C. A. Lantz, and R. C. Carpenter. 2014. Water flow modulates the response of coral reef communities to ocean acidification. Scientific Reports 2014 4:1 **4**: 1–6. doi:10.1038/srep06681

Comeau, S., P. J. Edmunds, N. B. Spindel, and R. C. Carpenter. 2013. The responses of eight coral reef calcifiers to increasing partial pressure of CO2 do not exhibit a tipping point. Limnology and Oceanography **58**: 388–398. doi:10.4319/lo.2013.58.1.0388

Costanza, R., R. D'Arge, R. de Groot, and others. 1997. The value of the world's ecosystem services and natural capital. Nature 1997 387:6630 **387**: 253–260. doi:10.1038/387253a0

Costanza, R., R. de Groot, P. Sutton, S. van der Ploeg, S. J. Anderson, I. Kubiszewski, S. Farber, and R. K. Turner. 2014. Changes in the global value of ecosystem services. Global Environmental Change **26**: 152–158. doi:10.1016/j.gloenvcha.2014.04.002

Crabbe, M. J. C., E. Martinez, C. Garcia, J. Chub, L. Castro, and J. Guy. 2008. Growth modelling indicates hurricanes and severe storms are linked to low coral recruitment in the Caribbean.

Cyronak, T., A. J. Andersson, C. Langdon, and others. 2018. Taking the metabolic pulse of the world's coral reefs C.R. Voolstra [ed.]. PLOS ONE **13**: e0190872. doi:10.1371/journal.pone.0190872

Cyronak, T., and B. D. Eyre. 2016. The synergistic effects of ocean acidification and organic metabolism on calcium carbonate (CaCO3) dissolution in coral reef sediments. Marine Chemistry **183**: 1–12. doi:10.1016/J.MARCHEM.2016.05.001

Cyronak, T., I. R. Santos, and B. D. Eyre. 2013. Permeable coral reef sediment dissolution driven by elevated p CO $_2$ and pore water advection. Geophysical Research Letters **40**: 4876–4881. doi:10.1002/grl.50948

Cyronak, T., Y. Takeshita, T. A. Courtney, and others. 2020. LETTER Diel temperature and pH variability scale with depth across diverse coral reef habitats. Limnology and Oceanography Letters **5**: 193–203. doi:10.1002/lol2.10129

Dam, B. van, P. Polsenaere, A. Barreras-Apodaca, and others. 2021. Global Trends in Air-Water CO2 Exchange Over Seagrass Meadows Revealed by Atmospheric Eddy Covariance. Global Biogeochemical Cycles **35**: e2020GB006848. doi:10.1029/2020GB006848

Darling, E. S., L. Alvarez-Filip, T. A. Oliver, T. R. Mcclanahan, and I. M. Côté. 2012. Evaluating life-history strategies of reef corals from species traits. Ecology Letters **15**: 1378–1386. doi:10.1111/j.1461-0248.2012.01861.x

Davis, K. L., A. P. Colefax, J. P. Tucker, B. P. Kelaher, and I. R. Santos. 2021. Global coral reef ecosystems exhibit declining calcification and increasing primary productivity. Communications Earth & Environment 2021 2:1 **2**: 1–10. doi:10.1038/s43247-021-00168-w

Dennison, W. C., and D. J. Barnes. 1988. Effect of water motion on coral photosynthesis and calcification. Journal of Experimental Marine Biology and Ecology **115**: 67–77. doi:10.1016/0022-0981(88)90190-6

Diaz-Pulido, G., K. R. N. Anthony, D. I. Kline, S. Dove, and O. Hoegh-Guldberg. 2012. Interactions between ocean acidification and warming on the mortality and dissolution of coralline algae. Journal of Phycology **48**: 32–39. doi:10.1111/j.1529-8817.2011.01084.x

Done, T. J. 1992. Phase shifts in coral reef communities and their ecological significance. Hydrobiologia **247**: 121–132. doi:10.1007/BF00008211

Doney, S. C., D. S. Busch, S. R. Cooley, and K. J. Kroeker. 2020. The Impacts of Ocean Acidification on Marine Ecosystems and Reliant Human Communities. https://doi.org/10.1146/annurev-environ-012320-083019 **45**: 83–112. doi:10.1146/ANNUREV-ENVIRON-012320-083019

Dorenbosch, M., M. G. G. Grol, M. J. A. Christianen, I. Nagelkerken, and G. van der Velde. 2005. Indo-Pacific seagrass beds and mangroves contribute to fish density and diversity on adjacent coral reefs. Marine Ecology Progress Series **302**: 63–76. doi:10.3354/MEPS302063

Doropoulos, C., S. Ward, G. Diaz-Pulido, O. Hoegh-Guldberg, and P. J. Mumby. 2012. Ocean acidification reduces coral recruitment by disrupting intimate larval-algal settlement interactions. Ecology Letters **15**: 338–346. doi:10.1111/j.1461-0248.2012.01743.x

Du, J., W. Hu, I. Nagelkerken, and others. 2020. Seagrass meadows provide multiple benefits to adjacent coral reefs through various microhabitat functions. Ecosystem Health and Sustainability **6**. doi:10.1080/20964129.2020.1812433

Duarte, C. M., and J. Cebrián. 1996. The fate of marine autotrophic production. Limnology and Oceanography **41**: 1758–1766. doi:10.4319/lo.1996.41.8.1758

Duarte, C. M., and C. L. Chiscano. 1999. Seagrass biomass and production: a reassessment. Aquatic Botany **65**: 159–174. doi:10.1016/S0304-3770(99)00038-8

Duarte, C. M., H. Kennedy, N. Marbà, and I. Hendriks. 2013a. Assessing the capacity of seagrass meadows for carbon burial: Current limitations and future strategies. Ocean & Coastal Management **83**: 32–38. doi:10.1016/J.OCECOAMAN.2011.09.001

Duarte, C. M., I. J. Losada, I. E. Hendriks, I. Mazarrasa, and N. Marbà. 2013b. The role of coastal plant communities for climate change mitigation and adaptation. Nature Climate Change 2013 3:11 **3**: 961–968. doi:10.1038/nclimate1970

Duarte, C. M., N. Marbà, E. Gacia, J. W. Fourqurean, J. Beggins, C. Barrón, and E. T. Apostolaki. 2010. Seagrass community metabolism: Assessing the carbon sink capacity of seagrass meadows. Global Biogeochemical Cycles **24**: 1–8. doi:10.1029/2010GB003793

Duarte, C. M., T. Sintes, and N. Marbà. 2013c. Assessing the CO2 capture potential of seagrass restoration projects. Journal of Applied Ecology **50**: 1341–1349. doi:10.1111/1365-2664.12155

Earle, S. A., D. J. Wright, S. Joye, D. Laffoley, J. Baxter, C. Safina, and P. Elkus. 2018. Ocean deoxygenation: Time for action. Science (1979) **359**: 1475–1476. doi:10.1126/SCIENCE.AAT0167

Eddy, T. D., V. W. Y. Lam, G. Reygondeau, and others. 2021. Global decline in capacity of coral reefs to provide ecosystem services. One Earth **4**: 1278–1285. doi:10.1016/J.ONEEAR.2021.08.016

Edmunds, P. J., and R. C. Carpenter. 2001. Recovery of Diadema antillarum reduces macroalgal cover and increases abundance of juvenile corals on a Caribbean reef. Proc Natl Acad Sci U S A **98**: 5067–71. doi:10.1073/pnas.071524598

Edmunds, P. J., S. Comeau, C. Lantz, and others. 2016. Integrating the Effects of Ocean Acidification across Functional Scales on Tropical Coral Reefs. BioScience **66**: 350–362. doi:10.1093/biosci/biw023

Edmunds, P. J., G. Tsounis, R. Boulon, and L. Bramanti. 2018. Long-term variation in light intensity on a coral reef. Coral Reefs **37**: 955–965. doi:10.1007/s00338-018-1721-y

Enochs, I. C., D. P. Manzello, P. R. Jones, S. J. Stamates, and T. P. Carsey. 2019. Seasonal Carbonate Chemistry Dynamics on Southeast Florida Coral Reefs: Localized Acidification Hotspots From Navigational Inlets. Front Mar Sci **6**: 160. doi:10.3389/fmars.2019.00160

Enríquez, S., N. Marbà, C. M. Duarte, B. I. van Tussenbroek, and G. Reyes-Zavala. 2001. Effects of seagrass Thalassia testudinum on sediment redox. Marine Ecology Progress Series **219**: 149–158. doi:10.3354/meps219149

Estrada-Saldívar, N., E. Jordán-Dalhgren, R. E. Rodríguez-Martínez, C. Perry, and L. Alvarez-Filip. 2019. Functional consequences of the long-term decline of reef-building corals in the Caribbean: Evidence of across-reef functional convergence. Royal Society Open Science **6**. doi:10.1098/rsos.190298

Eyre, B. D., A. J. Andersson, and T. Cyronak. 2014. Benthic coral reef calcium carbonate dissolution in an acidifying ocean. Nature Climate Change **4**: 969–976. doi:10.1038/nclimate2380

Eyre, B. D., T. Cyronak, P. Drupp, E. H. de Carlo, J. P. Sachs, and A. J. Andersson. 2018. Coral reefs will transition to net dissolving before end of century. Science **359**: 908–911. doi:10.1126/science.aao1118

Falkowski, P. G., Z. Dubinsky, L. Muscatine, and J. W. Porter. 1984. Light and the Bioenergetics of a Symbiotic Coral. BioScience **34**: 705–709. doi:10.2307/1309663

Falter, J. L., R. J. Lowe, M. J. Atkinson, S. G. Monismith, and D. W. Schar. 2008. Continuous measurements of net production over a shallow reef community using a modified Eulerian approach. **113**: 7035. doi:10.1029/2007JC004663

Ferrario, F., M. W. Beck, C. D. Storlazzi, F. Micheli, C. C. Shepard, and L. Airoldi. 2014. The effectiveness of coral reefs for coastal hazard risk reduction and adaptation. Nature Communications **5**: 1–9. doi:10.1038/ncomms4794

Ferse, S. C. A., M. Y. Hein, and L. Rölfer. 2021. A survey of current trends and suggested future directions in coral transplantation for reef restoration. PLOS ONE **16**: e0249966. doi:10.1371/JOURNAL.PONE.0249966

Flato, G. M., J. Marotzke, B. Abiodun, and others. 2013. Evaluation of climate models. Climate Change 2013 the Physical Science Basis: Working Group I Contribution to the Fifth Assessment Report of the Intergovernmental Panel on Climate Change **9781107057999**: 741–866. doi:10.1017/CBO9781107415324.020

Fonseca, M., and J. Fisher. 1986. A comparison of canopy friction and sediment movement between four species of seagrass with reference to their ecology and restoration. Marine Ecology Progress Series **29**: 15–22. doi:10.3354/meps029015

Forsman, Z. H., C. A. Page, R. J. Toonen, and D. Vaughan. 2015. Growing coral larger and faster: micro-colony-fusion as a strategy for accelerating coral cover. PeerJ **3**: e1313. doi:10.7717/peerj.1313

Fourqurean, J. W., C. M. Duarte, H. Kennedy, and others. 2012. Seagrass ecosystems as a globally significant carbon stock. Nature Geoscience **5**: 505–509. doi:10.1038/ngeo1477

Frankignoulle, M., C. Canon, and J.-P. J. -P Gattuso. 1994. Marine calcification as a source of carbon dioxide: Positive feedback of increasing atmospheric CO_2. Limnology and Oceanography **39**: 458–462. doi:10.4319/lo.1994.39.2.0458

Furla, P., I. Galgani, I. Durand, and D. Allemand. 2000. Sources and mechanisms of inorganic carbon transport for coral calcification and photosynthesis. Journal of Experimental Biology **203**: 3445–3457. doi:10.1242/JEB.203.22.3445

Gattuso, J., and R. W. Buddemeier. 2000. Calcification and CO_2. Nature **407**: 311–313. doi:10.1038/35030280

Gattuso, J. P., D. Allemand, M. Frankignoulle, and others. 1999a. Photosynthesis and calcification at cellular, organismal and community levels in coral reefs: A review on interactions and control by carbonate chemistry. American Zoologist **39**: 160–183. doi:10.1093/icb/39.1.160

Gattuso, J. P., M. Frankignoulle, S. v Smith, J. R. Ware, and R. Wollast. 1996. Coral reefs and carbon dioxide. Science **271**: 1298a. doi:10.1126/science.271.5253.1298a

Gattuso, J.-P., M. Frankignoulle, and S. v. Smith. 1999b. Measurement of community metabolism and significance in the coral reef CO2 source-sink debate. Proceedings of the National Academy of Sciences **96**: 13017–13022. doi:10.1073/pnas.96.23.13017

Gattuso, J.-P., S. Reynaud-Vaganay, P. Furla, S. Romaine-Lioud, J. Jaubert, I. Bourge, and M. Frankignoulle. 2000. Calcification does not stimulate photosynthesis in the zooxanthellate scleractinian coral Stylophora pistillata. Limnology and Oceanography **45**: 246–250. doi:10.4319/lo.2000.45.1.0246

Gingerich, P. D. 2019. Temporal Scaling of Carbon Emission and Accumulation Rates: Modern Anthropogenic Emissions Compared to Estimates of PETM Onset Accumulation. Paleoceanography and Paleoclimatology **34**: 329–335. doi:10.1029/2018PA003379

González-Barrios, F. J., and L. Álvarez-Filip. 2018. A framework for measuring coral species-specific contribution to reef functioning in the Caribbean. Ecological Indicators **95**: 877–886. doi:10.1016/J.ECOLIND.2018.08.038

Goreau, T. F. 1959. The physiology of skeleton formation in corals. A method for measuring the rate of calcium deposition by corals under different conditions. The Biological Bulletin **116**: 59–75. doi:10.2307/1539156

Goreau, T. F., and N. I. Goreau. 1959. The physiology of skeleton formation in corals. II. Calcium deposition by hermatypic corals under various conditions in the reef. https://doi.org/10.2307/1538903 **117**: 239–250. doi:10.2307/1538903

Goreau T F, Goreau N I, and Yonge C M. 1971. Reef corals: autotrophs or heterotrophs? Biol. Bull. **141**: 247–260.

Goreau, T. J. F., and R. L. Hayes. 2021. Global warming triggers coral reef bleaching tipping point: This article belongs to Ambio's 50th Anniversary Collection. Theme: Climate change impacts. Ambio **50**: 1137–1140. doi:10.1007/S13280-021-01512-2/FIGURES/2

Gove, J. M., M. A. McManus, A. B. Neuheimer, and others. 2016. Near-island biological hotspots in barren ocean basins. Nature Communications 2016 7:1 **7**: 1–8. doi:10.1038/ncomms10581

Green, D. H. D., P. P. J. Edmunds, and R. R. C. Carpenter. 2008. Increasing relative abundance of Porites astreoides on Caribbean reefs mediated by an overall decline in coral cover. Marine Ecology Progress Series **359**: 1–10. doi:10.3354/meps07454

Greiner, J. T., K. J. McGlathery, J. Gunnell, and others. 2013. Seagrass Restoration Enhances "Blue Carbon" Sequestration in Coastal Waters J. Cebrian [ed.]. PLoS ONE **8**: e72469. doi:10.1371/journal.pone.0072469

Guannel, G., K. Arkema, P. Ruggiero, and G. Verutes. 2016. The Power of Three: Coral Reefs, Seagrasses and Mangroves Protect Coastal Regions and Increase Their Resilience. PLOS ONE **11**: e0158094. doi:10.1371/JOURNAL.PONE.0158094

Harborne, A. R., P. J. Mumby, F. Micheli, C. T. Perry, C. P. Dahlgren, K. E. Holmes, and D. R. Brumbaugh. 2006. The Functional Value of Caribbean Coral Reef, Seagrass and Mangrove Habitats to Ecosystem Processes. Advances in Marine Biology **50**: 57–189. doi:10.1016/S0065-2881(05)50002-6

Harianto, J., N. Carey, and M. Byrne. 2019. respR—An R package for the manipulation and analysis of respirometry data S. Price [ed.]. Methods in Ecology and Evolution **10**: 912–920. doi:10.1111/2041-210X.13162

Harris, D. L., A. Rovere, E. Casella, and others. 2018. Coral reef structural complexity provides important coastal protection from waves under rising sea levels. Science Advances **4**. doi:10.1126/SCIADV.AAO4350/SUPPL_FILE/AAO4350_SM.PDF

He, Q., and B. R. Silliman. 2019. Climate Change, Human Impacts, and Coastal Ecosystems in the Anthropocene. Current Biology **29**: R1021–R1035. doi:10.1016/J.CUB.2019.08.042

Hein, M. Y., R. Beeden, A. Birtles, and others. 2020. Coral Restoration Effectiveness: Multiregional Snapshots of the Long-Term Responses of Coral Assemblages to Restoration. Diversity 2020, Vol. 12, Page 153 **12**: 153. doi:10.3390/D12040153

Hein, M. Y., B. L. Willis, R. Beeden, and A. Birtles. 2017. The need for broader ecological and socioeconomic tools to evaluate the effectiveness of coral restoration programs. Restoration Ecology **25**: 873–883. doi:10.1111/rec.12580

Hemminga, M. A. , M. A., and C. M. C. M. Duarte. 2000. No Title G. Balint, B. Antala, C. Carty, J.-M.A. Mabieme, I.B. Amar, and A. Kaplanova [eds.]. Uniwersytet śląski 343–354. doi:10.2/JQUERY.MIN.JS

Hendriks, I. E., Y. S. Olsen, L. Ramajo, L. Basso, A. Steckbauer, T. S. Moore, J. Howard, and C. M. Duarte. 2014. Photosynthetic activity buffers ocean acidification in seagrass meadows. Biogeosciences **11**: 333–346. doi:10.5194/BG-11-333-2014

Hendriks, I. E., T. Sintes, T. J. Bouma, and C. M. Duarte. 2008. Experimental assessment and modeling evaluation of the effects of the seagrass Posidonia oceanica on flow and particle trapping. Marine Ecology Progress Series **356**: 163–173. doi:10.3354/MEPS07316

Hernández, A. L. M., and B. I. van Tussenbroek. 2014. Patch dynamics and species shifts in seagrass communities under moderate and high grazing pressure by green sea turtles. Marine Ecology Progress Series **517**: 143–157. doi:10.3354/MEPS11068

van Heuven, S. M. A. C., A. E. Webb, D. M. de Bakker, E. Meesters, F. C. van Duyl, G.-J. Reichart, and L. J. de Nooijer. 2018. In-situ incubation of a coral patch for community-scale assessment of metabolic and chemical processes on a reef slope. PeerJ **6**: e5966. doi:10.7717/peerj.5966

Heyward, A. J., and A. P. Negri. 1999. Natural inducers for coral larval metamorphosis. Coral Reefs **18**: 273–279. doi:10.1007/s003380050193

Hoegh-Guldberg, O., L. Pendleton, and A. Kaup. 2019. People and the changing nature of coral reefs. Regional Studies in Marine Science **30**: 100699. doi:10.1016/j.rsma.2019.100699

Holzer, K. K., and K. J. McGlathery. 2016. Cultivation grazing response in seagrass may depend on phosphorus availability. Marine Biology **163**: 88. doi:10.1007/s00227-016-2855-5

Hoogenboom, M., K. Anthony, and S. Connolly. Energetic cost of photoinhibition in corals. Marine Ecology Progress Series **313**: 1–12.

Howard, J., A. Sutton-Grier, D. Herr, J. Kleypas, E. Landis, E. Mcleod, E. Pidgeon, and S. Simpson. 2017. Clarifying the role of coastal and marine systems in climate mitigation. Frontiers in Ecology and the Environment **15**: 42–50. doi:10.1002/fee.1451

Huettel, M., and G. Gust. 1992. Solute release mechanisms from confined sediment cores in stirred benthic chambers and flume flows. Marine Ecology Progress Series **82**: 187–197.

Hughes, T. P. 1987. Skeletal density and growth form of corals.

Hughes, T. P., A. H. Baird, D. R. Bellwood, and others. 2003. Climate change, human impacts, and the resilience of coral reefs. Science (1979) **301**: 929–933. doi:10.1126/science.1085046

Hughes, T. P., J. T. Kerry, M. Álvarez-Noriega, and others. 2017a. Global warming and recurrent mass bleaching of corals. Nature **543**: 373–377. doi:10.1038/nature21707

Hughes, T. P., J. T. Kerry, A. H. Baird, and others. 2018. Global warming transforms coral reef assemblages. Nature **556**: 492–496. doi:10.1038/s41586-018-0041-2

Hughes, T. P., M. J. Rodrigues, D. R. Bellwood, and others. 2007. Phase Shifts, Herbivory, and the Resilience of Coral Reefs to Climate Change,.

Hughes, T. P. T., M. L. Barnes, D. R. Bellwood, and others. 2017b. Coral reefs in the Anthropocene. Nature **546**: 82–90. doi:10.1038/nature22901

Hyndes, G. A., I. Nagelkerken, R. J. Mcleod, R. M. Connolly, P. S. Lavery, and M. A. Vanderklift. 2014. Mechanisms and ecological role of carbon transfer within coastal seascapes. Biological Reviews **89**: 232–254. doi:10.1111/brv.12055

Idjadi, J., R. Haring, and W. Precht. 2010. Recovery of the sea urchin Diadema antillarum promotes scleractinian coral growth and survivorship on shallow Jamaican reefs. Marine Ecology Progress Series **403**: 91–100. doi:10.3354/meps08463

Iluz, D., and Z. Dubinsky. 2015. Coral photobiology: New light on old views. Zoology **118**: 71–78. doi:10.1016/j.zool.2014.08.003

IPCC. 2013. IPCC. 2013. Climate change 2013: the physical science basis. In: Contribution of working group I to the fifth assessment report of the intergovernmental panel on climate change. Press.e.

IUCN. 2019. Ocean deoxygenation: Everyone's problem.doi:10.2305/IUCN.CH.2019.13.en

Jackson, J., M. Donovan, K. Cramer, and V. Lam. 2014. Status and trends of Caribbean coral reefs: 1970-2012, Global Coral Reef Monitoring Network, IUCN, Gland, Switzerland.

Jassby, A. D., and T. Platt. 1976. Mathematical formulation of the relationship between photosynthesis and light for phytoplankton. Limnology and Oceanography **21**: 540–547. doi:10.4319/lo.1976.21.4.0540

Johnson, M. D., J. J. Scott, M. Leray, N. Lucey, L. M. R. Bravo, W. L. Wied, and A. H. Altieri. 2021a. Rapid ecosystem-scale consequences of acute deoxygenation on a Caribbean coral reef. Nature Communications 2021 12:1 **12**: 1–12. doi:10.1038/s41467-021-24777-3

Johnson, M. D., S. D. Swaminathan, E. N. Nixon, V. J. Paul, and A. H. Altieri. 2021b. Differential susceptibility of reef-building corals to deoxygenation reveals remarkable hypoxia tolerance. Scientific Reports 2021 11:1 **11**: 1–12. doi:10.1038/s41598-021-01078-9

Jokiel, P. L. 1978. Effects of water motion on reef corals. **35**: 87–97. doi:10.1016/0022-0981(78)90092-8

Jokiel, P. L. 2016. Predicting the impact of ocean acidification on coral reefs: evaluating the assumptions involved. ICES Journal of Marine Science **73**: 550–557. doi:10.1093/ICESJMS/FSV091

Jokiel, P. L., C. P. Jury, I. B. Kuffner, P. L. Jokiel, C. P. Jury, and I. B. Kuffner. 2016. Coral Calcification and Ocean Acidification. 7–45. doi:10.1007/978-94-017-7567-0_2

Jokiel, P. L., C. P. Jury, and K. S. Rodgers. 2014. Coral-algae metabolism and diurnal changes in the CO $_2$ -carbonate system of bulk sea water. PeerJ **2**: e378. doi:10.7717/peerj.378

Jokiel, P. L., J. E. Maragos, and L. Franzisket. 1978. Measurement of the skeletal growth in scleractinian corals by buoyant weight technique. 529–542.

Jones, N. S., A. Ridgwell, and E. J. Hendy. 2015. Evaluation of coral reef carbonate production models at a global scale. Biogeosciences **12**: 1339–1356. doi:10.5194/bg-12-1339-2015

Jury, C., F. Thomas, M. Atkinson, and R. Toonen. 2013. Buffer Capacity, Ecosystem Feedbacks, and Seawater Chemistry under Global Change. Water (Basel) **5**: 1303–1325. doi:10.3390/w5031303

Kapsenberg, L., and T. Cyronak. 2019. Ocean acidification refugia in variable environments. Global Change Biology **25**: 3201–3214.

Kennedy, H., J. Beggins, C. M. Duarte, and others. 2010. Seagrass sediments as a global carbon sink: Isotopic constraints. Global Biogeochemical Cycles **24**. doi:10.1029/2010GB003848

Kinsey, D., and E. Kinsey. 1967. Diurnal changes in oxygen content of the water over the coral reef platform at Heron I. Marine and Freshwater Research **18**: 23–34. doi:10.1071/MF9670023

Kinsey, D. W. 1978. Alkalinity changes and coral reef calcification. Limnology and Oceanography **23**: 989–991. doi:10.4319/lo.1978.23.5.0989

Kinsey, D. W. 1983. Standards of performance in coral reef primary production and carbon turnover. 209–220.

Kleypas, J. A., K. R. N. Anthony, and J.-P. Gattuso. 2011. Coral reefs modify their seawater carbon chemistry - case study from a barrier reef (Moorea, French Polynesia). Global Change Biology **17**: 3667–3678. doi:10.1111/j.1365-2486.2011.02530.x

Kleypas, J., and K. Yates. 2009. Coral Reefs and Ocean Acidification. Oceanography **22**: 108–117. doi:10.5670/oceanog.2009.101

Knowlton, N., R. E. Brainard, R. Fisher, M. Moews, L. Plaisance, and M. J. Caley. 2010. Coral Reef Biodiversity, p. 65–78. *In* Life in the World's Oceans. Wiley-Blackwell.

Kornder, N. A., B. M. Riegl, and J. Figueiredo. 2018. Thresholds and drivers of coral calcification responses to climate change. Global Change Biology **24**: 5084–5095. doi:10.1111/gcb.14431

Koweek, D. A., R. C. Zimmerman, K. M. Hewett, and others. 2018. Expected limits on the ocean acidification buffering potential of a temperate seagrass meadow. Ecological Applications **28**: 1694–1714. doi:10.1002/EAP.1771

Koweek, D., R. B. Dunbar, J. S. Rogers, G. J. Williams, N. Price, D. Mucciarone, and L. Teneva. 2015. Environmental and ecological controls of coral community metabolism on Palmyra Atoll. Coral Reefs **34**: 339–351. doi:10.1007/s00338-014-1217-3

Kubicek, A., B. Breckling, O. Hoegh-Guldberg, and H. Reuter. 2019. Climate change drives trait-shifts in coral reef communities. Scientific Reports **9**: 3721. doi:10.1038/s41598-019-38962-4

Kuffner, I. B., E. Bartels, A. Stathakopoulos, I. C. Enochs, G. Kolodziej, L. T. Toth, and D. P. Manzello. 2017. Plasticity in skeletal characteristics of nursery-raised staghorn coral, Acropora cervicornis. Coral Reefs **36**: 679–684. doi:10.1007/s00338-017-1560-2

Lamb, J. B., J. A. J. M. van de Water, D. G. Bourne, and others. 2017. Seagrass ecosystems reduce exposure to bacterial pathogens of humans, fishes, and invertebrates. Science (1979) **355**: 731–733. doi:10.1126/SCIENCE.AAL1956/SUPPL_FILE/LAMB.SM.PDF

Lang, M. A. 2012. Coral reef research: Advances through the use of SCUBA. Underwater Technology **31**: 21–27. doi:10.3723/UT.31.021

Lange, I. D., and C. T. Perry. 2020. A quick, easy and non-invasive method to quantify coral growth rates using photogrammetry and 3D model comparisons N. Cooper [ed.]. Methods in Ecology and Evolution **11**: 714–726.

Lange, I. D., C. T. Perry, and L. Alvarez-Filip. 2020. Carbonate budgets as indicators of functional reef "health": A critical review of data underpinning census-based methods and current knowledge gaps. Ecological Indicators **110**. doi:10.1016/j.ecolind.2019.105857

Lantz, C., W. Leggat, J. Bergman, A. Fordyce, C. Page, T. Mesaglio, and T. Ainsworth. 2021. Will community calcification reflect reef accretion on future, degraded coral reefs? Biogeosciences Discussions 1–31. doi:10.5194/BG-2021-61

Larkum, A. W. D., R. J. Orth, and C. M. Duarte. 2006. Seagrasses: Biology, ecology and conservation. Seagrasses: Biology, Ecology and Conservation 1–691. doi:10.1007/978-1-4020-2983-7

Lau, J. D., C. C. Hicks, G. G. Gurney, and J. E. Cinner. 2019. What matters to whom and why? Understanding the importance of coastal ecosystem services in developing coastal communities. Ecosystem Services **35**: 219–230. doi:10.1016/J.ECOSER.2018.12.012

Lesser, M. P., V. M. Weis, M. R. Patterson, and P. L. Jokiel. 1994. Effects of morphology and water motion on carbon delivery and productivity in the reef coral, Pocillopora damicornis (Linnaeus): Diffusion barriers, inorganic carbon limitation, and biochemical plasticity. Journal of Experimental Marine Biology and Ecology **178**: 153–179. doi:10.1016/0022-0981(94)90034-5

Lessios, H. A. 2016. The Great *Diadema antillarum* Die-Off: 30 Years Later. Annual Review of Marine Science **8**: 267–283. doi:10.1146/annurev-marine-122414-033857

Lessios, H. A., D. R. Robertson, and J. D. Cubit. 1984. Spread of Diadema Mass Mortality Through the Caribbean. Science (1979) **226**: 335–337. doi:10.1126/SCIENCE.226.4672.335

Lewis, B., E. v. Kennedy, and G. Diaz-Pulido. 2017. Seasonal growth and calcification of a reef-building crustose coralline alga on the Great Barrier Reef. Marine Ecology Progress Series **568**: 73–86. doi:10.3354/meps12074

Lirman, D. 2000. Fragmentation in the branching coral Acropora palmata (Lamarck): Growth, survivorship, and reproduction of colonies and fragments. Journal of

Experimental Marine Biology and Ecology **251**: 41–57. doi:10.1016/S0022-0981(00)00205-7

Littler, M. M., and D. S. Littler. 2013. The Nature of Crustose Coralline Algae and Their Interactions on Reefs,.

Long, M. H., P. Berg, D. de Beer, J. C. Zieman, D. de Beer, and J. C. Zieman. 2013. In Situ Coral Reef Oxygen Metabolism: An Eddy Correlation Study A. Davies [ed.]. PLoS ONE **8**: e58581. doi:10.1371/journal.pone.0058581

Long, M. H., P. Berg, and J. L. Falter. 2015a. Seagrass metabolism across a productivity gradient using the eddy covariance, Eulerian control volume, and biomass addition techniques. Journal of Geophysical Research: Oceans **120**: 3624–3639. doi:10.1002/2014JC010352

Long, M. H., P. Berg, K. J. McGlathery, and J. C. Zieman. 2015b. Sub-tropical seagrass ecosystem metabolism measured by eddy covariance. Marine Ecology Progress Series **529**: 75–90. doi:10.3354/meps11314

Long, M. H., J. E. Rheuban, D. C. McCorkle, D. J. Burdige, and R. C. Zimmerman. 2019. Closing the oxygen mass balance in shallow coastal ecosystems. Limnology and Oceanography **64**: 2694–2708. doi:10.1002/LNO.11248

López-Mendoza, P. G., A. C. Ruiz-Fernández, J. A. Sanchez-Cabeza, B. I. van Tussenbroek, T. Cuellar-Martinez, and L. H. Pérez-Bernal. 2020. Temporal trends of organic carbon accumulation in seagrass meadows from the northern Mexican Caribbean. CATENA **194**: 104645. doi:10.1016/J.CATENA.2020.104645

Macreadie, P. I., A. Anton, J. A. Raven, and others. 2019. The future of Blue Carbon science. Nature Communications **10**: 1–13. doi:10.1038/s41467-019-11693-w

Macreadie, P. I., M. E. Baird, S. M. Trevathan-Tackett, A. W. D. Larkum, and P. J. Ralph. 2014. Quantifying and modelling the carbon sequestration capacity of seagrass meadows – A critical assessment. Marine Pollution Bulletin **83**: 430–439. doi:10.1016/J.MARPOLBUL.2013.07.038

Macreadie, P. I., M. D. P. Costa, T. B. Atwood, and others. 2021. Blue carbon as a natural climate solution. Nature Reviews Earth & Environment 2021 2:12 **2**: 826–839. doi:10.1038/s43017-021-00224-1

Macreadie, P. I., O. Serrano, D. T. Maher, C. M. Duarte, J. Beardall, and O. S. T. M. D. M. D. C. J. B. I Macreadie Peter. 2017. Addressing calcium carbonate cycling in blue carbon accounting. Limnology and Oceanography Letters **2**: 195–201. doi:10.1002/lol2.10052

Mallon, J., T. Cyronak, E. R. Hall, A. T. Banaszak, D. A. Exton, and A. M. Bass. 2022. Light-driven dynamics between calcification and production in functionally diverse coral reef calcifiers. Limnology and Oceanography **9999**: 1–16. doi:10.1002/LNO.12002

Manzello, D. P., I. C. Enochs, N. Melo, D. K. Gledhill, and E. M. Johns. 2012. Ocean Acidification Refugia of the Florida Reef Tract. PLOS ONE **7**: e41715. doi:10.1371/JOURNAL.PONE.0041715

Marsh, J. A., and S. v. Smith. 1978. Productivity measurements of coral reefs in flowing water. 361–377.

Mass, T., A. Genin, U. Shavit, M. Grinstein, and D. Tchernov. 2010. Flow enhances photosynthesis in marine benthic autotrophs by increasing the efflux of oxygen from the organism to the water. Proceedings of the National Academy of Sciences **107**: 2527–2531. doi:10.1073/PNAS.0912348107

McConnaughey, T. A., and J. F. Whelan. 1997. Calcification generates protons for nutrient and bicarbonate uptake. Earth-Science Reviews **42**: 95–117. doi:10.1016/S0012-8252(96)00036-0

McGillis, W. R., C. Langdon, B. Loose, K. K. Yates, and J. Corredor. 2011. Productivity of a coral reef using boundary layer and enclosure methods. Geophysical Research Letters **38**: n/a-n/a. doi:10.1029/2010GL046179

McKinley, G. A., A. R. Fay, N. S. Lovenduski, and D. J. Pilcher. 2017. Natural Variability and Anthropogenic Trends in the Ocean Carbon Sink. http://dx.doi.org/10.1146/annurev-marine-010816-060529 **9**: 125–150. doi:10.1146/ANNUREV-MARINE-010816-060529

McMahon, A., I. R. Santos, K. G. Schulz, T. Cyronak, and D. T. Maher. 2018. Determining coral reef calcification and primary production using automated alkalinity, pH and pCO2 measurements at high temporal resolution. Estuarine, Coastal and Shelf Science **209**: 80–88. doi:10.1016/J.ECSS.2018.04.041

Mehvar, S., T. Filatova, A. Dastgheib, E. de Ruyter van Steveninck, and R. Ranasinghe. 2018. Quantifying Economic Value of Coastal Ecosystem Services: A Review. Journal of Marine Science and Engineering **6**: 5. doi:10.3390/jmse6010005

Millero, F. J. 2007. The Marine Inorganic Carbon Cycle. Chemical Reviews **107**: 308–341. doi:10.1021/CR0503557

Moberg, F., and P. Rönnbäck. 2003. Ecosystem services of the tropical seascape: interactions, substitutions and restoration. Ocean & Coastal Management **46**: 27–46. doi:10.1016/S0964-5691(02)00119-9

Molina-Hernández, A., F. J. González-Barrios, C. T. Perry, and L. Álvarez-Filip. 2020. Two decades of carbonate budget change on shifted coral reef assemblages: are these reefs being locked into low net budget states? Proceedings of the Royal Society B: Biological Sciences **287**: 20202305. doi:10.1098/rspb.2020.2305

Moore, T. S., K. M. Mullaugh, R. R. Holyoke, A. S. Madison, M. Yucel, and G. W. Luther. 2009. Marine chemical technology and sensors for marine waters: Potentials and limits. Annual Review of Marine Science **1**: 91–115. doi:10.1146/annurev.marine.010908.163817

Muehllehner, N., C. Langdon, A. Venti, and D. Kadko. 2016. Dynamics of carbonate chemistry, production, and calcification of the Florida Reef Tract (2009-2010): Evidence for seasonal dissolution. Global Biogeochemical Cycles **30**: 661–688. doi:10.1002/2015GB005327

Mumby, P. J., A. J. Edwards, J. E. Arias-González, and others. 2004. Mangroves enhance the biomass of coral reef fish communities in the Caribbean. Nature 2004 427:6974 **427**: 533–536. doi:10.1038/nature02286

Murphy, B. A., C. H. Mazel, R. Whitehead, and A. M. Szmant. 2012. CISME: A self-contained diver portable metabolism and energetics system. *OCEANS 2012 MTS/IEEE: Harnessing the Power of the Ocean.*

Muscatine, L. 1973. Nutrition of corals. 77–115.

Muscatine, L. 1990. The role of symbiotic algae in carbon and energy flux in reef corals. Ecosystems of the world **25**.

Nagelkerken, I., C. M. Roberts, G. van der Velde, M. Dorenbosch, M. C. van Riel, E. Cocheret de la Morinière, and P. H. Nienhuis. 2002. How important are mangroves and seagrass beds for coral-reef fish? The nursery hypothesis tested on an island scale. Marine Ecology Progress Series **244**: 299–305. doi:10.3354/MEPS244299

Nakamura, T., K. Nadaoka, A. Watanabe, T. Yamamoto, T. Miyajima, and A. C. Blanco. 2017. Reef-scale modeling of coral calcification responses to ocean acidification and sea-level rise. Coral Reefs 1–17. doi:10.1007/s00338-017-1632-3

Naumann, M. S., C. Richter, C. Mott, M. el-Zibdah, R. Manasrah, and C. Wild. 2012. Budget of coral-derived organic carbon in a fringing coral reef of the Gulf of Aqaba, Red Sea. Journal of Marine Systems **105–108**: 20–29. doi:10.1016/J.JMARSYS.2012.05.007

Nellemann, C., E. Corcoran, C. M. Duarte, L. Valdés, C. de Young, L. Fonseca, and G. Grimsditch. 2009. Blue carbon: A Rapid Response Assessment.,.

Nelson, H. R., and A. H. Altieri. 2019. Oxygen: the universal currency on coral reefs,.

Nordlund, L. M., E. L. Jackson, M. Nakaoka, J. Samper-Villarreal, P. Beca-Carretero, and J. C. Creed. 2018. Seagrass ecosystem services – What's next? Marine Pollution Bulletin **134**: 145–151. doi:10.1016/J.MARPOLBUL.2017.09.014

Odum, H. T. 1956. Primary Production in Flowing Waters. Limnology and Oceanography **1**: 102–117. doi:10.4319/LO.1956.1.2.0102

Odum, H. T. 1957. Trophic Structure and Productivity of Silver Springs, Florida. Ecological Monographs **27**: 55–112. doi:10.2307/1948571

Olivé, I., J. Silva, M. M. Costa, and R. Santos. 2016. Estimating Seagrass Community Metabolism Using Benthic Chambers: The Effect of Incubation Time. Estuaries and Coasts **39**: 138–144. doi:10.1007/s12237-015-9973-z

van Oppen, M. J. H. H., R. D. Gates, L. L. Blackall, and others. 2017. Shifting paradigms in restoration of the world's coral reefs. Global Change Biology **23**: 3437–3448. doi:10.1111/gcb.13647

Oreska, M. P. J., G. M. Wilkinson, K. J. McGlathery, M. Bost, and B. A. McKee. 2018. Non-seagrass carbon contributions to seagrass sediment blue carbon. Limnology and Oceanography **63**: S3–S18. doi:10.1002/LNO.10718

Orr, J. C., V. J. Fabry, O. Aumont, and others. 2005. Anthropogenic ocean acidification over the twenty-first century and its impact on calcifying organisms. Nature **437**: 681–686. doi:10.1038/NATURE04095

Page, C. A., E. M. Muller, and D. E. Vaughan. 2018. Microfragmenting for the successful restoration of slow growing massive corals. Ecological Engineering **123**: 86–94. doi:10.1016/J.ECOLENG.2018.08.017

Page, H. N., T. A. Courtney, A. Collins, E. H. de Carlo, and A. J. Andersson. 2017. Net Community Metabolism and Seawater Carbonate Chemistry Scale Non-intuitively with Coral Cover. Front Mar Sci **4**: 161. doi:10.3389/fmars.2017.00161

Patterson, M. R., K. P. Sebens, and R. R. Olson. 1991. In situ measurements of flow effects on primary production and dark respiration in reef corals. Limnology and Oceanography **36**: 936–948. doi:10.4319/lo.1991.36.5.0936

Perry, C. T., and L. Alvarez-Filip. 2018. Changing geo-ecological functions of coral reefs in the Anthropocene, N. Graham [ed.]. Blackwell Publishing Ltd.

Perry, C. T., E. N. Edinger, P. S. Kench, G. N. Murphy, S. G. Smithers, R. S. Steneck, and P. J. Mumby. 2012. Estimating rates of biologically driven coral reef framework production and erosion: A new census-based carbonate budget methodology and applications to the reefs of Bonaire. Coral Reefs **31**: 853–868. doi:10.1007/s00338-012-0901-4

Piñón-González, V. M., and A. T. Banaszak. 2018. Effects of Partial Mortality on Growth, Reproduction and Total Lipid Content in the Elkhorn Coral Acropora palmata. Front Mar Sci **5**: 396. doi:10.3389/fmars.2018.00396

Platz, M. C., Y. Takeshita, E. Bartels, and M. E. Arias. 2020. Evaluating the potential for autonomous measurements of net community production and calcification as a tool for monitoring coral restoration. Ecological Engineering **158**: 106042. doi:10.1016/j.ecoleng.2020.106042

Precht, W. F., A. W. Bruckner, R. B. Aronson, and R. J. Bruckner. 2002. Endangered acroporid corals of the Caribbean. Coral Reefs **21**: 41–42. doi:10.1007/s00338-001-0209-2

Quéré, C., R. Andrew, P. Friedlingstein, and others. 2018. Global Carbon Budget 2018. Earth System Science Data **10**: 2141–2194. doi:10.5194/essd-10-2141-2018

R Core Team. 2019. R: A language and environment for statistical computing.

Reguero, B. G., C. D. Storlazzi, A. E. Gibbs, J. B. Shope, A. D. Cole, K. A. Cumming, and M. W. Beck. 2021. The value of US coral reefs for flood risk reduction. Nature Sustainability 2021 4:8 **4**: 688–698. doi:10.1038/s41893-021-00706-6

Reverter, M., S. B. Helber, S. Rohde, J. M. de Goeij, | Peter, and J. Schupp. 2021. Coral reef benthic community changes in the Anthropocene: Biogeographic heterogeneity, overlooked configurations, and methodology. Global Change Biology **00**: 1–16. doi:10.1111/GCB.16034

Ricart, A. M., M. Ward, T. M. Hill, and others. 2021. Coast-wide evidence of low pH amelioration by seagrass ecosystems. Global Change Biology **27**: 2580–2591.

Ricart, A. M., P. H. York, C. v. Bryant, M. A. Rasheed, D. Ierodiaconou, and P. I. Macreadie. 2020. High variability of Blue Carbon storage in seagrass meadows at the estuary scale. Scientific Reports 2020 10:1 **10**: 1–12. doi:10.1038/s41598-020-62639-y

Richardson, L. E., N. A. J. Graham, and A. S. Hoey. 2017. Cross-scale habitat structure driven by coral species composition on tropical reefs. Scientific Reports **7**. doi:10.1038/s41598-017-08109-4

Rinkevich, B., and Y. Loya. 1985. Intraspecific competition in a reef coral: effects on growth and reproduction. Oecologia **66**: 100–105. doi:10.1007/BF00378559

Rodolfo-Metalpa, R., M. O. Hoogenboom, C. Rottier, A. Ramos-Esplá, A. C. Baker, M. Fine, and C. Ferrier-Pagès. 2014. Thermally tolerant corals have limited capacity to acclimatize to future warming. Global Change Biology **20**: 3036–3049. doi:10.1111/GCB.12571

Rodríguez-Martínez, R. E., A. T. Banaszak, M. D. McField, A. U. Beltrán-Torres, and L. Álvarez-Filip. 2014. Assessment of Acropora palmata in the mesoamerican reef system B. Ruttenberg [ed.]. PLoS ONE **9**: 1–7. doi:10.1371/journal.pone.0096140

Romanó de Orte, M., D. A. Koweek, T. Cyronak, and others. 2021. Unexpected role of communities colonizing dead coral substrate in the calcification of coral reefs. Limnology and Oceanography **9999**: lno.11722. doi:10.1002/lno.11722

Roth, F., C. Wild, S. Carvalho, and others. 2019. An in situ approach for measuring biogeochemical fluxes in structurally complex benthic communities C. Trueman [ed.]. Methods in Ecology and Evolution **10**: 712–725. doi:10.1111/2041-210X.13151

Roth, M. S. 2014. The engine of the reef: Photobiology of the coral-algal symbiosis. Frontiers in Microbiology **5**: 422. doi:10.3389/fmicb.2014.00422

Sabine, C. L., R. A. Feely, N. Gruber, and others. 2004. The Oceanic Sink for Anthropogenic CO2. Science (1979) **305**.

Sargent, M. C., and T. S. Austin. 1949. Organic productivity of an Atoll. Eos, Transactions American Geophysical Union **30**: 245–249.

Sawall, Y., E. J. Hochberg, Y. Sawall Id, and E. J. Hochberg. 2018. Diel versus time-integrated (daily) photosynthesis and irradiance relationships of coral reef organisms and communities C. Linares [ed.]. PLOS ONE **13**: e0208607. doi:10.1371/journal.pone.0208607

Schlecker, L., C. Page, M. Matz, and R. M. Wright. 2022. Mechanisms and potential immune tradeoffs of accelerated coral growth induced by microfragmentation. PeerJ **10**: e13158. doi:10.7717/PEERJ.13158/SUPP-13

Schneider, C. A., W. S. Rasband, and K. W. Eliceiri. 2012. NIH Image to ImageJ: 25 years of image analysis. Nature Methods **9**: 671–675. doi:10.1038/nmeth.2089

Schopmeyer, S. A., D. Lirman, E. Bartels, and others. 2017. Regional restoration benchmarks for Acropora cervicornis. Coral Reefs **36**: 1047–1057. doi:10.1007/s00338-017-1596-3

Serrano, O., C. E. Lovelock, T. B. Atwood, and others. 2019. Australian vegetated coastal ecosystems as global hotspots for climate change mitigation. Nature Communications **10**: 1–10. doi:10.1038/s41467-019-12176-8

Shamberger, K. E. F. E. F., R. A. A. Feely, C. L. L. Sabine, M. J. J. Atkinson, E. H. H. DeCarlo, F. T. T. Mackenzie, P. S. S. Drupp, and D. A. A. Butterfield. 2011. Calcification and organic production on a Hawaiian coral reef. Marine Chemistry **127**: 64–75.

Shamberger, K. E. F., S. J. Lentz, and A. L. Cohen. 2018. Low and variable ecosystem calcification in a coral reef lagoon under natural acidification. Limnology and Oceanography **63**: 714–730. doi:10.1002/lno.10662

Shaw, E. C., B. I. McNeil, and B. Tilbrook. 2012. Impacts of ocean acidification in naturally variable coral reef flat ecosystems. Journal of Geophysical Research: Oceans **117**: n/a-n/a. doi:10.1029/2011JC007655

Shaw, E. C., S. R. Phinn, B. Tilbrook, and A. Steven. 2014. Comparability of slack water and Lagrangian flow respirometry methods for community metabolic measurements. PLoS ONE **9**: e112161–e112161. doi:10.1371/journal.pone.0112161

Short, F. T., and C. A. Short. 1984. The seagrass filter: purification of estuarine and coastal waters. The Estuary As a Filter 395–413. doi:10.1016/B978-0-12-405070-9.50024-4

Silbiger, N. J., and C. J. B. Sorte. 2018. Biophysical feedbacks mediate carbonate chemistry in coastal ecosystems across spatiotemporal gradients. Scientific Reports 2018 8:1 **8**: 1–11. doi:10.1038/s41598-017-18736-6

Smith, J. E., N. N. Price, C. E. Nelson, and A. F. Haas. 2013. Coupled changes in oxygen concentration and pH caused by metabolism of benthic coral reef organisms. Marine Biology **160**: 2437–2447. doi:10.1007/s00227-013-2239-z

Smith, S. v., and J. T. Hollibaugh. 1993. Coastal metabolism and the oceanic organic carbon balance. Reviews of Geophysics **31**: 75–89. doi:10.1029/92RG02584

Smith, S. v., and D. W. Kinsey. 1976. Calcium carbonate production, coral reef growth, and sea level change. Science (1979) **194**: 937–939. doi:10.1126/science.194.4268.937

Smith, S. v., and D. W. Kinsey. 1978. Calcification and organic carbon metabolism as indicated by carbon dioxide, p. 469–484. *In* D.R. Stoddart and R.E. Johannes [eds.], Coral Reefs: Research Methods. UNESCO.

Sorek, M., E. M. Díaz-Almeyda, M. Medina, and O. Levy. 2014. Circadian clocks in symbiotic corals: The duet between Symbiodinium algae and their coral host. Marine Genomics **14**: 47–57. doi:10.1016/j.margen.2014.01.003

Sorek, M., and O. Levy. 2012. Influence of the quantity and quality of light on photosynthetic periodicity in coral endosymbiotic Algae. PLoS ONE **7**. doi:10.1371/journal.pone.0043264

Spalding, M., L. Burke, S. A. Wood, J. Ashpole, J. Hutchison, and P. zu Ermgassen. 2017. Mapping the global value and distribution of coral reef tourism. Marine Policy **82**: 104–113. doi:10.1016/j.marpol.2017.05.014

Stoltenberg, L., K. G. Schulz, T. Cyronak, and B. D. Eyre. 2019. Seasonal variability of calcium carbonate precipitation and dissolution in shallow coral reef sediments. Limnology and Oceanography **65**: lno.11357. doi:10.1002/lno.11357

Storlazzi, C. D., B. G. Reguero, K. A. Cumming, and others. 2021. Rigorously valuing the coastal hazard risks reduction provided by potential coral reef restoration in Florida and Puerto Rico. Open-File Report. doi:10.3133/OFR20211054

Suggett, D. J., L. F. Dong, T. Lawson, E. Lawrenz, L. Torres, and D. J. Smith. 2013. Light availability determines susceptibility of reef building corals to ocean acidification. Coral Reefs **32**: 327–337. doi:10.1007/s00338-012-0996-7

Sun, C.-Y. Y., C. A. Stifler, R. v. Chopdekar, and others. 2020. From particle attachment to space-filling coral skeletons. **117**: 30159–30170.

Takeshita, Y. 2017. Understanding feedbacks between ocean acidification and coral reef metabolism. Journal of Geophysical Research: Oceans **122**: 1639–1642. doi:10.1002/2017JC012740

Takeshita, Y., T. Cyronak, T. R. Martz, T. Kindeberg, and A. J. Andersson. 2018. Coral Reef Carbonate Chemistry Variability at Different Functional Scales. Front Mar Sci **5**: 175. doi:10.3389/fmars.2018.00175

Takeshita, Y., W. McGillis, E. M. Briggs, A. L. Carter, E. M. Donham, T. R. Martz, N. N. Price, and J. E. Smith. 2016. Assessment of net community production and calcification of a coral reef using a boundary layer approach. Journal of Geophysical Research: Oceans **121**: 5655–5671. doi:10.1002/2016JC011886

Teneva, L., R. B. Dunbar, D. A. Mucciarone, J. F. Dunckley, and J. R. Koseff. 2013. High-resolution carbon budgets on a Palau back-reef modulated by interactions between hydrodynamics and reef metabolism. Limnology and Oceanography **58**: 1851–1870. doi:10.4319/lo.2013.58.5.1851

Toth, L. T., A. Stathakopoulos, I. B. Kuffner, R. R. Ruzicka, M. A. Colella, and E. A. Shinn. 2019. The unprecedented loss of Florida's reef-building corals and the emergence of a novel coral-reef assemblage. Ecology **100**: e02781. doi:10.1002/ECY.2781

Trevathan-Tackett, S. M., J. Kelleway, P. I. Macreadie, J. Beardall, P. Ralph, and A. Bellgrove. 2015. Comparison of marine macrophytes for their contributions to blue carbon sequestration. Ecology **96**: 3043–3057. doi:10.1890/15-0149.1.sm

Tunnicliffe, V. 1981. Breakage and propagation of the stony coral Acropora cervicornis. Proceedings of the National Academy of Sciences **78**: 2427–2431. doi:10.1073/pnas.78.4.2427

Turk, D., K. Yates, M. Vega-Rodriguez, and others. 2015. Community metabolism in shallow coral reef and seagrass ecosystems, lower Florida Keys. Marine Ecology Progress Series **538**: 35–52. doi:10.3354/meps11385

UNEP. 2006. Marine and coastal ecosystems and human well-being: A synthesis report based on the findings of the Millennium Ecosystem Assessment. UNEP 76pp.

Unsworth, R. K. F., L. J. McKenzie, L. M. Nordlund, and L. C. Cullen-Unsworth. 2018. A changing climate for seagrass conservation? Current Biology **28**: R1229–R1232. doi:10.1016/J.CUB.2018.09.027

Ver, L. M. B., F. T. Mackenzie, and A. Lerman. 1999. Carbon cycle in the coastal zone: effects of global perturbations and change in the past three centuries. Chemical Geology **159**: 283–304. doi:10.1016/S0009-2541(99)00042-X

Veron, J. E. N. 2011. Ocean Acidification and Coral Reefs: An Emerging Big Picture. Diversity (Basel) **3**: 262–274. doi:10.3390/d3020262

van Vuuren, D. P., J. Edmonds, M. Kainuma, and others. 2011. The representative concentration pathways: An overview. Climatic Change **109**: 5–31. doi:10.1007/S10584-011-0148-Z/TABLES/4

Waltham, N. J., M. Elliott, S. Y. Lee, and others. 2020. UN Decade on Ecosystem Restoration 2021–2030—What Chance for Success in Restoring Coastal Ecosystems? Front Mar Sci **0**: 71. doi:10.3389/FMARS.2020.00071

Ware, J. R., S. v Smith, and M. L. Reaka-Kudla. 1991. Coral reefs: sources or sinks of atmospheric CO_2. Coral Reefs **11**: 127–130.

Watanabe, A., and T. Nakamura. 2019. Carbon Dynamics in Coral Reefs, p. 273–293. *In* Blue Carbon in Shallow Coastal Ecosystems. Springer Singapore.

Webb, A. E., D. M. de Bakker, K. Soetaert, T. da Costa, S. M. A. C. van Heuven, F. C. van Duyl, G.-J. Reichart, and L. J. de Nooijer. 2021. Quantifying functional consequences of habitat degradation on a Caribbean coral reef. Biogeosciences **18**: 6501–6516. doi:10.5194/BG-18-6501-2021

Wickham, H. 2016. ggplot2: Elegant Graphics for Data Analysis.

Wickham, H. 2019. Welcome to the tidyverse. Journal of Open Source Software, 4(43), 1686,.

Williams, G. J., and N. A. J. Graham. 2019. Rethinking coral reef functional futures C. Fox [ed.]. Functional Ecology **33**: 942–947. doi:10.1111/1365-2435.13374

Williams, S. M., C. Sánchez-Godínez, S. P. Newman, and J. Cortés. 2017. Ecological assessments of the coral reef communities in the Eastern Caribbean and the effects of herbivory in influencing coral juvenile density and algal cover. Marine Ecology **38**: e12395. doi:10.1111/maec.12395

Woodhead, A. J., C. C. Hicks, A. v. Norström, G. J. Williams, and N. A. J. Graham. 2019. Coral reef ecosystem services in the Anthropocene. Functional Ecology **33**: 1023–1034. doi:10.1111/1365-2435.13331

Yates, K. K., and R. B. Halley. 2003. Measuring coral reef community metabolism using new benthic chamber technology. Coral Reefs **22**: 247–255. doi:10.1007/S00338-003-0314-5

Yeakel, K. L., A. J. Andersson, N. R. Bates, T. J. Noyes, A. Collins, and R. Garley. 2015. Shifts in coral reef biogeochemistry and resulting acidification linked to offshore productivity. Proc Natl Acad Sci U S A **112**: 14512–7. doi:10.1073/pnas.1507021112

Young, C., S. Schopmeyer, and D. Lirman. 2012. A Review of Reef Restoration and Coral Propagation Using the Threatened Genus <I>Acropora</I> in the Caribbean and Western Atlantic. Bulletin of Marine Science **88**: 1075–1098. doi:10.5343/bms.2011.1143